

**Synaptic vesicle protein 2A (SV2A) and connexin 43
(Cx43) as targets for epilepsy: establishment of assays
and identification of ligands**

Dissertation

zur

Erlangung des Doktorgrades (Dr. rer. nat.)

der

Mathematisch-Naturwissenschaftlichen Fakultät

der

Rheinischen Friedrich-Wilhelms-Universität Bonn

vorgelegt von

Azeem Danish

aus

Pakistan

Bonn 2017

Angefertigt mit Genehmigung der Mathematisch-Naturwissenschaftlichen Fakultät der Rheinischen Friedrich-Wilhelms-Universität Bonn.

1. Gutachter: Prof. Dr. Christa E. Müller

2. Gutachter: PD Dr. Anke Schiedel

Tag der Promotion: 18.07.2017

Erscheinungsjahr: 2017

Die vorliegende Arbeit wurde in der Zeit von Juli 2013 bis April 2017 am Pharmazeutischen Institut der Rheinischen Friedrich-Wilhelms-Universität Bonn unter der Leitung von Frau Prof. Dr. Christa E. Müller durchgeführt.

Mein ganz besonderer Dank gilt Frau Prof. Dr. Christa E. Müller für die kompetente Betreuung sowie für die inspirierenden Diskussionen während meiner Promotion.

Frau PD Dr. Anke Schiedel danke ich ganz herzlich für die Übernahme des Korreferats. Herrn Prof. Dr. Christian Steinhäuser danke ich für die freundliche Zusammenarbeit sowie für die Mitwirkung in meiner Promotionskommission. Herrn Prof. Dr. Rainer Manthey danke ich für die Mitwirkung in meiner Promotionskommission.

Ich danke der Friedrich-Ebert-Stiftung für die finanzielle sowie ideelle Unterstützung in Form eines Stipendiums. Ich danke der BIGS-DrugS-Graduiertenschule für die interessanten Seminare und Workshops.

Dedicated to

Child labor and street children

Abstract

Epilepsy is a chronic neurological disorder affecting around 1% of the human population worldwide. The antiepileptic drugs (AEDs) available on the market provide symptomatic relief from epilepsy but do not cure the disease. Moreover, around 30% of epileptic patients remain resistant to treatment with the available AEDs. There is an unmet need for new AEDs exhibiting novel mechanism(s) of action resulting in disease-modifying properties. The AEDs **levetiracetam** (LEV, Keppra[®]) and its more potent derivative **brivaracetam** (BRV, Briviact[®]) exert their anticonvulsive effects through a unique mechanism of action, which is, however, still not well understood. The synaptic vesicle protein 2A (**SV2A**) was previously identified as the main target of LEV and BRV. However, LEV was also shown to modulate connexin43 (**Cx43**) gap junction (GJ) channels in astrocytes, which may also contribute to its antiepileptic efficacy.

In the present study, a **radioligand competition assay** suitable for compound library screening was established using [³H]BRV and cellular homogenates of Chinese hamster ovary (CHO) cells stably expressing human SV2A. A library of 500 approved drugs was tested for interaction with SV2A resulting in the identification of three new SV2A-interacting compounds, **loratadine**, **quinine**, and **rimonabant**. This discovery prompted us to screen an in-house library of 80 cannabinoids, which resulted in the identification of cannabidiol (**CBD**) as a potent ligand of SV2A with a K_i value below 1 μM. Thus CBD (K_i 0.719 μM) is similarly potent as LEV (K_i 1.74 μM) at SV2A. Our results support the idea that the already established anticonvulsive properties of quinine might be – at least partly – attributed to its interaction with SV2A. In fact, CBD has shown antiepileptic effects and was recently approved for the treatment of epilepsy syndromes (Dravet syndrome and Lennox-Gastaut syndrome). SV2A interaction may contribute to its antiepileptic activity which has so far been unknown. Binding studies with [³H]BRV at SV2A variants to investigate a potential role of the long **intracellular cytoplasmic loop 3** (ICL3) of SV2A for LEV/BRV binding point towards the importance of the ICL3 for racetam binding. Previously proposed interaction partners of SV2A, namely galactose and botulinum neurotoxin A (BoNT/A) did not modulate [³H]BRV binding. Binding studies with [³H]BRV on recombinant Cx43 did not indicate the presence of a high-affinity binding site. Moreover, we developed a new screening assay for **Cx43 GJ** modulators which should be suitable for high-throughput screening. Lastly, the development of a novel method using capillary gel electrophoresis with a laser-induced fluorescence detector (**CGE-LIF**) for the quantification of green fluorescent protein (**GFP**)-tagged **membrane proteins** in a complex matrix such as cellular homogenates was reported. In conclusion, herein identified compounds interacting with SV2A may provide a basis for the development of new classes of antiepileptic drugs. The newly developed Cx43 GJ screening assay will help to screen large compound libraries to identify selective and potent modulators of Cx43 GJ channels. Furthermore, the new CGE-LIF based method provides a fast, robust, and reproducible approach to quantify various classes of membrane proteins containing a fluorescent tag.

Keywords: brivaracetam, cannabidiol, CGE-LIF, Cx43, epilepsy, gap junctions, HTS assay, levetiracetam, radioligand binding, SV2A

TABLE OF CONTENTS

1	Introduction.....	1
1.1	Epilepsy.....	1
1.2	Antiepileptic drugs and their targets.....	3
1.2.1	Levetiracetam (Keppra®) and Brivaracetam (Briviact®)	11
1.3	Newer antiepileptic drug targets	13
1.3.1	Biology of SV2A	13
1.3.2	Gap junction channels.....	16
1.4	Interaction of botulinum neurotoxins with SV2A	17
1.5	Objectives	19
2	Characterization of SV2A and its ligands	21
2.1	Identification and characterization of new SV2A ligands	21
2.1.1	Interaction of approved drugs with SV2A	21
2.1.2	Interaction of cannabinoids with SV2A.....	39
2.1.3	Summary.....	52
2.2	Modulation of [³ H]BRV binding	53
2.2.1	Impact of monosaccharides on [³ H]BRV binding	53
2.2.2	Impact of botulinum neurotoxin A on [³ H]BRV binding.....	54
2.3	Potential interaction of the intracellular loop 3 of SV2A with [³ H]BRV ...	57
2.3.1	Introduction.....	57
2.3.2	Molecular cloning and recombinant expression	60
2.3.3	Heterologous expression of wt SV2A and its variants	62
2.3.4	Binding of [³ H]BRV to SV2A-R383Q mutant	64
2.3.5	Binding of [³ H]BRV to chimeric SV2A and SV2B proteins.....	67
2.3.6	Summary.....	70
3	Screening assay for connexin 43 (Cx43) gap junctions.....	71
3.1	Introduction.....	71
3.1.1	Gap junction channels.....	71
3.1.2	Synthesis and degradation of Cx43 GJs.....	73
3.1.3	Phosphorylation mediated regulation of Cx43 GJs	75
3.1.4	Pharmacological relevance of GJs	76

3.1.5	Interaction of levetiracetam with Cx43 GJs.....	78
3.1.6	GJ functional assays.....	79
3.2	Development of Cx43 GJ assay	81
3.2.1	Evaluation of levetiracetam binding to Cx43 protein.....	81
3.2.2	Cx43 expression in cell lines	82
3.2.3	Strategies for developing a new Cx43 GJ screening assay.....	84
3.2.4	Cx43 GJ screening assay design.....	86
3.2.5	Optimization of cAMP detection in Cx43 GJ assay	90
3.2.6	Cell-to-cell communication in native HeLa cells	94
3.2.7	Inhibition of Cx43 GJs with carbenoxolone	96
3.2.8	Suitability as a HTS assay.....	98
3.3	Summary	101
4	Quantification of GFP-tagged membrane proteins by CGE-LIF	102
4.1	Introduction.....	102
4.1.1	CGE-LIF setup.....	105
4.1.2	Calibration curve with GFP using CGE-LIF	106
4.1.3	Calibration curve with GFP using direct fluorimetry	108
4.1.4	Quantification of recombinant GFP-fused proteins.....	108
4.1.5	Quantification of SV2A and A _{2A} AR by radioligand binding assays....	112
4.2	Summary	114
5	Summary and outlook	115
6	Experimental section	122
6.1	Materials	122
6.1.1	Chemicals.....	122
6.1.2	Instruments and consumables	124
6.1.3	Software	126
6.1.4	Materials for molecular biology.....	127
6.1.5	Plasmids	128
6.1.6	Media and supplements for cell culture	128
6.1.7	Primers	129
6.1.8	Bacteria and growth media	130
6.1.9	Cell lines and culture media.....	131

6.1.10	Buffers, media and gels.....	131
6.1.11	Radioligands	133
6.2	Molecular Biology	134
6.2.1	Transformation.....	134
6.2.2	Isolation and purification of plasmids.....	135
6.2.3	Preparation of glycerol stocks.....	135
6.2.4	Gel electrophoresis.....	136
6.2.5	Restriction digest with endonucleases	136
6.2.6	Ligation.....	138
6.2.7	Polymerase chain reaction (PCR).....	138
6.2.8	Site-directed mutagenesis	140
6.2.9	Primer design	141
6.2.10	Sequencing.....	142
6.2.11	Gibson assembly: one-step assembly of multiple DNA fragments	142
6.3	Expression and purification of BoNT/A-HCR	144
6.4	Cell culture.....	145
6.4.1	Cultivation of cells.....	145
6.4.2	Cryopreservation of cells	145
6.4.3	Counting and seeding of cells	145
6.4.4	Lipofection.....	146
6.5	Protein sample preparations	150
6.5.1	Rat cortical membrane preparations	150
6.5.2	Preparation of cellular homogenates.....	150
6.5.3	Cell membrane and cell debris preparations.....	151
6.6	Recombinant protein analysis.....	152
6.6.1	Fluorescence microscopy.....	152
6.6.2	Bradford assay	152
6.6.3	Fluorimetric measurement	153
6.6.4	Capillary gel electrophoresis system	154
6.6.5	SDS PAGE.....	156
6.6.6	Western Blot analysis	156
6.7	Radioligand binding assays	157
6.7.1	Competition radioligand binding assay	158

6.7.2	Homologous competition binding assay	160
6.8	Cx43 gap junction assay	162
6.8.1	Plasmids and cell lines for Cx43 gap junction assay	162
6.8.2	Plate preparation for the Cx43 gap junction assay.....	163
6.9	Pharmacophore modeling	164
7	Abbreviations	166
8	References.....	172
9	Appendices.....	199
	Curriculum Vitae	203
	Acknowledgements	206

1 Introduction

1.1 Epilepsy

The term “epilepsy” originates from the Greek word “epilambanein”, which means to seize, to take hold of, or to attack.¹ Epilepsy is one of the most common chronic neurological disorders affecting around 1% of the human population worldwide.² One of the striking facts about epilepsy is that one third of the patients are under the age of 16.³ Epilepsy with a prevalence of about 3 million patients alone in the U.S. is the fourth most common neurological disorder after migraine, stroke, and Alzheimer’s disease.²

Epilepsy is characterized by epileptic seizure(s) – a transient occurrence of signs and/or symptoms due to abnormal excessive or synchronous neuronal activity in the brain. This is a consensus definition of epileptic seizures proposed by the International League Against Epilepsy (ILAE) and the International Bureau for Epilepsy (IBE).⁴ Seizures may vary from brief lapses of attention and muscle jerks to prolonged convulsions that can occur less than once per year to several times per day. Epilepsy is not characterized by one particular condition, but rather represents a spectrum of neurological conditions, all with the common hallmark characteristic of enhanced predisposition to epileptic seizures. The multifaceted nature of this brain disorder results in debatable diagnostic criteria, like on the one hand “two or more unprovoked seizures occurring more than 24 h apart” and on the other hand “at least one seizure with enduring alteration in the brain with the likelihood of future seizures”.¹ However, these definitions are of more theoretical nature and not sufficient for clinical diagnosis of epilepsy. Therefore, the ILAE in 2014 proposed revised diagnosis criteria for epilepsy; a person is considered to have epilepsy if any of the following criteria is met, i) two or more unprovoked seizures occurring more than 24 h apart, ii) one unprovoked seizure with 60% probability of future seizures and two unprovoked seizures occurring within the next 10 years, and iii) diagnosis of epilepsy syndrome. Epilepsy syndrome is defined by group of features occurring together such as type of seizures, typical age of seizures onset, and certain electroencephalogram (EEG) patterns and imaging features.⁵⁻⁶ Individuals with epilepsy syndrome are considered to be epilepsy free, in case they have either passed the typical age of seizures onset or they have been remained seizure-free for the last 10 years with no antiseizure

1 Introduction

medication for the last 5 years.⁵ Under these criteria ILAE emphasizes to differentiate epilepsy-mediated seizures from seizures due to other causes such as febrile seizures.⁴

A synchronized release of excitatory and inhibitory neurotransmitters is required to maintain membrane potentials for signal transmission in the central nervous system (CNS).⁷ Seizures are a consequence of neuronal hypersynchronisation (“electrical storm”) impairing the normal activity of the brain. Based on the initial clinical findings like magnetic resonance imaging (MRI) and EEG patterns, seizures are divided into two broad categories, namely partial (focal) and generalized ones. Seizures initiated from a limited part of one cerebral hemisphere are classified as partial or focal seizures, whereas seizures with the involvement of both hemispheres are classified as generalized seizures.¹ Based on the clinical manifestations seizures are further subclassified into absence, atonic, myoclonic, tonic-clonic seizures and so on. Epilepsy may be i) primary (idiopathic) due to unknown cause – presumably involving a genetic predisposition, ii) secondary (symptomatic) due to an underlying pathophysiological condition such as brain insults, infection, tumour, stroke, and syndromes, iii) provoked due to external factors like fever, alcohol, and photosensitivity, and iv) cryptogenic due to an unknown cause but presumably symptomatic.^{4, 8} Several epilepsy syndromes are described including the treatment-resistant Dravet syndrome and Lennox-Gastaut syndrome. Dravet syndrome is an infantile epileptic encephalopathy beginning in the first year of life and results in the development of different seizure types like prolonged febrile and generalized tonic-clonic seizures. It is characterized by intractable epilepsy and neurodevelopmental disabilities. Up to 85% of children with Dravet syndrome exhibit a *de novo* mutation in the sodium channel 1 α (*SCN1A*) gene.⁹ Lennox-Gastaut represents another form of treatment-resistant pediatric epilepsy which is characterized by multiple seizure types (tonic, atonic, and generalized tonic-clonic seizures) and impaired cognition. Approximately 75% of children with Lennox-Gastaut syndrome have a brain malformation, which is likely the underlying cause of the syndrome.¹⁰ It is worthy to note that six out of ten epileptic patients suffer from idiopathic epilepsy with no known pathology. Proper classification of epilepsy is decisive to understand the clinical course, prognosis, and treatment strategy.⁸

1 Introduction

1.2 Antiepileptic drugs and their targets

More than 20 antiepileptic drugs (AEDs) are available on the market including barbiturates, e.g. phenobarbital, phenytoin, ethosuximide, valproic acid, carbamazepine, and second generation AEDs such as felbamate, oxcarbazepine, lamotrigine, vigabatrin, gabapentin, pregabalin, tiagabine, topiramate, levetiracetam, and zonisamide (see Table 1).¹¹ Most of the AEDs exert their antiseizure effects by either decreasing excitatory or by increasing inhibitory neurotransmission. Their main molecular mechanisms of action comprise modulation of voltage-gated ion channels (Na^+ , Ca^{2+} and K^+), augmentation of γ -aminobutyric acid (GABA) or inhibition of glutamate neurotransmission.¹¹

Voltage-gated ion channels undergo conformational changes allowing ion flux in response to changes in membrane potential and thereby regulate the release of neurotransmitters. This common characteristic of voltage-gated sodium (Na^+), calcium (Ca^{2+}), and potassium (K^+) channels make them key molecular targets for the majority of AEDs.^{7, 12}

Voltage-gated sodium channels (Na^+ -channels) are crucial for the generation and propagation of action potential (AP) in neurons.¹³ Sodium channels exhibit three conformational states, resting (closed), conducting (open), and non-conducting (inactive) depending on the AP threshold. Upon depolarization of neurons Na^+ -channels transit from the resting to the conducting state allowing the influx of Na^+ ions into the neuron. The channels then enter immediately – within milliseconds – into a non-conducting state ceasing the ion influx. After hyperpolarization of the neuron, these channels return to their resting state and become responsive to new AP. The cycle of these three conformational states continue in response to high-frequency APs to ensure efficient neurotransmission.¹² AEDs such as phenytoin, lamotrigine, carbamazepine, oxcarbazepine, and valproic acid bind to Na^+ -channels in their non-conducting state and by stabilizing this state inhibit Na^+ currents (see Figure 1 & Table 1).³

The voltage-gated calcium channels are important targets for AEDs due to their involvement in neuronal excitability and neurotransmitter release. Based on their biophysical and pharmacological properties calcium channels in the brain can be classified into L-, N-, P/Q-, and T-type channels.¹⁴ L-, N-, and P/Q -type channels are high voltage-activated channels (HVA) opening at higher depolarization, while the T-type is a low voltage-activated (LVA)

1 Introduction

channel opening at lower depolarization. L-type channels are mainly found in postsynaptic neurons and allow sustained calcium entry after depolarization due to their slow inactivation characteristic.¹⁵ Carbamazepine has been proposed to bind to these L-type channels. P/Q-, and N-type channels are present at boutons of the presynaptic neurons. These are fast inactivating channels mediating the calcium entry required for neurotransmitter release. AEDs such as gabapentin and pregabalin inhibit calcium channels by binding to their $\alpha 2\gamma$ auxiliary subunit and significantly decrease the neurotransmitter release (see Figure 1 & Table 1).¹⁵ T-type channels are involved in the generation of physiological rhythms within the thalamus. AEDs like ethosuximide, zonisamide, and valproate are proposed to exert their antiepileptic effects via acting on T-type channels.¹⁵ Voltage-gated potassium channels are important for maintaining resting membrane potentials and for repolarization after AP. The AED retigabine or ezogabine (US adopted name) targets KCNQ2/3 potassium channels as a positive allosteric modulator and opens these channels (see Figure 1 & Table 1).¹⁶⁻¹⁷

γ -Aminobutyric acid (GABA) is the most important inhibitory neurotransmitter in the brain. GABA is released in the synaptic cleft, where it acts through fast chloride-permeable ionotropic GABA_A receptors and also through slow metabotropic GABA_B receptors to decrease neuronal excitability.¹² However, GABA_A receptors are more relevant as AED targets due to the complex role of GABA_B receptors in decreasing neuronal excitability both pre- and postsynaptically.¹⁵ Several AEDs like benzodiazepines (clonazepam), barbiturates (phenobarbital), and topiramate act as positive allosteric modulators at GABA_A receptors, consequently increasing receptor affinity for GABA and potentiating sustained chloride channel opening.¹² GABA is removed from the synaptic cleft by glial and neuronal cells through GABA transporters. Inhibition of GABA transporters for reuptake is also an antiepileptic mechanism for AEDs like tiagabine (see Figure 1 & Table 1).¹⁵ Glutamic acid decarboxylase (GAD) catalyzes the conversion of glutamate to GABA. GABA is then degraded by GABA transaminase (GABA-T) to succinic semialdehyde (SSA), which is further oxidized by SSA-dehydrogenase (SSA-D) to succinic acid. Succinic acid inhibits GAD in a negative-feedback mechanism inhibiting the conversion of glutamate to GABA. Some AEDs enhance the GABA concentration either by increasing the GAD activity or by inhibiting the GABA-T and SSA-D activity. Valproate presumably blocks GABA-T and SSA-D thereby exerting its antiepileptic effects (see Figure 1).³ Another AED vigabatrin exerts its

1 Introduction

anticonvulsive activity by selectively and irreversibly inhibiting the GABA-T to increase the GABA supply in the brain.¹⁸

Glutamate is the main excitatory neurotransmitter in the central nervous system.¹⁵ Glutamate receptors are subdivided into ionotropic and metabotropic receptors. Only ionotropic receptors, named after their ligands, *N*-methyl-*D*-aspartate (NMDA), α -amino-3-hydroxy-5-methyl-4-isoxazole propionic acid (AMPA), and kainic acid (KA), currently represent targets for AEDs. NMDA receptors are blocked by Mg^{2+} at resting potential. However, upon activation by glutamate in the presence of the co-agonist glycine, the channel becomes permeable to Ca^{2+} , Na^{+} , and K^{+} ions.^{3, 19} The anticonvulsive effects of the AED felbamate are in part attributed to its ability to inhibit NMDA receptors.²⁰ The recently approved AED perampanel for adjunctive therapy is the first selective and a non-competitive antagonist of AMPA receptors.²¹⁻²² The AED topiramate beside its other targets is reported to interact non-selectively with KA receptors which may also contribute to its anticonvulsive activity (see Figure 1 & Table 1).²³ It is worthy to mention that inhibition of these receptors may result in severe side effects like psychosis and neuropsychiatric disorders, e.g. memory impairment and cognitive decline.^{15, 24}

1 Introduction

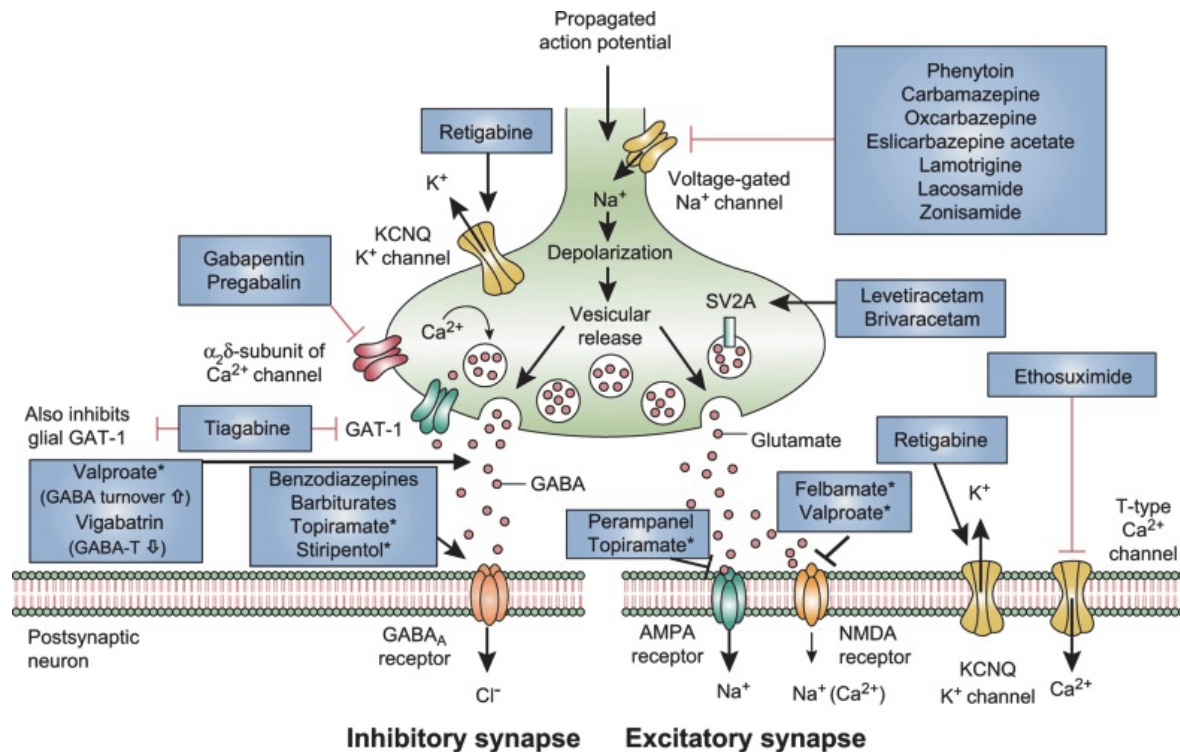


Figure 1: Schematic drawing indicating the mechanism(s) of action of clinically used antiepileptic drugs on inhibitory and excitatory synapses. Na⁺, Ca²⁺, and K⁺-channels, voltage-gated sodium-, calcium, and potassium channels; NMDA, N-methyl-D-aspartate receptors, AMPA, α -amino-3-hydroxy-5-methyl-4-isoxazole propionic acid receptors; GABA, γ -Aminobutyric acid, GAT-1, sodium and chloride dependent GABA transporter 1; GABA-T, GABA transaminase; KCNQ, family of voltage-gated potassium channels; *asterisk indicates drugs with more than one mechanism of action. Figure adapted from Löscher et al. (2016).²⁵

In addition to the aforementioned classical targets for AEDs, the ubiquitously expressed synaptic vesicle protein 2A (SV2A) in the brain represents a novel target for the broad spectrum AEDs levetiracetam (Keppra[®]) and its newly approved derivative brivaracetam (Briviact[®]) (see Figure 1). The SV2A has been discussed as an AED target in detail in section 1.3.1. Furthermore, growing evidence regarding the role of non-neuronal cells such as astrocytes in the spread of epilepsy and depression suggests connexin 43 gap junctions as potential targets for novel AEDs. These gap junctions are described in detail in section 1.3.2 and chapter 3.

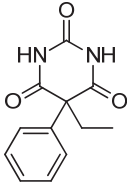
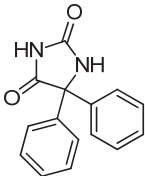
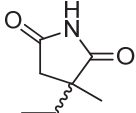
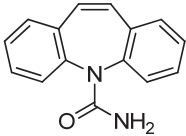
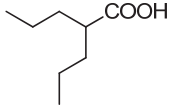
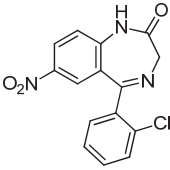
Approximately 70% of the epilepsy patients respond to initially provided pharmacological treatment. Of these, 50% of the patients get symptomatic relief from the first medication (monotherapy) and 20% need a second medication or polytherapy to respond. An alarmingly

1 Introduction

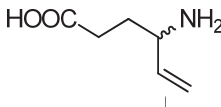
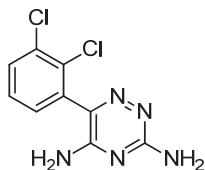
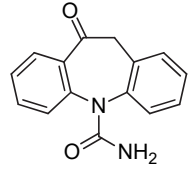
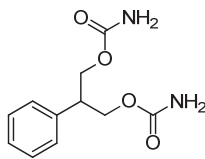
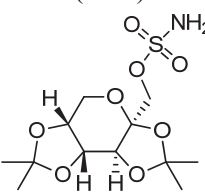
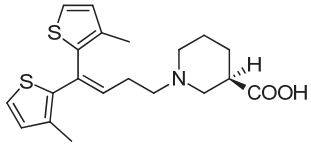
high number of epilepsy patients (30%) suffer from drug resistant epilepsies and do not even respond to polytherapy.²⁶⁻²⁷ Most of the AEDs have been discovered based on their antiepileptic efficacy in animal models of seizures, more or less by chance without prior knowledge of their mechanism of action. Once the antiseizure efficacy of a drug was confirmed, investigation started to reveal the potential mechanism of action.^{15,21} Levetiracetam is a good example of this scenario, where an AED was first approved for clinical use and later its binding site SV2A was identified and proposed as its main target. The currently available AEDs provide symptomatic relief from epilepsy but do not target the underlying cause.²⁸ Development of mechanism-driven AEDs should lead to highly selective, potent, and efficacious AEDs with less adverse effects. There is a significant unmet medical need for third generation AEDs, which are expected to show disease-modifying properties.²⁵

1 Introduction

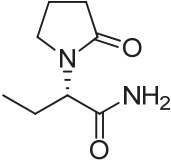
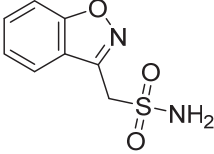
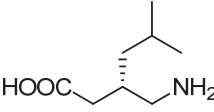
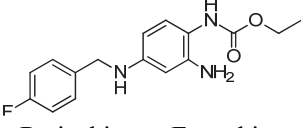
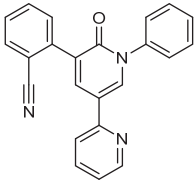
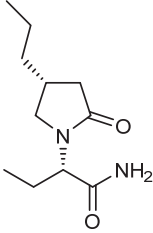
Table 1: Mechanism(s) of action of clinically used antiepileptic drugs ^{21, 29-38}

Antiepileptic drugs ¹⁾	Mechanism(s) of action	Therapeutic Plasma concentrations (μM)	Side-effects ²⁾
First generation drugs			
 Phenobarbital (1912)	GABA _A receptors (positive allosteric modulation)	43-172	↑↑↑ Somnolence Behavioral problems Cognitive issues
 Phenytoin (1938)	Na ⁺ -channel blockade	40-79	↑↑ Dizziness Encephalopathy Behavioral problems
 Ethosuximide (1958)	Ca ²⁺ -channel blockade	284-709	↑↑ GI problems Psychotic episodes Depression
 Carbamazepine (1964)	Na ⁺ -channel blockade	13-51	↑↑ Lukopenia Seizure exacerbation Cognition issues
 Valproic acid (1967)	Na ⁺ -channel blockade Ca ²⁺ -channel blockade GABA supply increase	347-694	↑↑↑ Thrombocytopenia Teratogenicity Retinal dysfunction
 Clonazepam (1968)	GABA _A receptor (positive allosteric modulation)	79-95	↑ Behavioral problems Dizziness

1 Introduction

Antiepileptic drugs ¹⁾	Mechanism(s) of action	Therapeutic Plasma concentrations (μM)	Side-effects ²⁾
Second generation drugs			
 Vigabatrin (1989)	Irreversible GABA-T inhibition	6.2-279	↑↑↑ Seizure exacerbation Encephalopathy Behavioral problems Psychotic episodes
 Lamotrigine (1990)	Na^+ -channel blockade Ca^{2+} -channel blockade	3.9-16	↑ Somnolence Dizziness
 Oxcarbazepine (1990)	Na^+ -channel blockade Ca^{2+} -channel blockade	29-79 (Monohydroxy metabolite)	↑ Dizziness GI problems
 Felbamate (1993)	NMDA receptor blockade Na^+ -channel blockade Ca^{2+} -channel blockade GABA modification	76-348	↑↑ Aplastic anemia Weight loss Hypersensitivity
 Gabapentin (1993)	Ca^{2+} -channel blockade ($\alpha_2\delta$ subunit)	≥ 12	↑ Somnolence Dizziness
 Topiramate (1995)	KA/AMPA receptor Na^+ -channel Ca^{2+} -channel GABA modification carboanhydrase inhibition	31	↑↑↑ Somnolence Dizziness Behavioral problems
 Tiagabine (prodrug) (1997)	GABA transporter GAT-1 inhibition	0.05-0.5	↑↑ Somnolence Dizziness Behavioral problems

1 Introduction

Antiepileptic drugs ¹⁾	Mechanism(s) of action	Therapeutic Plasma concentrations (μM)	Side-effects ²⁾
Second generation drugs			
 Levetiracetam (1999)	SV2A modulation Ca ²⁺ -channel blockade GABA _A receptor modulation	41-235	↑ Somnolence Dizziness
 Zonisamide (2000)	Na ⁺ -channel blockade Ca ²⁺ -channel blockade	94-141	↑ Somnolence Weight loss
 Pregabalin (2004)	Ca ²⁺ -channel blockade (α ₂ δ subunit)	12-31	↑ Weight gain Somnolence
 Retigabine or Ezogabine (2011)	K ⁺ -channel opener (KCNQ2/KCNQ3 subunits)	nd	↑ Retinal dysfunction
 Perampanel (2012)	AMPA receptor blockade	nd	- Behavioral problems
 Brivaracetam (2016)	SV2A modulation	10-16	↑ Somnolence Dizziness

↑, only one high risk early or late onset adverse event; ↑↑, two high risk early or late onset adverse events; ↑↑↑, three or more high risk early or late onset adverse events; -, one medium risk side-effect. n.d., not determined.

¹⁾Year of the drug approval or market entry in the USA or Europe.

1 Introduction

1.2.1 Levetiracetam (Keppra®) and Brivaracetam (Briviact®)

The majority of AEDs exhibits a large spectrum of side-effects. A considerable number of patients changes their medications due to severe side-effects such as psychotic episodes, anemia, leukopenia, osteoporosis etc., affecting their quality of life.³⁹ Another challenge is the epilepsy treatment in special groups of patients such as pregnant women, elderly patients, and patients with comorbidities.²¹ Thus, there is a continued need for better tolerated and more effective AEDs for good clinical care.⁴⁰ The approval of levetiracetam (Keppra®, LEV, (2S)-2-(2-oxopyrrolidin-1-yl)butanamide) by the Food and Drug Administration (FDA) and the European Medicines Agency (EMA) in 1999 as a novel AED extended the spectrum for epilepsy treatment in terms of efficacy and safety.⁴¹ Initially LEV was approved for adjunctive therapy and later on approved as first-line monotherapy for partial and generalized seizures.²¹ LEV is a relatively safe drug with a good pharmacokinetic profile in terms of absorption, binding to plasma protein, enzyme (cytochrome P450) induction, drug interactions and metabolism.⁴²

The exact mechanism of action of LEV is still not well understood, however it may modulate the release of neurotransmitters by binding to the synaptic vesicle 2A (SV2A) protein that is ubiquitously expressed in the brain.⁴³ LEV, unlike other AEDs, lacks anticonvulsant activity in any of the two conventional acute seizure tests, e.g. maximal electroshock (MES) and s.c. pentylenetetrazole (PTZ) induced seizures.^{42,44} However, LEV showed suppression of seizures in genetic animal models of partial and generalized epilepsy such as audiogenic seizure-susceptible and amygdala-kindled models, which are difficult to treat with other AEDs.⁴⁵⁻⁴⁶ Some evidence support the idea that LEV has additional mechanisms of action like inhibition of high-voltage gated (N-type) calcium channels and AMPA receptors, inhibition of intracellular calcium release, and reversal of the inhibitory effects of zinc on GABA_A receptors.⁴⁷ In addition, it was shown to modulate the function of connexin 43 (Cx43), the predominant gap junction (GJ) protein on astrocytes. LEV treatment fully restored the lipopolysaccharide-induced uncoupling of astrocytes *in vivo*.⁴⁸ Despite involving additional mechanisms, the correlation of SV2A affinities of LEV analogs with their anticonvulsive effects in various mouse and rat models suggests that SV2A is the principal target site of LEV for its anticonvulsant activity.^{43, 49-50}

1 Introduction

As over time several mechanisms of action for LEV were revealed, it was hypothesized that a more selective and high-affinity ligand for SV2A may result in a more potent AED with less side-effects. Based on this rationale UCB Pharma, Belgium, started a drug discovery campaign and consequently identified two highly potent SV2A ligands, brivaracetam (BRV) and seletracetam (SEL) (see Figure 2).⁴⁰ Both racetam compounds displayed antiseizure activity, however BRV was superior to SEL in inhibiting neuronal hyperexcitability in an *in vitro* model. Moreover, in contrast to SEL and LEV, BRV demonstrated seizure protection in the MES and s.c. PTZ seizure tests, although at higher concentrations.²⁵ Eventually, development of SEL was discontinued after Phase II clinical trials by UCB and development of BRV was continued.⁵¹

Brivaracetam (Briviact[®], BRV, (2*S*)-2-[(4*R*)-2-oxo-4-propylpyrrolidin-1-yl]butanamide) is a 4-propyl derivative of LEV and has been approved in February 2016 by the EMA and the FDA as an add-on AED to treat partial onset seizures.⁵²⁻⁵³ BRV selectively binds to SV2A and is almost 15-fold more potent than LEV.⁵⁴ Moreover, BRV shows complete seizure protection in partial, generalized, and drug resistant animal models.⁴⁰ Unlike LEV, BRV does not have a direct action on AMPA and GABA_A receptors, and HVA calcium channels, however it shows weak inhibition of NMDA receptor at therapeutically irrelevant concentrations.⁴⁰ In a small open-label study, switching of the treatment from LEV to BRV in patients showed reduction in LEV associated non-psychotic behavioral adverse events.⁵⁵ The different pharmacological efficacies of LEV and BRV can probably be explained based on their differential binding characteristics at SV2A. The positive allosteric modulator (UCB 1244283) increased the affinity of SV2A for [³H]BRV by 10-fold and to [³H]LEV by only 2-fold, while maximum binding capacity was increased by 1.3-fold for [³H]BRV compared to 2-fold for [³H]LEV.⁵⁶ Hence, to date BRV represents the first AED selectively binding to SV2A to exert its antiseizure effects.

Our group has developed LEV and BRV in radiolabeled form and established radioligand binding assays with both radioligands.⁵⁷⁻⁵⁸ [³H]LEV and [³H]BRV were expected to be useful tools for (i) identifying their exact binding site on the SV2A, (ii) to potentially identify additional targets that might contribute to the compounds' antiepileptic activity, and (iii) to find new compounds interacting with the SV2A by competition studies.

1 Introduction

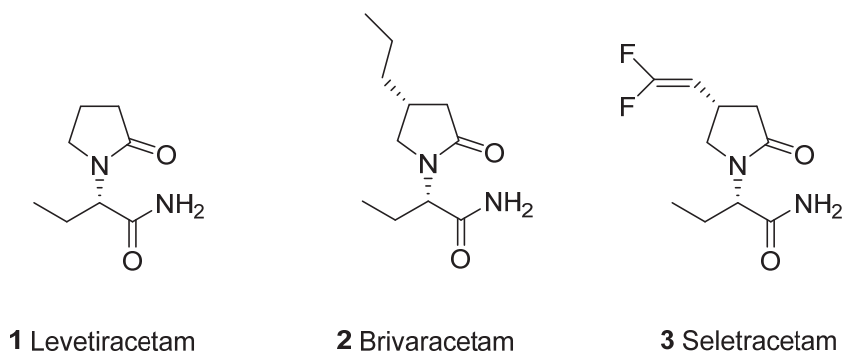


Figure 2: Chemical structures of the racetams levetiracetam, brivaracetam and seletracetam.

1.3 Newer antiepileptic drug targets

1.3.1 Biology of SV2A

The elucidation of SV2A as the binding site for LEV led to an increased interest in the synaptic vesicle 2 (SV2) proteins in the epilepsy treatment scenario.⁴³ To date three isoforms of synaptic vesicle protein 2 (SV2A, SV2B and SV2C) have been identified, which differ in size, sequence and distribution pattern in the brain.⁵⁹⁻⁶⁰ They are localized at the secretory vesicles of neurons and endocrine cells, with the highest prevalence in the brain.⁶¹ SV2A shows ubiquitous expression across the brain, while the expression of SV2B and SV2C is limited to certain brain regions.^{59, 62} SV2A shows 65% identity to SV2B and 62% identity to SV2C in the amino acid sequence.⁶³⁻⁶⁴

The human SV2A (ca. 90 kDa) is encoded by the *SV2A* gene located in the q-arm of chromosome 1 at locus 21.2.⁶⁴ SV2A is putatively a 12-transmembrane domain (TMD) protein and belongs to the major facilitator superfamily (MFS) comprising most of the membrane transporters, e.g. sugar, citrate and drug transporters in bacteria and glucose transporters in mammalian cells (see Figure 3).^{61, 64-65} Recently, the galactose transport function of SV2A has been demonstrated in *Saccharomyces cerevisiae*.⁶⁵ Loops between the TMDs of SV2A are relatively short compared to the intracellular cytoplasmic loop three (ICL3) between TMDs six and seven, and a long luminal loop four (L4) between TMDs seven and eight containing three *N*-glycosylation sites.⁶⁶ All three SV2 isoforms share a high degree of sequence homology within the 12-TMDs, whereas they are less conserved in ICL3 and least conserved in L4 and *N*-terminus.³⁸ SV2A exists in two major conformations demonstrated by protein

1 Introduction

tomography, one has a funnel-structure with an opening towards the cytosol and the other has a “V” shape broader opening towards the vesicular lumen.⁶⁷ These conformations suggest a high-flexibility and valve-like transporter function of SV2A. Interestingly, LEV does not seem to cause a significant change of either conformation of SV2A, since both conformations were represented in control (saline) and LEV treated samples.⁶⁷

The exact role of SV2A in synaptic vesicle (SV) function under normal and pathological conditions is not well understood.^{25,64} However, some important functions proposed for SV2A include calcium-dependent neurotransmitter release,⁶⁸ neurotransmitter immobilization within SVs,⁶⁹⁻⁷⁰ galactose transport,⁶⁵ function as an ATP-regulated protein,⁷¹ and a role in SV priming.⁷²

SV2A^(-/-) knockout mice appeared normal at birth, but developed severe seizures and died within 2-3 weeks.⁷³ Moreover, SV2A^(+/-) audiogenic mice demonstrated a proepileptic phenotype with reduced anticonvulsive activity and binding of LEV by 50%.⁷⁴ Furthermore, the established correlation of SV2A affinities of a series of LEV derivatives and analogs with their anticonvulsive effects in epilepsy models advocates for SV2A as a validated neuronal AED target.⁵⁰ LEV and BRV have been described to reduce the synaptic transmission and neurotransmitter release.⁷⁵⁻⁷⁷ However, the exact mechanism of action and downstream changes upon LEV and BRV binding to SV2A still remain elusive. In addition, LEV was shown to be efficacious in treatment-resistant animal models such as phenytoin-resistant kindled rats suggesting that SV2A may be a valuable target for novel AEDs to combat pharmacoresistant epilepsies.⁷⁸⁻⁷⁹ Growing evidence suggests that LEV may also have disease-modifying properties.²⁵

1 Introduction

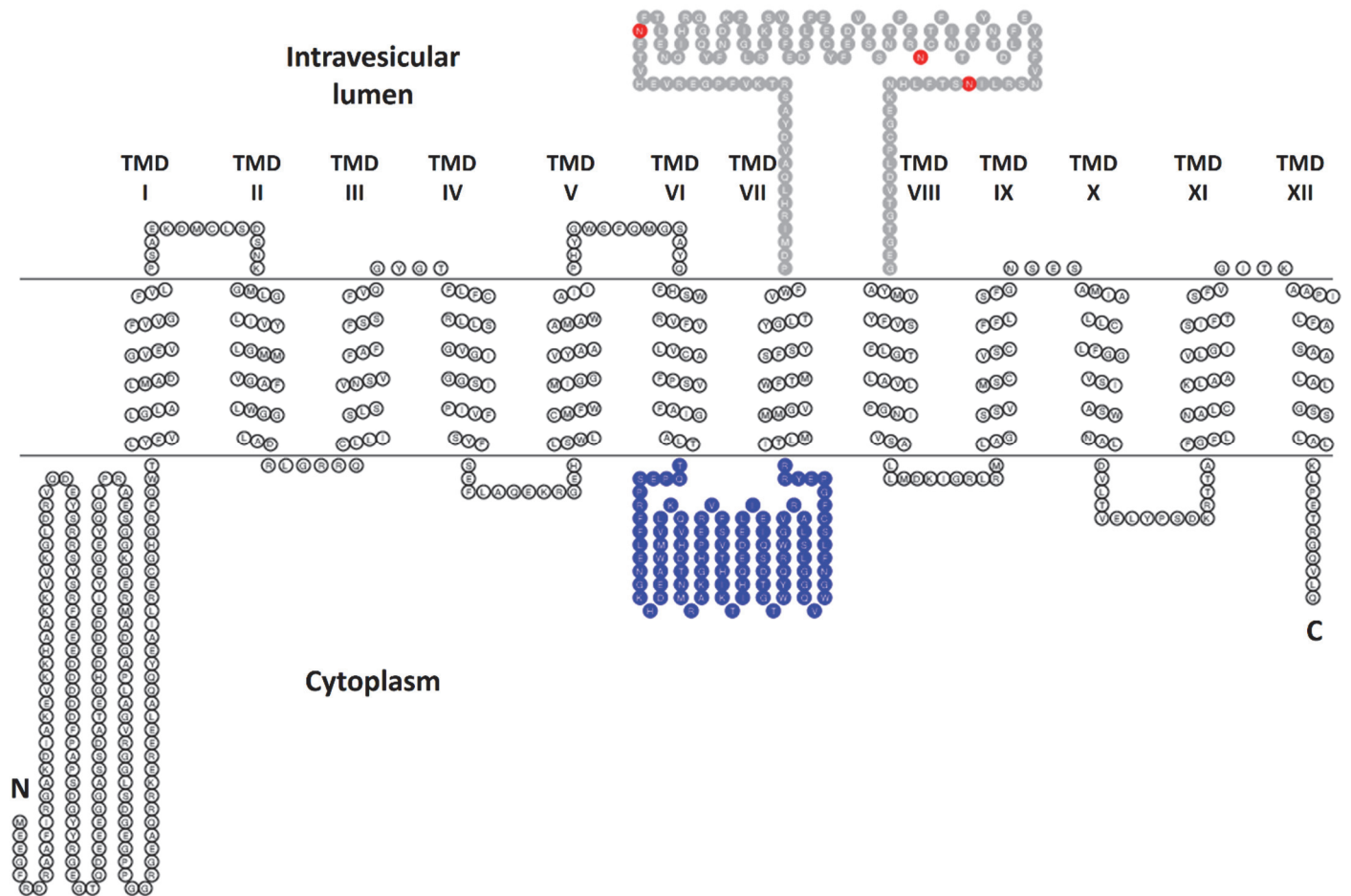


Figure 3: Topology model of the human SV2A. The snake plot diagram was prepared by using the TOPO2 program along with the transmembrane domain predictions using the HMMTOP software.⁸⁰⁻⁸¹ The 12-transmembrane domains (TMD) are indicated with Roman numbers. Amino acids depicted in dark blue color comprise the intracellular cytoplasmic loop 3 (ICL3). Amino acids presented in red color are the putative N-glycosylation sites. N, N-terminus; C, C-terminus.

1.3.2 Gap junction channels

Gap Junction (GJ) channels are important for cell-to-cell communication in almost all cells and tissues with some exceptions such as spermatocytes, erythrocytes, thrombocytes, skeletal muscles, and some neuronal subpopulations.⁸² GJs mediate the exchange of amino acids, second messengers, ions, glucose and its metabolites, and molecules < 1000 Da between the cytoplasm of connected cells.⁸³ Gap junctional intercellular communication (GJIC) regulates embryonic development, coordinated smooth and cardiac muscle contraction, tissue homeostasis, apoptosis, metabolic transport, cell growth and cell differentiation.⁸⁴ GJs are found in many different brain cell types but with the highest prevalence in glial cells, particularly in astrocytes. Astrocytes are involved in gliotransmission, extracellular neurotransmitter uptake, and metabolic processes, thereby contributing to neuronal transmission and plasticity.⁸⁵

Connexin (Cx) is a structural subunit of a GJ channel; 21 Cx subtypes have been identified in humans. Among all Cx types in humans, Cx43 is the most abundantly and widely expressed Cx with its presence in more than 34 tissues and 46 cell types.⁸⁶ Cx43 and Cx30 are the major astroglial Cxs, which are not found in the other brain cell populations.⁸⁵ Cx43 GJs are considered to be associated with several diseases, in particular brain disorders like epilepsy, depression, and brain metastasis.^{48, 85, 87} It has been recognized that astrocytic uncoupling occurs in patients with temporal lobe epilepsy, which leads to neuronal death and accelerated epileptogenesis. Most interestingly, LEV has been shown to restore the Cx43 GJ coupling in an animal model suggesting a novel therapeutic target to combat epilepsy.⁴⁸ Although the importance of Cx43 GJs as a promising therapeutic target is rising, the development of its modulators is still impeded by the lack of suitable high-throughput screening assays. A more detailed introduction on Cx43 GJs and available functional assays is given in chapter 3.

1 Introduction

1.4 Interaction of botulinum neurotoxins with SV2A

Botulinum neurotoxins (BoNTs) are the most potent known protein toxins produced by the bacterium *Clostridium botulinum*.⁸⁸ They cause flaccid paralysis by blocking neurotransmitter (acetylcholine) release from the presynaptic nerve terminals.⁸⁹ There are seven distinct serotypes of BoNTs (BoNT/A – BoNT/G).⁹⁰ BoNTs are produced as 150 kDa di-chain proteins containing a 50 kDa *N*-terminal catalytic light chain (LC) connected by a disulfide bond to a 100 kDa *C*-terminal heavy chain (HC). The HC is further organized into two functional domains, the *N*-terminal translocation domain (HCT) and the *C*-terminal receptor binding domain (HCR).⁸⁸ Enrichment of BoNTs at the nerve terminal takes place by binding to the non-protein polysialogangliosides which in turn facilitates the interaction of the toxin with its protein counterparts, the synaptic vesicle (SV) proteins. Dependent on the BoNT serotype, it binds either to SV2 proteins or to synaptotagmin at the presynaptic membrane.⁹¹⁻⁹² The HCR domains of BoNTs bind to the SV proteins and eventually the whole toxin gets internalized via the SV recycling pathway. Once inside the vesicle, owing to the acidification of the SV by the ATPase proton pump, HCT becomes active and translocates LC to the cytosol. LC is a Zn²⁺ metalloprotease domain which cleaves proteins of the SV release machinery and impairs neurotransmitter secretion.^{90, 93}

BoNT/A is one of the seven BoNTs serotypes with wide-spread applications ranging from serious clinical indications to cosmetic use. Three preparations of BoNT/A, namely onabotulinumtoxinA (Botox), abobotulinumtoxinA (Dysport), and incobotulinumtoxinA (Xeomin) have been approved by the FDA and EMA for different clinical indications such as strabismus, hemifacial spasm, and urinary tract disorders to cosmetic use.^{89, 94-95} The HCR of BoNT/A binds to the longest luminal loop four (L4) of SV2 homologous proteins (SV2A, SV2B and SV2C) for internalization into neuronal cells, and inhibits neurotransmitter release by cleaving the 25 kDa synaptosome-associated protein (SNAP-25).⁹⁶

1 Introduction

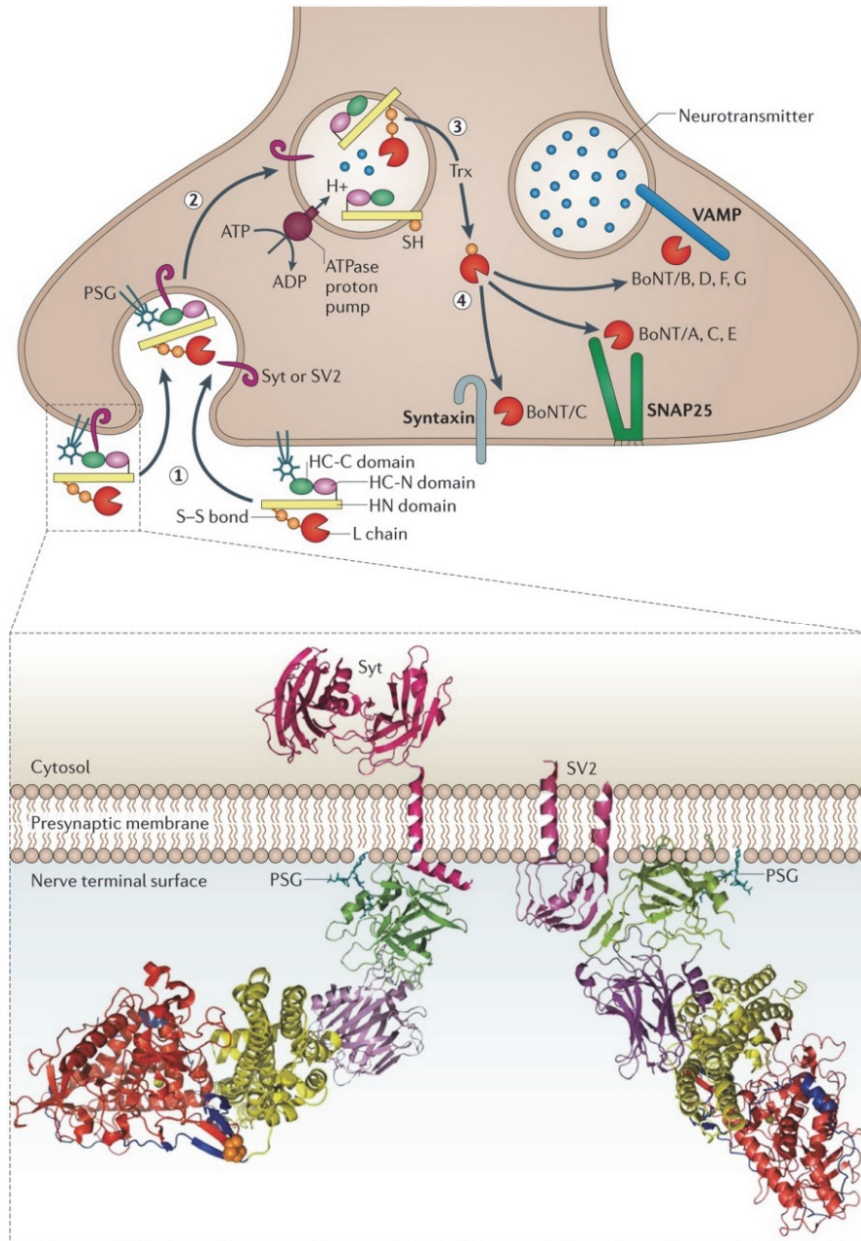


Figure 4: Mechanism of action of botulinum neurotoxin (BoNTs) serotypes. (1) The receptor binding heavy chain C-terminal domain (HC-C or HCR) of BoNTs initially binds to polysialoganglioside (PSG) for toxin enrichment at the nerve terminal. The BoNT serotype either binds to synaptotagmin (Syt) or to SV2 proteins located on the presynaptic nerve membrane. (2) The BoNT is then endocytosed via SV recycling. (3) Upon acidification of the vesicle via ATPase proton pump, the catalytic light chain (LC) is translocated into the cytosol and set free by the action of the thioredoxin reductase system (Trx) on the disulfide bond (S-S). (4) Eventually the LC (Zn²⁺-metalloprotease) of BoNTs cleaves the proteins of the vesicle release machinery (VAMP, SNAP25, and syntaxin) resulting in the inhibition of neurotransmitter release. VAMP, vesicle-associated membrane protein; SNAP25, synaptosomal-associated protein of 25 kDa (SNAP25). Adapted from Rossetto et al. (2014).⁹⁷

1.5 Objectives

1.5 Objectives

Levetiracetam (LEV) is a widely prescribed antiepileptic drug (AED) for the treatment of generalized and partial **epilepsy**. LEV unlike other AEDs exerts its anticonvulsive effects via a unique mechanism of action by modulating the synaptic vesicle protein 2A (SV2A).^{43, 50, 74} Considering the importance of SV2A as a novel AED target, a derivative of LEV **brivaracetam** (BRV), which is about 10-fold more potent and highly SV2A-selective has been developed. BRV was recently (2016) approved in Europe and the USA as an adjunctive therapy for the treatment of partial onset seizures. BRV has a better pharmacokinetic profile than LEV and is expected to be superior to LEV in terms of tolerability, onset of action, and antiepileptogenic potential. Nevertheless, the exact binding site of LEV/BRV within the SV2A is unknown and the underlying mechanism of action of these drugs is poorly understood.

Only few SV2A ligands have been reported so far, and most of the published compounds are directly related to LEV (pyrrolidones) or to known antiepileptic drugs. The SV2A project was designed:

- i) to screen compounds of different chemical classes for binding to SV2A and
- ii) to contribute to the identification of the binding site of LEV/BRV on SV2A.

Previously established binding assays using radiolabeled BRV – [³H]BRV – were performed with transiently transfected intact cells. This approach was not suitable for the screening of larger compound libraries in terms of costs and reproducibility. In order to be able to conduct the aforementioned studies, an **improved assay** using [³H]BRV binding to highly SV2A expressing preparations was to be established.

Another goal was to investigate the potential involvement of the **intracellular loop 3** (ICL3) of SV2A in the binding of LEV/BRV. To this end chimeric proteins in which the whole ICL3 of SV2A was exchanged for that of SV2B, and the reverse chimera in which the ICL3 of SV2B was replaced by that of SV2A, as well as a specific point mutant observed in a LEV-resistant patient were to be cloned and heterologously expressed. Botulinum neurotoxin A (**BoNT/A**) was reported to enter neurons via binding to the luminal loop 4 (**L4**) of **SV2** proteins.⁹⁶ Moreover, SV2A has recently been proposed to function as a **galactose** transporter.⁶⁵ One goal of the present project was to investigate whether BoNT/A- and monosaccharides can modulate [³H]BRV binding to SV2A.

1.5 Objectives

Astrocyte coupling occurs predominantly by connexin 43 (**Cx43**) gap junctions (GJ). Uncoupling of astrocytes was suggested to be involved in the etiology of mesial temporal lobe epilepsy (MTLE).⁴⁸ Interestingly, Cx43 GJ coupling was restored upon LEV treatment.^{48, 98-99} Whether LEV exerts these effects by directly binding to Cx43 GJs or by acting indirectly via some other mode of action remains elusive. The identification of molecules which can enhance GJ coupling may lead to the development of novel AEDs with disease-modifying properties. However, despite the potential of **Cx43 GJs** as novel AED targets, potent and selective ligands are not available most likely due to the difficulty in developing suitable **high-throughput screening** (HTS) assays. As a contribution to address the aforementioned issues we planned the following experiments:

- i) radioligand binding studies with [³H]BRV on Cx43 expressed in CHO cells;
- ii) establishment of a new HTS assay to screen for inhibitors as well as enhancers of the formation of GJs.

Fluorescence microscopy, flow cytometry, and fluorimetric measurements can be used to detect and quantify green fluorescent protein (**GFP**)-tagged membrane proteins. However, these methods have limitations including low sensitivity, inaccurate quantification, and high background due to autofluorescence. Most of the recombinant proteins implemented in the current study were to be GFP-tagged to monitor their expression. Therefore, an optimal method for the quantification of GFP-tagged membrane proteins was to be established using capillary gel electrophoresis with laser-induced fluorescence detector (**CGE-LIF**). This method should ideally be fast, robust, reproducible, and precise.

In summary, the current project was designed to investigate two promising new AED targets, SV2A and Cx43. Studies on SV2A focused on the identification of novel SV2A ligands and on understanding the interaction of LEV/BRV with the ICL3 of SV2A. Studies on Cx43 were aimed at developing a new HTS assay for the identification of Cx43 GJ modulators. Additionally a novel analytical method using CGE-LIF was developed to quantify the expression of GFP-tagged membrane proteins.

2 Characterization of SV2A and its ligands

2.1 Identification and characterization of new SV2A ligands

2.1.1 Interaction of approved drugs with SV2A

The AEDs levetiracetam (**1**, LEV, (2*S*)-2-(2-oxopyrrolidin-1-yl)butanamide) and its 4-propyl derivative brivaracetam (**2**, BRV, (2*S*)-2-[(4*R*)-2-oxo-4-propylpyrrolidin-1-yl]butanamide) (see Figure 5) have been reported to act via a unique mechanism of action – they interact with the synaptic vesicle protein 2A (SV2A).²⁵ Only few studies demonstrating new SV2A ligands have been reported so far, and most of the published compounds are directly related to LEV (pyrrolidones) such as piracetam and aniracetam or to known antiepileptic drugs like, pentobarbital, ethosuximide, and chlordiazepoxide (see Figure 5 and see Table 2).^{49-50, 54, 57-58, 100-103}

Interestingly, co-incubation of [³H]LEV with an allosteric modulator (UCB1244283) (see Figure 5) was shown to have only a minor effect on its SV2A affinity, however the maximum binding capacity of the radioligand was increased by 2-fold.¹⁰² Conversely, the same treatment on [³H]BRV resulted in a 10-fold increase in its affinity for SV2A but almost no effect on its maximum binding capacity.⁵⁶ These findings are evidence for different interactions of LEV and BRV with the SV2A and probably the explanation for their distinct pharmacological effects.⁵⁶ Similarly new ligands from diverse chemical classes may stabilize different SV2A conformations and open avenues for more effective novel AEDs.

Several radioligands including a PET (positron emission tomography) ligand for the labeling of SV2A have been developed.^{54, 100, 104-108} Recently, [³H]LEV and [³H]BRV with high specific activity (> 90 Ci/mmol) were obtained by our group; the radioligands were demonstrated to be useful for binding studies at rat and human brain membrane preparations.⁵⁷⁻⁵⁸ Since BRV is about 10-fold more potent than LEV (see Table 2), [³H]BRV has been selected in the present study to search for compounds that compete with its binding and to identify suitable lead structures for the development of novel antiepileptic drugs.

2 Characterization of SV2A and its ligands

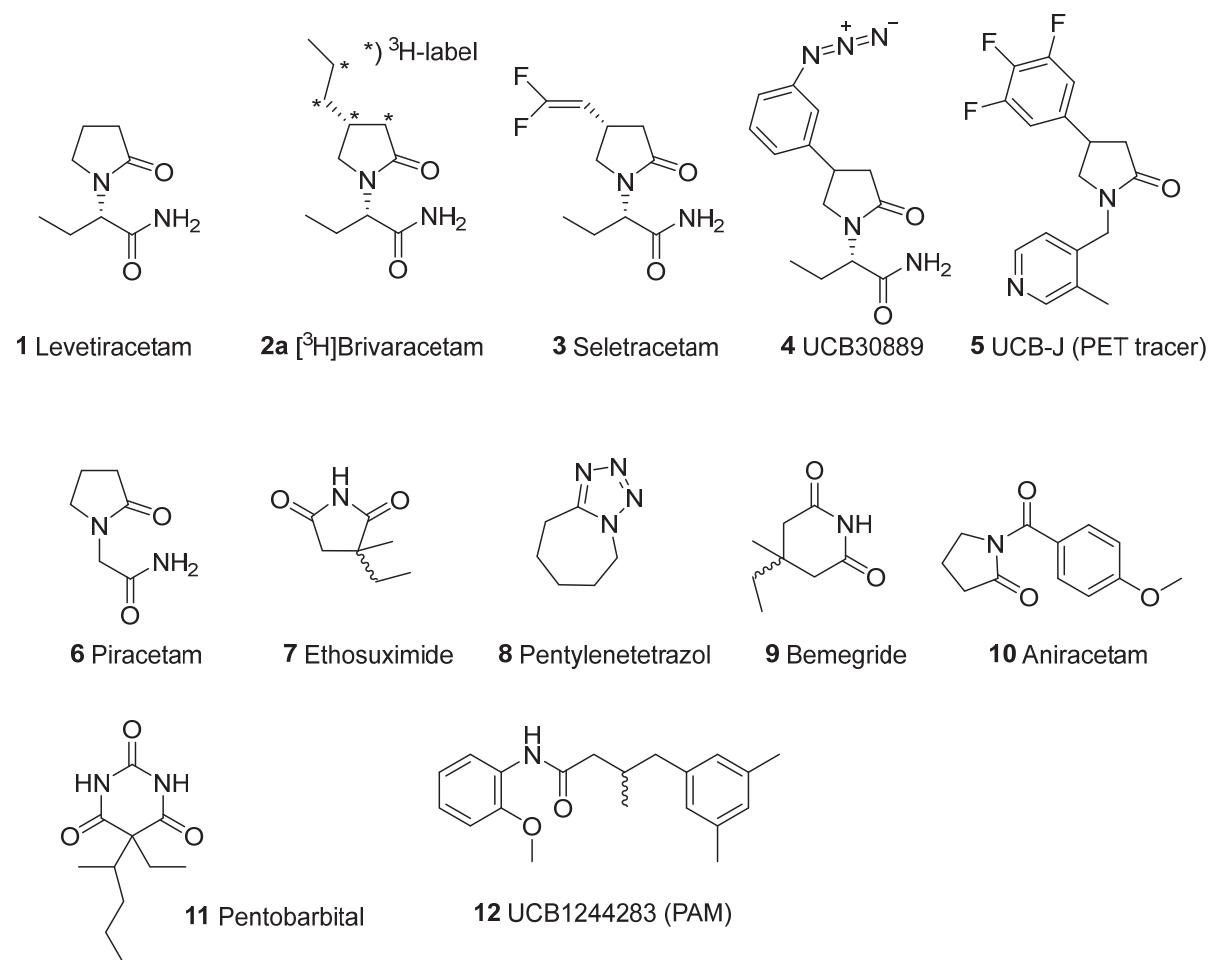


Figure 5: Chemical structures of SV2A ligands.^{49, 54, 57-58, 100-101, 103} PET, Positron emission tomography; PAM, positive allosteric modulator.

Approved drugs with well-established drug metabolism and pharmacokinetic and safety profile have been suggested as suitable starting points for the development of novel drugs. Already optimized physicochemical properties of a drug can accelerate the hit-to-lead as well as the lead optimization procedure.¹⁰⁹

In the present study, a radioligand competition binding assay was established, that is suitable for high-throughput screening, using [³H]BRV and crude cellular homogenates of monoclonal Chinese hamster ovary (CHO) cells stably overexpressing recombinant human SV2A. Subsequently a library of approved drugs was screened, a sublibrary of the Pharma-Zentrum Bonn compound library, to identify compounds that interact with SV2A.

2 Characterization of SV2A and its ligands

Table 2: Potencies of selected compounds at SV2A

Compound		K_i values [μ M]				
		vs. [3 H]UCB30889		vs. [3 H]LEV		vs. [3 H]BRV
		rat	rat	human	rat	human
1	LEV	1.25 ⁵⁶	1.26 ⁵⁶	3.16 ⁵⁶	1.71 ⁶⁰	2.05 ³⁹
2	BRV	0.079 ⁵⁶	n.d.	n.d.	0.079 ⁵⁶	0.126 ⁵⁶
3	Seletracetam	0.079 ¹⁰³	n.d.	n.d.	n.d.	-
4	UCB308889	0.079 ⁵⁶	0.100 ¹⁰³	n.d.	0.063 ⁵⁶	0.100 ⁵⁶
5	UCB-J	n.d.	n.d.	0.006 ^{105*}	n.d.	n.d.
6	Piracetam	n.d.	31.6 ⁵¹	n.d.	63.8 ³⁹	n.d.
7	Ethosuximide	n.d.	424 ³⁹	n.d.	312 ³⁹	n.d.
8	Pentylentetrazol	126 ⁵⁶	72.5 ³⁹	n.d.	116 ³⁹	n.d.
9	Bemegride	20.0 ⁵⁶	6.68 ³⁹	n.d.	11.9 ³⁹	n.d.
10	Aniracetam	n.d.	1000 ⁵¹	n.d.	> 1000 ³⁹	n.d.
11	Pentobarbital	158 ¹⁰²	158 ¹⁰²	n.d.	n.d.	n.d.

⁵⁴Gillard et al. 2011; ⁵⁸Hildenbrand et al. 2012; ³⁸Hildenbrand 2012; ⁴⁹Noyer et al. 1995; ¹⁰³Mercier et al. 2014; ¹⁰⁰Gillard et al. 2003; ¹⁰¹Matagne et al. 2009; rat, rat cortical membranes; human, recombinant human SV2A; *IC₅₀; n.d., not determined.

The results shown in the following section are included in this publication:

- Danish, A.; Namasivayam, V.; Schiedel, A. C.; Müller, C. E. Interaction of Approved Drugs with Synaptic Vesicle Protein 2A. *Arch. Pharm.* **2017**, DOI: 10.1002/ardp.201700003 (ahead of print).

2 Characterization of SV2A and its ligands

2.1.1.1 Plasmid design for SV2A expression

Previously low stable heterologous expression of a wild-type human SV2A-GFP construct (ca. 3.0 kbp) in CHO cells was reported using a retroviral transfection method.³⁸ The reason could be that the insert (pQCXIH-hSV2A-GFP) is close to the packaging limit of 9-12 kb for retroviruses.¹¹⁰ In this study, reliable expression was achieved by transient transfection with linearized plasmids obtained after restriction digest.³⁸ In order to improve the heterologous expression of hSV2A-GFP and to simplify the transfection procedure, a mammalian expression vector pcDNATM4/*myc*-His-A vector with a strong (cytomegalovirus) CMV promoter was selected.¹¹¹ For construction of the plasmid pcDNA4-hSV2A-GFP (see Figure 6), the cDNA of hSV2A-GFP was amplified from the mother plasmid by using a 5'-end forward primer with an overhang-containing HindIII restriction site and a 3'-end reverse primer with an overhang-containing XhoI restriction site (see Section 6.1.7 for primers). The amplified insert and the vector were digested with HindIII and XhoI restriction enzymes and ligated by following the procedure explained in Section 6.2.6.

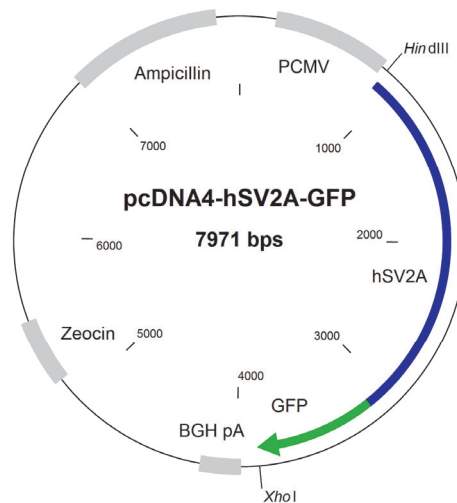


Figure 6: Plasmid map of the pcDNA4-hSV2A-GFP construct. The cDNA of wt hSV2A (blue) at its C-terminus tagged to GFP (green) was inserted into the vector using HindIII and XhoI restriction digest. Regions of the important functional elements such as cytomegalovirus promoter (PCMV), bovine growth hormone polyadenylation signal (BGH pA), zeocin, and ampicillin are indicated.

2 Characterization of SV2A and its ligands

2.1.1.2 Characterization of SV2A expression in CHO cells

CHO cells were chosen for recombinant expression of SV2A as previously described by Gillard et al. (2006).¹⁰⁴ Transient transfection of the human SV2A in CHO cells, similarly as described by Lynch et al. for COS-7 cells (2004), resulted in measurable binding of [³H]BRV to the intact transfected CHO cells.⁴³ However, for the screening of compound libraries, a stably transfected cell line was required to reduce costs and to ensure high reproducibility. Therefore, CHO cells were transfected by lipofection with human SV2A tagged at the C-terminus with green fluorescent protein (GFP) using the pcDNA4-hSV2A-GFP plasmid. GFP tagging allowed to select strongly fluorescent monoclonal cell lines by fluorescence-activated cell sorting (FACS) to ensure high and stable SV2A expression. Crude cellular homogenates were prepared from the monoclonal cell culture of early passages (P5-P8). Moreover, it was discovered that instead of intact cells cellular homogenates were better suitable for performing radioligand binding assays with [³H]BRV. The exact procedure for performing the radioligand binding assays is described in the next Section 6.7.1. To further characterize the heterologous expression of SV2A in the cell membranes, the latter were separated from the cell debris by centrifugation using the cellular homogenate as explained in Section 6.5.3. As shown in Figure 7A, the cellular homogenate displayed highest cpm values with [³H]BRV in radioligand binding assays. In contrast, the cell membranes and the cell debris resulted in lower specific binding of the radioligand (see Figure 7A). The cellular preparations demonstrated specific [³H]BRV binding according to the sequence: cell homogenate > membrane preparation > cell debris.

Furthermore, all three protein fractions were monitored for the GFP-mediated fluorescence signal by direct fluorimetric measurements (for procedure see Section 6.6.3). For this experiment, homogenate of non-transfected CHO cells was used as a negative control. While cellular homogenate produced the strongest fluorescence signal followed by moderate fluorescence signal with cell membranes, much weaker fluorescence signal was observed in cell debris. The strength of fluorescence signal from different protein fractions was obtained in the following order: cell homogenate > membrane preparation > cell debris. These findings are well in line with the results obtained from the radioligand binding assays (Figure 7A and 7B). The same protein samples were further used in Western blot to re-confirm the results.

2 Characterization of SV2A and its ligands

Western blots were performed using the mouse monoclonal anti-GFP primary antibodies and horseradish peroxidase (HRP) conjugated anti-mouse secondary antibodies (see Section 6.6.6). The expression profile of hSV2A-GFP in various protein fractions obtained from the Western blot method indicated the same sequence: cell homogenate > membrane preparation > cell debris, determined by the intensity of the bands (see Figure 7c). These results are well in agreement with the data obtained from the radioligand binding assays and fluorimetric measurements.

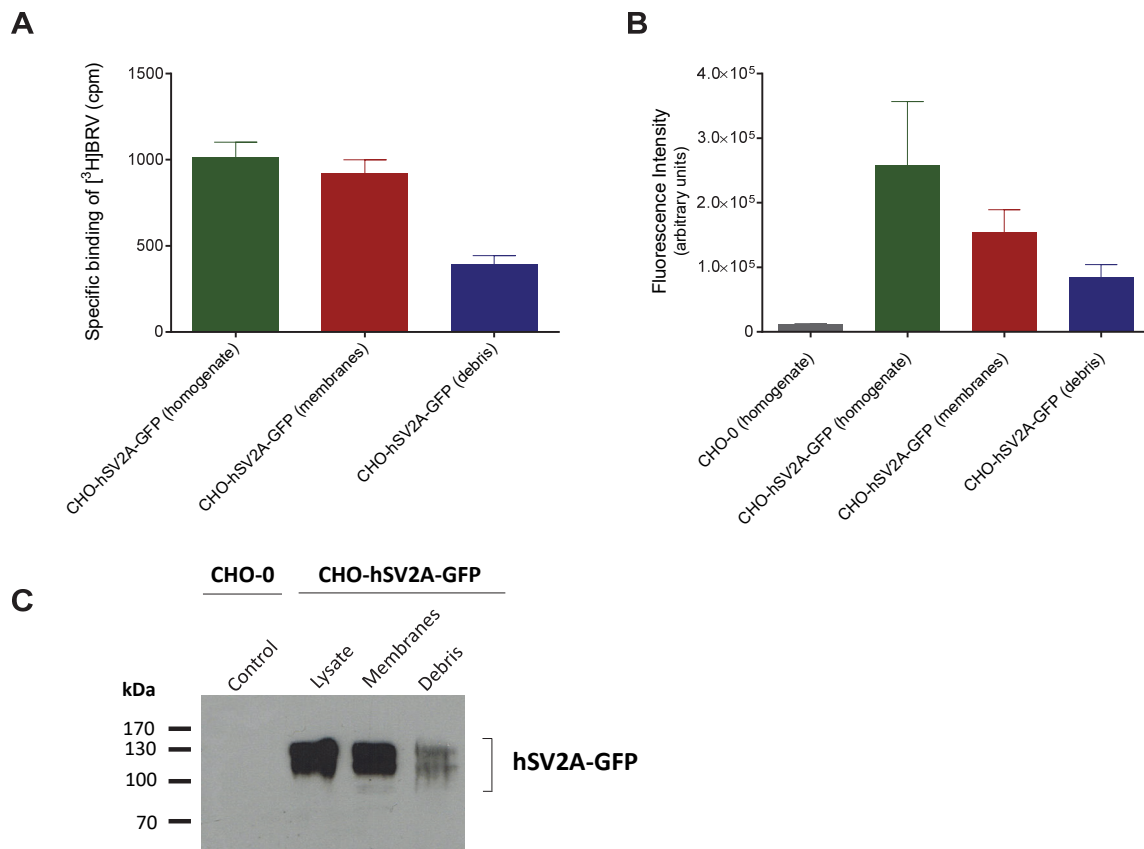


Figure 7: Characterization of recombinant human SV2A in CHO cells. **(A)** Radioligand binding assay with cell homogenate, membranes, and debris of CHO-hSV2A-GFP cells. Protein (200 μ g) was incubated with [³H]BRV (3 nM) for 240 min at 4°C. Non-specific binding was obtained in the presence of LEV (1 mM). **(B)** Direct fluorimetric measurements (excitation = 450/30 nm and emission = 510/12 nm) of protein samples with a fluorimeter. **(C)** Western blot analysis of the expression of hSV2A-GFP. Homogenate of non-transfected CHO-0 cells was used as a negative control and samples include homogenate of CHO-hSV2A-GFP, separated membranes and cellular debris separated from homogenate. An amount of 50 μ g protein sample was loaded on 10% SDS-gel. Primary mouse anti-GFP antibodies (1:3000) and secondary HRP conjugated anti-mouse antibodies (1:4500) were used for the detection of the protein. Data shown are means \pm SEM of at least three independent experiments performed in duplicate.

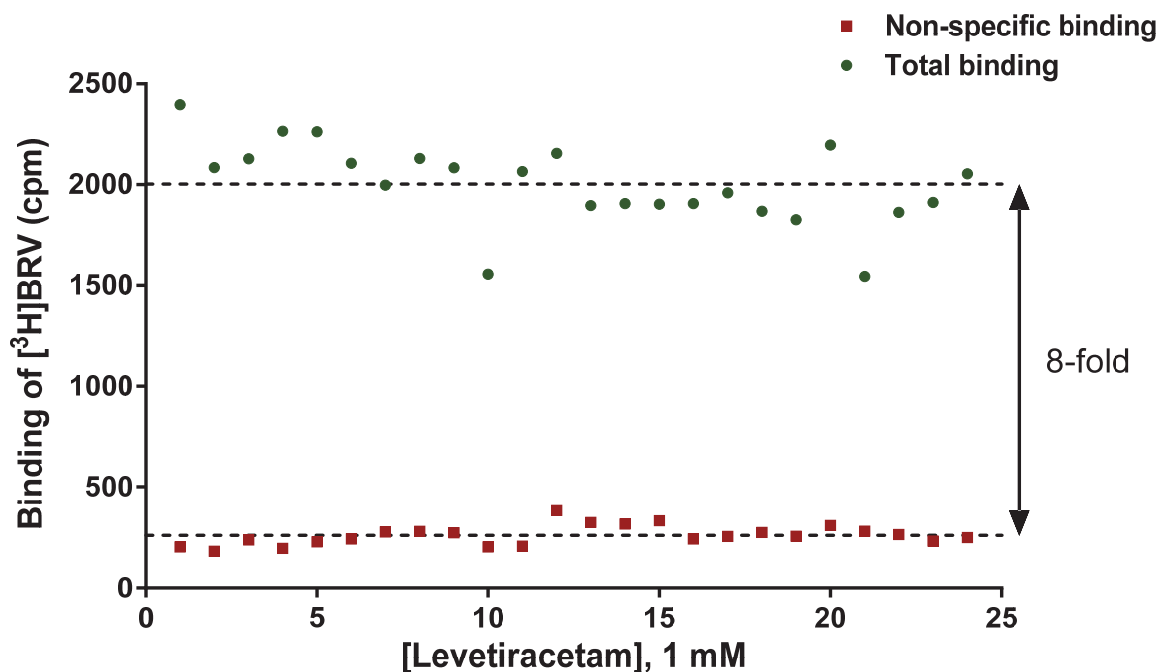
2 Characterization of SV2A and its ligands

Taken together the current data suggest that a fraction of the hSV2A is integrated into the cell membrane of the overexpressing CHO cells. Both, cell homogenate as well as membranes, can be used for [³H]BRV binding assays. However, cell homogenate can be more readily prepared without the requirement of ultracentrifugation as needed for membrane preparations, and they can be stored similarly as membranes at -80°C for long-term usage. Moreover, homogenates are more uniform than membrane suspensions and are therefore easier to handle and less prone to errors. Based on these results cellular homogenates were implemented for subsequent radioligand binding assays.

2.1.1.3 Establishment of a [³H]BRV binding assay for compound screening

Radioligand competition assays were performed by incubating [³H]BRV (3 nM), test compound and crude cellular homogenate of CHO cells expressing the human SV2A for 4 h. Non-specific binding of the radioligand was determined in the presence of a high concentration of LEV (1 mM) and amounted to approximately 10% of total binding (see Figure 8). The quality of the radioligand competition assay and its suitability for compound library screening was assessed by calculating the screening window co-efficient (*Z'*-factor), which is a dimensionless statistical characteristic for a screening assay.¹¹² The *Z'*-factor was calculated to be 0.6, which represents a suitable assay with a large separation window between negative and positive controls (see Figure 8). The current assay with some further adaptations should be suitable for high-throughput screening (HTS) of large compound libraries. The execution of HTS will include transfer of the current assay to a 96-well plate format with an automated assay performance. Scintillation proximity assay would be another approach to upgrade the current assay for HTS purpose.¹¹³

2 Characterization of SV2A and its ligands



$$Z' = 1 - \frac{(3\sigma_{c+} + 3\sigma_{c-})}{|\mu_{c+} - \mu_{c-}|}$$

$$Z' = 0.6$$

Figure 8: Assay quality for compound screening was evaluated by calculating the Z' -factor. Total binding was determined by incubating [^3H]BRV (3 nM) with cell homogenate (200 μg of protein) at 4°C for 240 min, and non-specific binding was determined in the presence of unlabeled LEV (1 mM). σ_{c+} , standard deviation of total binding; σ_{c-} , standard deviation of non-specific binding; μ_{c+} , mean of total binding (cpm); μ_{c-} , mean of non-specific binding (cpm).

The applicability of the assay was further verified by performing concentration-dependent specific [^3H]BRV inhibition by unlabeled LEV and BRV. As shown in Figure 9, LEV displayed a K_i value of 1.74 μM , which is in agreement with the previously reported K_i values of 3.16 μM ,⁵⁴ and 2.05 μM ,³⁸ respectively. Similarly, BRV displayed a K_i value of 0.098 μM , which very well relates to the previously reported K_i value of 0.126 μM .⁵⁴

2 Characterization of SV2A and its ligands

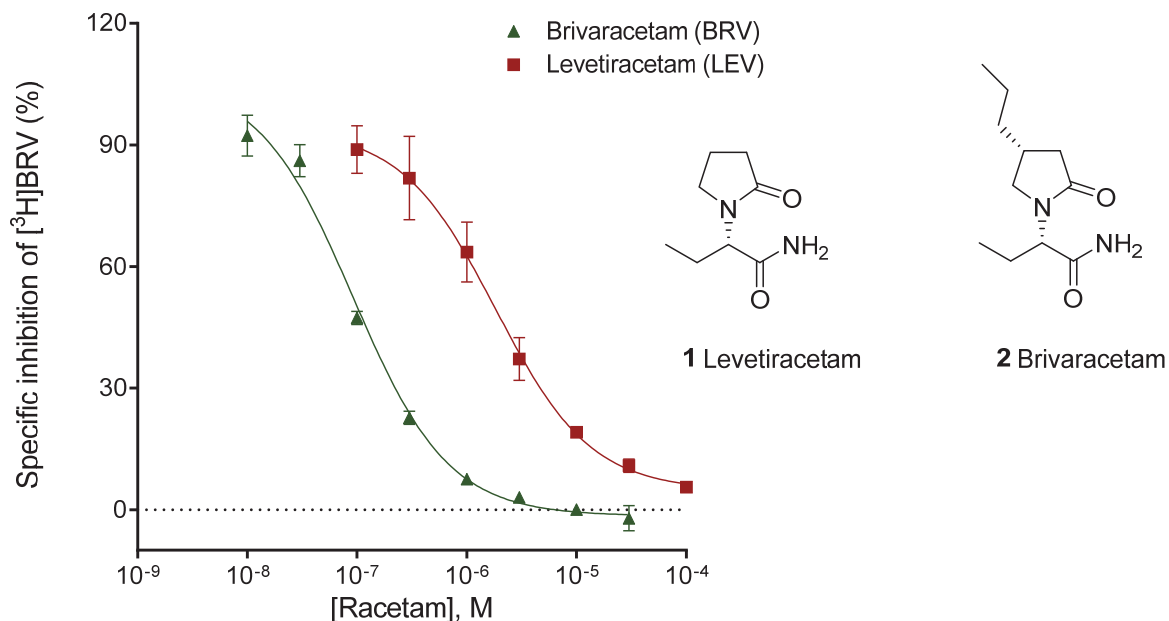


Figure 9: Competitive radioligand binding assays. Concentration-dependent inhibition of [³H]BRV binding to recombinant hSV2A by levetiracetam resulting in a K_i value of $1.74 \pm 0.27 \mu\text{M}$, and by brivaracetam, K_i value: $0.098 \pm 0.015 \mu\text{M}$. Increasing concentrations of unlabeled test compounds were incubated with cell homogenate (200 μg of protein) and [³H]BRV (3 nM) at 4°C for 240 min. Non-specific binding was determined in the presence of LEV (1 mM). Data points represent means \pm SEM of at least three independent experiments performed in duplicate.

2.1.1.4 Screening of an approved drugs library

Using the established assay an in-house collection of 500 approved drugs was screened for their ability to compete with [³H]BRV at the SV2A. An initial screening concentration of 20 μM was employed. Compounds that inhibited [³H]BRV binding by at least 90% were considered as hits. A hit rate of 3% (15 compounds) was obtained. These hits were further re-evaluated at a 10-fold lower concentration of 2 μM . Three compounds, loratadine (**13**), quinine (**18**), and rimonabant (**25a**), from which the first two are listed by the WHO as essential medicines (WHO list of essential medicines 2015),¹¹⁴ displayed > 50% inhibition of [³H]BRV binding at that low concentration (hit rate: 0.6%). Subsequently concentration-dependent inhibition curves were determined for all three drugs. The inhibition curve with rimonabant and preliminary structure-activity relationships (SARs) with other cannabinoids are presented in Section 2.1.2.

2 Characterization of SV2A and its ligands

2.1.1.5 Loratadine

A K_i value of 1.16 μM was determined for loratadine (**13**), which is in the same order of magnitude as the affinity of LEV for SV2A (K_i 1.74 μM) (see Figure 10). Loratadine is a potent histamine H_1 receptor antagonist prodrug and broadly used for its anti-allergic activity.¹¹⁵ It is a second generation non-sedative anti-histamine with a chemical structure related to tricyclic antidepressants.¹¹⁶⁻¹¹⁷ *In vivo*, loratadine, is hydrolyzed (see Figure 11) yielding the active metabolite desloratadine (K_i 0.9 nM).¹¹⁸ Peak therapeutic plasma concentrations of both loratadine and desloratadine were reported to be around 4 ng/mL (10 nM) in humans.¹¹⁹ Only minor amounts of loratadine are reported to cross the blood-brain barrier (BBB), and at a therapeutical dose of 10 mg/day the drug shows no sedative effects in humans.^{37, 116} The K_i value of loratadine for SV2A is 100-fold higher than the compound's therapeutic plasma concentration in humans. Moreover, it does not penetrate the blood-brain barrier in significant amounts, and to date no anticonvulsive activity has been reported for loratadine. Nevertheless, the structure of loratadine may be used as a starting point for the development of novel SV2A-interacting AEDs, e.g. by replacing the carbamate by a metabolically stable structure. This is expected to reduce interactions with histamine receptors, and to potentially increase the affinity for SV2A.

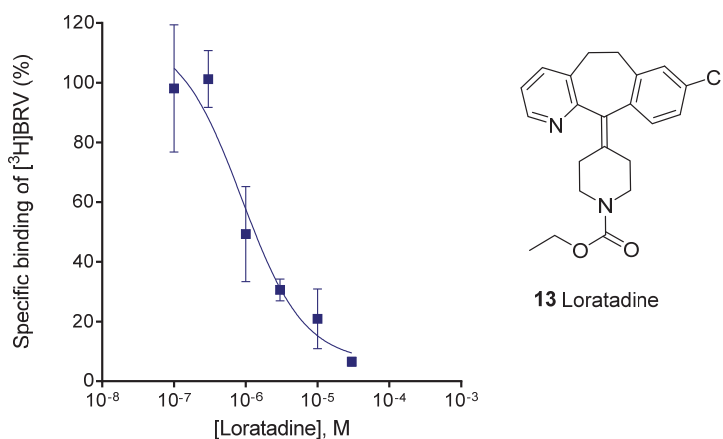


Figure 10: Competitive radioligand binding assay. Concentration-dependent inhibition of [³H]BRV binding to recombinant human SV2A by loratadine resulting in a K_i value of $1.16 \pm 0.44 \mu\text{M}$. Increasing concentrations of unlabeled test compounds were incubated with cellular homogenate (200 μg of protein) and [³H]BRV (3 nM) at 4°C for 240 min. Non-specific binding was determined in the presence of LEV (1 mM). Data points represent means \pm SEM of at least three independent experiments performed in duplicate.

2 Characterization of SV2A and its ligands

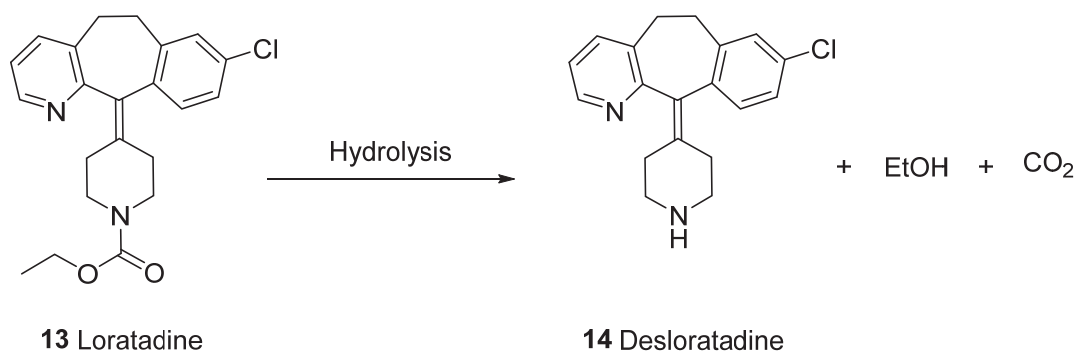


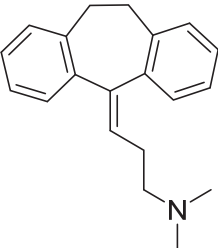
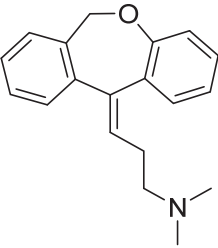
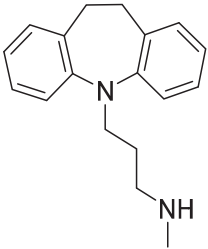
Figure 11: Hydrolysis of the prodrug loratadine releases the active metabolite desloratadine, a potent histamine H₁ receptor antagonist.

In contrast to loratadine, its metabolite desloratadine (**14**) showed very low affinity for SV2A inhibiting radioligand binding by only 25% at a high concentration of 20 μ M (see Table 3). This result indicates that the substituent on the piperidine ring (ethoxycarbonyl) is essential for SV2A binding (also see Section 2.1.1.8 on pharmacophore modeling below).

Additionally, several tricyclic antidepressants, structurally related to desloratadine, including amitriptyline (**15**), doxepine (**16**) and desipramine (**17**), were tested for their SV2A affinity. All of them displayed a low to moderate degree of specific interaction with SV2A and showed inhibition of radioligand binding according to the following order: doxepine (**60%**) > desipramine (**30%**) > amitriptyline (**5%**). The oxygen atom in the tricyclic ring system of doxepine appears to increase SV2A affinity (compare **15** and **16**). The current results indicate that the tricyclic drugs **14-17** only possess part of the pharmacophoric structure that is required for high SV2A affinity (see Table 3).

2 Characterization of SV2A and its ligands

Table 3: Affinities of loratadine, desloratadine and selected tricyclic drugs for human SV2A

Compound	Structure	Human SV2A
		$K_i \pm \text{SEM}$ (μM) or (% inhibition at 20 μM) vs. [^3H]BRV
Loratadine (13)	see Figure 11	1.16 ± 0.44
Desloratadine (14)	see Figure 11	(25%) ^{a)}
Amitriptyline (15)		(5%) ^{a)}
Doxepine (16)		(60%) ^{a)}
Desipramine (17)		(30%) ^{a)}

^{a)} inhibition (%) of [^3H]BRV binding by 20 μM of the test compound. Data represent means of three independent experiments performed in duplicate.

2 Characterization of SV2A and its ligands

2.1.1.6 Quinine

Quinine (**18**) is a natural product, which still plays an important role in the treatment of malaria.¹²⁰ Its mechanism of action is not completely understood, however it is widely accepted that quinine interferes with the hemoglobin breakdown process in parasites resulting in the accumulation of free heme which intoxicates and eventually kills the parasites.¹²¹ In the competitive radioligand binding assay, quinine displaced [³H]BRV from SV2A with a K_i value of 2.03 μ M (see Figure 12) and thus possesses the same affinity as the important antiepileptic drug LEV (K_i 1.74 μ M).

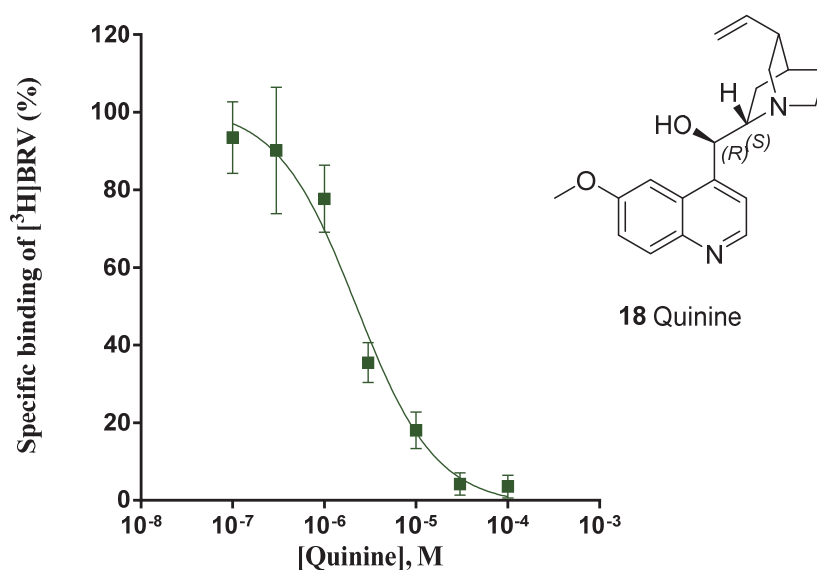


Figure 12: Competitive radioligand binding assay. Concentration-dependent inhibition of [³H]BRV binding at recombinant human SV2A by quinine resulted in a K_i value of 2.03 ± 0.31 μ M. Data points represent means \pm SEM of three independent experiments performed in duplicate.

Subsequently six compounds were tested that are structurally related to quinine, i.e. quinidine (**19**), cinchonine (**20**), cinchonidine (**21**), (\pm)-mefloquine (**22**), chloroquine (**23**), and primaquine (**24**), at a concentration of 20 μ M for their interaction with SV2A (see Table 4). Cinchonine and cinchonidine are diastereoisomers and differ from each other in the stereochemistry at positions C8 and C9 (see Table 4). While cinchonine exhibited relatively low inhibition of radioligand binding of 21% at 20 μ M, cinchonidine was more potent inhibiting radioligand by around 80%. Therefore we determined a full inhibition curve and

2 Characterization of SV2A and its ligands

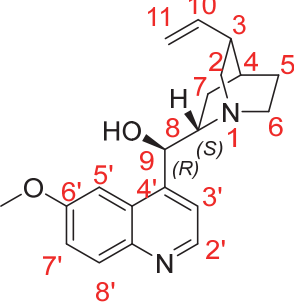
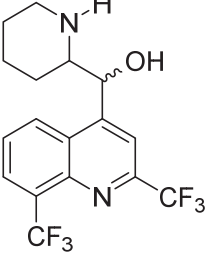
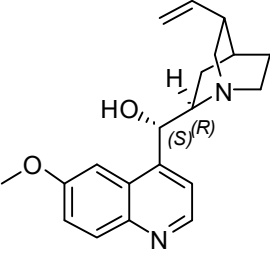
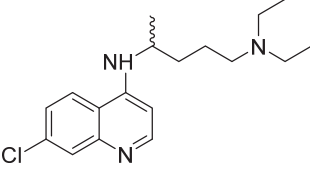
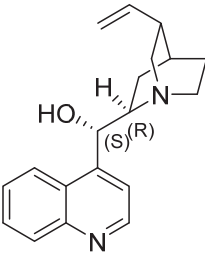
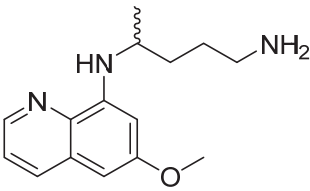
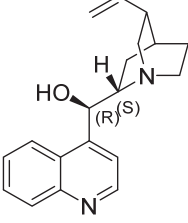
calculated a K_i value of 12.2 μM for cinchonidine. Cinchonine (**20**) at position C9 has a hydroxyl group with (*S*)-configuration, whereas cinchonidine (**21**) - similarly to quinine - is (*R*)-configured (see Table 4). This indicates that (*R*)-configuration of the OH group at position 9 improves the binding of cinchonidine to SV2A. Quinidine and quinine are diastereoisomers, again with different stereochemistry at C8 and C9, similar to cinchonine and cinchonidine, but with an additional 6'-methoxy substituent on the quinoline ring system. Quinidine in contrast to quinine displayed much lower affinity for SV2A with only 31% inhibition of radioligand binding, showing however slightly better affinity than cinchonine. The difference in the affinities of quinine and quinidine under the same assay conditions is due to stereoselective binding of SV2A. Interestingly, quinidine - like cinchonine - contains a hydroxyl group with (*S*)-configuration at position C9, but an additional methoxy group at position C6', and the latter appears to be responsible for a slight improvement in its affinity.

The synthetic anti-malaria drug mefloquine has a simplified structure as compared to quinine and related compounds. It showed inhibition of [^3H]BRV binding to SV2A by 48% at 20 μM . Mefloquine has two trifluoromethyl substituents at position C2' and C8' of the quinoline core structure, and at the position corresponding to C9 in quinine a hydroxyl group is present; mefloquine is a racemate and represents a mixture of the *R*- and *S*-enantiomers. Chloroquine is a 4-aminoquinoline derivative and primaquine is an 8-aminoquinolone derivative. Chloroquine inhibited radioligand binding by 23%, whereas primaquine showed no inhibition at 20 μM .

Altogether, these results suggest that (*R*)-configuration of the hydroxyl group at position C9 in quinine and related compounds has a strong impact on the compounds' affinity for SV2A and a 6'-methoxy residue further potentiates their affinity for SV2A. Hence, among all quinine-related compounds tested, quinine exhibited the highest affinity for SV2A with a low micromolar K_i value.

2 Characterization of SV2A and its ligands

Table 4: Affinities of quinine and related antimalarial drugs for hSV2A

Compound	Human SV2A	Compound	Human SV2A
	$K_i \pm \text{SEM}$ (μM) (% inhibition) vs. [^3H]BRV		$K_i \pm \text{SEM}$ (μM) (% inhibition) vs. [^3H]BRV
 <p>Quinine (18)</p>	2.03 ± 0.31	 <p>(<i>R,S</i>)-Mefloquine (22)</p>	(48%) ^{a)}
 <p>Quinidine (19)</p>	(31%) ^{a)}	 <p>(<i>R,S</i>)-Chloroquine (23)</p>	(23%) ^{a)}
 <p>Cinchonine (20)</p>	(21%) ^{a)}	 <p>(<i>R,S</i>)-Primaquine (24)</p>	(0%) ^{a)}
 <p>Cinchonidine (21)</p>	12.2 ± 4.4		

^{a)}inhibition (%) of [^3H]BRV binding by 20 μM of test compound. Data represent means of three independent experiments performed in duplicate.

2 Characterization of SV2A and its ligands

2.1.1.7 Anticonvulsive action of quinine

Severe malaria infections can be associated with acute seizures that may lead to neurological damage.¹²² Interestingly, anticonvulsant activity of quinine has been demonstrated in several animal models of epilepsy including 4-aminopyridine-, penicillin-, and pentylenetetrazole (PTZ)-induced epilepsy at concentrations of 35 μM , 1 μM (intracerebroventricular administration), or 185 μM , respectively.¹²³⁻¹²⁵ In these studies, the anticonvulsant properties of quinine had been attributed to its ability to prevent connexin 36 (Cx36) GJ-mediated neuronal communication; an IC_{50} value of 32 μM was determined for Cx36 inhibition.¹²⁶ In a recent study, quinine at high concentration (500 μM) was proconvulsive while paradoxically only lower doses (30 μM) resulted in anticonvulsive effects. This study questioned the involvement of Cx36 in quinine-mediated anticonvulsive effects and proposed the possibility of another, unknown target.¹²⁷ Studies on the anticonvulsive effects of quinine in humans are still limited,¹²² although seizures are frequently observed in children with cerebral malaria infections. The average therapeutic plasma concentration for quinine was reported to be 3.4 $\mu\text{g/ml}$ (10.5 μM),¹²⁸ which is 5-fold higher than its K_i value of 2.03 μM for the human SV2A. Data is scarce regarding quinine concentrations in brain, however the ratio of cerebrospinal fluid (CSF) to plasma was found to be 0.55 in patients infected with *Plasmodium*.¹²⁹ Thus, the anticonvulsive effects of quinine observed in animal studies and also seen in some clinical studies might be due to its interaction with the SV2A.

2 Characterization of SV2A and its ligands

2.1.1.8 Pharmacophore modeling

To establish a pharmacophore model for SV2A, the structural features of the newly identified SV2A-binding drugs were compared with those of the known SV2A ligands LEV and its propyl derivative BRV. BRV is about 10-fold more potent than LEV.⁵⁸ Figure 13A shows an overall alignment of BRV (orange), loratadine (magenta), and quinine (yellow) with the consensus pharmacophore model. Each drug is separately shown in Figure 13B with the consensus pharmacophore features. All three structures overlay very well with several features that are known to be important for high-affinity binding of the racetams:

- (i) two hydrogen bond acceptors: two carbonyl groups in brivaracetam, a pyridine N atom and a carbonyl group in loratadine, and a hydroxyl group and quinoline N atom in quinine (pharmacophore features F3 and F4 shown as cyan-colored spheres in Figure 13A-C);
- (ii) a lipophilic (cyclo)alkyl or an aromatic group: propyl in brivaracetam, chlorobenzene in loratadine, allyl-substituted cycloalkyl in quinine (pharmacophore feature F2 shown as orange-colored large sphere in Figure 13A-C);
- (iii) a short alkyl or alkoxy group: ethyl in brivaracetam, ethoxy in loratadine, methoxy in quinine (pharmacophore feature F1 shown as orange-colored small sphere in Figure 13A-C).

The steric and electronic fit of the three structures is excellent and in agreement with known structure-activity relationships (SARs). The additional amide-NH₂ group in BRV, which is about 10-fold more potent than the other compounds, might improve its SV2A binding in comparison to loratadine and quinine. The created pharmacophore model may allow the transfer of SARs from the known SV2A modulators LEV and BRV to the newly identified scaffolds.

2 Characterization of SV2A and its ligands

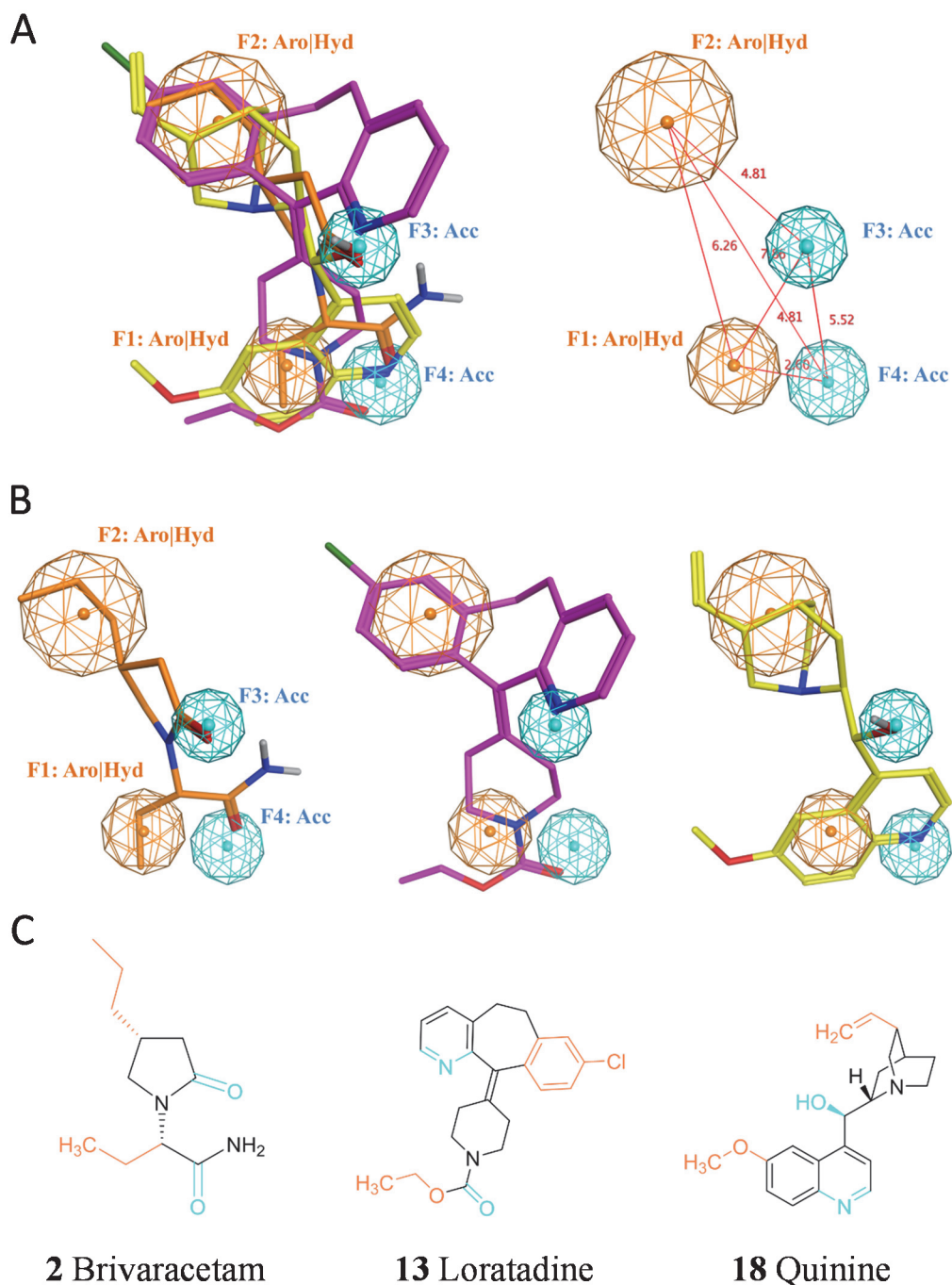


Figure 13. (A) The overall alignment of the selected drugs brivaracetam (orange), loratadine (magenta) and quinine (yellow) with the four pharmacophore features (F1 and F2: Aromatic/Hydrophobic, F3 and F4: Acceptor) and on the right side the distances between the pharmacophore features are shown in Å as red lines. (B) Each individual drug is shown with the four identified pharmacophore features (F1-F4). Oxygen atoms are colored in red, nitrogen atoms in blue, chlorine atoms in green, hydrogen atoms in silver white and non-polar hydrogen atoms are omitted. (C) Pharmacophore features are indicated in 2D representation of the selected drugs brivaracetam, loratadine and quinine (cyan = hydrogen bond acceptor atoms, orange = aromatic/hydrophobic). Molecular modeling was performed by Dr. Vigneshwaran Namasivayam.

2 Characterization of SV2A and its ligands

2.1.2 Interaction of cannabinoids with SV2A

In ancient times cannabis was used for different therapeutic applications including seizure management. However, it was scientifically evaluated and documented only in the early 19th century.^{130 131-132} Cannabinoid receptor (CB₁R and CB₂R) ligands can be subdivided into three major classes: i) endocannabinoids, ii) phytocannabinoids, and iii) synthetic cannabinoids.¹³³

Endocannabinoids refer to the lipids produced within the brain that interact with CB receptors. Two major endocannabinoids are *N*-arachidonylethanolamide (anandamide) and 2-arachidonylglycerol (2-AG). They are synthesized from postsynaptic membrane phospholipid precursors and after release interact with presynaptic neurons. Upon binding of anandamide and 2-AG to CB₁ receptors, a signaling cascade is triggered resulting in reduced presynaptic neurotransmitter release.¹³⁴ The complexity of endocannabinoid-mediated signaling is due to the involvement of several targets such as the transient receptor potential vanilloid receptor type 1 (TRPV1), the voltage-gated potassium channels (K_v7), the orphan G protein-coupled receptor (GPR55) and the orphan GPR18.¹³⁵⁻¹³⁸

In recent years there has been an increased research interest in exploring the therapeutic potential of cannabis in the treatment of seizures. The two major constituents (cannabinoids) of the cannabis plant which have gained most attention are the primary psychoactive component Δ^9 -Tetrahydrocannabinol (THC) and the non-psychoactive component cannabidiol (CBD).¹³⁰ CBD was demonstrated to exhibit potential in managing intractable epilepsy, however its mode(s) of action in ameliorating epilepsy appears to be complex and may involve several targets, however it is not yet fully understood.¹³⁹ Two CBD-enriched preparations Epidiolex[®] (98% CBD, 2% THC) and realm oil (94% CBD, 6% THC) made their way to clinical trials against Dravet and Lennox-Gastaut syndromes (for definition see Section 1.1) of intractable epilepsy in children.¹³⁰ An open-label trial with Epidiolex[®] reported a significant reduction of seizure frequency in treatment-resistant epilepsy (TRE) patients. Oral Epidiolex[®] administration at a maximum dose of 25-50 mg/kg/day (80-160 μ M) for 12 weeks significantly reduced seizure frequency in TRE patients and Dravet syndrome (DS) patients.¹⁴⁰ Quite recently Epidiolex[®] received orphan drug designation from EMA and FDA for the treatment of childhood-onset epilepsy syndromes, Lennox-Gastaut syndrome (LGS) and Dravet syndrome.¹⁴¹

2 Characterization of SV2A and its ligands

Several studies have demonstrated that the activation of cannabinoid receptors, particularly CB₁R due to its predominance in the brain, led to anticonvulsive effects, and blockade of these receptors exerted proconvulsive effects.¹⁴²⁻¹⁴³ Rimonabant (**25a**, SR141716A, Acomplia[®], see Figure 14), a potent CB₁R antagonist and a proconvulsive compound was paradoxically found to have antiepileptogenic effects. Intriguingly, a single-time administration of rimonabant (2.16 μM) after a short interval of traumatic brain injury (TBI) in rats abolished the long-term seizure susceptibility.¹⁴⁴ However, how the post-traumatic application of the proconvulsive drug rimonabant is translated into long-term antiepileptogenic effects remains to be clarified.

The current study demonstrates the interaction of rimonabant with SV2A using radioligand binding with [³H]BRV. Moreover, within the scope of this study 80 cannabinoid-like compounds were tested for interaction with recombinant human SV2A versus [³H]BRV inhibition. This study identifies for the first time cannabinoids which compete with [³H]BRV for SV2A with K_i values in the low micomolar range.

The results shown in the next section are included in the manuscript (in preparation):

- Danish, A.; Namasivayam, V.; Müller, C. E. Cannabidiol (CBD) interacts with the levetiracetam binding site of synaptic vesicle protein SV2A.

2 Characterization of SV2A and its ligands

2.1.2.1 Rimonabant

Rimonabant (**25a**, SR141716A, Acomplia[®], see Figure 14) is a potent synthetic CB₁R antagonist with a K_i value of 1.98 nM (see Table 6). It was approved in 2006 as an antiobesity drug and for smoking cessation. However, due to severe side-effects like depression and emergence of suicidal tendencies, the drug was withdrawn from the market in 2007.^{134, 145} In our screening campaign of approved drugs at SV2A, rimonabant was identified to compete with [³H]BRV for binding to SV2A. As shown in Figure 14, concentration-dependent specific [³H]BRV inhibition by rimonabant resulted in a K_i value of 2.73 μM, which is similar to the K_i value of LEV (1.74 μM). The cannabinoid-like compounds AM-251 (**25b**) and AM-281 (**25c**) (see Table 5 for structures) are close structural derivatives of rimonabant and potent CB₁R antagonists with K_i values of 7.94 nM and 12.6 nM, respectively (see Table 6).¹⁴⁶⁻¹⁴⁷ Similar to rimonabant, AM-251 competed with [³H]BRV for SV2A in the radioligand binding assay resulting in a K_i value of 2.75 μM (see Table 5). In contrast AM-281 displayed low affinity with a K_i value of 40.4 μM (see Table 5). The K_i values of both analogs rimonabant and AM-251 are almost identical. However, replacement of the piperidine in rimonabant and AM-251 for morpholine in AM-281 appears to drastically decrease its affinity for SV2A, whereas substitution of 4-chlorophenyl in rimonabant for 4-iodophenyl in AM-251 are equipotent (see Table 5).

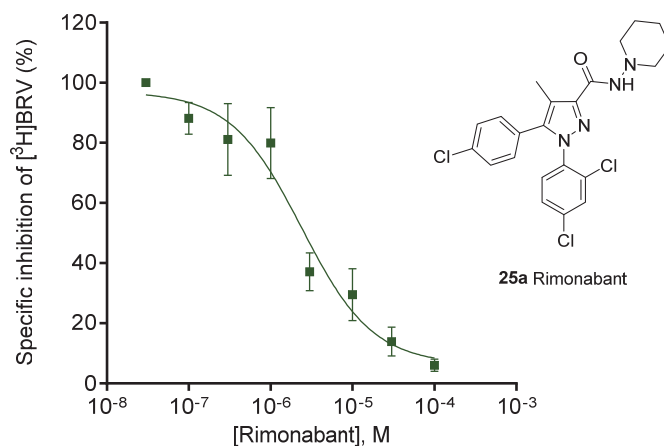


Figure 14: Concentration-dependent specific inhibition of [³H]BRV binding to recombinant SV2A by unlabeled rimonabant resulted in a K_i value of 2.73 ± 0.78 μM. For performing the competition experiments, cellular homogenate of CHO-hSV2A-GFP cells (200 μg of protein) was incubated at 4°C for 240 min with [³H]BRV (3 nM) and increasing concentrations of test compound. Data points show means ± SEM of three independent experiments performed in duplicate.

2 Characterization of SV2A and its ligands

2.1.2.2 Indole and pyrrole derivatives

AM-2232 (**26a**, for structure see Figure 15) is an indole derivative, which acts as a highly potent agonist at CB₁ and CB₂ receptors with K_i values of 0.28 nM and 1.48 nM, respectively (see Table 6).¹⁴⁸ In the present study, AM-2232, which contains a 2-naphthyl carbonyl residue at position C3 and a 4-cyanobutyl residue at position N1 of indole, was identified as a relatively strong displacer of [³H]BRV at SV2A with a K_i value of 0.401 μM (see Table 5). Subsequently, a series of selected indoles such as STS-135 (**26b**), AM-679 (**26c**), JWH-234 (**26d**), JWH-175 (**26e**), AM-630 (**26f**), JWH-016 (**26g**) and WIN55, 212-2 (**26i**) were also profiled for their SV2A affinity (see Table 5 for structures). However, they were all weaker than AM-2232.

The compound STS-135 (**26b**) inhibited [³H]BRV binding by 79% at a high concentration of 10 μM, which suggests that the substitution with an adamantylamino residue connected via a carbonyl amide linkage at position C3 and a 5-fluoropentyl residue at position N1 of indole are tolerable for SV2A interaction (see Table 5). AM-679 (**26c**) with a 2-iodophenyl carbonyl residue at position C3 and a pentyl residue at position N1 of indole showed similar affinity as AM-2232 for SV2A with a K_i value of 8.43 μM. Comparison of AM-679 (**26c**) with JWH-234 (**26d**) indicates that the replacement of the 2-iodophenyl moiety with a 7-ethyl-1-naphthyl residue abolished affinity for SV2A (9% inhibition at 2 μM). JWH-016 (**26g**) with a butyl residue at position N1 and a 1-naphthylcarbonyl residue at position C3 of indole displayed a K_i value of 4.88 μM. On the other hand, substituting butyl for pentyl and carbonyl for a methylene residue in compound JWH-175 (**26e**) resulted in inhibition of the radioligand by only 33% at 10 μM. Furthermore, AM-630 (**26f**) with a relatively bulky morpholinoethyl residue at N1 and a 4-methoxyphenyl moiety connected via a carbonyl linkage at position C3 of indole resulted in a K_i of 19.9 μM. More detailed structure-relationship studies are warranted to elucidate a pharmacophore model.

WIN55, 212-2 (**26i**, see Table 5 for structure) is a potent agonist of the CB₂ receptor with a K_i value of 3.30 nM and a K_i value of 62.3 nM at CB₁ receptor (see Table 6).¹⁴⁹ WIN55, 212-2 (**26i**) was found to compete with [³H]BRV for SV2A binding and displayed a K_i value of 4.15 μM (see Table 5). According to a recent report, co-administration of WIN55, 212-2 (11.7 μM) in a 6 Hz seizure mouse model significantly enhanced the anticonvulsive effects of the AEDs LEV (42.9 μM) and gabapentin (249 μM).¹⁵⁰ Comparing the *in vivo* effective dosage (11.7

2 Characterization of SV2A and its ligands

μM) of WIN55, 212-2 and the herein determined K_i value of $4.15 \mu\text{M}$ at SV2A are in the same order of magnitude. In view of that, WIN55, 212-2 (**26i**) might potentially contribute to the enhancement of LEV-mediated anticonvulsive effects via acting on SV2A. Nonetheless, data is scarce on this topic and further studies are warranted to elucidate the downstream effects upon interaction of cannabinoids with SV2A.

Among the pyrrole-derived cannabinoid-like compounds listed in Table 5, JWH-031 (**27a**, see Figure 15 for structure) was found to displace [^3H]BRV with a K_i value of $0.618 \mu\text{M}$. JWH-031 shows similar affinity for CB_1R (K_i 399 nM) where it acts as an agonist (see Table 6).¹⁵¹ The related pyrroles JWH-368 (**27b**) and JWH-309 (**27c**) that bear rather bulky substituents at position C2 of pyrrole ring displayed much lower affinities for SV2A (see Table 5 for structures). JWH-368 (**27b**) inhibited [^3H]BRV binding to SV2A by 28% at $2 \mu\text{M}$ and JWH-309 (**27c**) by only 20% at $10 \mu\text{M}$ (see Table 5). Based on the compound structures and their affinities for SV2A, a pyrrole residue at position C4 connected to a 2-naphthyl residue via a carbonyl linkage and a long hydrophobic substituent at N1 of pyrrole are favorable for interaction with SV2A. Introducing a bulky substituent like 3-fluorobenzyl or 1-naphthyl at pyrrole reduces SV2A affinity, whereas a hexyl substituent at N1 of pyrrole in terms of SV2A affinity has a clear advantage over a pentyl substituent (see Table 5).

2 Characterization of SV2A and its ligands

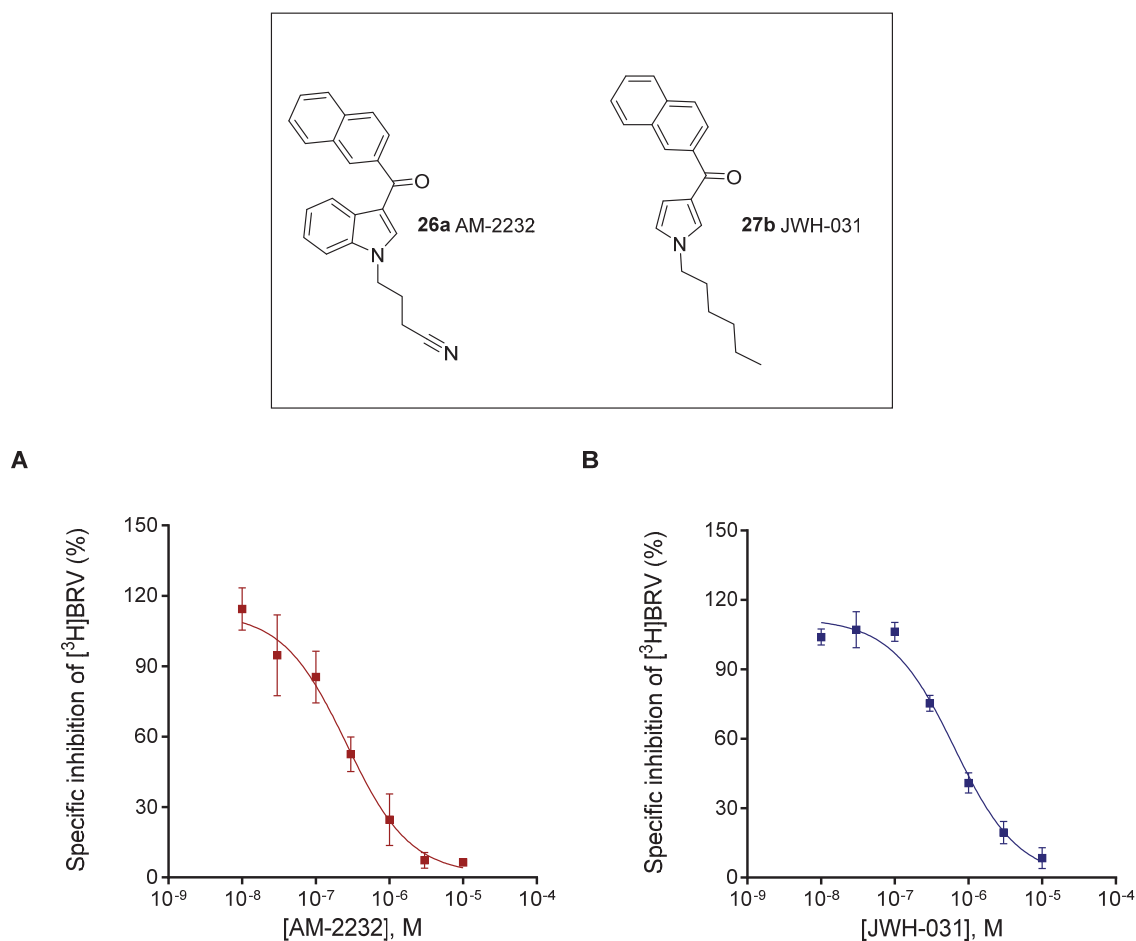


Figure 15: Concentration-dependent specific inhibition of [³H]BRV binding to SV2A by (A) AM-2232 resulted in a K_i value of $0.401 \pm 0.144 \mu\text{M}$, and by (B) JWH-031 a K_i value of $0.618 \pm 0.083 \mu\text{M}$. For performing the competition binding experiments, homogenate of CHO cells expressing recombinant SV2A (200 μg of protein) was incubated at 4°C for 240 min with [³H]BRV (3 nM) and increasing concentrations of test compound. Data points show means \pm SEM of three independent experiments performed in duplicate.

2.1.2.3 Δ^9 -Tetrahydrocannabinol (THC) and cannabidiol (CBD)

Two of the most abundant phytocannabinoids, cannabidiol (**28a**, CBD) and Δ^9 -tetrahydrocannabinol (**28b**, THC) (see Table 5 for structures), were evaluated in the current study for their SV2A affinity. THC and CBD are similar in structure, THC representing the cyclized form of CBD (see Table 5). THC has higher affinity for both CB₁ and CB₂ receptors with reported K_i values of 5.05 nM and 3.13 nM, respectively, as compared to CBD (K_i at CB₁ 4.35 μM) and (K_i at CB₂ 2.86 μM) (see Table 6).¹⁵²⁻¹⁵³ While THC showed negligible affinity for SV2A and inhibited [³H]BRV by only 24% at 20 μM in competition binding assays, CBD displaced [³H]BRV with a K_i value of 0.719 μM for human SV2A and a K_i value of 4.85 μM

2 Characterization of SV2A and its ligands

for rat SV2A (see Figure 16). Although the K_i values at human and rat SV2A are differed considerably from each other (two-tailed t -test, $p < 0.05$), both still lie in the same order of magnitude as the K_i value of LEV (see Figure 16). Interestingly, similar observations were made by Daniel et al. (2013) with the SV2A PAM (UCB1244283), which displayed higher potency (EC_{50} 1 – 4 μ M) for recombinant rat and human SV2A compared to native SV2A in rat cortical membranes ($EC_{50} > 8\mu$ M).¹⁰² The exact mechanism(s) underlying these differences in affinities remains elusive. However, some potential contributing factors to these differences have been suggested like, i) differences in SV2A conformation between recombinant and native tissue, ii) interaction with synaptotagmin, adenine-containing nucleotides and macromolecules in native expression system, iii) and posttranslational modifications such as glycosylation.¹⁰²

CBD is a multi-target drug and around 65 distinct molecular targets for CBD have been described including transporters, receptors, ion channels and enzymes with which CBD interacts at low to high micromolar concentrations either as inhibitor or activator. Of these, only few represent relevant pharmacological targets for neurological disorders.¹⁵⁴ CBD showed significant anticonvulsant effects in mouse models including classical seizure models of maximal electroshock (MES) and pentylenetetrazol (PTZ) with ED_{50} values of 381 μ M and 318 μ M, respectively.^{131, 155} While LEV lacked anticonvulsant activity in both of these mouse models,⁴⁴ BRV demonstrated seizure protection in MES and PTZ mouse models with ED_{50} values of 359 μ M and 95 μ M, respectively.⁴⁴ SV2A is considered to be the main target for LEV and BRV for their anticonvulsive effects. However, the plausible pharmacological targets and mechanism(s) by which CBD exerts its antiseizure effects are still not well understood.^{131,}

154

It is noteworthy that both THC and CBD have been shown to exhibit anticonvulsant properties in a retrospective analysis of 34 preclinical studies. In contrast to THC (dosage 3 – 600 μ M) none of these studies showed proconvulsive effects for CBD (dosage 3 – 1200 μ M).¹³⁴ The evaluation of anticonvulsant effects of cannabinoids for instance in MES model displayed an ED_{50} value of 134 μ M for THC and an ED_{50} value of 255 μ M for CBD.¹⁵⁶ Furthermore, in another study CBD has been demonstrated to significantly synergize with the effect of LEV, when both administered at a 1:1 fixed ratio displaying an experimental ED_{50} value of 172 μ M

2 Characterization of SV2A and its ligands

in a preclinical seizure model.¹⁵⁷ Due to scarce data on tissue distribution of CBD in humans, it is currently difficult to estimate the concentration of CBD in brain required for its antiepileptic effects and to compare it with the herein obtained K_i value of $0.719 \mu\text{M}$ at SV2A. Despite the high structural resemblance between CBD and THC, only CBD binds to SV2A with high affinity (see Figure 16 and Table 5). Further research is required to clarify the CBD-mediated anticonvulsive effects, for example in the presence of negative allosteric modulator of SV2A in animal models.

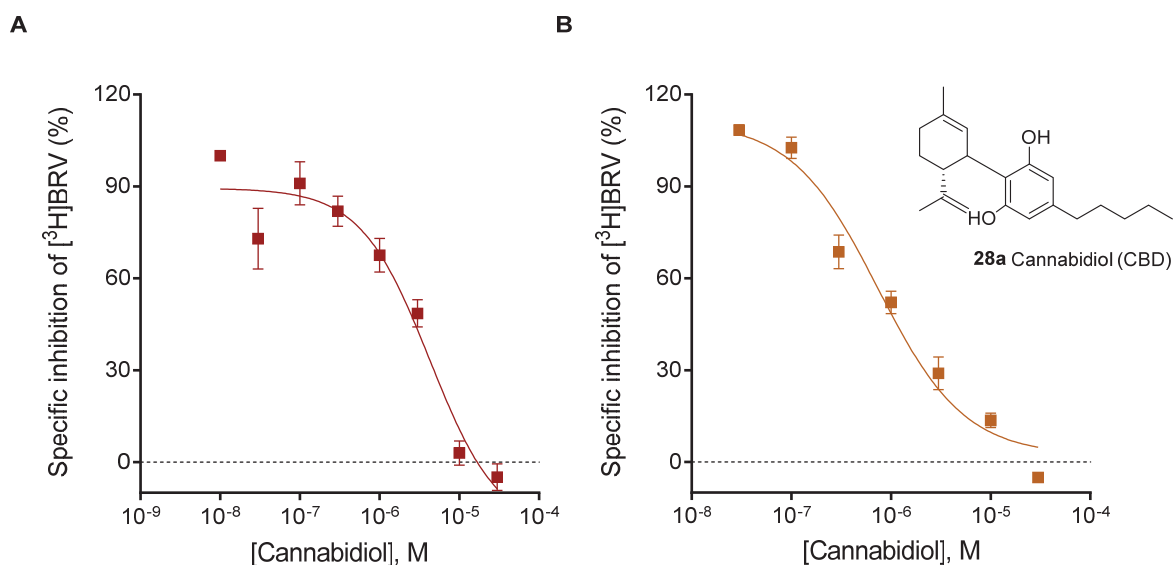


Figure 16: Concentration-dependent specific inhibition of [³H]BRV binding to SV2A by cannabidiol (CBD) at (A) rat brain cortical membranes, K_i value: $4.85 \pm 1.01 \mu\text{M}$, and (B) at recombinant human SV2A, K_i value: $0.719 \pm 0.166 \mu\text{M}$. For performing the competition binding assay, rat cortical membranes or cellular homogenate of CHO-hSV2A-GFP cells (200 μg of protein) was incubated at 4°C for 240 min with [³H]BRV (3 nM) and increasing concentrations of CBD. Data points show means \pm SEM of three independent experiments performed in duplicate.

2.1.2.4 Drug metabolism and pharmacokinetic profile of cannabidiol

Cannabidiol (CBD) upon oral administration by humans undergoes excessive first-pass metabolism and therefore results in low peroral bioavailability of only about 6%. Conversely, administration in form of aerosols or vapors results in a rapid increase in peak plasma concentrations within less than 10 min and a bioavailability of around 31%. CBD is a highly lipophilic drug with high volume of distribution and rapid transport into brain and adipose tissue.¹³¹ Administration of a cannabis-based sublingual formulation (Sativex[®]) at a dose of 40

2 Characterization of SV2A and its ligands

mg (20 mg THC + 20 mg CBD) resulted in mean peak plasma concentrations of CBD (ca. 8 nM) and THC (ca. 21 nM) after 100 min.¹⁵⁸ Interestingly, higher concentrations of CBD on average up to 21.3 nM were reported in the brains of 5 postmortem cases, however the amount of intake and time-point was unknown.¹⁵⁹

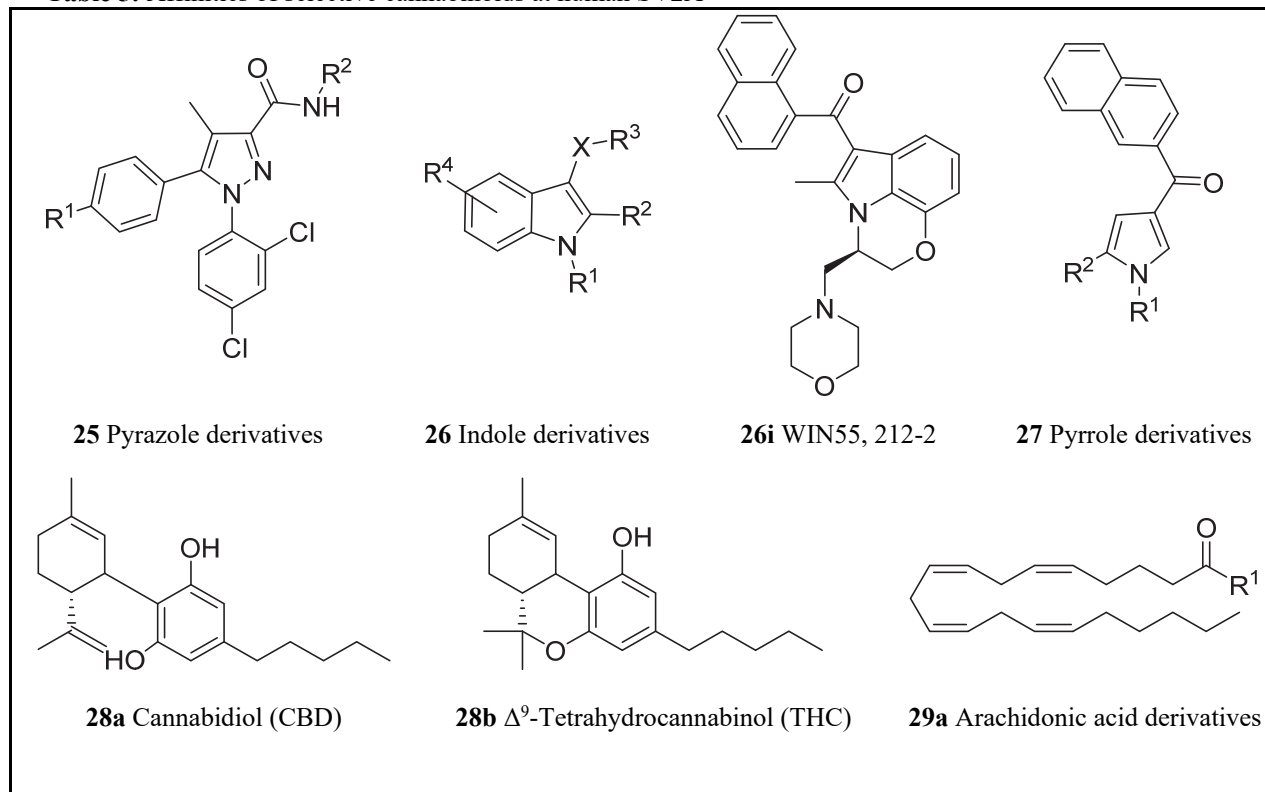
CBD is a substrate and inhibitor of cytochrome CYP450, predominantly via isozymes CYP3A (2/4) and CYP2C (8/9/19). Therefore, co-administration of CBD with other AEDs that are metabolized by these isozymes has to be considered. It may result in a change of serum concentrations of the background AEDs and their active metabolites, as shown for clobazam, levetiracetam, and other AEDs.¹⁶⁰ Around 100 CBD metabolites from urinal excretion have been characterized in different species. Not much is known about CBD-derived metabolites regarding their biological activity in humans. However, CBD-derived hydroxylated metabolites are the most abundant ones, which are excreted either unchanged or as glucuronide conjugates.¹⁶¹

2.1.2.5 Specific [³H]BRV inhibition by endocannabinoids

In addition to synthetic and phytocannabinoids, we investigated the interaction of SV2A with highly lipophilic endocannabinoids, i.e. *N*-arachidonylethanolamide (**29b**, anandamide), 2-arachidonylglycerol (**29c**, 2-AG), *N*-arachidonylserotonin (**29d**, AA-5HT), and the acetaminophen metabolite *N*-arachidonylaminophenol (**29e**, AM-404).¹⁶² All of these compounds share a membrane phospholipid precursor in synthesis and structurally resemble each other (see Table 5 for structures). However, upon evaluating their affinity for SV2A, anandamide and 2-AG displayed minor specific inhibition of [³H]BRV binding to SV2A (33% and 16% at 10 μM, respectively), while AA-5HT and AM-404 were found to be more potent with K_i values of 27.7 μM and 22.9 μM, respectively (see Table 5). However the affinity of these lipids was moderate.

2 Characterization of SV2A and its ligands

Table 5: Affinities of selective cannabinoids at human SV2A



Compound	R ¹	R ²	R ³	R ⁴	X	Human SV2A [³ H]BRV vs. Compound K _i ± SEM (μM) % inhibition ± SEM ^a
1 Levetiracetam (LEV)		For structure see Figure 5				1.74 ± 0.27
2 Brivaracetam (BRV)		For structure see Figure 5				0.098 ± 0.015
Synthetic cannabinoids						
25 Pyrazole derivatives						
25a Rimonabant	Cl					2.73 ± 0.78
25b AM-251	I					2.75 ± 0.34
25c AM-281	I					40.4 ± 20.0

Table 5 continued

2 Characterization of SV2A and its ligands

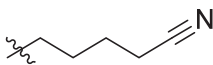
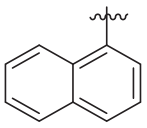
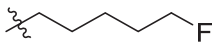
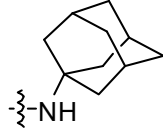
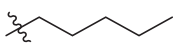
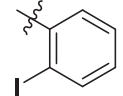
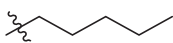
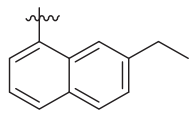
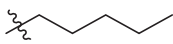
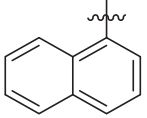
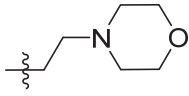
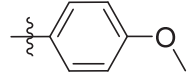
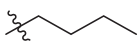
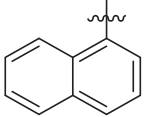
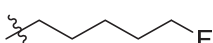
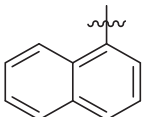
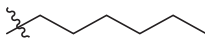
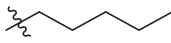
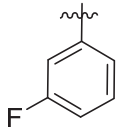
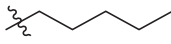
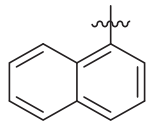
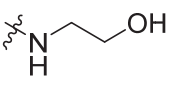
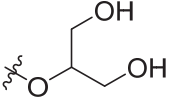
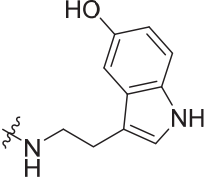
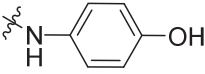
Compound	R ¹	R ²	R ³	R ⁴	X	Human SV2A [³ H]BRV vs. Compound K _i ± SEM (μM) % inhibition ± SEM ^a	
26	Indole derivatives						
26a	AM-2232		H		H	C=O	0.401 ± 0.144
26b	STS-135		H		H	C=O	79% at 10 μM
26c	AM-679		H		H	C=O	8.43 ± 1.68
26d	JWH-234		H		H	C=O	9% at 2 μM
26e	JWH-175		H		H	CH ₂	33% at 10 μM
26f	AM-630		CH ₃		6-I	C=O	19.9 ± 7.01
26g	JWH-016		CH ₃		H	C=O	4.88 ± 1.82
26h	AM-1235		H		6- NO ₂	C=O	18% at 10 μM
26i	WIN55, 212-2			For structure see above			4.15 ± 0.89

Table 5 continued

2 Characterization of SV2A and its ligands

							Human SV2A	
							[³ H]BRV vs.	
							Compound	
Compound	R ¹	R ²	R ³	R ⁴	X	K _i ± SEM (μM)		
							% inhibition ± SEM ^a	
27	Pyrrole derivatives							
27a	JWH-031		H	H			0.618 ± 0.083	
27b	JWH-368			H			28% at 2 μM	
27c	JWH-309			H			20% at 10 μM	
28	Phytocannabinoids							
28a	CBD	For structure see above					0.719 ± 0.166	
28b	Δ ⁹ -THC	For structure see above					24% at 20 μM	
29	Endocannabinoids							
29a	Arachidonic acid							
29b	Anandamide							33% at 10 μM
29c	2-AG							16% at 10 μM
29d	AA-5HT							27.7 ± 10.3
29e	AM-404							22.9 ± 6.15

^aScreening was performed at one indicated test compound concentration and percent inhibition of [³H]BRV (3 nM) is given relative to LEV (1 mM) mediated 100% inhibition at hSV2A. Data show means ± SEM of at least three independent experiments performed in duplicate until and otherwise indicated.

2 Characterization of SV2A and its ligands

Table 6: Potencies of selected cannabinoids at SV2A and cannabinoid receptors

Cannabinoid	Human SV2A	CB ₁	CB ₂
	K _i ± SEM (nM)	K _i ± SEM (nM)	K _i ± SEM (nM)
25a Rimonabant	2730 ± 780	2.0 ¹⁴⁵ 12.6 ± 3.9*	> 1000 ¹⁴⁵ 900 ± 310*
25b AM-251	2750 ± 340	7.49 ¹⁶³	2290 ¹⁶³
25c AM-281	40400 ± 20000	12 ¹⁶³	4200 ¹⁶³
26a AM-2232	401 ± 144	0.28 ¹⁴⁸	1.48 ¹⁴⁸
26b STS-135	79% at 10000 nM	2.51 ± 0.35 ¹⁶⁴	0.794 ± 0.071 ¹⁶⁴
26c AM-679	8430 ± 1680	13.5 ¹⁴⁸	49.5 ¹⁴⁸
26d JWH-234	9% at 2000 nM	8.4 ± 1.8 ¹⁶⁵	3.8 ± 0.6 ¹⁶⁵
26e JWH-175	33% at 10000 nM	22 ± 2 ¹⁶⁶	n.d.
26f AM-630	19900 ± 7010	5152 ¹⁶³	93.3 ± 23.8 ¹⁶³
26g JWH-016	4880 ± 1820	22.0 ± 1.5 ¹⁶⁸	4.29 ± 1.63 ¹⁶⁸
26h AM-1235	18% at 10000 nM	1.5 ¹⁴⁸	20.4 ¹⁴⁸
26i WIN55,212-2	4150 ± 890	1.89-123 ¹⁶³	0.28-16.2 ¹⁶³
27a JWH-031	618 ± 83.0	399 ± 109 ¹⁵¹	n.d.
27b JWH-368	28% at 2000 nM	16 ± 1 ¹⁶⁷	9.1 ± 0.7 ¹⁶⁷
27c JWH-309	20% at 10000 nM	41 ± 3 ¹⁶⁷	49 ± 7 ¹⁶⁷
28a CBD	719 ± 166	4350 ± 390 ¹⁵³ 2950 ± 2100*	2860 ± 1230 ¹⁵³ 2150 ± 4010*
28b THC	24% at 20000 nM	40.7 ± 1.7 ¹⁵³ 3.89 ± 0.9*	36.4 ± 10.0 ¹⁵³ 71.6 ± 24.1*
29b Anandamide	33% at 10000 nM	61-543 ¹⁶³	279-1940 ¹⁶³
29c 2-AG	16% at 10000 nM	58.3-472 ¹⁶³	145-1400 ¹⁶³
29d AA-5HT	27700 ± 10300	572 ± 148*	661 ± 81.7*
29e AM-404	22900 ± 6150	2150 ± 105*	3080 ± 754*

n.d., not determined; ¹⁶³Pertwee et al. 2010; ¹⁴⁸Makriyanis & Deng 2005; ¹⁶⁴Hess et al. 2016; ¹⁶⁵Huffman et al. 2005; ¹⁶⁶Huffman et al. 2003; ¹⁵¹Wiley et al. 1998; ¹⁶⁷Huffman et al. 2006; ¹⁶⁸Aung et al. 2000; ¹⁴⁵Rinaldi et al. 1995; ¹⁵³Showalter et al. 1996; *AK Müller (determined by Clara Schöder and Andhika B Mahardhika).

2 Characterization of SV2A and its ligands

2.1.3 Summary

In the present study, 500 approved drugs were tested for their interaction with the human SV2A expressed in CHO cells. Competition binding studies were performed using [³H]brivaracetam as a radioligand. A hit rate of 3% was obtained defined as compounds that inhibited radioligand binding by more than 90% at a screening concentration of 20 μM. Subsequent concentration-inhibition curves revealed the antihistaminic prodrug loratadine (K_i 1.16 μM), the antimalarial drug quinine (K_i 2.03 μM), and the anti-obesity drug rimonabant (K_i 2.73 μM) to be the most potent SV2A ligands of the investigated drug library. All three compounds were similarly potent as levetiracetam (K_i 1.74 μM). A pharmacophore model was established using flexible alignment of brivaracetam, loratadine, and quinine, which indicated steric and electronic conformities of brivaracetam with the new SV2A ligands, and preliminary structure-activity relationships were analyzed. The anticonvulsive effects of the natural product quinine previously observed in animal models may - at least in part - be explained by interaction with SV2A. Loratadine and quinine could serve as new lead structures for antiepileptic drug development.

Based on the interaction of rimonabant with SV2A, a panel of 80 cannabinoids was screened against SV2A, which resulted in the identification of new potent ligands for SV2A, i.e. cannabidiol (CBD) (K_i 0.719), AM-2232 (K_i 0.401), and JWH-031 (K_i 0.618). THC displayed very low binding affinity for SV2A. Subsequently, selected derivatives of CBD, AM-2232, and JWH-031 with diverse substitutional patterns were analysed for preliminary structure-activity relationships (SARs). The resulting SARs may provide a basis for the development of dual-target drugs for epilepsy. Although further rigorous research is required this study supports the idea that the anticonvulsive effects of CBD might be – at least partly – attributed to its interaction with SV2A.

2 Characterization of SV2A and its ligands

2.2 Modulation of [³H]BRV binding

2.2.1 Impact of monosaccharides on [³H]BRV binding

A transporter like function of SV2A has been widely discussed, owing to its homology with the major facilitator superfamily (MFS) of transporters, however its substrate has not been elucidated so far.^{59, 61, 64} Recently Madeo et al. (2014) claimed that SV2A may be a transporter for galactose.⁶⁵ Authors of this study have demonstrated that expression of recombinant human SV2A in hexose transport-deficient yeast cells enables them to grow on galactose-containing medium. However, these yeast cells with recombinant SV2A were not able to grow on other sugars such as sucrose, glucose, or fructose. Furthermore, growth of these yeast cells could be inhibited by LEV (4 μ M) treatment. Moreover, this study demonstrated the cellular uptake of [³H]galactose and time-dependent accumulation of the radioligand in yeast cells expressing recombinant SV2A.⁶⁵ This study prompted us to investigate the potential interaction of galactose and glucose with [³H]BRV binding to SV2A. Increasing concentrations (10 mM – 300 mM) of each sugar was added, and the radioligand binding assay was performed as described in Section 6.7.1. High concentration of LEV (1 mM) was used to determine the non-specific binding of the radioligand. As shown in Figure 17 neither galactose nor glucose up to concentrations of 300 mM significantly modulated the binding of the radioligand to SV2A.

Normal physiological blood concentrations of galactose and glucose in humans are reported to be 0.08 mM and 4.72 mM, respectively.¹⁷⁰ If at supraphysiological concentrations galactose does not modulate the [³H]BRV binding, it is not likely that it shares the same binding site with LEV/BRV on SV2A and that it may modulate LEV/BRV binding to SV2A. It is tempting to speculate that LEV may block the SV2A pore, thereby impeding the transport of galactose. Galactose is an important structural component of membrane carbohydrates and glycoproteins.¹⁷¹ Furthermore, a disaccharide fucose- α (1-2)galactose is proposed to have an effect on cognition, synaptic plasticity, and turnover of synaptic vesicle-associated protein, synapsin.^{65, 172} Understanding the association of SV2A with galactose will help to elucidate the exact role of SV2A in the brain and the mode of action of LEV/BRV. Further research is warranted in this area and LEV-mediated inhibition of galactose via SV2A should be assessed in primary neuronal cultures for their reproducibility.

2 Characterization of SV2A and its ligands

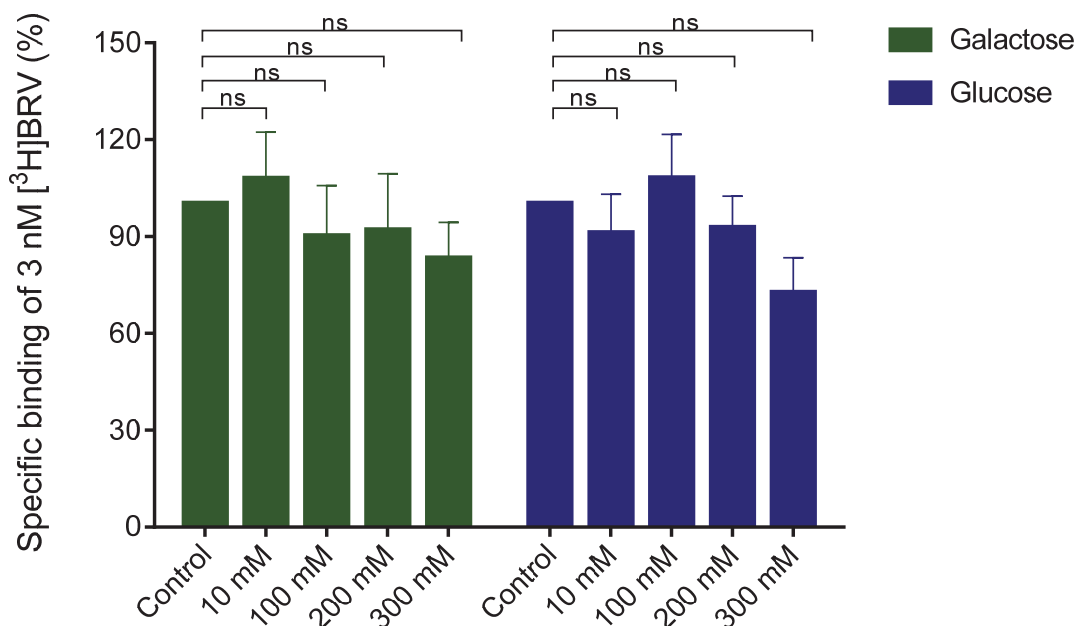


Figure 17: [³H]BRV binding to recombinant SV2A in the presence of glucose and galactose. Bars demonstrate [³H]BRV binding to SV2A in the presence of different concentrations of monosaccharides. Cellular homogenate preparation (200 µg of protein) was incubated with [³H]BRV (3 nM) together with sugar for 240 min at 4°C. Total binding was determined in the absence of LEV and non-specific binding was measured in the presence of LEV (1 mM). Data shown are means ± SEM of four individual experiments performed in duplicate. Statistical analysis was performed by one-way-ANOVA with Dunnett's test for multiple comparisons, where control assay was compared with sugar-treated assays. ns, not significant (p > 0.05).

2.2.2 Impact of botulinum neurotoxin A on [³H]BRV binding

Botulinum neurotoxin A (BoNT/A) first binds to gangliosides to facilitate anchoring at the synaptic membrane and then enters neurons by specifically binding to synaptic vesicle SV2 proteins.⁸⁹ The heavy chain C-terminal receptor binding domain (HCR) of BoNT/A was mapped to be the critical region for associating with the luminal loop 4 (L4) of SV2 (SV2A, SV2B and SV2C) proteins in the pull-down assays.⁹⁶ In the present study potential HCR-mediated modulation of [³H]BRV binding to SV2A was investigated. The 6xHis-tagged BoNT/A-HCR (~50 kDa) was expressed in *E. coli* and purified over Ni-columns via affinity chromatography (see Figure 18).

2 Characterization of SV2A and its ligands

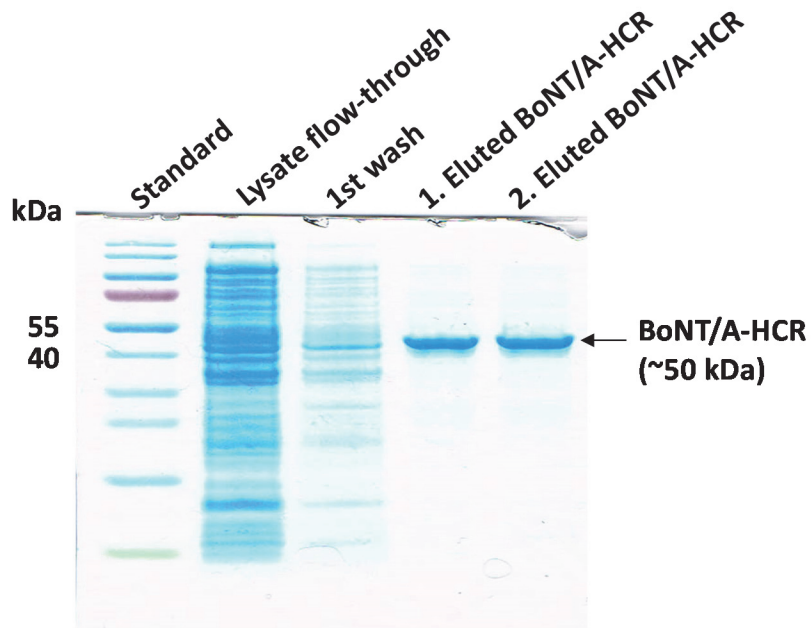


Figure 18: Purification and SDS-PAGE analysis of the C-terminal receptor binding domain (HCR) of BoNT/A (BoNT/A-HCR). Lysate containing the 6xHis-tagged BoNT/A-HCR was incubated in the Ni-NTA-columns for 1 h at 4°C under mild shaking. The flow-through of lysate was collected and the column was washed three times with wash buffer (10 mM imidazole). Subsequently, BoNT/A-HCR was eluted in elution buffer (250 mM imidazole).

For the assay, a constant amount of cellular homogenate containing exogenous human SV2A (200 µg of protein) was incubated with three different concentrations of BoNT/A-HCR, i.e. 6.7 µM, 5.0 µM, 2.5 µM, and control without BoNT/A-HCR, respectively. After an overnight incubation at 4°C under shaking, the mixture of proteins was used in the assay. As illustrated in Figure 19, there is no significant impact of BoNT/A-HCR on the binding of [³H]BRV to SV2A compared to control without BoNT/A-HCR.

Recently Benoit et al. (2014) have determined the high-resolution crystal structure of the BoNT/A-HCR in complex with the luminal loop four of the SV2C (SV2C-L4) to characterize the molecular interactions between the toxin and the SV2C.¹⁷³ In that study, they have reported a dissociation constant K_d of 0.26 µM for the SV2C-L4 at the BoNT/A-HCR by performing fluorescence anisotropy experiments.¹⁷³ Although the same amino-acid sequence of BoNT/A-HCR as described by Benoit et al. was used in this study and even with 25-fold K_d concentration (6.7 µM) of BoNT/A-HCR at pH 7.4, no significant change in [³H]BRV binding was observed. It is noteworthy that BoNT/A displays affinity for SV2 protein isoforms

2 Characterization of SV2A and its ligands

following the order SV2C > SV2A > SV2B.⁹⁶ The lethal dose of BoNTs is around 1 ng/kg (6.7 fM),⁹⁰ which indicates its extremely high potency. Since SV2A was expressed in CHO cells, presumably the *N*-linked glycosylation at Asp⁵⁷³ of SV2A was preserved, which is known to enhance the BoNT/A-HCR binding.¹⁷⁴ Overall, our findings demonstrate that the BoNT/A binding site within SV2A-L4 does not overlap with the [³H]BRV binding site, and BoNT/A does not affect [³H]BRV binding by allosteric modulation.

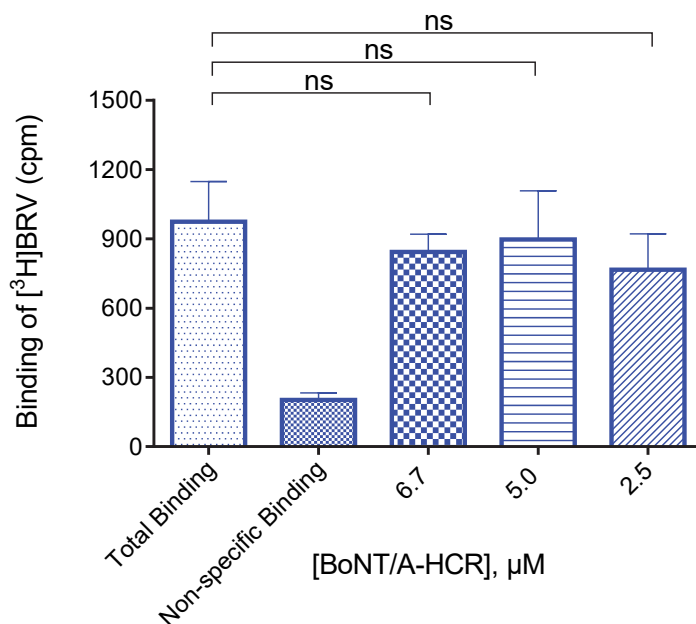


Figure 19: Analysis of BoNT/A-HCR-mediated modulation of [³H]BRV binding to SV2A using radioligand binding assay. No significant difference in the [³H]BRV binding to SV2A in the presence of BoNT/A-HCR was observed as compared to control without BoNT/A-HCR. Statistical analysis was performed by one-way-ANOVA with Dunnett's test for multiple comparisons, in which [³H]BRV binding expressed in counts per minute (cpm) in control assay was compared to BoNT/A-HCR treated assays ($p > 0.05$). For performing the assay, a constant amount of CHO cells homogenate expressing SV2A (200 µg of protein) was incubated with different concentrations of purified BoNT/A-HCR for 16 h at 4°C under shaking. Control proteins without BoNT/A-HCR were also treated under same conditions. These pre-inubated protein mixtures were then incubated with [³H]BRV (3 nM) at 4°C for 240 min prior to harvesting of the radioligand-protein complex. Total [³H]BRV binding was determined in the absence of unlabeled compound and non-specific binding was determined in the presence of unlabeled LEV (1 mM). Data represent the means \pm SEM of at least three independent experiments performed in duplicate. cpm, counts per minute; and ns, not significant.

2 Characterization of SV2A and its ligands

2.3 Potential interaction of the intracellular loop 3 of SV2A with [³H]BRV

2.3.1 Introduction

Data is scarce on genetic variations (polymorphisms) of SV2A which may be present in LEV non-responders.¹⁷⁵ However, a point mutation from nucleotide guanine (G) to adenine (A) at position 169 in intron 6 leading to a splice variant of SV2A with a deleted portion of exon 6 and complete exon 7 was previously reported to result in a LEV non-responder phenotype.¹⁷⁵ Recently, a homozygous mutation resulting in the exchange of arginine to glutamine in position 383 (Arg383Gln) in exon 5 of SV2A, has been suggested to be a candidate mutation causing intractable epilepsy. Moreover, a patient exhibiting this mutation was found to be a LEV non-responder.¹⁷⁶ It is noteworthy that exon 5 (Asn³⁶⁴ – Ser³⁹³), exon 6 (Val³⁹⁴ – Gln⁴³⁰) and large portion of exon 7 (Val⁴³¹ – Ser⁴⁶⁰) constitute the longest cytosolic loop of the SV2A (UniProt: Q7L0J3). Knowledge of the amino acid residues in SV2A involved in LEV and BRV binding will help to design better SV2A-binding drugs. Moreover, mutations of these amino acid residues may additionally serve as a biomarker to predict treatment response to LEV in epileptic patients harbouring these mutations.

Radiolabeled LEV surrogate [³H]UCB30889 and [³H]BRV have been shown to bind to SV2A (see Figure 20), but they exclusively bind to SV2A and not to SV2B and SV2C.^{38, 43, 64} This implies that there is a unique binding site for pyrrolidone derivatives in SV2A, which is absent in SV2B and SV2C. The SV2A contains a long, relatively non-conserved *N*-terminus, an intracellular cytoplasmic loop three (ICL3) between TMDs 6 and 7, a highly glycosylated long intravesicular/luminal loop four (L4) between TMDs 7 and 8, and a short *C*-terminus (see Figure 21).⁶¹⁻⁶²

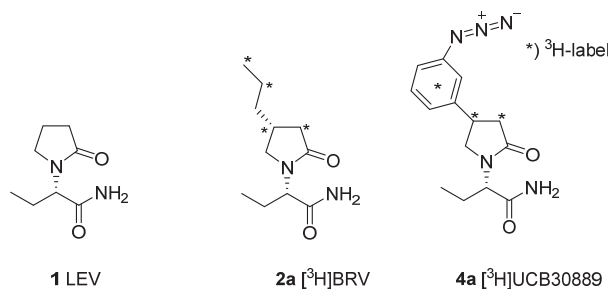


Figure 20: Chemical structures of pyrrolidone derivatives levetiracetam (LEV), and radiolabeled brivaracetam (BRV), and UCB30889. *) ³H-label.

2 Characterization of SV2A and its ligands

Within the major facilitator superfamily (MFS), lactose permease (LacY) with a known crystal structure is the closest homolog to SV2A with 16% sequence identity.¹⁷⁷ From the homology model of SV2A based on the LacY transporter and mutagenesis studies, 14 amino acid residues in the TMDs interacting with LEV were proposed (see Figure 21).¹⁷⁸ This work was further extended by implementing the SV2A homology model with inward-open and outward-open conformational states, which led to the identification of Asp⁶⁷⁰, conserved in all three SV2 isoforms, as an indispensable racetam interaction partner.¹⁷⁷ Asp⁶⁷⁰ is the third last amino acid of TMD 10 (UniProtKB: Q7L0J3). It is noteworthy that these studies used [³H]UCB30889, which possesses a rather bulky, aromatic phenyl residue, which may not accurately represent LEV and BRV. Shortly after this work, again several new amino acid residues were identified as putative racetam-interaction partners by docking studies (see Figure 21).¹⁷⁹ However, among these newly identified amino acid residues, only Trp⁶⁶⁶ as a racetam-interaction partner was found to be consistent with previous studies.¹⁷⁹

Previously reported homology models focused on the TMDs of SV2A to elucidate LEV binding residues.¹⁷⁷⁻¹⁷⁹ Interestingly, most of the proposed amino acid residues are conserved in all three SV2 protein isoforms. Moreover, the role of the ICL3 and the L4 that contain several SV2A-unique and non-conserved amino acids for LEV binding has not been investigated. The ICL3 of SV2A contains 25 unique amino acids and the TMDs 6 and 7 are relatively rich in amino acid residues specific for the SV2A isoform (see multiple sequence alignment in appendix Figure A3).

It has been previously shown by Hildenbrand (2012) that [³H]BRV binding was abolished in the exon 5 and/or 6 deletion mutants of rat SV2A.³⁸ Furthermore, single and double mutants containing amino acid mutations within the ICL3 of SV2A, i.e. N364K, H387Q, H387Q-T395I, T395I, and E403D did not show any significant effect on the IC₅₀ value of LEV.³⁸ The current study is an extension to the previous work to further investigate the role of ICL3 in the binding of LEV. Within this study, the point mutant R383Q of hSV2A was expressed in CHO cells and affinities of LEV, BRV, JWH-031, and CBD were evaluated. Subsequently, chimeric human SV2A with the ICL3 of the human SV2B (hSV2A-hSV2B-ICL3) and the chimeric human SV2B with the ICL3 of the human SV2A (hSV2B-hSV2A-ICL3) were expressed in CHO cells and evaluated for their [³H]BRV affinity.

2 Characterization of SV2A and its ligands

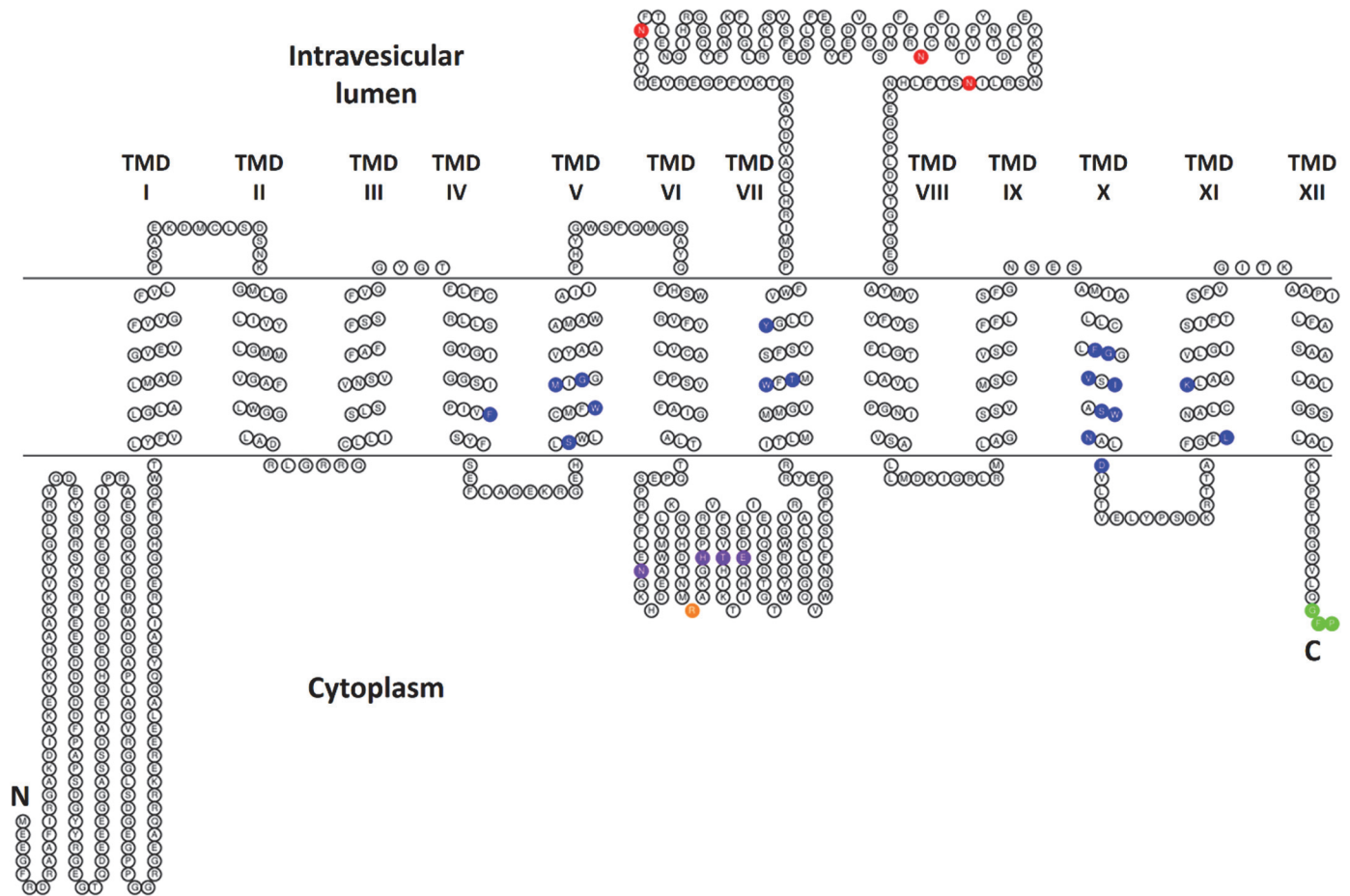


Figure 21: Topology model of the human SV2A. The snake plot diagram was prepared by using the TOPO2 program along with the transmembrane domain predictions using the HMMTOP software.⁸⁰⁻⁸¹ Transmembrane domains are indicated with Roman numbers and N & C represent *N*- and *C*-termini. The amino acids depicted in blue color have been previously demonstrated to alter racetam binding by mutagenesis and docking studies.¹⁷⁷⁻¹⁷⁹ Amino acids shown in purple within ICL3 have been previously mutated to test the affinity of mutants for racetams, however binding was not altered.³⁸ The mutation of arginine within ICL3 depicted in orange color at position 383 is suggested to be a causal factor in intractable epilepsy. The green GFP tag at the *C*-terminus indicates a green fluorescent protein (GFP) and the amino acids in red color are the *N*-glycosylation sites.

The results shown in the following section are planned to be included in a manuscript (in preparation).

2 Characterization of SV2A and its ligands

2.3.2 Molecular cloning and recombinant expression

2.3.2.1 Construct of the SV2A-R383Q mutant and heterologous expression

The mutation replacing arginine at position 383 for glutamine is the first identified point mutation in SV2A suggested to be linked with intractable epilepsy (see Figure 22).¹⁷⁶ Considering the significance of this mutation for proper SV2A function, it was decided to characterize the SV2A-R383Q protein variant for its affinity to LEV/BRV. To construct the SV2A-R383Q mutant, mutagenesis primers with exchanged nucleotides at the corresponding position were designed (see Section 6.1.7 for primers). Site-directed mutagenesis was performed by using the plasmid pcDNA4-hSV2A-GFP and mutagenesis primers. Subsequently, SV2A-R383Q-GFP was excised out of the mother plasmid by restriction digest using XhoI and HindIII enzymes. The SV2A-R383Q-GFP was subcloned into a linearized vector pcDNATM4/myc-His A also digested with XhoI and HindIII enzymes. The plasmid map is the same as shown in the Figure 6 with the only exception of the introduced point mutation (Arg383Gln).

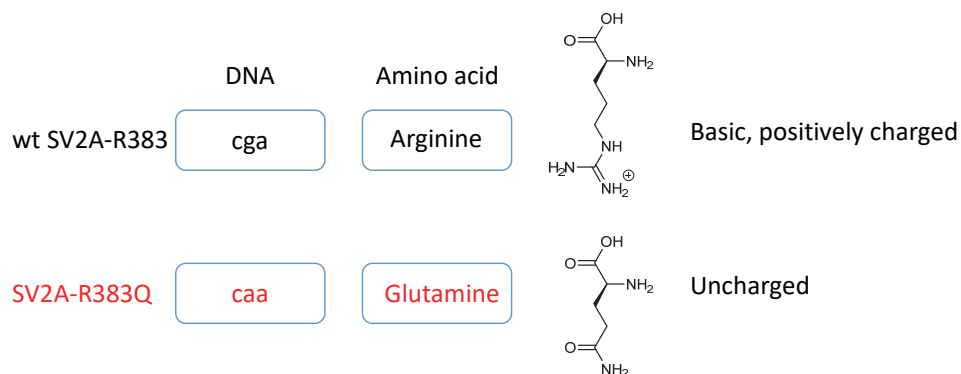


Figure 22: Point mutation located in the hSV2A-ICL3. Mutation of arginine at position 383 in SV2A to glutamine is a candidate mutation for intractable epilepsy.¹⁷⁶

2.3.2.2 Constructs of SV2A and SV2B chimeras

In the previous study, four out of 25 amino acids unique to the ICL3 of SV2A were randomly exchanged against another amino acid, i.e. N364K, H387Q, T395I and E403D.³⁸ However, none of these mutants showed significant difference in LEV affinity in competition radioligand binding assay against [³H]BRV.³⁸ Generating and testing of single point mutants of the

2 Characterization of SV2A and its ligands

remaining 21 amino acids at first place would have been tedious and time-consuming. Therefore, to study a potential role of the ICL3 of SV2A for the binding of LEV/BRV, chimeric proteins were designed: chimeric SV2A containing the ICL3 of SV2B (SV2A-SV2B-ICL3) and chimeric SV2B protein containing the ICL3 of SV2A (SV2B-SV2A-ICL3). Construction of chimeric proteins posed various challenges due to absence of suitable restriction sites that do not cut within the vector-backbone. Initial attempts such as, i) loop exchange by introducing restriction sites using site-directed mutagenesis,¹⁸⁰ ii) ligation of multiple DNA fragments,¹⁸¹ and iii) PCR-after-ligation of multiple DNA inserts,¹⁸² did not result in intact plasmids. Consequently, a novel strategy – the Gibson assembly method – designed for ligation of multiple DNA fragments was employed.¹⁸³⁻¹⁸⁴ In order to use this method overlapping primers were designed to amplify adjacent DNA fragments with overlaps sharing terminal sequence (see Section 6.1.7 for primers).

The Gibson assembly collectively makes use of three enzymes, a) 5'-T5 exonuclease (5'-exo), b) Phusion[®] DNA polymerase (DNA pol), and c) *Thermus aquaticus* ligase (*Taq* ligase), in a one-step isothermal reaction.¹⁸⁴ When the double-stranded DNA (dsDNA) fragments to be ligated are subjected to the Gibson assembly mixture, 5'-exo cuts off nucleotides at the 5'-end of (dsDNA) leaving behind a 3'-overhang. The complementary 3'-overhangs of adjacent DNA fragments are annealed and gaps are filled by the action of DNA pol and subsequently nicks are sealed by *Taq* ligase resulting in a seamless DNA construct.¹⁸⁴ As shown in the Figure 23, for construction of the plasmid pcDNA4-hSV2A-hSV2B-ICL3, vector pcDNATM4/myc-His A was linearized by the restriction digest using XhoI and HindIII enzymes, followed by mixing the linearized vector and amplified DNA fragments with Gibson assembly mixture as explained in Section 6.2.11. Similarly, the plasmid pcDNA4-hSV2B-hSV2A-ICL3 was constructed, however initially the vector was linearized by the restriction digest using XbaI and HindIII (see Figure 23).

2 Characterization of SV2A and its ligands

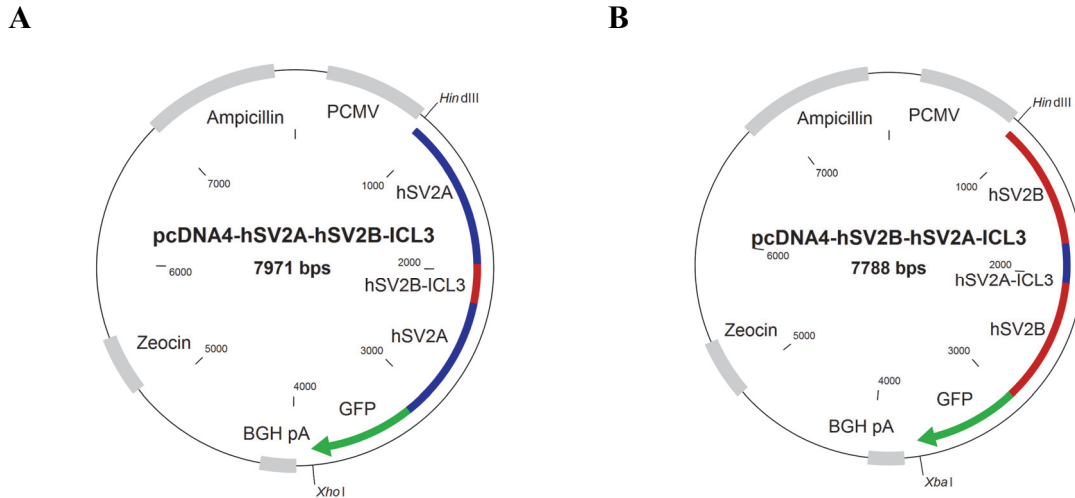


Figure 23: Plasmid maps of the hSV2A and hSV2B chimeric constructs. (A) The wt hSV2A sequence (blue) contains the ICL3 (red) from wt hSV2B and a GFP-tag (green) is fused at its C-terminus. (B) The wt hSV2B sequence (red) contains the ICL3 (blue) from wt hSV2A and a GFP-tag (green) is fused at its C-terminus. Regions of the most important functional elements such as promoter region (PCMV), termination/polyadenylation signal (BGH pA), zeocin, and ampicillin are indicated accordingly within the map.

2.3.3 Heterologous expression of wt SV2A and its variants

Expression and intracellular localization of the GFP-tagged wt SV2A, SV2A-R383Q, and chimeric proteins was investigated by fluorescence microscopy. CHO cells were transiently transfected with each plasmid and slides were prepared for confocal fluorescence microscopy (see Section 6.6.1). As shown in the Figure 24, the expression of wt SV2A and SV2A-R383Q was found to be similar in CHO cells and both proteins were not only localized to the plasma membrane but also to intracellular compartments. However, lower fractions of chimeric proteins were found to be localized at the plasma membrane compared to the intracellular compartments. To further specify the compartments for protein localization, detailed and more specialized studies using the plasma membrane, cytosolic and nuclear markers could be conducted, which however lies out of the focus of this study. Nevertheless, these results demonstrate that all aforementioned proteins tagged with GFP at their C-terminus were successfully expressed in CHO cells.

2 Characterization of SV2A and its ligands

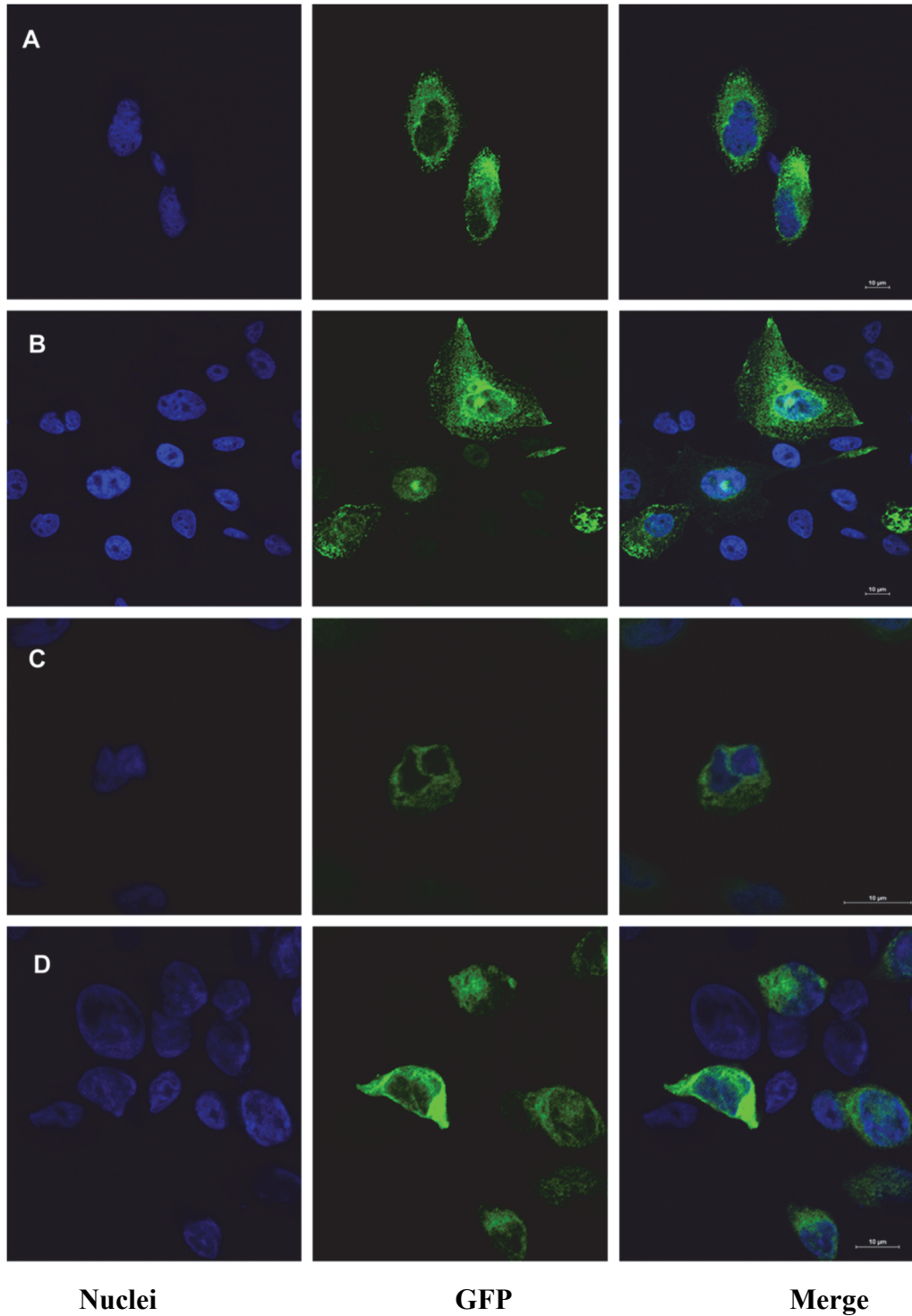


Figure 24: Fluorescence microscope images of CHO cells expressing GFP-tagged proteins, (A) wt hSV2A, (B) hSV2A-R383Q, (C) chimeric hSV2A (hSV2A-hSV2B-ICL3), and (D) chimeric hSV2B (hSV2B-hSV2A-ICL3). Nuclei were stained with DAPI and a DAPI filter was used for detection. GFP fused proteins were detected by a FITC filter indicating protein expression. The scale bar represents 10 µm. DAPI, 4',6-diamidino-2-phenylindole; FITC, fluorescein isothiocyanate.

2 Characterization of SV2A and its ligands

2.3.4 Binding of [³H]BRV to SV2A-R383Q mutant

The homozygous missense mutation R383Q in a LEV non-responder patient lies within the ICL3 of SV2A.¹⁷⁶ Notably, arginine at this position is conserved in all three SV2 isoforms (alignment performed with ClustalW, NCBI). SV2A contains two ATP binding sites, the first at the *N*-terminus and the second at the ICL3 within which Arg³⁸³ is located and perhaps has influence on ATP and/or LEV binding to SV2A.^{64, 71} Recombinant wt SV2A and SV2A-R383Q were expressed in CHO cells with the goal to perform radioligand competition assays using [³H]BRV. Both proteins expressed a GFP-tag at their *C*-termini which allowed monitoring of expression by direct fluorimetric measurements using a fluorimeter (see Figure 25).

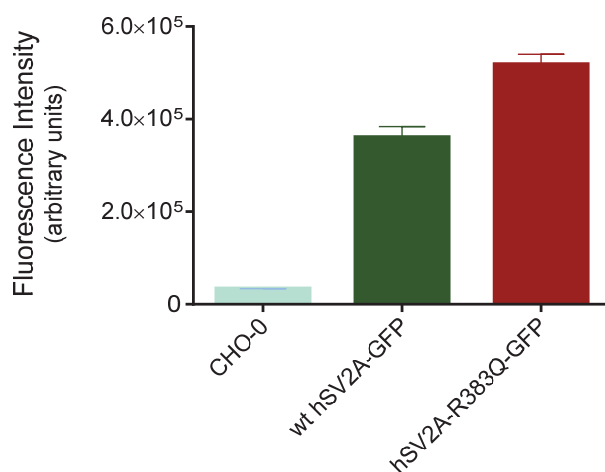


Figure 25: Expression of recombinant wt hSV2A-GFP and hSV2A-R383Q-GFP proteins in CHO cells determined by fluorimetric measurements. The same amount of cellular homogenate for all three cell lines was used for measurements. Bars shown are means \pm SEM of three individual experiments performed in duplicate.

Concentration-dependent inhibition of specific [³H]BRV binding by LEV, BRV, JWH-031 and cannabidiol (CBD) was determined. LEV displayed similar affinity for wt SV2A and SV2A-R383Q with IC₅₀ values of $1.81 \pm 0.28 \mu\text{M}$ and $2.14 \pm 0.46 \mu\text{M}$, respectively. Similarly, BRV also showed comparable affinities with an IC₅₀ value of $0.099 \pm 0.015 \mu\text{M}$ for wt SV2A and an IC₅₀ value of $0.116 \pm 0.054 \mu\text{M}$ for SV2A-R383Q. The differences in IC₅₀ values of LEV and BRV for wt and mutant SV2A proteins are not significantly different as determined by a

2 Characterization of SV2A and its ligands

two tailed *t*-test analysis. These results suggest that R383Q mutation does not directly affect the affinity of LEV and BRV for SV2A. Previously binding of LEV was observed in both inside-open and outside-open conformations of SV2A identified by protein tomography, and LEV binding had no major impact on either of the conformations.⁶⁷ This finding implies the presence of more than one LEV binding site in SV2A. This idea was further supported by the work of Daniels et al. (2013), which showed that the SV2A PAM UCB1244283 had no significant effect on LEV affinity but on that of UCB30889.¹⁰² Based on the latter findings Daniels et al. concluded that LEV has multiple binding sites on SV2A which are dependent on SV2A conformations.¹⁰² Since LEV and BRV display similar affinity for SV2A and SV2A-R383Q, respectively, this mutation does not interfere with LEV/BRV binding but may interact with the compounds function. The mutation may cause a conformational change disturbing ATP binding or transporter like physiological function of SV2A contributing to intractable epilepsy and a LEV non-responder phenotype.

Intriguingly, the newly identified cannabinoid ligands of SV2A displayed significant differences in their IC₅₀ values at wt SV2A and SV2A-R383Q. Competitive binding of the synthetic cannabinoid JWH-031 versus [³H]BRV resulted in an IC₅₀ value of 0.643 ± 0.086 μM for SV2A, whereas an IC₅₀ value of 5.99 ± 1.47 μM corresponding to a 9-fold shift was observed for SV2A-R383Q. Similarly, while CBD exhibited an IC₅₀ value of 0.748 ± 0.173 μM for wt SV2A, an IC₅₀ value of 20.7 μM was obtained for SV2A-R383Q (28-fold shift) (see Table 7 and Figure 26). The shifts in the IC₅₀ values for JWH-031 and CBD at SV2A-R383Q are significantly different from those at wt SV2A as concluded per unpaired two tailed *t*-test with *p* < 0.05. An explanation for this shift in the IC₅₀ values for both compounds could either be their direct interaction with Arg³⁸³ and/or a mutation-mediated change in the protein conformation. How exactly this mutation affects the downstream consequences of LEV binding to SV2A and translates into LEV non-responsiveness is still to be elucidated. Nonetheless, it is warranted to further characterize the R383Q mutation using *in vitro* and *in vivo* models.

2 Characterization of SV2A and its ligands

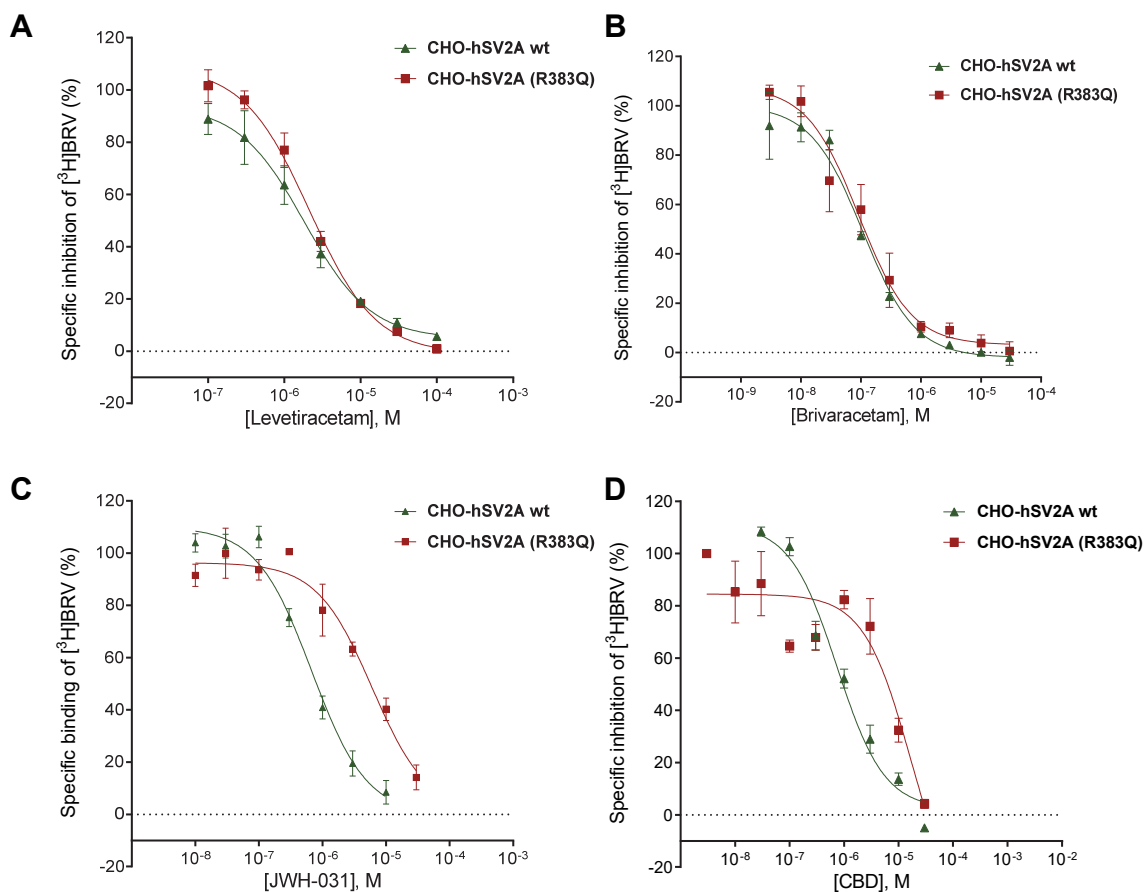
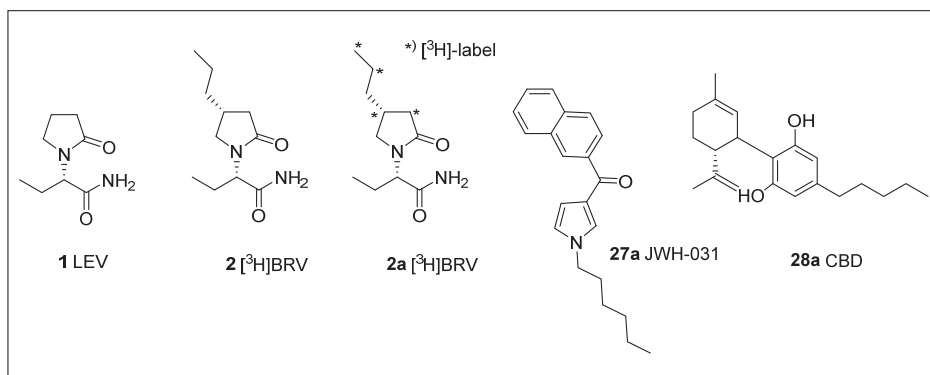


Figure 26: Concentration-dependent inhibition of specific [³H]BRV binding to recombinantly expressed wt human SV2A (green) and SV2A-R383Q (red) by selected compounds, **(A)** levetiracetam, **(B)** brivaracetam, **(C)** JWH-031, and **(D)** cannabidiol (CBD). For performing the assay cellular homogenate of each cell line (200 μ g of protein) was incubated at 4°C for 240 min with [³H]BRV (3 nM) and increasing concentrations of compound. Total binding was determined in the absence of LEV and non-specific binding was obtained in the presence of LEV (1 mM). Data shown are means \pm SEM of three individual experiments performed in duplicate until otherwise indicated.

2 Characterization of SV2A and its ligands

Table 7: Affinities of selected ligands for SV2A and SV2A-R383Q determined by inhibition of [³H]BRV binding

Compound	wt hSV2A	hSV2A-R383Q	Fold shift ^a
	IC ₅₀ ± SEM (μM)	IC ₅₀ ± SEM (μM)	
Levetiracetam	1.81 ± 0.28	2.14 ± 0.46 ^{ns}	1.2
Brivaracetam	0.099 ± 0.015	0.116 ± 0.054 ^{ns}	1.2
JWH-031	0.643 ± 0.086	5.99 ± 1.47 [*]	8.9
Cannabidiol (CBD)	0.748 ± 0.173	20.7 ± 1.11 ^{****}	27.7

Data show means ± SEM of at least three independent experiments performed in duplicate until otherwise indicated. ^a Fold shift = IC₅₀ (mutant) / IC₅₀ (wild-type); h, Human; ^{ns}, no significant difference as per two tailed *t*-test; * *p* < 0.05; **** *p* < 0.0001

2.3.5 Binding of [³H]BRV to chimeric SV2A and SV2B proteins

Using radioligand binding assays with [³H]BRV and exons 5 and/or 6 deletion mutants of SV2A, it has been already demonstrated that the deletion of large parts of ICL3 abolished radioligand binding.³⁸ However these results have to be interpreted carefully. It cannot be completely excluded that deletion of a protein region in SV2A may perhaps alter the native protein conformation, which might lead to the alteration of the LEV/BRV binding site or hinder the access of the ligand to the binding site. A more suitable strategy is to exchange all amino acids unique to the SV2A-ICL3. To exchange all of these amino acids simultaneously a SV2A chimeric protein containing the ICL3 of SV2B was constructed. Similarly, a chimeric SV2B protein containing ICL3 of SV2A was constructed to evaluate any gain in [³H]BRV binding to chimeric SV2B protein due to SV2A-specific amino acids. Both chimeric proteins were tagged with GFP at their C-terminus and recombinant protein expression was monitored by direct fluorimetry (see Figure 25a). To ensure high chimeric protein expression, early cell culture passages (P4-P5) of FACS-selected clones were used for the preparation of cellular homogenate (see Figure 25a).

2 Characterization of SV2A and its ligands

The chimeric protein approach appeared to be more suitable than deletion mutants for deciphering the binding pocket of LEV within the large SV2A (742 aa). In the future, it may be more rational to systematically exchange shorter regions of SV2A with corresponding regions of SV2B protein. In conclusion, the current data highlights the possible involvement of ICL3 of SV2A in LEV/BRV binding and suggests an important strategy of chimeric protein construction to study the interaction of SV2A with its ligands.

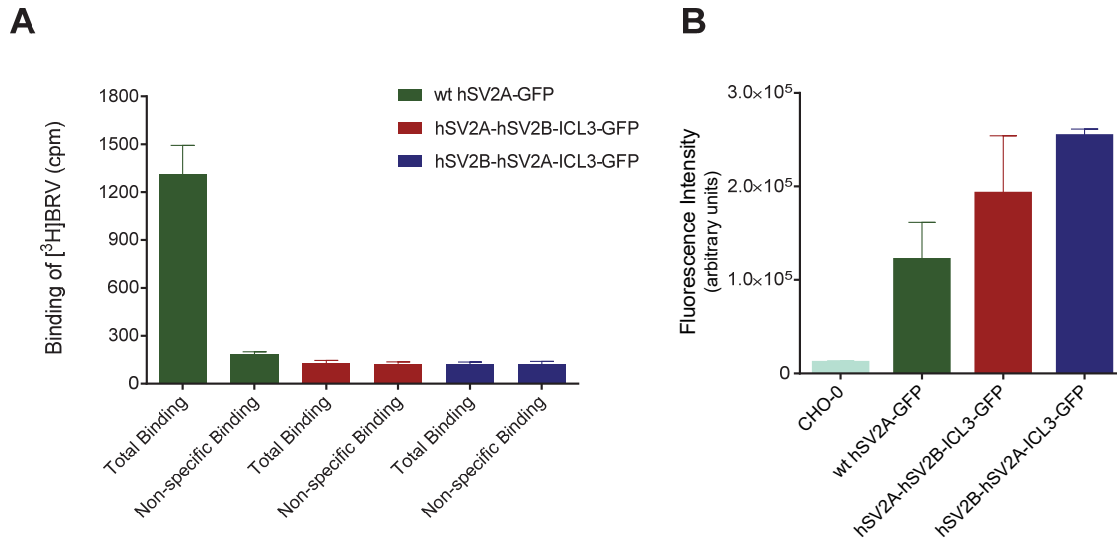


Figure 28: (A) Evaluation of [³H]BRV binding to recombinant wt hSV2A-GFP (green), hSV2A chimera (red), and hSV2B chimera (blue). For performing the assay cellular homogenate (200 μ g of protein) of each cell line was incubated at 4°C for 240 min with [³H]BRV (2 nM). Total binding was determined in the absence of LEV and non-specific binding was determined in the presence of LEV (1 mM). (B) The expression of GFP-tagged wt SV2A and chimeric proteins in CHO cells was determined by direct fluorimetric measurements using a fluorimeter. The color of the bars corresponds to the respective bars indicated in figure A. Data shown are means \pm SEM of three individual experiments performed in duplicate.

2 Characterization of SV2A and its ligands

2.3.6 Summary

The main target of LEV is believed to be SV2A to which it binds with moderate affinity (K_i 1.74 μM). Efforts involving homology modeling and site-directed mutagenesis indicated several amino acid residues in the TMDs of SV2A, to be potentially involved in the interaction with racetams. Despite several approaches, however, the LEV binding site within SV2A has remained elusive. However, its identification and characterization may lead to the design of improved SV2A-binding drugs. Moreover, it will help to understand the unique mode of action of LEV. The third long intracellular cytoplasmic loop (ICL3) of SV2A contains an ATP binding site, which may have a functional role and potentially be modulated by interactions with small molecules. The point mutation R383Q, which is located in the ICL3 of human SV2A, has been described in a patient as a candidate point mutation responsible for intractable epilepsy and LEV non-responsiveness. The rationale of the current study was to investigate the interaction of racetams (LEV and BRV) and two newly identified SV2A ligands (CBD and the synthetic cannabinoid JWH-031) with the SV2A variants using radioligand binding assays with [^3H]BRV. In this study, concentration-dependent inhibition of specific [^3H]BRV binding on wt SV2A and SV2A-R383Q by LEV, BRV, JWH-031 and CBD was determined. While LEV and BRV displayed no significantly altered binding on the SV2A-R383Q mutant, statistically significant differences in IC_{50} values of JWH-031 (9-fold rightward shift) and CBD (28-fold rightward shift) were observed. The ICL3 of SV2A contains several non-conserved SV2A-specific amino acid residues. To investigate a potential role of the ICL3 for the binding of LEV/BRV, chimeric proteins were constructed: chimeric SV2A containing the ICL3 of SV2B (SV2A-SV2B-ICL3) and chimeric SV2B containing the ICL3 of SV2A (SV2B-SV2A-ICL3). It should be noted that LEV/BRV do not bind to SV2B. Similar to the previously reported exon 5 and/or 6 deletion mutants of SV2A, specific [^3H]BRV binding was completely abolished in both chimeric proteins.³⁸ The current data suggest a possible involvement of the ICL3 of SV2A in addition to other TMD residues reported previously in the binding of LEV and BRV.

3 Screening assay for connexin 43 (Cx43) gap junctions

3.1 Introduction

3.1.1 Gap junction channels

Gap Junction (GJ) channels between two adjacent cells are formed by the head-to-head docking of hemichannels (Connexons). Undocked hemichannels (HCs) are also physiologically relevant and mediate the release of small molecules like prostaglandins, NAD^+ , ATP, neurotransmitters like glutamate in an autocrine and/or paracrine fashion. However, the effect of HCs is less pronounced than that of GJs under normal physiological conditions.¹⁸⁵ A single connexon is formed by hexameric assembly of structural protein subunits called connexins (Cxs).¹⁸⁶ Cxs are a class of integral membrane proteins, comprising four-transmembrane domains (TMDs), two extracellular loops (ELs), one cytoplasmic loop (CL), and cytosolic C- and N-termini (see Figure 29).

Cxs constitute a multigene family whose members are distinguished based on their molecular weight. In humans, 21 Cx types have been identified and more than one Cx types can be found on the same cell.¹⁸⁵⁻¹⁸⁶ Oligomerization of six Cxs to form a single connexon can either be heteromeric or homomeric. Furthermore, docking of two connexons to form intercellular channel may also result in either homotypic or heterotypic, or combined heterotypic/heteromeric arrangements of GJs.^{84,187} Among all Cxs in humans, Cx43 is the most abundantly and widely expressed Cx type with its presence in many tissues and cell types.⁸⁶ Cx43 and Cx30 are exclusively expressed in astroglial cells and are not found in other brain cell populations.⁸⁵

3 Screening assay for connexin 43 gap junctions

3.1.2 Synthesis and degradation of Cx43 GJs

Like other integral membrane proteins, Cx43 follows the secretory pathway from the ER through the Golgi apparatus. The half-life of Cx43 is rather short as compared to many other proteins and ranges between 1 and 5 h. The Cx43 mRNA is transcribed from the GJ alpha-1 gene (*GJA1*) located on chromosome 6 in humans.¹⁸⁸ The nascent Cx43 protein, P0 (42 kDa) matures by undergoing several phosphorylation steps to produce isoforms with lower electrophoretic mobilities on SDS-PAGE, i.e. P1 (44 kDa) phosphorylated at Ser³⁶⁵ and P2 (46 kDa) phosphorylated at Ser³²⁵/Ser³²⁸/Ser³³⁰.^{86, 186} As a next step, oligomerization of Cx43 into a hexameric connexon takes place in the *trans*-Golgi network. Following the secretory pathway, connexons are trafficked within vesicles to the plasma membrane to become a part of the GJ plaque (see Figure 30). Eventually, calcium-dependent cell adhesion molecules cadherins (L, A, and N) and cadherin-associated intracellular protein α -catenin facilitate the head-on docking of two connexons of neighboring cells to form functional GJs. It is noteworthy to mention another important Cx43 interaction protein zona occludens-1 (ZO-1) of around 220 kDa, a scaffolding protein facilitating the assembly of multi-protein complexes at the plasma membrane. It has been demonstrated that the hydrophobic C-terminus of Cx43 specifically fits in the hydrophobic cleft of ZO-1. Fusion of a GFP tag at the C-terminus of Cx43 resulted in GJ plaques of unusually large size. The significance of ZO-1 for GJ at various stages from assembly to degradation is widely accepted, however its exact mechanism of action is yet to be clarified.¹⁸⁹

Once GJs are formed, they are not separable into hemichannels under physiological conditions and are internalized by either of the cell as a double-membrane vesicle known as annular junction or connexosome for lysosomal degradation. Presumably the misfolded Cx proteins from the ER/Golgi apparatus undergo proteasomal degradation, whereas GJs from the plasma membrane follow lysosomal degradation (see Figure 30). It has been shown that a tyrosine-based sorting signal in the C-terminus initiates the invagination of Cx43 GJs for lysosomal degradation.¹⁹⁰ In general cellular proteins doomed to undergo proteasomal degradation are marked by polyubiquitination, which is recognized by proteasomes. Polyubiquitination in Cx43 has been already demonstrated and it is considered to be the main pathway of Cx43

3 Screening assay for connexin 43 gap junctions

degradation.¹⁹¹ However, it is still under debate which of the two mechanisms of Cx43 degradation, is the major one.¹⁸⁶

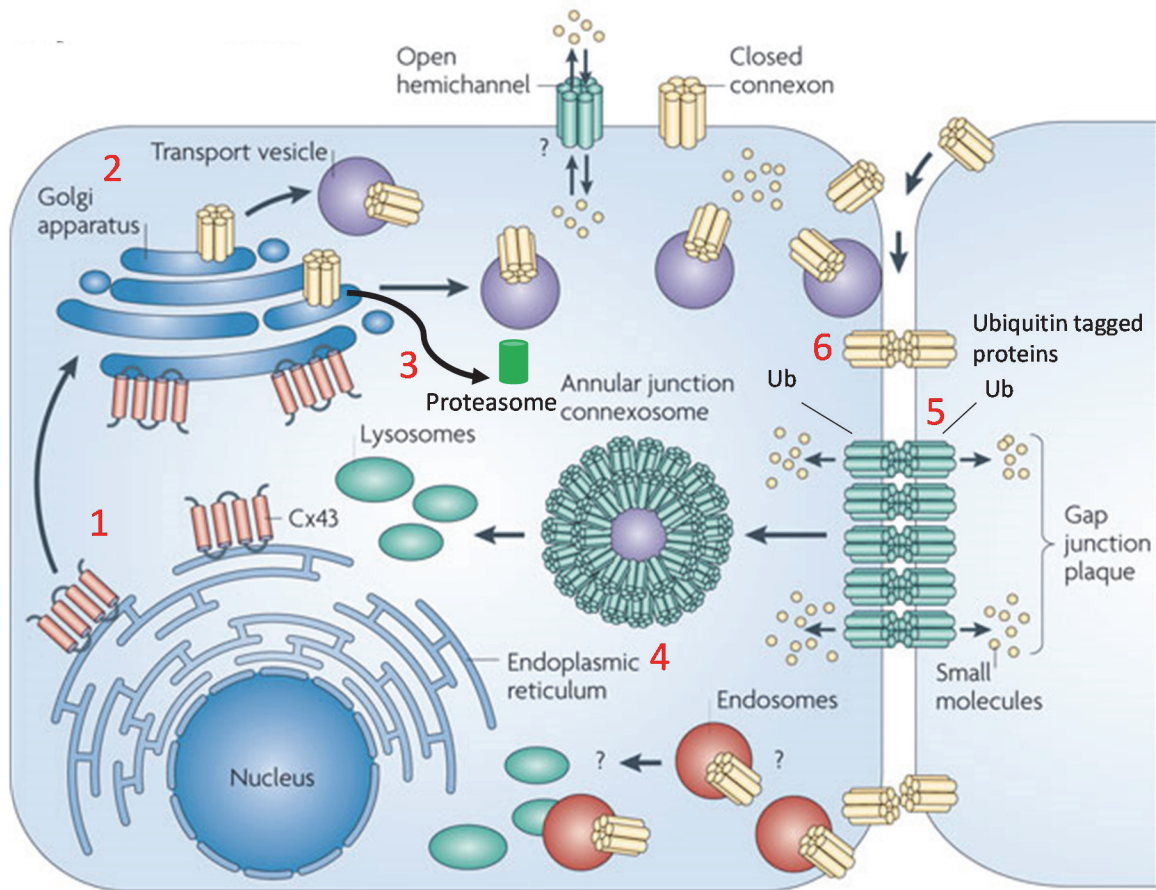


Figure 30: Life cycle of Cx43 GJs. (1) The Cx43 protein is synthesized by endoplasmic reticulum (ER) bound ribosomes and co-translationally inserted in the ER. (2) Upon reaching the Golgi apparatus six Cx43 molecules oligomerize into connexons (hemichannels) which are transported in vesicles to the plasma membrane to the periphery of preexisting GJ plaques. (3) Any misfolded proteins are degraded by proteasomes. (4) The older GJs are either degraded by internalization as double-membrane structure “annular junction” and their fusion with lysosomes or (5) by proteasomes if polyubiquitinated. (6) New connexons from the periphery replace the older GJs. Subsequently, new functional GJs capable of intercellular exchange of small molecules (< 1000 Da) are formed by the head-to-head docking of connexons from the neighboring cells. Figure taken and modified from Naus et al. 2010.¹⁹²

3 Screening assay for connexin 43 gap junctions

3.1.3 Phosphorylation mediated regulation of Cx43 GJs

GJ turnover, assembly, and size in cells dynamically changes depending on the phosphorylation pattern at specific sites within Cxs.¹⁹³ Since Cx43 is the most abundantly expressed one, phosphorylation-mediated regulation of Cx43 is well researched. Gap junctional communication (GJIC) is controlled in response to various extracellular cues such as growth factors, neurotransmitters, and cytokines. These molecules act as the activators of downstream kinases, which upon activation phosphorylates Cx43 at specific sites leading to channel closure and opening. The long cytosolic C-terminal domain in Cx43 is the major site of phosphorylation, however with exception some Cxs such as Cx36 and Cx56 can be phosphorylated within cytoplasmic loops.⁸⁶

A total of 19 phosphorylation sites have been identified within Cx43. Early phosphorylation occurs in the ER and Golgi apparatus which may facilitate the transport of Cx43 to the plasma membrane, and initial phosphorylation at membrane can occur within 15 min of Cx43 connexon synthesis.¹⁹³ Activation of cAMP dependent protein kinase A (PKA) promotes Cx43 synthesis, export to the plasma membrane, and enhances the GJ assembly.¹⁹⁴ It is well established that increased cAMP concentration leads to phosphorylation of Ser³⁶⁴ and Ser³⁶⁵ at the C-terminus with substantial increase in the export of Cx43 to the GJ plaques.⁸⁶ Phosphorylation of Cx43 at the sites Ser³²⁵, Ser³²⁸, and/or Ser³³⁰ by casein kinase 1 (CK1) has been shown to promote GJ assembly at the plasma membrane.¹⁹³ Activated protein kinase C (PKC) phosphorylates Ser³⁶⁸ at the C-terminus resulting in the down-regulation of the Cx43 expression and impairment of GJ assembly. Similarly, activation of Src kinases negatively regulates the GJ communication by phosphorylating Cx43 via Src, MAPK and PKC at the sites Tyr²⁴⁷, Tyr²⁶⁵, Ser²⁶², Ser²⁷⁹, Ser²⁸² and Ser³⁶⁸. Additionally, activation of Src decreases the PKA-mediated phosphorylation at Ser³⁶⁴ and Ser³⁶⁵.¹⁹³ Both, cGMP dependent protein kinase (PKG) and PKC are reported to exert similar effects on Cx43.¹⁹⁴

3 Screening assay for connexin 43 gap junctions

3.1.4 Pharmacological relevance of GJs

More than ten distinct human diseases have been linked to germline mutations of Cx family members.¹⁹³ For instance mutations in Cx26 result in Keratitis-ichthyosis-deafness and mutations in Cx32 causes an X-linked Charcot-Marie-Tooth disease.¹⁹⁵ Other Cxs are also linked to diseases, however the current project focuses on Cx43, the predominant GJ protein found in astrocytes.

Mutations in Cx43 are linked to the disease ODDD (Oculodentodigital Dysplasia) characterized by developmental abnormalities, and total disruption of this gene causes cardiac arrhythmias.¹⁹⁵ Changes in the expression levels of Cx43 has been reported for some neurological disorders in humans such as epilepsy, depression, and brain metastasis, implying its crucial role in the etiologies of these diseases.^{48, 85, 87} It has been demonstrated that Cx43 knockout mice died shortly after birth. Moreover, mouse models with a truncated Cx43 at the C-terminus exhibited rigid, easy-to-peel skin with mislocalized Cx43 GJs, which also resulted in the death of animals soon after birth.¹⁹³

Pharmacological modulators of GJ channels are therefore considered to have promising therapeutic potentials. For instance, naturally occurring antiarrhythmic peptide AAP10 exerts its effects by enhancing Cx43 and Cx45 GJs activities.¹⁹⁶ The active non-peptide derivative of AAP10, GAP134 reduces post-operative atrial fibrillation. Another synthetic peptide, Gap26, protects the heart from ischemic injury by specifically blocking Cx43 hemichannel activity.¹⁹⁵ Tonabersat, a GJ inhibitor is suggested to be beneficial against cortical spreading depression and could be a potential remedy against migraine.¹⁹⁷ Some of the important Cx43 GJ modulators with their effects on GJ activity are listed in Table 8.

3 Screening assay for connexin 43 gap junctions

Table 8: Cx43 gap junction modulators (adapted and modified from Jeanson et al., 2015).⁸⁵

Compound	Cx43 expression	Cx43 GJ coupling	Test model	Treatment conditions	References
Antidepressants					
Amitriptyline	↑ n.e.	↑ ↓	Primary rat astrocytes culture Primary mouse astrocytes culture	25 μM, 48 h 20 μM, 24 h	Marioka et al., 2014 ¹⁹⁸ Jeanson et al., 2015 ⁸⁵
Clomipramine	↑	n.d.	Primary rat astrocytes culture	10 μM, 48 h	Marioka et al., 2014 ¹⁹⁸
Fluoxetine	↑	n.d.	Rat prefrontal cortex (<i>in vivo</i>)	64 μM, 21 days	Fatemi et al., 2008 ¹⁹⁹
	↑	n.d.	Native human Astrocytoma cell line	32.5 - 65 μM, 24 h	Mostafavi et al., 2014 ²⁰⁰
	↑	ne	Rat prefrontal cortex (<i>in vivo</i>)	32 μM, 21 days	Sun et al., 2012 ²⁰¹
	n.e.	↓	Primary mouse astrocytes culture	10 μM, 24 h	Jeanson et al., 2015 ⁸⁵
	↓	↓	Mouse hippocampus (<i>in vivo</i>)	52 μM, 30 days	Quesseveur et al., 2015 ²⁰²
Duloxetine	↑	n.e.	Rat prefrontal cortex (<i>in vivo</i>)	34 μM, 21 days	Sun et al., 2012 ²⁰¹
	n.e.	n.e.	Primary mouse astrocytes culture	5 μM, 24 h	Jeanson et al., 2015 ⁸⁵
Fluvoxamine	↑	n.d.	Primary rat astrocytes culture	25 μM, 48 h	Marioka et al., 2014 ¹⁹⁸
Imipramine	n.e.	n.e.	Primary mouse astrocytes culture	20 μM, 24 h	
Paroxetine	n.e.	↑	Primary mouse astrocytes culture	5 μM, 24 h	Jeanson et al., 2015 ⁸⁵
Reboxetine	n.e.	n.e.	Primary mouse astrocytes culture	10 μM, 24 h	
Venlafaxine	n.e.	↓	Primary mouse astrocytes culture	5 μM, 24 h	
Tonabersat	n.d.	↓	Primary human astrocytes culture	200 μM, 12 h	Chen et al., 2016 ⁸⁷
Anesthetics					
Propofol	n.d.	↓	Mouse acute cortical slices (<i>in situ</i>)	150 μM, 30 min	
Ketamine	n.d.	Weak ↓	Mouse acute cortical slices (<i>in situ</i>)	300 μM, 30 min	Liu et al., 2015 ²⁰³
Dexmedetomidine	n.d.	Weak ↓	Mouse acute cortical slices (<i>in situ</i>)	10 μM, 30 min	
Antiarrhythmic					
Gap26	n.d.	↓	Mouse acute cortical slices (<i>in situ</i>)	200 μM, 90 min	Liu et al., 2015 ²⁰³
Flecainide	n.d.	↓ (Cx30)	Mouse acute cortical slices (<i>in situ</i>)	500 μM, 2 h	Duchene et al., 2016 ²⁰⁴
	n.d.	↓	Cx43 transfected RIN cell line	100 μM*, 3 h	
Rotigaptide (ZP123)	n.e.	↑	HL-1 atrial cardiomyocytes culture Rat neonatal cardiomyocytes culture Cx43 transfected HeLa cell line	0.05 μM, 5 h	Clarke et al., 2006 ²⁸⁸
Analgesics					
Meclofenamate	n.d.	↓	Cx43 transfected RIN cell line	50 μM*, 3 h	Duchene et al., 2016 ²⁰⁴
	n.d.	↓	Primary human astrocytes culture	100 μM, 12 h	Chen et al., 2016 ⁸⁷
Psychotropics					
Modafinil	n.d.	↑ (Cx30)	Mouse acute cortical slices (<i>in situ</i>)	200 μM, 2 h	Duchene et al., 2016 ²⁰⁴
Antiepileptics					
Levetiracetam	↑	↑	Primary rat astrocytes culture	300 μM, 24 h	Haghikia et al., 2008 ⁹⁸
Macromolecules					
LPS	↓	↓	Mouse acute cortical slices (<i>in situ</i>)	1 μg/ml, 3 - 4.5 h	Bedner et al., 2015 ⁴⁸
IL-1β	n.d.	↓	Mouse acute cortical slices (<i>in situ</i>)	10 ng/ml, 3 - 4.5 h	
Glycyrrhetic acid derivatives					
18α-GA	n.d.	↓	Cx43 transfected HeLa cell line	17 μM*, Instantly	Haq et al., 2013 ¹⁹⁵
18β-GA	↓	↓	Native WB-F344 rat liver cell line	40 μM, 1 - 4 h	Guan et al., 1996 ²⁰⁵
Carbenoxolone	n.d.	↓	Native LN215 cell line	2.1 μM*, 10 min	Lee et al., 2015 ²⁰⁶
cAMP analog					
db-cAMP	n.d.	↑	Mouse acute cortical slices (<i>in situ</i>)	100 μM, 3 - 4.5 h	Bedner et al., 2015 ⁴⁸
Quinoline derivative					
PQ1	↑	↑	Mouse mammary carcinoma cell line	5 μM, 24 h 1 μM, 2 h	Shishido et al., 2016 ²⁸⁹

↑, increase; ↓, decrease; n.e., no effect; n.d., no data; *IC₅₀, half maximal inhibitory concentration; RIN, rat insulinoma; IL-1β, Interleukin-1β; LPS, lipopolysaccharide; 18α-GA, 18α-glycyrrhetic acid; 18β-GA, 18β-glycyrrhetic acid; db-cAMP, Dibutyryl-cyclic AMP.

3 Screening assay for connexin 43 gap junctions

3.1.5 Interaction of levetiracetam with Cx43 GJs

In the past, a dysfunction of neurons was considered to be involved in the pathogenesis of epilepsy. In the development of novel antiepileptic drugs (AEDs) the focus was therefore on compounds affecting neuronal functions. However, the recognition of glial cells as active communication partners in the CNS has raised the question of their putative role in the pathogenesis of epilepsy. Glial cells, in particular astrocytes have multiple functions, e.g. metabolic support of neurons, and maintenance of extracellular K^+ ions and neurotransmitter homeostasis. These functions can be properly performed when the astrocytic syncytium is intact through GJ proteins. Functional GJ coupling in astrocytes is constituted predominantly by Cx43 and Cx30. A clinically effective and well established AED, LEV (294 μ M) successfully restored functional GJ coupling and impaired resting membrane potentials in an *in vitro* astrocytic inflammatory model.⁹⁸ Moreover, in the same model LEV treatment rescued inflammation-mediated disruption of gap junctional coupling to the same functional levels as the antiinflammatory cytokine transforming growth factor β 1 (TGF β 1).⁹⁹

More recently, it has been recognized that the surviving glial cells in the hippocampi of patients with mesial temporal lobe epilepsy (MTLE) have a major loss of GJ coupling. Additionally, by implementing a mouse model of MTLE and hippocampal sclerosis (MTLE-HS), it has been shown that astrocytic uncoupling leads to neuronal death and hyperactivity, thus supporting the strong role of GJ uncoupling in epileptogenesis. In mice, the lipopolysaccharide-induced (5 mg/kg) inhibition of coupling was reversed to normal coupling upon i.p. administration of LEV (882 μ M) for 5 days (first LEV injection 6 h post LPS).⁴⁸

Cumulatively, taken into consideration the above presented results, it is tempting to speculate that there might be a direct effect of LEV on Cx43, which restores the uncoupled GJs in astrocytes. One possibility is the presence of a LEV binding site on Cx43 protein. To answer this question, we investigated the binding of [³H]BRV, a 10-fold more active analogue of LEV, at Cx43 protein using radioligand binding assay. The results of these studies will give us a better understanding of mechanism of action of LEV on the restoration of uncoupled GJs in astrocytes.

3 Screening assay for connexin 43 gap junctions

3.1.6 GJ functional assays

Until recently, no high-throughput screening (HTS) assays were established to identify modulators of GJs. The majority of the techniques established to assess the GJIC are either based on measuring cell-to-cell dye transfer, electrical conductance, or metabolic interdependence. The dye transfer experiments make use of non-toxic tracers (<1 kDa) which on their own shall be ideally impermeable across the non-junctional membranes or upon entering into the cells acquire charge and become trapped inside the cell.⁸² Lucifer yellow (LY) is a fluorescent dye with a molecular weight of 443 Da and is extensively employed in microinjection,²⁰⁷ scrape loading,²⁰⁸ and electroporation²⁰⁹ techniques for investigating GJ activities.⁸² Another tracer is calcein-acetoxymethyl ester (calcein-AM) which is non-fluorescent and cell-permeable, however once inside the cell the acetomethoxy group is cleaved by cytoplasmic esterases resulting in highly fluorescent, hydrophilic, and membrane impermeable free calcein. This fluorescent tracer is used in techniques such as fluorescence recovery after photobleaching (gap-FRAP) and preloading assays with flow cytometry (FC).²¹⁰⁻²¹¹ Other techniques to study coupling in individual cell pairs include local activation of molecular fluorescence probe (LAMP) imaging assays using photocaged fluorescent dyes, and the dual whole-cell patch clamp conductance measurement method.²¹²⁻²¹³ Despite the diverse applicability of all aforementioned techniques in investigating GJs, none of them is well suited for screening compound libraries for GJ modulators. These methods have certain constraints in terms of applicability in screening assays such as i) only limited numbers of cells can be analyzed, ii) requirement of special equipment or expertise, and iii) time-consuming experimental set-up.⁸²

The first HTS assay for Cx43 GJ modulators based on real-time detection of intercellular Ca^{2+} transport was designed and established by Haq et al. (2013) from GlaxoSmithKline.¹⁹⁵ This assay system used HeLa donor cells and recipient cells. Donor cells co-expressed Cx43 and a G_q protein-coupled $\alpha 1\text{A}$ adrenergic receptor or TrpVI ion channel, whereas recipient cells co-expressed Cx43 and Ca^{2+} -sensitive codon-optimized cytoplasmic aequorin (cytoAeq) protein. Both donor and recipient cells were co-cultured to allow formation of Cx43 GJs. Activation of $\alpha 1\text{AR}$ by epinephrine or in case of TrpVI ion channel by capsaicin led to an increase in intracellular Ca^{2+} ions in the donor cells which diffused into the recipient cells via Cx43 GJs.

3 Screening assay for connexin 43 gap junctions

The cytoAeq protein detects the free calcium producing a luminescence readout.¹⁹⁵ Although the assay has been excellently executed in 40 s for single-point measurement, it is noteworthy that Ca^{2+} activates PKC-mediated phosphorylation of Cxs, which impairs the Cx43 GJ channels.¹⁹⁴ It is well established that increased intracellular Ca^{2+} binds to calmodulin (CaM), which directly inhibits the Cx43 GJs within seconds (30-90 s).²¹⁴⁻²¹⁵ Furthermore, alone intracellular Ca^{2+} overload can close GJ, however it is not well understood whether Ca^{2+} ions directly bind to GJs and close them.¹⁹⁴ The authors of this method have also proposed the development of an alternative assay using other second messengers like cAMP and cGMP.

Another HTS assay was reported for modulators of Cx43 GJs by Lee et al., (2015).²⁰⁶ For this assay system LN215 glioma cells with endogenous Cx43 expression were used for establishing donor and acceptor cells. Donor cells were engineered to express the iodide transporter (solute carrier family 26 anion exchanger member 4, SLC2A4) and acceptor cells to express the iodide ion-sensing yellow fluorescent protein H148Q/I152L (YFP^{QL}). The donor and acceptor cells were co-cultured to allow GJ formation and when iodide was added to the co-culture, the iodide ions which are otherwise cell membrane impermeable entered through SLC2A4 transporters into the donor cells, diffused via GJs to the acceptor cells and quenched fluorescent YFP^{QL}. In the absence of SLC2A4 in donor cells or the presence of Cx43 GJ inhibitors, the fluorescence of YFP^{QL} was not quenched.²⁰⁶ Despite the low cost of this method, maximum fluorescence quenching of around 45% has been shown for a control co-culture. The small signal window of this method may pose a challenge to identify hits in screening campaigns, especially for GJ inhibitors that are not highly potent. Additionally, this assay system requires a cell line which is impermeable to iodide ions.

In addition to these assays some other Cx43 GJ HTS assays have also been reported, however they are based on sophisticated experimental setups requiring high expertise such as automated fluorescence microscopy imaging,²¹⁶ automated incuCyte imaging,²¹⁷ and microfluidic method.²¹⁸

Taking into consideration the limitations of the aforementioned Cx43 GJ HTS assays, the current project focuses on the development of a relatively simple and new GJ HTS assay for a 96-well format based on intracellular cAMP detection.

3 Screening assay for connexin 43 gap junctions

3.2 Development of Cx43 GJ assay

3.2.1 Evaluation of levetiracetam binding to Cx43 protein

It had been shown that LEV successfully restored the functional coupling in inflammation-induced uncoupled Cx43 GJs in astrocytes.⁴⁸ To investigate whether LEV exerts these effects by directly binding to Cx43 GJs, two stable CHO cell lines expressing human and mouse Cx43 respectively, were established using the mCherry lentiviral expression system.²¹⁹⁻²²⁰ Since mCherry is a red fluorescent protein, this characteristic allowed the selection of strongly fluorescent monoclonal cells by fluorescence-assisted cell sorting (FACS) to ensure high and stable Cx43 expression.

Using homogenates of the cells expressing Cx43 protein, radioligand binding assays with [³H]BRV (5 nM) was performed. To validate the assay, homogenate of SV2A expressing cells were incubated and treated in parallel under the same assay conditions. Non-specific binding of the radioligand was determined in the presence of a high concentration of LEV (1 mM). As shown in Figure 31 total binding in counts per minute (cpm) of radioligand to SV2A containing cell homogenate (positive control) is around 6-fold higher than non-specific binding (negative control). The screening window between the positive and negative controls is well separated which confirms the successful execution of the assay. However, no specific binding (difference of total and non-specific binding) of the radioligand could be observed either with mCx43 or with hCx43 proteins. More importantly, non-specific binding of the radioligand for all different protein samples including homogenate of SV2A expressing cells displayed similar cpm values signifying assay uniformity. Similar results were obtained when assays were performed with higher concentration (15 nM) of the radioligands [³H]BRV and [³H]LEV (preliminary data).

FACS-picked monoclonal cells were used to prepare homogenates to ensure high expression of Cx43. However, they resulted in a similar expression level of Cx43 as for that of nontransfected CHO cells, which is also relatively high (see Section 3.2.2). One reason could be the absence of a resistance (selection) marker in the mCherry system, which may allow non-transfected cells to outnumber transfected cells in culture. These results in general indicate that Cx43 might not possess a direct high-affinity LEV binding site, and LEV may act on Cx43 through another mechanism of action. However, it cannot be excluded that the affinity of LEV/BRV and the

3 Screening assay for connexin 43 gap junctions

expression level of Cx43 are too low to demonstrate specific binding in a radioligand binding assay.

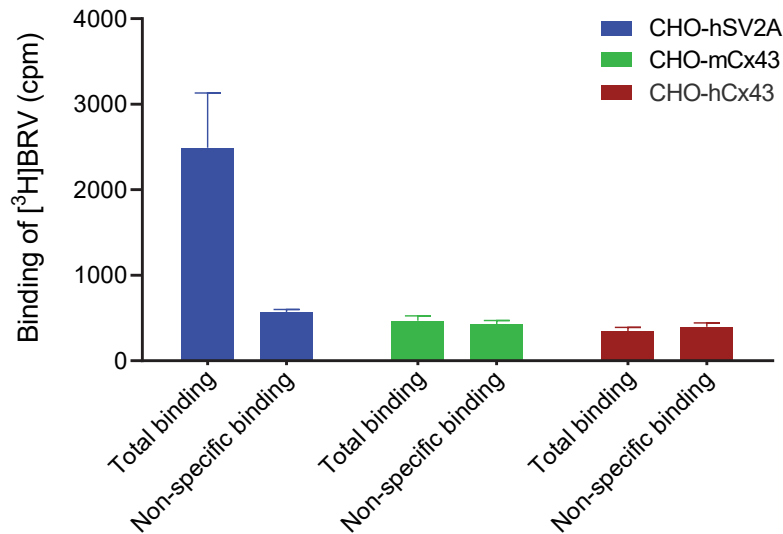


Figure 31: Evaluation of [³H]BRV binding to recombinant human and mouse Cx43 expressed in CHO cells using radioligand binding assays. Cellular homogenate (200 µg of protein) of each cell line per vial was incubated with [³H]BRV (5 nM) for 240 min at 4°C. Non-specific binding was determined in the presence of unlabeled LEV (1 mM) and total binding was determined in the absence of LEV. Data are means ± SEM of at least three individual experiments performed in duplicate.

3.2.2 Cx43 expression in cell lines

Cx43 is the most widely expressed and predominant GJ protein found in almost all mammalian cell types with the exception of brain cell populations, where it is exclusively expressed in astrocytes.⁸⁵ This wide expression pattern of Cx43 makes it difficult to find a mammalian cell line for experiments where low to no expression of Cx43 is desired. In this context, human cervix carcinoma (HeLa) cell line is the first choice when it comes to investigate GJs, since HeLa cells are known to be communication deficient.²²¹ Western blotting was performed to investigate the endogenous and/or heterologous Cx43 expression levels in CHO, astrocytoma 1321N1, and HeLa cell line. As shown in Figure 32A, non-transfected CHO cells show endogenous expression of Cx43, which is comparable to that of the stably transfected CHO cells, expressing mouse or human Cx43, respectively. One explanation for the similar expression levels is the use of mCherry system,²²⁰ which lacks a resistance marker for selection in culture. This might result in the outgrowth of the non-transfected CHO cells in culture. On

3 Screening assay for connexin 43 gap junctions

the other hand as expected non-transfected astrocytoma cells showed much high endogenous expression compared to CHO cells. In contrast to CHO and astrocytoma cell lines, non-transfected HeLa cell line showed much lower endogenous expression of Cx43, which was improve in HeLa cells transiently transfected with mCx43 (see Figure 32B). Low expression of Cx43 in non-transfected HeLa cell line is in agreement as reported earlier.²²¹ Overall these results suggest that among CHO, astrocytoma, and HeLa cell line, the latter exhibits the lowest Cx43 expression and is well suited for experiments where the lowest possible background of Cx43 GJs is desired. Based on these findings and previous reports, HeLa cells were selected for the development of a new functional Cx43 GJ assay.

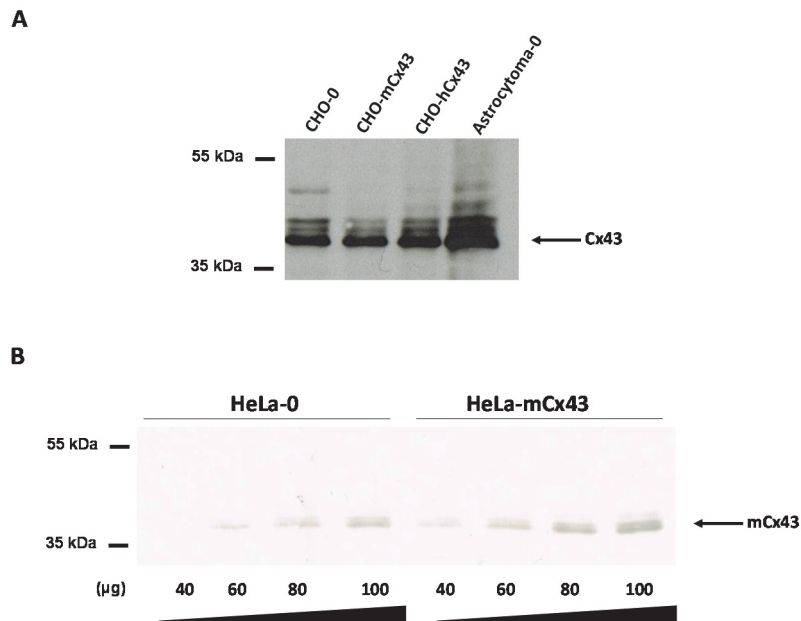


Figure 32: Expression profiling of Cx43 in wild-type and Cx43-transfected cell lines. (A) Western blot analysis of heterologous expression of human and mouse Cx43 in stable CHO cell lines and endogenous expression of Cx43 in native CHO and astrocytoma cell lines. For the analyses 30 µg of each protein sample per well was loaded onto SDS-gel. (B) Western blot analysis of endogenous Cx43 expression in native HeLa cell line and heterologous expression of mouse Cx43 in HeLa cells post 48 h transient transfection. Cells were lysed using radioimmunoprecipitation assay (RIPA) buffer, cleared by centrifugation, and the supernatants were subsequently used for analysis. The Cx43 protein bands were detected using primary polyclonal rabbit anti-Cx43 antibodies (1:2500) and secondary horseradish peroxidase (HRP) conjugated anti-rabbit antibodies (1:4000). The chemoluminescence from nitrocellulose blots was captured on X-ray films which were developed in fixing solutions.

3 Screening assay for connexin 43 gap junctions

3.2.3 Strategies for developing a new Cx43 GJ screening assay

Despite the established pharmacological relevance as a potential druggable target, only few moderately selective and potent modulators of Cx43 GJ (see Table 8) are available which may be due to difficulties in developing suitable HTS assays. In order to establish a new assay system to screen modulators of Cx43 GJ, several strategies were taken into consideration. Of these only the following ones were subsequently executed and evaluated in the lab.

3.2.3.1 Cx43 GJ assay using *Renilla* luciferase

HeLa cells were constructed as biosensor cells that exogenously co-express mouse Cx43 and *Renilla* luciferase8 (*R. luc8*). On the other hand HeLa cells were created as donor cells that express only mCx43 and were loaded with the substrate of *R. luc8* coelenterazine. The enzyme *R. luc8* catalyzes the mono-oxygenation of coelenterazine to coelenteramide yielding luminescence. Most of the commercially available preparations of coelenterazine and its analogs designed for high intensity luminescence such as coelenterazine-h require cell lysis to be used with recombinant *R. luc8*. The availability of *R. luc8* substrates for intact living cells is however limited, therefore a protected form of coelenterazine-h (EnduRen™ Live Cell Substrate, Promega) was used in this study. In the EnduRen™ substrate, the active site of oxygenation within coelenterazine-h is protected by esters which is available for *R. luc8* only when the protecting groups are cleaved by esterases inside the living cells and no luminescence is produced in dead or lysed cells.²²² Other advantages of EnduRen™ substrate over native coelenterazine-h included a reduced rate of degradation, high signal-to-background ratios, and a luminescence signal measurable for at least 24 hours. The strategy behind using EnduRen™ was that upon loading of the donor cells with EnduRen™ substrate, hydrolysis of esters will increase retention of the active substrate coelenterazine-h in the donor cells, which can then be transported to the *R. luc8* containing biosensor cells via Cx43 GJs producing a luminescence signal. The intensity of the luminescence signal will be associated with GJ formation.

Typically a ratio of three donor cells to one recipient cell is recommended for the assessment of coupling using nonfluorescent fluorogenic esters.²²³ Once inside the cell, the ester groups are cleaved by cellular esterases making this compound fluorescent. In these experiments fluorogenic ester-loaded donor cells were co-cultured with unloaded recipient cells, which have labeled cell membranes with a lipophilic dye such as dialkylcarbocyanine (Di-I), for 15

3 Screening assay for connexin 43 gap junctions

min to 24 h dependent on the type of cell and assay. The coupling of donor and recipient cells is then analyzed by fluorescence microscopy.²²³

Preliminary experiments performed with biosensor cells (40,000 cells/well in a 96-well plate) and 15 μ M EnduRen™ substrate produced a good luminescence signal. For the Cx43 GJ assay both cell types were mixed and co-cultured in a ratio of two donor cells (80,000 cells/well) to one biosensor cell (40,000 cells/well) in a 96-well plate for 3 h at 37°C to allow the formation of GJs. It was observed that exceeding a total number of 120,000 cells/well resulted in floating cell clumps and poor adherence to the well surface. That is why the ratio of donor cells in co-culture was reduced from 3 to 2 cells. The duration of 3 h has been previously demonstrated to be optimal for the Cx43 GJs formation in HeLa cells.¹⁹⁵

The luminescence signal obtained from the co-culture of donor and biosensor cells was found to be not significantly different to that of the control co-culture of donor and biosensor cells not transfected with Cx43 protein (preliminary data). One reason of this outcome was the poor retention of the EnduRen™ substrate within the cells, since after hydrolysis of the ester it is still uncharged and therefore can still move across the cell membrane based on the concentration gradient. Thus the substrate may have directly permeated from the medium into the control biosensor cells independent of Cx43 GJs, which resulted in a poorly distinguishable luminescence window between Cx43 transfected and non-transfected co-cultures.

Based on these results it was hypothesized that using another fluorogenic acetoxymethyl ester designed for cell loading may fulfill the criteria for developing the Cx43 GJ assay. To evaluate this hypothesis, two acetoxymethyl esters (AMs) of Ca²⁺-sensing dyes namely Fluo-4 (ThermoFischer Scientific) and Calcium-5 (Molecular Devices) were selected. After their hydrolysis by cellular esterases both AM dyes are negatively charged and become highly polar, which prevents them from exiting the cells. These dyes are frequently used by our group in HTS assays to measure intracellular Ca²⁺ concentration inside living cells in response to activation of G_q protein-coupled receptors.

In the preliminary experiments to test the duration of dye retention inside the cells, the astrocytoma 1321N1 cell line that expressed G_q protein-coupled P2Y₂-receptor already existing in our group was used. Cells were loaded with each dye followed by incubation for 1 h, 2 h, and 3 h at 37°C. Cells incubated for 1 h produced the highest fluorescent signal for both

3 Screening assay for connexin 43 gap junctions

dyes upon stimulating the P2Y₂-receptor with UTP (1 μM). However, the fluorescence signal for the dye-loaded cells incubated for 2 h and 3 h reduced to control levels (preliminary data). The retention of AM dyes inside the cells for a maximum of about one hour is much shorter than the duration of 3 h required for the formation of Cx43 GJs. Moreover, the AM dyes can be actively exported out of cells by multidrug resistance proteins.²²⁴ These findings indicated that AM dyes may not be a suitable choice for developing the Cx43 GJ screening assay.

3.2.3.2 Cx43 GJ assay using cAMP-sensing luciferase

This assay system employed HeLa cells which were engineered to co-express the human adenosine receptor (A_{2A}AR) and the mouse Cx43 in donor cells, and the cAMP-sensing GloSensor luciferase (GSL) and Cx43 in biosensor cells. Activation of A_{2A}AR by its selective agonist (CGS21680) generated intracellular cAMP in the donor cells which then diffused via Cx43 GJs to the biosensor cells activating GSL, and eventually producing a luminescence signal, that can be quantified. Development of this assay is detailed in section 3.2.4.

3.2.4 Cx43 GJ screening assay design

Assays to investigate cell-to-cell transfer of the second messenger cAMP through Cx43 and Cx32 GJs have been previously reported.²²⁵⁻²²⁶ In these assays donor cells capable of generating cAMP via G_s protein-coupled receptor were co-cultured with biosensor cells harboring a cAMP-sensitive reporter – cAMP response element (CRE- luciferase reporter) – responding to cAMP by producing luminescence.²²⁵⁻²²⁶ These assays despite their usefulness require disruption of the cells to be able to measure the cAMP-dependent activity of the CRE-luciferase reporter and do not monitor cAMP transfer in real-time. This method is tedious, costly, and less suitable for screening larger compound libraries for GJ modulators.

In the current project, a new strategy was developed to investigate the Cx43 GJs based on the transport of cAMP molecules from donor to biosensor cells. HeLa cells exogenously co-expressing the human adenosine receptor (A_{2A}AR) and the mouse Cx43 were designed as donor cells, while cells co-expressing GloSensor luciferase (GSL) and mCx43 were created as biosensor cells.

The current assay design is based on the detection of (cAMP). It employs a genetically engineered firefly luciferase known as cAMP GloSensor-20F from Promega (GSL) which

3 Screening assay for connexin 43 gap junctions

allows real-time detection of intracellular cAMP (Figure 33A). Another variant of this protein GloSensor-22F (GSL-22F) from Promega has been previously demonstrated to be useful for monitoring endogenous G_s protein-coupled receptors-induced cAMP generation in primary cells and HEK-293 cells co-cultured with biosensor cells harboring GSL-22F.²²⁷ This assay system is primarily developed to monitor GPCR activity in primary cells indirectly through biosensor cells connected via GJs, since transfection of primary cells is less efficient. This assay is based on endogenous connexins of primary neurons and HEK-293 cells, predominantly Cx32, and it does not report the background against other connexin subtypes.

Native firefly luciferase catalyzes the oxidation of its substrate luciferin in the presence of Mg^{2+} , ATP and O_2 to produce oxyluciferin, AMP, CO_2 and luminescence signal (Figure 33B). GSL is a circularly permuted form of firefly luciferase where between native *N*- and *C*-terminus, a conserved cAMP-binding domain B from PKA regulatory subunit type II β (RII β B) is introduced. The binding of intracellular cAMP to GSL favors the functional conformation of luciferase which in turn metabolizes the luciferin containing cAMP GloSensor substrate (GSS) giving off yellow-green light.²²⁸

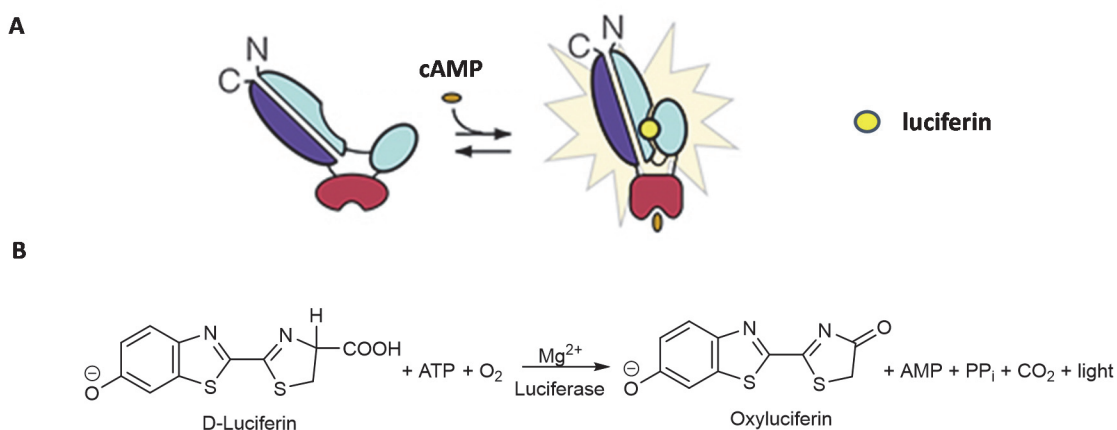


Figure 33: Principle of cAMP detection using engineered GloSensor luciferase (GSL). (A) GSL in the open conformation shows negligible luminescence activity, whereas binding of cAMP to (RII β B), the cAMP binding site within GSL, favors the closed conformation and hence activates the luciferase, which metabolizes luciferin to produce luminescence. (B) Luciferase catalyzes the oxygenation of luciferin using molecular oxygen and ATP in the presence of Mg^{2+} to produce oxyluciferin, which is highly unstable in electronically excited state and produces light upon falling back to its ground state. Figure taken and modified from Fan et al. (2008).²²⁸

3 Screening assay for connexin 43 gap junctions

According to the assay design the two cell populations will be co-cultured in a ratio of three donor cells to one biosensor cell for 4 h to allow the formation of GJs. The growth medium will then be replaced by the assay buffer supplemented with the luciferase substrate luciferin and the co-culture will be further incubated for 45 min in the dark at room temperature. Thereafter, stimulation of the A_{2A}AR by its selective agonist CGS21680 in the donor cells will activate adenylate cyclase, which converts ATP to cAMP. Binding of cAMP to GSL favors its functional conformation allowing it to metabolize luciferin and producing luminescence (see Figure 34). The mobilization of generated cAMP from donor to biosensor cells will take place via the heterologously expressed mCx43 GJs and could be detected in real-time by the GSL reaction in the established system. To initially evaluate the feasibility of the current assay design two preliminary experiments were performed:

i) Endogenous expression of adenosine receptors in HeLa cells: HeLa cells were selected for the development of a GJ assay due to low levels of endogenous Cx43 to maintain low background noise. In a preliminary study, the responses of endogenous G_s protein-coupled adenosine receptors, A_{2A} and A_{2B}, to non-selective and selective agonists in native HeLa cells were evaluated. HeLa cells were transiently transfected either with human A_{2A}AR and GSL (HeLa-hA_{2A}-GSL) or only with GSL (HeLa-GSL). HeLa-GSL produced a luminescence readout upon stimulation with forskolin (10 μM) that was used as an internal positive control. However, activation of HeLa-GSL with A_{2A}AR selective agonist CGS21680 (100 μM) produced a luminescence signal similar to vehicle (DMSO, 1%). A relatively moderate signal with HeLa-GSL was obtained with 50 μM NECA, a compound that is known to non-selectively activate A_{2A} and A_{2B} receptors. On the contrary, activation of HeLa-hA_{2A}-GSL with either NECA (50 μM) or CGS21680 (100 μM) produced luminescence readouts even higher than those produced by forskolin (10 μM). These results indicated that generation of cAMP in HeLa-GSL cells in response to NECA can be primarily attributed to A_{2B}ARs, since activation by the A_{2A}AR-selective agonist (CGS21680) did not generate detectable cAMP levels. In contrast, the high luminescence signal observed in HeLa-hA_{2A}-GSL in response to CGS21680 was primarily due to activation of overexpressed A_{2A}AR and that induced by NECA was due to activation of both, overexpressed A_{2A}AR and endogenous A_{2B}AR receptors.

3 Screening assay for connexin 43 gap junctions

Based on this preliminary experiment, it was concluded that native HeLa cells do not or only weakly express A_{2A}ARs. It makes the A_{2A}AR an excellent and selective cAMP generating tool using stimulation with the A_{2A}AR-selective agonist (CGS21680) in HeLa cells against a nearly zero background. These results were in good agreement with the previously reported expression profile of A_{2A}- and A_{2B}ARs in native HeLa cells, where A_{2B}AR expression was found to be higher than that of A_{2A}AR.²²⁹

ii) Effect of co-expression of proteins on luminescence signal: Co-expression of two or more proteins in the same cell may result in the reduced expression levels of each protein due to high occupancy of the cellular translational machinery. In the currently designed assay, biosensor cells transiently co-express GSL and mCx43. A comparison was therefore made between the transiently transfected HeLa cells expressing only GSL with the cells co-expressing GSL and mCx43 for their luminescence activity. Forskolin (10 µM) mediated activation of singly transfected HeLa cells with GSL gave an about 2-fold increased luminescence readout compared to the doubly transfected HeLa cells with GSL and mCx43. Similar results were obtained upon activation of both cell types with either 50 µM NECA or 50 µM adenosine with a 2-fold higher luminescence in singly transfected HeLa-GSL cells. Activation of both cell types by CGS21680 (10 & 100 µM) did not elicit luminescence signal indicating no expression of functional hA_{2A}ARs in native HeLa cells.

These preliminary results supported the concept that co-expression of Cx43 and GSL in HeLa cells appears to reduce the luminescence activity. Beside co-expression of proteins another reason could be that cAMP is released in the extracellular space through Cx43 hemichannels, since these channels are permeable to cAMP.²³⁰ However, luminescence readout in doubly transfected cells is still considerably above the basal luminescence, which indicates that the expressed amount of GSL is sufficient to detect changes in cellular cAMP levels.

3 Screening assay for connexin 43 gap junctions

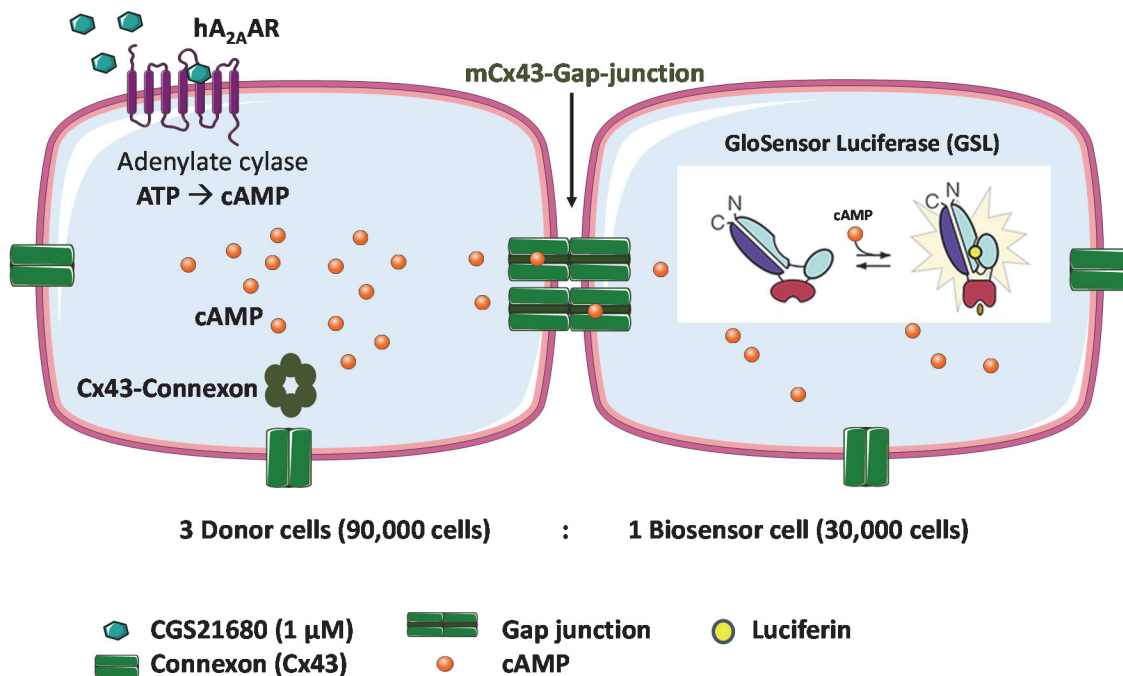


Figure 34: Design of the Cx43 GJ assay. HeLa cells expressing hA_{2A}AR and mCx43 are denoted as donor cells and HeLa cells expressing GSL and mCx43 are indicated as biosensor cells. Both cell lines are co-cultured in a ratio 3:1 of donor to biosensor cells for 4 h to allow the formation of Cx43 GJs. The coupled cells are then equilibrated with buffer containing the substrate (luciferin) of engineered luciferase. Upon activation of G_s-coupled A_{2A}ARs, cAMP levels are elevated in the donor cells, cAMP molecules move to biosensor cells via Cx43 GJs formed between donor and biosensor cells. Once inside the biosensor cells, cAMP binds to GSL causing a conformational shift activating GSL, which creates a luminescence signal by oxidizing luciferin.

3.2.5 Optimization of cAMP detection in Cx43 GJ assay

To investigate the GJ-mediated coupling, we next co-cultured the donor cells and biosensor cells in a ratio of three to one, and incubated then at 37°C for 4 h in full DMEM medium to allow the formation of GJs (see Section 6.8.2). Culture medium was then replaced by assay buffer containing the substrate of GSL without any phosphodiesterase (PDE) inhibitor and incubated the cells at room temperature for 2 h. Upon activation of the A_{2A}AR in donor cells with CGS21680 (1 μM), a subtle luminescence signal above that of the vehicle (DMSO, 1%) was detected. However, the A_{2A}AR-dependent luminescence signal was not sufficiently separable from the background to obtain a good assay window (see Figure 35).

3 Screening assay for connexin 43 gap junctions

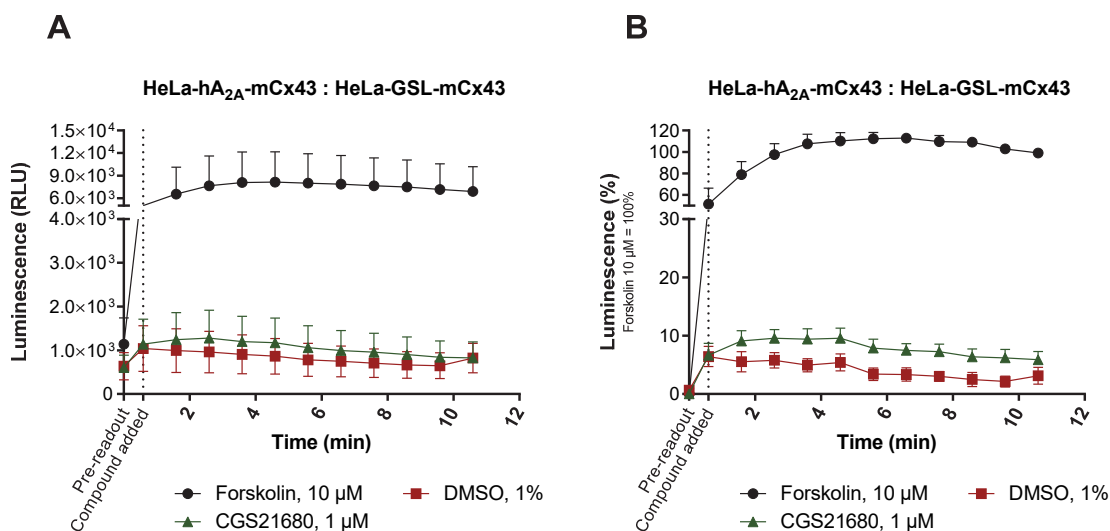


Figure 35: GJ-mediated transfer of cAMP from donor cells to biosensor cells in the absence of PDE inhibitor. **(A)** Activation of A_{2A}AR by the selective agonist CGS21680 in co-cultures produced a very small luminescence signal. Activation of adenylate cyclase by forskolin (10 µM) for cAMP generation represented an internal positive control and vehicle (DMSO, 1%) was used as a negative control. **(B)** Normalized representation of data. Data shown are means ± SEM of three individual experiments performed in duplicate.

It has been described previously that the addition of the non-specific PDE inhibitor 3-isobutyl-1-methylxanthine (IBMX) reduces the degradation of cAMP, allows cAMP accumulation and thereby enhances GSL activity.²²⁷ Therefore, co-cultures 4 h after incubation in full medium were transferred to incubation in assay buffer containing 200 µM IBMX for 45 min at room temperature in the dark. To monitor the intrinsic cAMP dependent luminescence activity in the biosensor cells, they were treated exactly like co-cultures in parallel experiments used as controls. Biosensor cells for control purpose were stimulated with either, i) 10 µM forskolin (positive control), ii) 1 µM CGS21680 (potential A_{2A}AR background signal), iii) 1% DMSO (vehicle), and iv) assay buffer (luminescence background). As expected, only forskolin-activated biosensor cells produced a high luminescence readout. Forskolin directly activates the adenylate cyclase resulting in the generation of cAMP. Biosensor cells treated with CGS21680, DMSO, or assay buffer, all produced similarly low background luminescence (see Figure 36A). The co-cultures were stimulated under the same conditions. Activation of co-cultures with forskolin elicited almost the same luminescence signal as that displayed by the biosensor cells alone, indicating no effect of the co-culture on the viability of the biosensor cells. On the other hand, CGS21680 activated A_{2A}ARs in co-culture producing an increase in

3 Screening assay for connexin 43 gap junctions

the luminescence readout which was significantly different from that produced by the vehicle (DMSO, 1%) and that observed in cells with assay buffer only (Figure 36C). These results suggest that without IBMX, the transport of cAMP from donor cells to biosensor cells is difficult to detect with reliability, similar issue was reported earlier by Trehan et al. (2014).²²⁷

The luminescence signal in response to A_{2A}AR activation by CGS21680 in co-culture is around 40% of the signal obtained in response to forskolin. The, increase in cAMP in response to forskolin is rapid and reaches the signal plateau much faster than the A_{2A}AR-dependent cAMP signal (see Figure 36D). This difference might be due to the fact, that only a fraction of cAMP generated in donor cells is transported via Cx43 GJs to the biosensor cells, whereas cAMP in response to forskolin is generated within the biosensor cells in addition to the donor cells. Similarly, in the previously reported Cx43 GJ assay, the Ca²⁺-dependent luminescence signal decreased in co-cultured cells compared to the intrinsic Ca²⁺ signal from control cells expressing both, receptor and sensor protein.¹⁹⁵

3 Screening assay for connexin 43 gap junctions

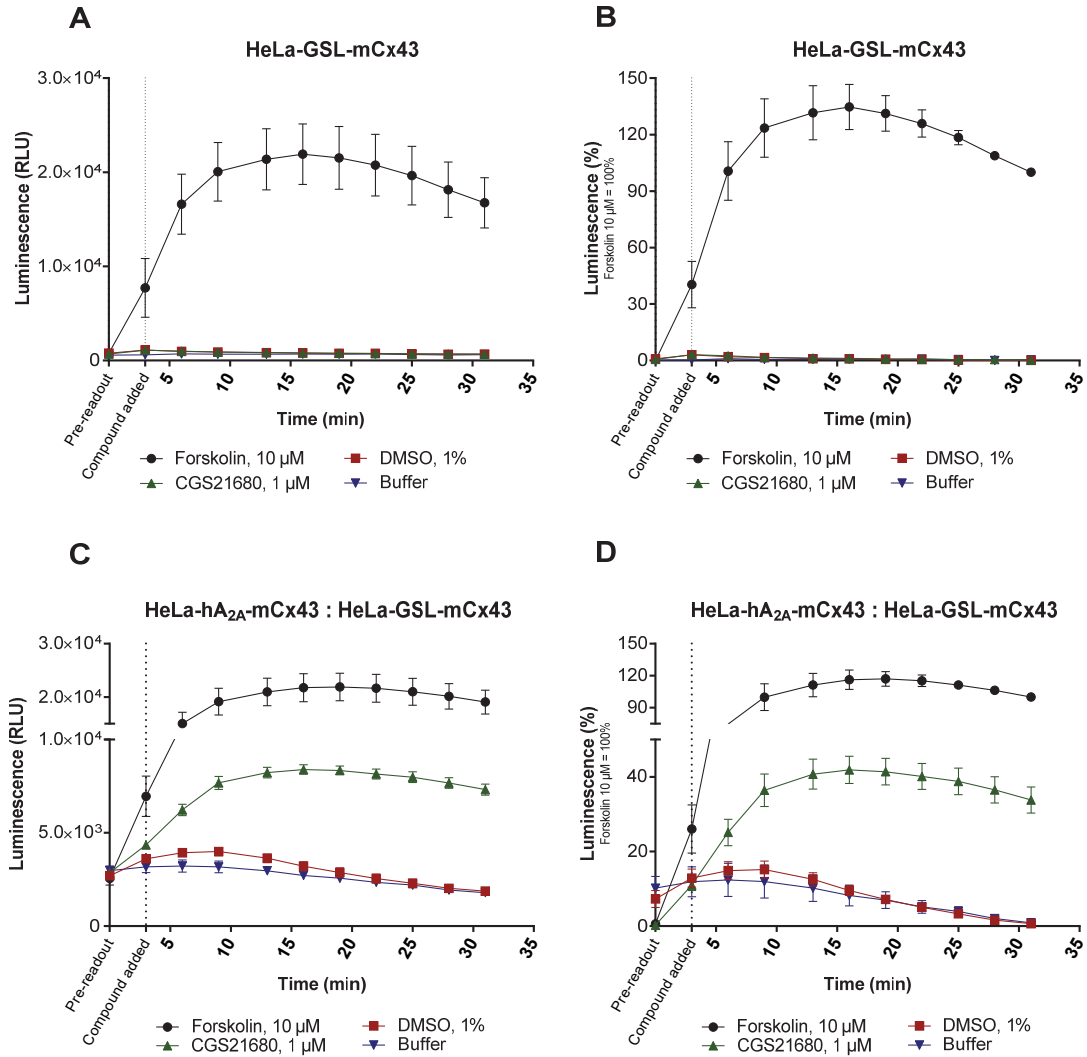


Figure 36: GJ-mediated transfer of cAMP from donor cells to biosensor cells in the presence of the PDE inhibitor IBMX. (A) Biosensor cells alone did not produce any luminescence in response to the A_{2A}AR-selective agonist CGS21680 (1 μ M). (B) Normalized representation of data obtained with biosensor cells. (C) Activation of hA_{2A}ARs in co-cultures by CGS21680 produced a strong luminescence signal. (D) Normalized representation of data obtained with co-cultures. Data are means \pm SEM of at least three individual experiments performed in duplicate.

3 Screening assay for connexin 43 gap junctions

3.2.6 Cell-to-cell communication in native HeLa cells

In order to verify that in the co-cultures, activation of GSL in the biosensor cells is entirely mediated by cAMP coming from the donor cells via Cx43 GJs, both, donor and biosensor cells, not transfected with mCx43 were studied. Donor cells (HeLa-hA_{2A}AR) and biosensor cells (HeLa-GSL) lacking mCx43 protein were co-cultured in a ratio of 3:1. The same procedure was followed as explained previously for the mCx43 GJs assay. As shown in Figure 37A, biosensor cells alone produced luminescence only in response to forskolin (10 μ M), whereas no luminescence was detected in response to DMSO (1%) or CGS21680 (1 μ M). However, this time in the absence of GJ proteins, upon stimulation of the co-cultured cells with CGS21680 (1 μ M) no increase in the luminescence signal above the basal luminescence level could be measured. In contrast, activation of co-cultured cells with forskolin (10 μ M) still elicited a high luminescence readout indicating the activity of the biosensor cells. These results suggest that native HeLa cells are devoid of efficient cell-to-cell communication and therefore cAMP generated in the donor cells can only be transported via transfected GJ proteins to the biosensor cells yielding luminescence. These results are well in line with our Western blot findings, performed to analyze endogenous Cx43 expression in HeLa cells. Although in the blots low levels of endogenous Cx43 were found in HeLa cells these are apparently not capable of forming GJs or at least not at detectable levels.

3 Screening assay for connexin 43 gap junctions

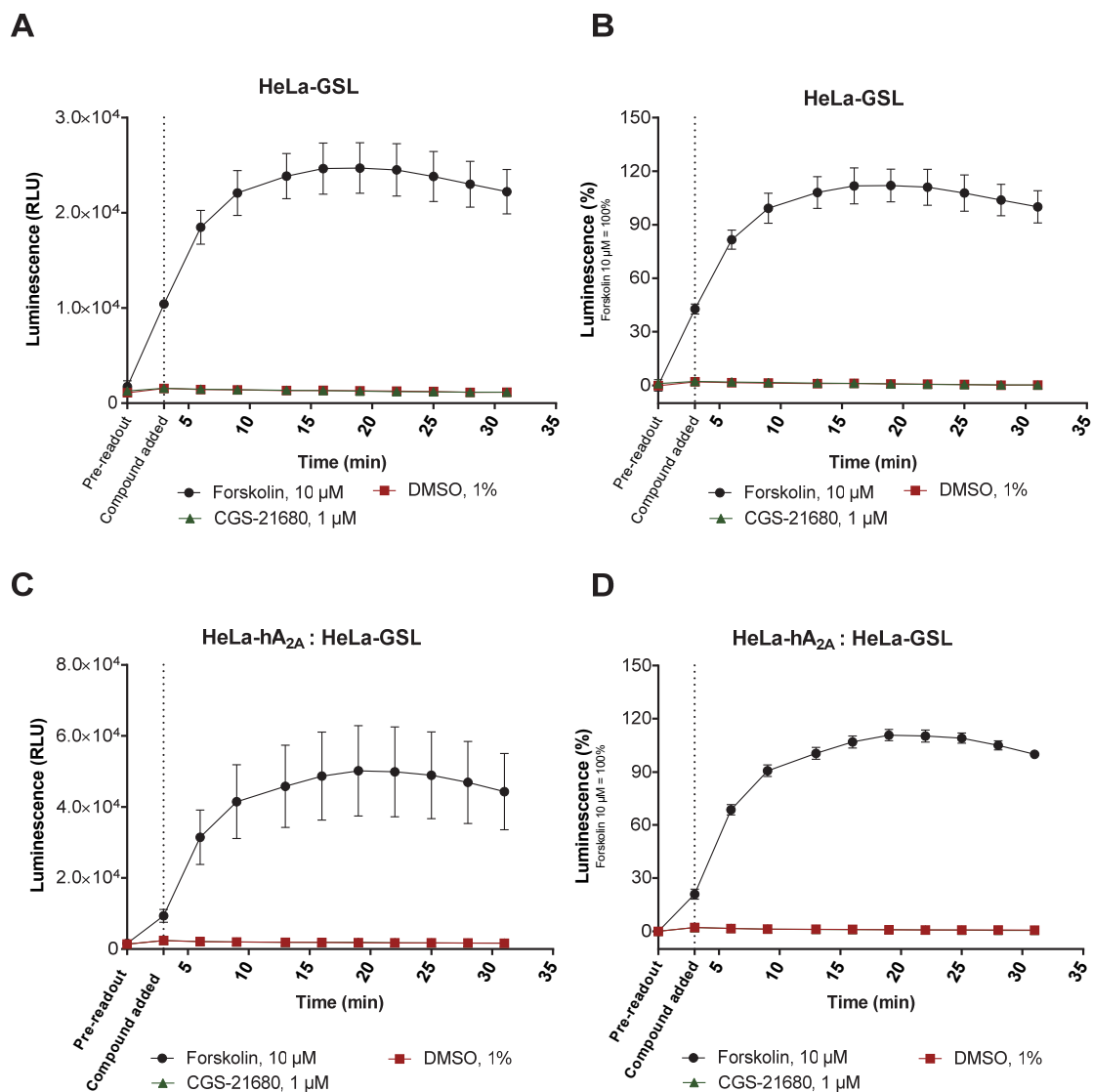


Figure 37: Evaluation of GJ-mediated intercellular transport of cAMP from donor cells to biosensor cells in native HeLa cells not transfected with Cx43. (A) Biosensor cells produced luminescence only in response to forskolin (10 μ M) used as a positive control and no luminescence in response to DMSO (1%) or A_{2A}AR-selective agonist CGS21680 (1 μ M) was measured. (B) Normalized representation of data obtained with biosensor cells. (C) Activation of co-cultures by forskolin (10 μ M) produced luminescence, whereas no luminescence could be detected in response to CGS21680 (1 μ M) or DMSO (1%). (D) Normalized representation of data obtained from co-cultured cells. Data are means \pm SEM of three individual experiments.

3 Screening assay for connexin 43 gap junctions

3.2.7 Inhibition of Cx43 GJs with carbenoxolone

As another proof of concept that the activation of GSL by cAMP in our Cx43 GJ assay is entirely attributed to GJs, we analyzed concentration-dependent inhibition of GJ by a broad-spectrum GJ inhibitor, carbenoxolone. The assay was exactly performed as explained earlier, except that after the replacement of full growth medium in the co-cultures by assay buffer, the GJ inhibitor carbenoxolone (CBX) was added followed by incubation for 45 min. To rule out that the inhibitor-mediated drop in the luminescence signal might not be Cx43 GJ-specific, biosensor cells were incubated with increasing concentrations of CBX under the same conditions.

As illustrated in Figure 38A CBX up to 30 μM had minor effects on the luminescence readout as compared to control. Conversely, as further depicted in Figure 38C, treatment with CBX (30 μM) completely blocked the GJ-mediated cAMP transfer in co-cultures, leading to a drop in the luminescence signal to control level. Treatment with CBX (3 μM) and (10 μM) resulted in about 50% and 80% reduction in luminescence after 30 min, respectively. The inhibition of cAMP-dependent luminescence determined by CBX is thought to be GJ-specific. In order to simplify the visualization of CBX-mediated inhibition of GJs, the maximal luminescence signals at a specific time point (19 min) for all samples are plotted as a bar-diagram (Figure 38B & 38D). These values were further used to draw an inhibition curve of CBX, resulting in an estimated IC_{50} value of $10.4 \pm 6.60 \mu\text{M}$ (Figure 38E). This estimated IC_{50} value is in the same order of magnitude as the previously reported IC_{50} value of 2.1 μM determined by iodide-sensing YFP^{QL} assay.²⁰⁶ The herein calculated IC_{50} value of 10.4 μM is an estimation, a more precise value can be obtained by performing the assay using stably transfected cell lines and using a broader range of CBX concentrations. However, our results clearly indicate that the current assay should be suitable for the identification of Cx43 GJ modulators in compound library screening campaigns.

3 Screening assay for connexin 43 gap junctions

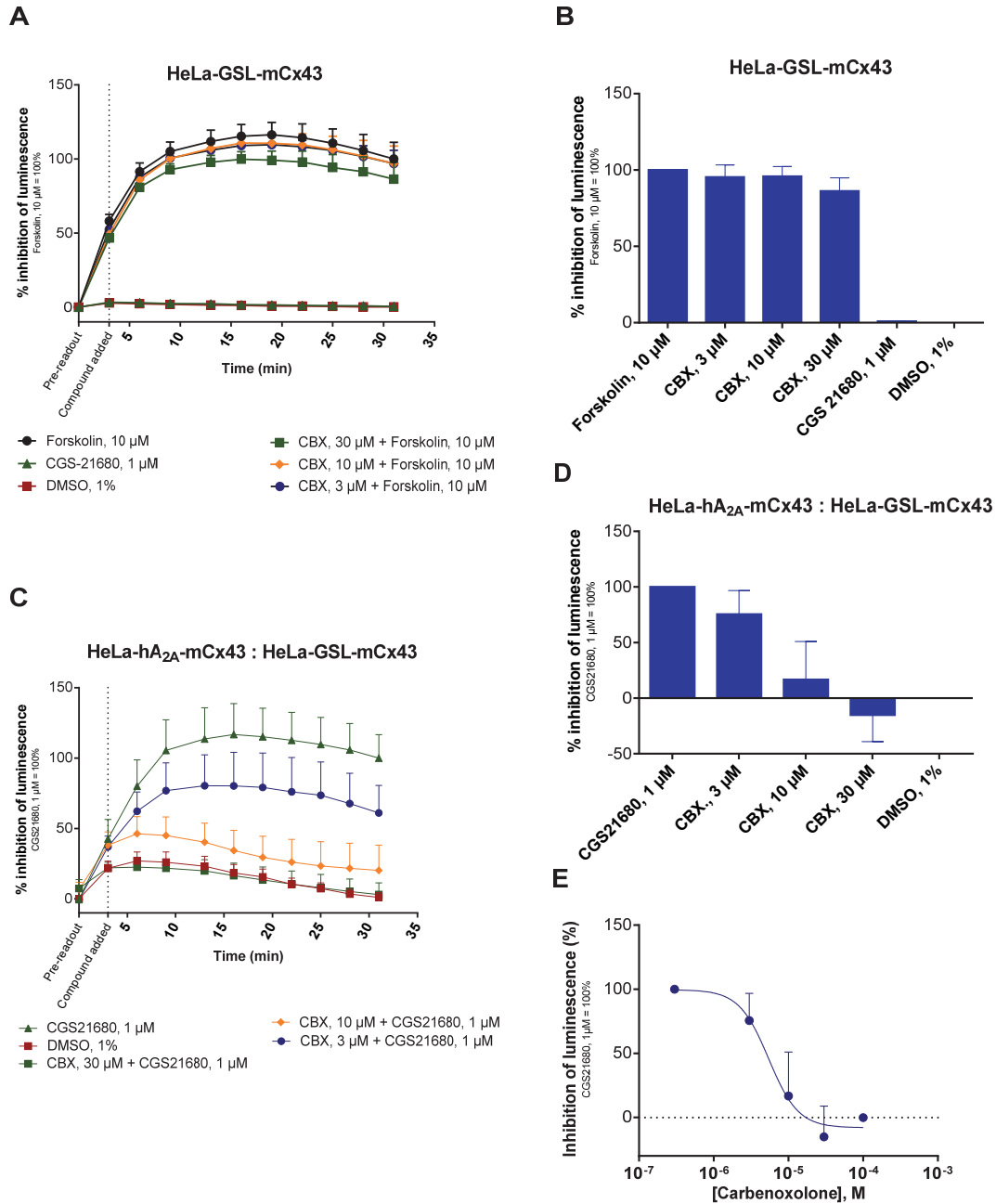


Figure 38: Concentration-dependent inhibition of Cx43 GJs by carbenoxolone (CBX). (A) Biosensor cells co-expressing mCx43 and GSL were incubated with increasing concentrations of CBX together with assay buffer for 45 min prior to activation by forskolin (10 μ M). Activation with Forskolin without inhibitor was taken as a positive control and incubation with 1% DMSO served as a negative control. (B) Concentration-dependent inhibition of maximal luminescence at a single time point after 19 min. (C) Co-cultured donor and biosensor cells (3:1) incubated with increasing concentrations of CBX together with assay buffer for 45 min prior to activation with CGS21680 (1 μ M). Activation of co-cultures with CGS21680 represents the positive control and incubation with 1% DMSO served as a negative control. (D) Concentration-dependent inhibition of GJs by CBX at a single time point after 19 min. (E) Estimated IC₅₀ value (10.4 \pm 6.60 μ M) of carbenoxolone at mCx43 GJs. Data are means \pm SEM of two to three individual experiments.

3 Screening assay for connexin 43 gap junctions

3.2.8 Suitability as a HTS assay

The ultimate goal of developing an HTS Cx43 GJ-assay was to efficiently and easily screen large compound libraries for Cx43 GJ modulators. We evaluated the suitability of the current assay by calculating the screening window coefficient known as Z' -factor. It is a dimensionless and statistical characteristic which provides valuable information that how good is the separation between positive and negative controls. The luminescence pre-readout of the co-cultures was used as a negative control and the luminescence signal upon reaching a plateau after 19 min of stimulation with CGS21680 (1 μ M) was taken as a positive control (see Figure 39). The Z' -factor for the current assay was calculated to be 0.5 corresponding to an HTS assay of good quality.¹¹² Thus, based on the evaluation of quality, the current assay can be implemented as an HTS platform.

Previously reported HTS assay measuring Ca^{2+} propagations through Cx43 GJs determined a $Z' > 0.4$.¹⁹⁵ In that assay Ca^{2+} generated in donor cells (HeLa- α 1A-Cx43) diffused via Cx43 GJs into recipient cells (HeLa- aequorin-Cx43), where the free calcium sensing protein aequorin produced a luminescence signal. It is well established that increased intracellular Ca^{2+} concentration can close Cx43 GJs via two key mechanisms, i) PKC-mediated phosphorylation of Ser³⁶⁸, and ii) Ca^{2+} bound calmodulin (CaM)-mediated direct inhibition. Since the reported assay measured integrated luminescence for only 40 s after the agonist addition, it is less likely that PKC-mediated GJ closure occurs, which was measured between 6 and 15 min. However CaM-mediated GJ closure was observed within seconds (30-90 s) particularly in the presence of extracellular Ca^{2+} up to 5 mM.²¹⁴⁻²¹⁵ Furthermore, alone intracellular Ca^{2+} overload can close GJ, however it is not well understood whether Ca^{2+} ions directly bind to GJs and close them.¹⁹⁴ Thus an assay based on Ca^{2+} propagation to investigate Cx43 GJs may only reflect a partial number of open GJ channels. In contrast, our assay holds a clear advantage over this assay, since cAMP-mediated closure of GJs has not been reported.

Another newly described Cx43 GJ assay, which measures the iodide propagations through the GJs reported a Z' of 0.7.²⁰⁶ This assay used a selective iodide transporter in donor cells and measured the iodide-mediated quenching of a yellow fluorescent protein variant (YFP^{QL}) in the recipient cells. However only a maximum quenching of about 45% in response to high

3 Screening assay for connexin 43 gap junctions

concentrations of NaI (70 mM) was demonstrated. This assay does not measure a physiological event which may additionally contribute to false-positive results.

Generally the GJ-mediated coupling in HTS format is measured indirectly with the aid of other components such as receptors, transporters, and ion sensing proteins, due to which the likelihood of false positive hits increases. Therefore hits should be reconfirmed using another testing system such as the scrape loading method. A detailed comparison of all three assays is presented in Table 9.

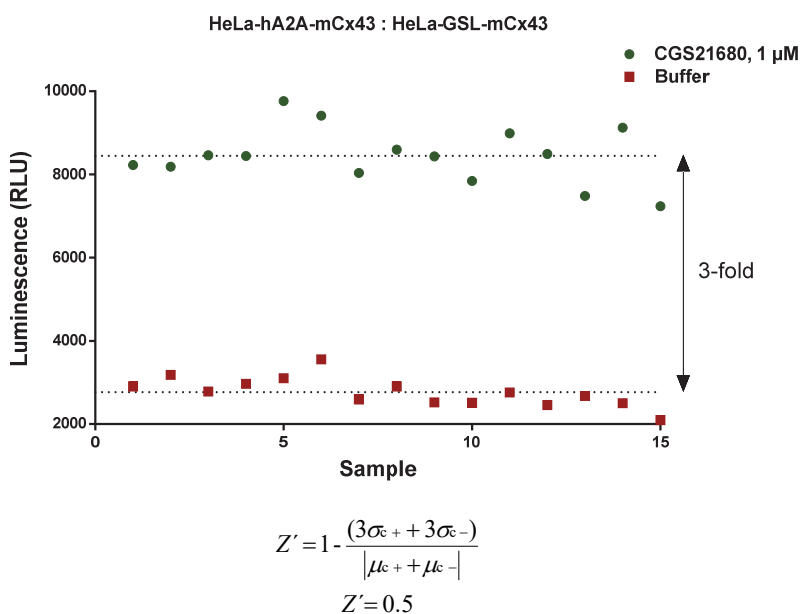


Figure 39: Suitability of cAMP assisted Cx43 GJ assay as a HTS assay. The quality of the assay was assessed by calculating the screening window co-efficient (Z' -Factor) as previously described by Zhang et al., (1999).¹¹² A co-culture of donor (90,000 cells/well) and biosensor (30,000 cells/well) cells at a ratio of 3:1 was incubated in assay buffer for 45 min as described in methods section. Prior to addition of CGS21680 (1 μM) to the co-culture, a pre-read of wells was taken which represented the negative control (red). The co-culture was then activated by adding CGS21680 (1 μM). The stabilized luminescence signal 19 min after stimulation was taken as a positive control (green). σ , standard deviation; μ , mean; c_+ , positive control; c_- , negative control.

3 Screening assay for connexin 43 gap junctions

Table 9: Comparison of cell based Cx43 gap junction high-throughput screening assays

	Ca ²⁺ -sensing aequorin assay ¹⁹⁵	Iodide-sensing YFP ^{QL} assay ²⁰⁶	cAMP-sensing luciferase assay
Invasiveness	Noninvasive	Noninvasive	Noninvasive
Cell line used	HeLa (Heterologous Cx43)	LN215 & HOS (Endogenous Cx43)	HeLa (Heterologous Cx43)
Reagent used	Coelenterazine	NaI	Luciferin
Read-out format	Luminescence enhancement	Fluorescence quenching	Luminescence enhancement
Measurement time	40 s / well	10 s / well	10 min / well
Cells / well in a 96-well plate	60,000*	not given	120,000
Z'-Factor	> 0.4	0.7	0.5
Advantages	Measures a physiological event (intracellular Ca ²⁺) Short measurement time in kinetic mode (40 s) Fully automated in 384-well format	Cost effective Short measurement time in kinetic mode (10 s) Partially automated in 96-well format	Measures a physiological event (intracellular cAMP) No cAMP-mediated GJ channel closure Highly potent A _{2A} -selective agonist CGS21680 (K _i 17.8 nM) ²³¹ Stable luminescence signal for up to 30 min
Disadvantages	Onset of Ca ²⁺ /CaM-mediated inhibition of GJs after ca. 30-90 s ²¹⁴⁻²¹⁵ Costly substrate Luminescence signal above background with 5 μM of phenylephrine in control co-culture with no Cx43 Moderately potent and less selective α1A agonist phenylephrine (K _i 6.3 μM) ²³²⁻²³³ Sources of false positives: i) α1A or TrpVI ii) Aequorin iii) Intracellular Ca ²⁺	Measures a non-physiological event (I ⁻ transport) High expression of a large SLC26A4 (780 aa) may be difficult Maximum quenching of YFP ^{QL} of about 45% by 70 mM NaI Background of other connexin subtypes not known Sources of false positives: i) SLC26A4 ii) I ⁻ permeability iii) YFP ^{QL}	Long measurement time in kinetic mode after about 10 min the agonist addition Costly substrate Temperature sensitive Sources of false positives: i) A _{2A} AR ii) Luciferase iii) Intracellular cAMP

LN215, LN215 glioma cells; HOS, Human osteosarcoma cells; CaM, calmodulin protein. DeFilippo et al. 2016,²³¹ (Churchill et al. 2001, Lurtz and Louis 2007),²¹⁴⁻²¹⁵ (Takanobu et al. 1999, Crassous et al. 2009).²³²⁻²³³

3.3 Summary

Cx43 is the most abundant and widely expressed GJ protein in humans, and it is the predominant Cx found in astrocytes. Changes in the expression pattern of Cx43 have been linked to neurological disorders such as depression, epilepsy, and brain metastasis. Lately it has been reported that the antiepileptic drug levetiracetam (LEV) restored the functional coupling of GJs in inflammation-induced uncoupled astrocytes. Due to the crucial role of Cx43 GJs in the crosstalk between astrocytes and of astrocytes and neurons to maintain a healthy neuronal microenvironment, Cx43 GJs are gaining increased attention as promising therapeutic targets for treating brain disorders.

In this project, we initially investigated the affinity of the Cx43 protein for the LEV derivative brivaracetam (BRV) in its ³H-labeled form using radioligand binding assay. The results from the binding assays indicated that there appears to be no direct high-affinity binding site for BRV neither on human nor on mouse Cx43. To date, only few, moderately potent and selective ligands of Cx43 are known. The development of potent Cx43 GJ modulators is probably hindered by the lack of suitable screening assays. The first HTS assay using the second messenger Ca²⁺ and its sensor aequorin to investigate Cx43 GJs was reported in 2013 by GlaxoSmithKline.¹⁹⁵ Another Cx43 GJ assay was reported by Lee et al. (2015), which used iodide and its sensor YFP^{QL}.²⁰⁶ Both assays exhibit a number of drawbacks, and therefore improved HTS assays are urgently required for the detection and characterization of Cx43 GJ modulators.

In this chapter the development of a new HTS assay was described for Cx43 GJ modulators. To execute the assay we established a donor cell line co-expressing A_{2A}ARs and Cx43, and a biosensor cell line co-expressing cAMP sensing luciferase and mCx43. The assay principle is relatively simple: activation of the G_s protein-coupled A_{2A}AR in the donor cells with a specific agonist (CGS21680) generates cAMP, which traverses via Cx43 GJs into the biosensor cells. Upon cAMP-mediated activation the luciferase catalyzes the oxidation of luciferin producing luminescence. The screening window coefficient Z'-factor of the current assay was calculated to be 0.5, which confirms its suitability as an HTS assay. The newly established assay has the potential to be applied to other Cx subtypes and may also be implemented for investigating heterotypic GJ coupling.

4 Quantification of GFP-tagged membrane proteins by CGE-LIF

4.1 Introduction

Proteins represent biological targets of the vast majority of approved drugs.²³⁴ The protein targets mainly include receptors (44%), enzymes (29%), and transporters (15%).²³⁵ Of these membrane proteins constitute targets for about 60% of all approved drugs, alone ca. 36% of the available drugs target G protein-coupled receptors (GPCRs).²³⁵⁻²³⁶ Detection and quantification of recombinant membrane proteins is mostly crucial for pharmacological investigations and therefore usually a reporter tag is attached to the *N*- or *C*-terminus of protein of interest (POI). Fluorescent labeling is the most powerful and widely used method for the detection of POIs. For such investigations POIs can be tagged with i) autofluorescent protein (e.g. green fluorescent protein, GFP), ii) self-labeling enzyme (e.g. Halo tags and SNAP/CLIP tags), and iii) short peptide sequence that covalently react with biarsenical dyes (e.g. FLAsH and ReAsH).²³⁷ However, autofluorescent proteins particularly GFP is still extensively used, since it offers robustness, produce low autofluorescent background, and do not require a secondary reaction component.²³⁷⁻²³⁸

The wild-type GFP (wt GFP) extracted from the jelly fish *Aequorea victoria* is a naturally fluorescent protein with a molecular mass of around 27 kDa.²³⁹ A tripeptide sequence of Ser⁶⁵-Tyr⁶⁶-Gly⁶⁷ in wt GFP makes up the chromophore located in the center of a β -sheet barrel structure.²⁴⁰ GFP is a very stable protein and resistant to high pressure (600 MPa), heat, alkaline pH, detergents, chaotropic salts, organic solvents, and several proteases.²⁴¹ GFP fused as a tag on either terminal of the protein of interest in most cases does not interfere with protein's native function.^{240, 242} Several mutants of GFP have been generated to improve and modify its stability and fluorescent properties. A commonly used variant is enhanced GFP which has a higher signal intensity than wt GFP. This variant displays two mutations (Phe64Leu and Ser65Thr) in the chromophore region with an excitation peak at 488 nm and an emission peak at 509 nm.²⁴³ GFP has a wide range of applications. It has been extensively used as a reporter for transfection and gene expression in mammalian cells.²³⁹ The applicability of GFP as a fluorescent reporter offers valuable information about the expression level and localization of the labeled protein in the given system, such as mammalian cells.²⁴⁴

4 Quantification of GFP-tagged proteins by CGE-LIF

Frequently applied methods to analyze GFP-fused proteins are fluorescence microscopy, flow cytometry, and fluorescence measurement in suspension or after solubilization by direct fluorimetry.²⁴⁵⁻²⁴⁶ Despite the usefulness of these methods, they pose limitations to, for example quantification of low-abundance GFP-tagged proteins and detection limit due to autofluorescence of cellular components, particularly in cellular homogenates.²⁴⁶ Western blotting, a gold standard for protein detection, can be also utilized to roughly quantify the GFP-tagged proteins by using primary antibodies against the GFP-tag.²⁴⁷ However, Western blotting is an error-prone multistep procedure and it can last up to more than 24 hours to obtain the final results.

Capillary electrophoresis (CE) is a fast, low-cost and powerful separation technique that has been highly useful in genomics and proteomics.²⁴⁸⁻²⁴⁹ CE coupled to a laser-induced fluorescence detector (CE-LIF) has been successfully used for the analysis of proteins,²⁵⁰⁻²⁵² especially free GFP or GFP-tagged proteins in various biological materials.^{246, 253-256} The CE-LIF has, for example, been successfully used to separate free GFP from the GFP-antibody complex with high resolution and sensitivity.²⁵³ Furthermore, the CE-LIF has been applied to analyze cell-to-cell variation in GFP expression in single bacteria.²⁴⁶ This technique has been also employed to analyze the conversion of I-form of GFP-tagged microtubule-associated protein light chain 3 (GFP-LC3), an autophagy marker, to its II-form in an extract of HeLa cells which were pretreated by starvation or application of chloroquine (CQ).²⁵⁴ The CE-LIF method has been also used to investigate the autophagy organelles isolated from rat L6 cells by counting GFP-LC3.²⁵⁵ Swearingen et al. (2010) has also applied the CE-LIF to quantify cell death by measuring the GFP released from cells due to membrane degradation in treating with staurosporine or exposing to H₂O₂.²⁵⁶ However, all those CE-LIF methods have limitation to quantify the GFP and GFP-labeled proteins since the protein adsorption on the capillary inner surface due to application of bare fused silica capillaries cannot be avoided in an aqueous buffer system.

To address this issue we came up with the idea of establishing a capillary gel electrophoresis method with laser-induced fluorescence detection (CGE-LIF) method to quantify recombinantly expressed GFP-fused proteins in a complex mixture of cellular homogenates. Here we have demonstrated that the CGE-LIF can be used to quantify different types of GFP-

4 Quantification of GFP-tagged proteins by CGE-LIF

fused membrane proteins in a crude cellular homogenate. Furthermore, we compared the newly developed CGE-LIF method with commonly used simple fluorimetric measurements. Finally, we compared the determined amounts of the GFP-fused proteins by using the CGE-LIF method with those obtained by applying radioligand binding assays.

The results shown in the next section are included in the manuscript (in preparation):

- Danish, A.*; Lee, SY.*; Müller, C. E. Quantification of green fluorescent protein (GFP)-tagged membrane proteins by capillary gel electrophoresis

*Both authors contributed equally to this study.

4 Quantification of GFP-tagged proteins by CGE-LIF

4.1.1 CGE-LIF setup

In order to avoid protein adsorption on the capillary inner surface, we applied here the capillary electrophoresis coupled with the laser-induced fluorescence detector (CE-LIF). The design of the detection set-up is illustrated in Figure 40. Firstly, a semi-liquid gel is filled into the fused-silica capillary. Application of pressure at both in- and outlet sides allows the maintenance of the gels inside. Since the proteins in the crude cellular homogenates are treated with a reaction buffer including 1% of sodium dodecylsulfate (SDS), they are incorporated into negatively charged micelles. All negatively charged proteins are then separated based on their molecular weights. Consequently, all proteins in the homogenate reach the detector, but only GFP-tagged proteins are selectively recorded at the LIF detector.

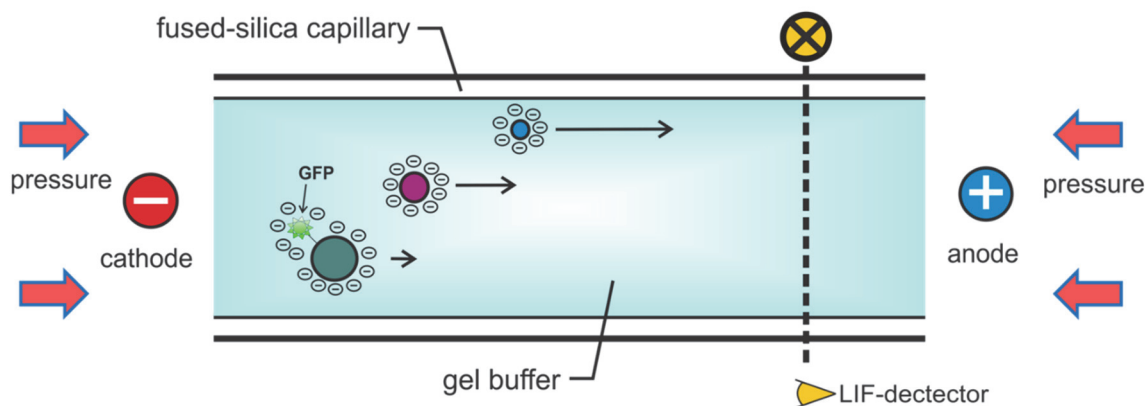


Figure 40: Schematic representation for the detection of GFP-tagged proteins using CGE-LIF. Crude cellular homogenate containing recombinant GFP-tagged protein (green circle) and non-fluorescent cellular proteins (violet and blue circles) is diluted in a Tris buffer containing 1% SDS. The sample is then electrokinetically injected into a fused-silica capillary filled with a gel buffer containing semi-liquid gels. The complex mixture of cellular proteins in the cellular homogenate is resolved in the applied electric field based on their molecular weights by applying a high voltage. The proteins are negatively charged due to their inclusion in SDS micelles and then migrate from cathode to anode. Only the GFP-tagged proteins are detected by a LIF detector. CGE: capillary gel electrophoresis, GFP, green fluorescent protein, LIF: laser-induced fluorescence, SDS: sodium dodecylsulfate.

4.1.2 Calibration curve with GFP using CGE-LIF

Initially the CGE-LIF method was used to monitor the concentration-dependent increase in peak area of various concentrations of free GFP ranging from 0.929 to 92.9 nM. A strict linearity was shown with a R^2 value of 0.9701 (see Figure 41). We determined a limit of detection (LOD) of 5 nM (0.168 $\mu\text{g/ml}$) and a limit of quantification (LOQ) of 15 nM (0.508 $\mu\text{g/ml}$). This value is similar to the determined LOD value of 3 nM by Korf et al., but considerably higher as compared to the determined LOD value of 2 pM in Turner et al., both using a free GFP standard protein but a CE-LIF method without filling with gels.^{246, 253} Turner et al. used a short and thin fused-capillary (20 cm of the effective length and 10 μm of the inner diameter) compared to the fused-capillary (50 cm of the effective length and 50 μm of the inner diameter) used in our investigations. This resulted in the better LOD into the picomolar range. Initially we also used a fused-silica capillary without any gels inside, however it resulted in high protein adsorption and non-reproducibility of measurements with the pure GFP protein, therefore we established a method using semi-liquid gel (in SDS-MW gel buffer). Our newly developed method showed high robustness and reproducibility of the results with less than 2% relative standard deviation (RSD) (see Table A1 in appendices). The calibration curve with the free GFP was subsequently used for quantification of recombinantly expressed GFP-fused transmembrane proteins in cellular homogenates.

4 Quantification of GFP-tagged proteins by CGE-LIF

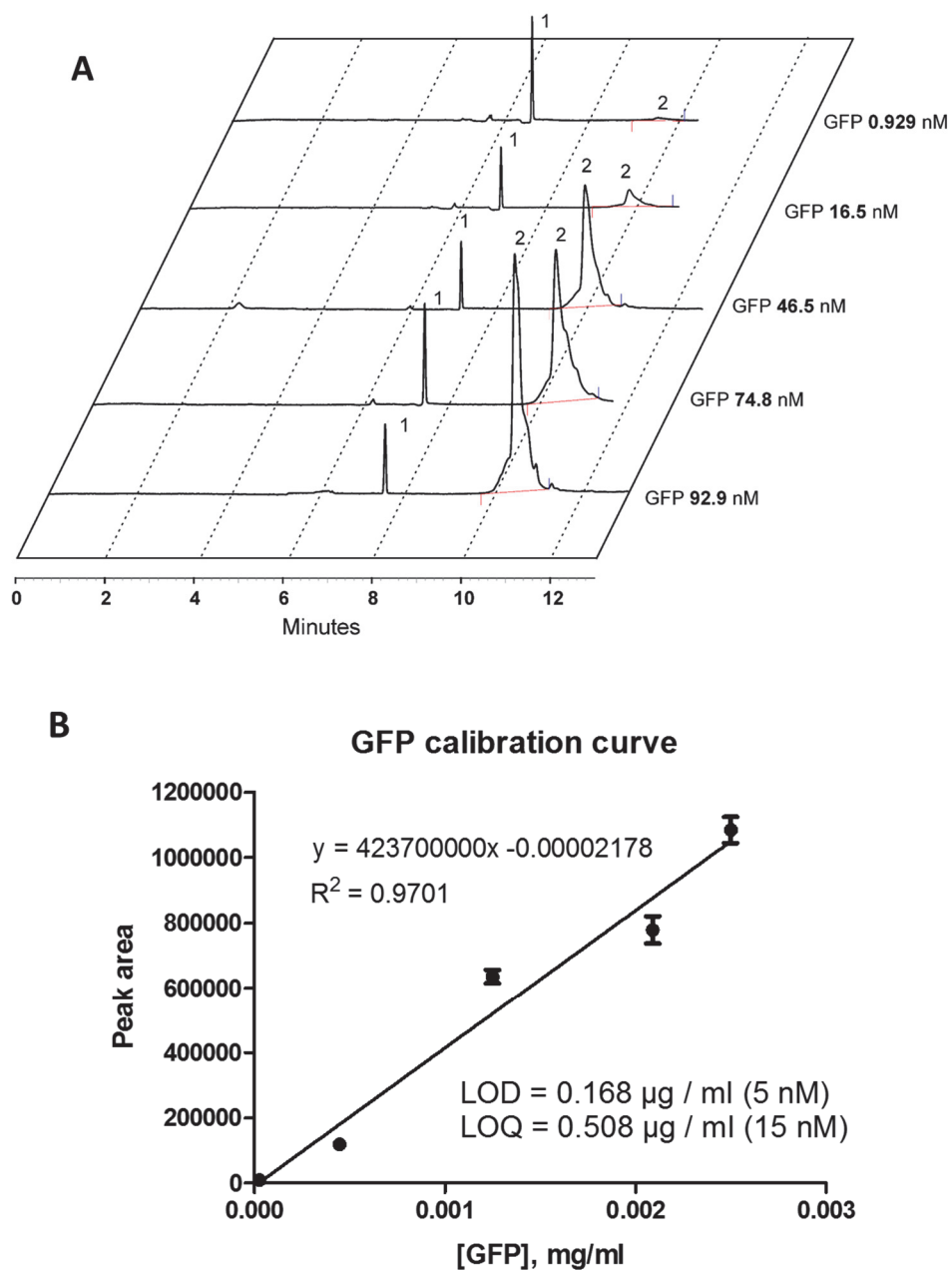


Figure 41: Calibration curve with free GFP standard protein by CGE-LIF. **(A)** Electropherogram of free GFP used as standard at different concentrations analyzed at -15 kV and electrokinetic injection (peak 1: autofluorescence, peak 2: GFP). **(B)** Calibration curve obtained by plotting free GFP concentration in mg/ml on the X-axis and corresponding peak area on the Y-axis. Data points in the calibration curve show means \pm SD of three independent experiments. LOD: limit of detection; LOQ: limit of quantification.

4 Quantification of GFP-tagged proteins by CGE-LIF

4.1.3 Calibration curve with GFP using direct fluorimetry

For comparison we determined the LOD of GFP using a microplate fluorimeter. Concentration-dependent fluorescent signals were observed and a LOD of 25.7 nM and a LOQ of 78.0 nM was determined (see Figure 42). Thus, the sensitivity was about 5-fold lower than that of the newly developed CGE-LIF method. Importantly, the CGE-LIF method offers the great advantage of protein separation and allows the distinction of the protein to be analyzed from its degradation products and impurities.

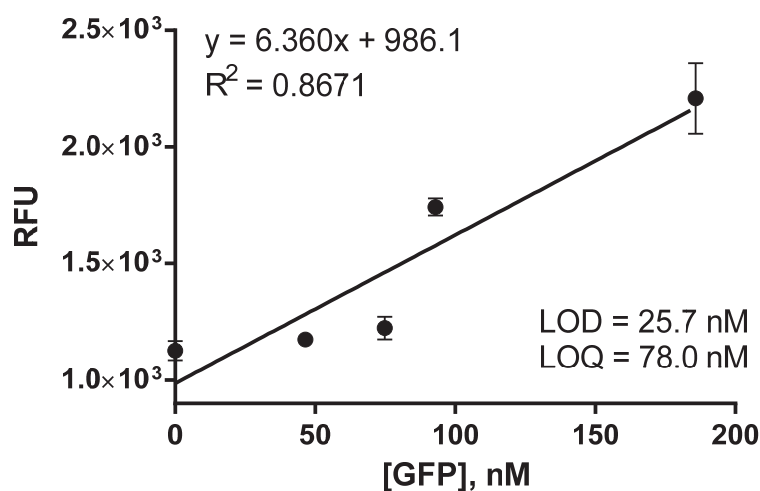


Figure 42: Calibration curve of GFP determined in a fluorimeter. The calibration curve was obtained by plotting the free GFP concentration in nM on the X-axis and the corresponding fluorescence intensity on the Y-axis. The fluorescence of free GFP was measured in a black solid-bottom 96 well plate with a fluorescence plate reader. Data points in calibration curve show means \pm SD of three independent measurements. LOD: limit of detection, LOQ: limit of quantification, RFU: Relative fluorescence units.

4.1.4 Quantification of recombinant GFP-fused proteins

We showed by determining a GFP standard curve that the CGE-LIF method can efficiently detect very low amounts of GFP. This method was exploited to detect and quantify recombinantly expressed GFP-fused transmembrane proteins in cellular homogenates without any prior isolation or purification of the proteins. For the analyses, membrane proteins of various classes such as 12-, 7- and 4- transmembrane proteins were selected to assess the scope of the new method. Synaptic vesicle 2A protein (SV2A) is a 12-transmembrane domain protein (ca. 90 kDa) with intracellular *N*- and *C*- termini. SV2A is ubiquitously found in brain

4 Quantification of GFP-tagged proteins by CGE-LIF

(neuronal cells) and involved in neurotransmitter exocytosis.^{43, 64} The A_{2A} adenosine receptor (A_{2A}AR) is a seven-transmembrane receptor (ca. 45 kDa) with an extracellular *N*-terminus and an intracellular *C*-terminus.²⁵⁷⁻²⁵⁸ The A_{2A}AR is expressed in the human body and mediates anti-inflammatory, immunosuppressive and hypotensive effects. It is a drug target for Parkinson's disease and a potential target in immunooncology.²⁵⁷⁻²⁵⁸ Connexin 43 (Cx43) is a four-transmembrane protein (ca. 43 kDa) with intracellular *N*- and *C*- termini. Oligomerization of six Cx43 proteins gives rise to Cx43 gap junctions, the most abundant and widely expressed types of gap junctions.⁸⁶ We used 1% SDS in sample buffer to solubilize the cell membrane preparations prior to CE analysis.

Human SV2A with a GFP-tag at its *C*-terminus was stably expressed in CHO cells and the monoclonal lines with the highest SV2A-GFP expression were picked by fluorescence assisted cell sorting (FACS). The cells were homogenized to prepare cellular homogenate. Before using the homogenate for the CGE-LIF method, we monitored the concentration-dependent fluorescence signals using a fluorimeter. The homogenate of non-transfected CHO cells was used as a negative control. The increase in fluorescence intensity was found to be directly proportional to the amount of homogenate containing SV2A-GFP, while for control, negligible increase in fluorescence could be determined (see Figure 43).

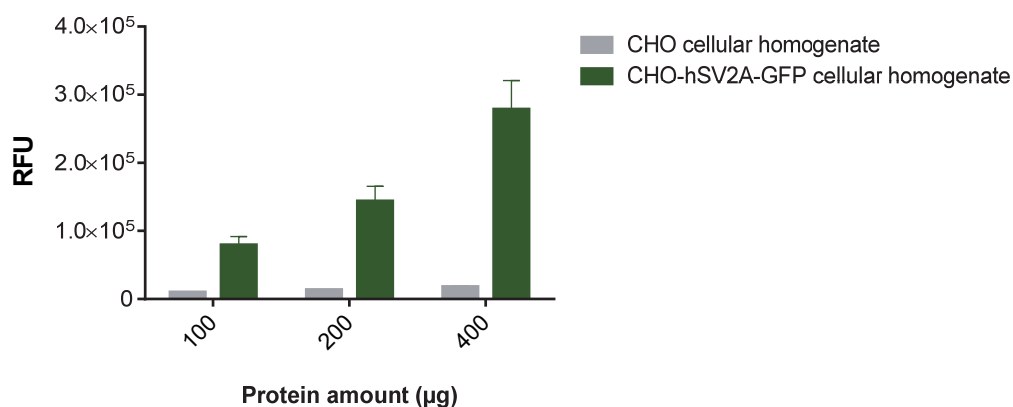


Figure 43: Determination of fluorescence in cellular homogenates of non-transfected CHO cells and hSV2A-GFP-expressing CHO cells. RFU: relative fluorescence unit. Data shown are means \pm SEM of three individual experiments performed in duplicate.

Next for the CGE-LIF analysis we used the cellular homogenates of three CHO cell lines expressing GFP-tagged hSV2A, hA_{2A}AR, and mCx43 proteins, respectively. As expected, the

4 Quantification of GFP-tagged proteins by CGE-LIF

electropherograms of SV2A-GFP-expressing solubilized cell homogenates showed reproducibly large peaks (see Figure 44A). A concentration of 26.7 pmol of SV2A-GFP per mg of protein was determined based on a calibration curve (see Figure 41 and for calculation see Section 6.6.4). Non-transfected CHO cell homogenates were used as negative controls. The electropherogram of the negative control was found to be background-free at the position of SV2A-GFP peak (see Figure 44A). Small peaks with shorter migration time in the electropherogram of SV2A-GFP might represent proteolytic degradation products. As an additional control to assess the resolution quality of proteins by this method, we spiked the SV2A-GFP-containing sample with free GFP and analyzed it with CGE-LIF. Two baseline-separated peaks were obtained, free GFP showing a shorter migration time, while SV2A-GFP had a longer migration time due to its higher protein size (see Figure A1 in appendices).

Next, the SDS-solubilized cellular homogenates containing GFP-tagged A_{2A}AR and Cx43 proteins, respectively, were subjected to CGE-LIF analysis. Figure 44B and C represent the electropherograms of the proteins. The calculated concentrations for the proteins based on the calibration curve for free GFP were 0.121 pmol of A_{2A}AR-GFP per mg of protein and 0.0398 pmol of Cx43-GFP per mg of protein.

To find out whether SDS lead to mediate protein degradation, the hSV2A-GFP cellular homogenate was incubated with 1% SDS for up to 4 h. The results showed that the protein was stable in the presence of 1%SDS (see Figure A2 in appendices).

4 Quantification of GFP-tagged proteins by CGE-LIF

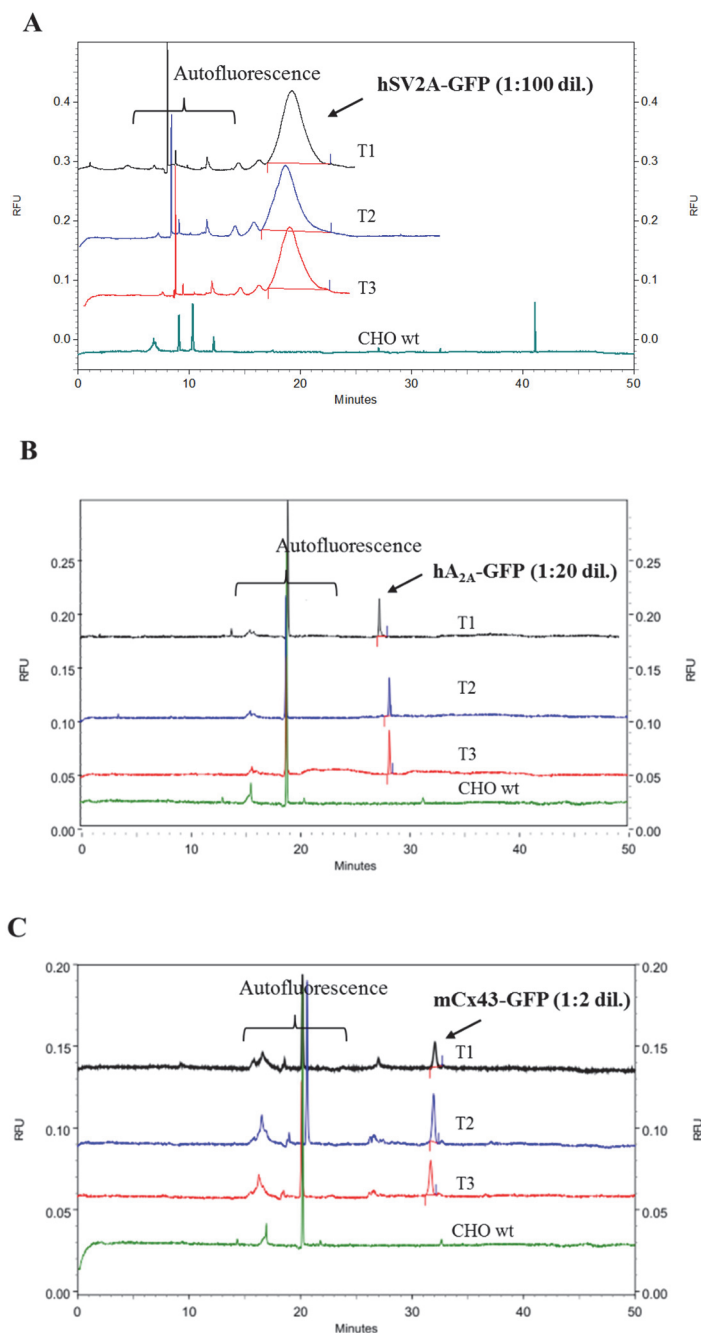


Figure 44: Detection and quantification of GFP-tagged recombinant proteins in SDS-solubilized CHO cell homogenates. (A) Electropherogram for the hSV2A-GFP (1:100 dilution), (B) Electropherogram for the hA_{2A}AR-GFP (1:20 dilution), and (C) Electropherogram for the mCx43-GFP (1:2 dilution). Samples were separated by -15 kV after electrokinetic injection. The calculated amounts of proteins were 26.7 ± 1.15 pmol of hSV2A-GFP per mg of protein, 0.121 ± 0.006 pmol of hA_{2A}AR-GFP per mg of protein, and 0.0398 ± 0.0040 pmol of mCx43-GFP per mg of protein. The experiments were performed in triplicates (T1 to T3) for each protein samples including wild-type CHO (wt CHO) as a negative control. RFU, relative fluorescence unit; m, Mouse; h, Human.

4 Quantification of GFP-tagged proteins by CGE-LIF

4.1.5 Quantification of SV2A and A_{2A}AR by radioligand binding assays

Radioligand binding assays are considered as important tools in pharmacology to determine the protein's affinity (K_d) for a ligand as well as the amount of protein (B_{max}) in a given biological sample. B_{max} values can be determined either by saturation binding assays or by homologous competition binding assays.²⁵⁹ In the latter method same compound in the labeled (single concentration) and the unlabeled (multiple concentrations) form is used in competition binding assays. Using this method for B_{max} value determination requires a lower amount of radioligand.²⁵⁹ In our lab radioligand binding assays for the SV2A and the A_{2A}AR are well established.²⁶⁰⁻²⁶¹ For Cx43 we could not determine its B_{max} value by radioligand binding since no radioligand is available for this protein. To validate our results obtained by the CGE-LIF method, we conducted homologous competition assays with hSV2A using [³H]BRV as a radioligand and unlabeled BRV as a competitor, whereas for hA_{2A}AR, [³H]MSX-2 was employed as a radioligand and unlabeled MSX-2 was used as a competitor (see Figure 45). It should be noted that the same batches of cellular homogenates were used for the radioligand assays and for the CGE-LIF analysis.

The density (B_{max}) of hSV2A-GFP per mg of protein in the cell homogenate was found to be 4.19 ± 0.52 pmol (see Figure 45A) which is significantly 5-fold lower than 26.7 ± 1.15 pmol obtained by CGE-LIF method (unpaired two-tailed *t*-test) (For B_{max} calculation see Section 6.7.2). As mentioned earlier that monoclonal cells with the highest expression of hSV2A-GFP, having highest plasmid copies, were used for preparation of homogenates. It is noteworthy that overexpression of heterologous proteins can lead to formation of protein aggregates and accumulation of unfolded proteins due to fully occupied cellular folding machinery.²⁶² These factors might compromise the binding sites of the ligands, while fluorophore might stay intact and contribute to the fluorescence. Since the intact binding pocket is critical for ligand binding, this hypothesis might explain the reason behind the difference. The B_{max} value for the hA_{2A}AR-GFP obtained in radioligand competition assays was found to be 0.319 ± 0.081 pmol/mg of protein (see Figure 45B) which is not significantly different from the value of 0.121 pmol/mg of protein determined by CGE-LIF (unpaired two-tailed *t*-test). These results indicate that the hA_{2A}ARs in the non-solubilized homogenate (no SDS added) are all in conformations with high-affinity for the radioligand and not partly in a denatured conformation. Considering the

4 Quantification of GFP-tagged proteins by CGE-LIF

comparison of the two methods, our results suggest that CGE-LIF is a reliable and sensitive method for the detection and quantification of GFP-tagged membrane proteins. Moreover, this kind of comparison can provide important information e.g. for crystallization, NMR structural studies, and cryo-electron microscopy.

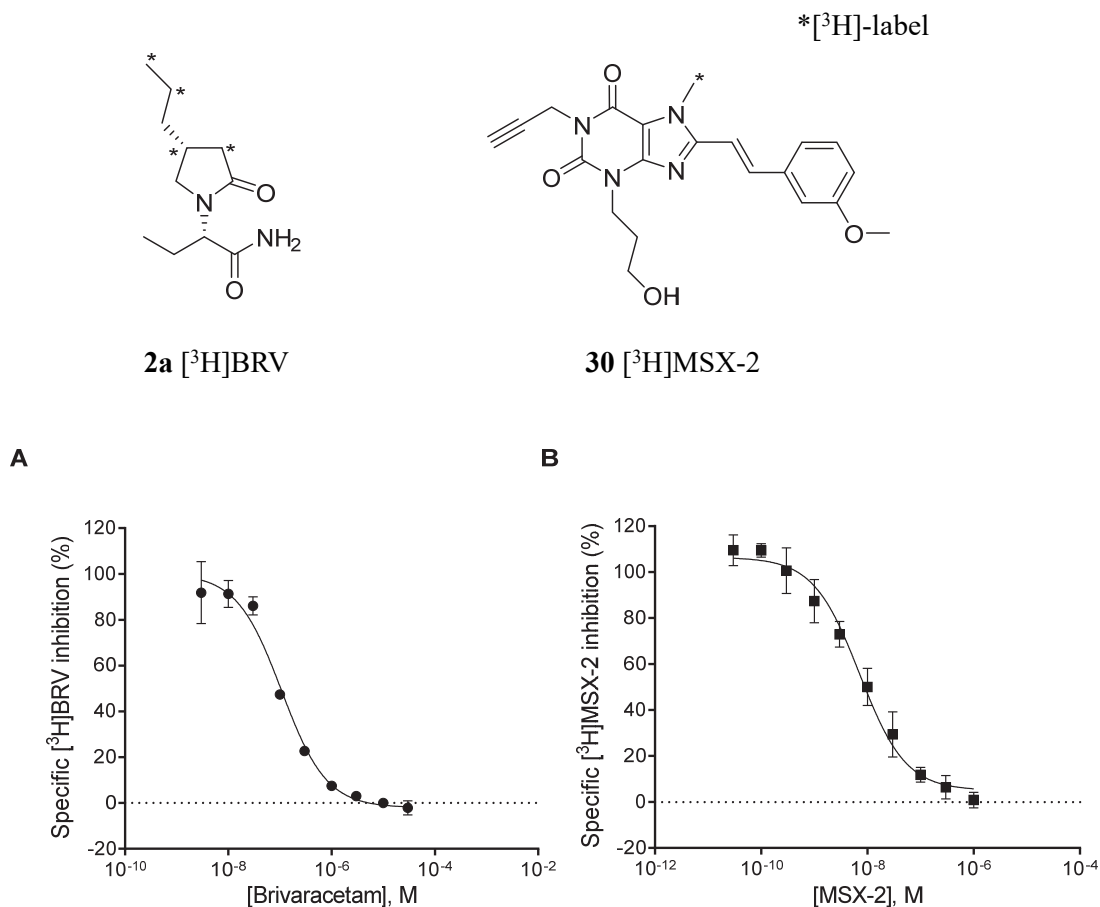


Figure 45: Homologous competition binding assays to determine the amount of radioligand binding sites (B_{\max}) in cell homogenates. Binding assays were performed with specific radioligands for hSV2A and hA_{2A}AR, respectively. **(A)** Concentration-dependent inhibition of [³H]BRV (3 nM) binding to hSV2A-GFP by unlabeled BRV yielded a B_{\max} value of 4.19 ± 0.52 pmol per mg of protein ($IC_{50} = 87.6 \pm 4.47$ nM; $K_i = 85.6 \pm 4.47$ nM). **(B)** Concentration-dependent inhibition of [³H]MSX-2 (1 nM) binding to hA_{2A}AR-GFP by unlabeled MSX-2 yielded a B_{\max} value of 0.319 ± 0.081 pmol per mg of protein ($IC_{50} = 7.46 \pm 1.83$ nM; $K_i = 6.76 \pm 1.83$ nM). Data points in the inhibition curves show means \pm SEM of at least three independent experiments. Protein determination was performed by the Bradford method.²⁶³

4.2 Summary

Detection and quantification of recombinant proteins fused to green fluorescent protein (GFP) are most frequently performed by fluorescence microscopy, flow cytometry, or by measuring fluorescence in suspension or in solution after solubilization. However, these methods have limitations such as low sensitivity and lack of precision due to high background autofluorescence. We have developed a fast, robust, and reproducible method to quantify GFP-tagged membrane proteins in a complex matrix of cell homogenates by using capillary gel electrophoresis coupled to a laser-induced fluorescence detector (CGE-LIF). A semifluid gel for CGE-LIF to reduce protein adsorption on the fused-silica capillary and to enhance peak resolution. Based on a calibration curve obtained with purified GFP using the CGE-LIF method, the amount of GFP-tagged protein of interest in solubilized cell homogenates was determined. CGE-LIF was found to be highly sensitive, displaying a limit of detection (LOD) of 0.168 µg/ml (5 nM) for GFP. The CGE-LIF method showed at least 5-fold higher sensitivity as compared to fluorimetric measurement in a microplate. Using CGE-LIF method three different types of GFP-tagged membrane proteins expressed in Chinese hamster ovary (CHO) cells, namely human synaptic vesicle protein 2A (hSV2A), human A_{2A} adenosine receptor (hA_{2A}AR), and mouse connexin 43 (mCx43) were quantified. Quantification of hSV2A and hA_{2A}AR using classical radioligand binding assays confirmed the results obtained with CGE-LIF. Comparison allows to distinguish between correctly folded protein and total protein. Importantly, the new method involves separation of the target proteins and their degradation products prior to quantification. In the future, the CGE-LIF method may be extended to other fluorescent proteins such as red fluorescent protein (RFP) and yellow fluorescent protein (YFP). Moreover, it may be applied to detect native proteins without GFP-tag in cell homogenates by using fluorophore-conjugated antibodies.

5 Summary and outlook

Despite the availability of more than twenty different antiepileptic drugs (AEDs) on the market, about one third of epileptic patients remains resistant to pharmacotherapy with existing drugs.²⁶⁴ All of the current AEDs exert their effects either by reducing excitatory or by enhancing inhibitory neurotransmission. Most of the AEDs produce these effects by modulating voltage-gated ion channels, ionotropic glutamate receptors, or by enhancing γ -aminobutyric acid (GABA)-mediated neurotransmission. Contemporary AEDs thus dampen epilepsy symptoms by targeting mechanisms involved in seizure generation, but do not provide a cure.²⁵ Thus major goals in the development of future AEDs include features like efficacy against refractory epilepsy, prevention for the onset of epilepsy “antiepileptogenic properties” in patients at risk (e.g. brain trauma, stroke, and tumor), disease-modifying properties, potential of broad use in non-epileptic central nervous system (CNS) disorders, and fewer adverse effects.^{47, 51} Investigating novel molecular targets and identifying antiepileptic agents with different mechanism(s) of action may substantially contribute to achieving these goals.

The discovery of synaptic vesicle protein 2A (SV2A) in 2004 to be the main target of the AED levetiracetam (LEV, Keppra[®]) demonstrated that novel targets for AED could be identified (see Figure I).⁴³ SV2A has been demonstrated to be involved in the recycling of vesicles containing neurotransmitters, however its exact function remains elusive. Moreover, SV2A-deficient mice showed a proepileptic phenotype with reduced anticonvulsive activity and binding of LEV.⁷⁴ LEV exhibits relatively a safe and tolerable profile and has shown promising disease-modifying properties in pharmaco-resistant animal models of epilepsy like in the kindled rats and the 6-Hz mouse model.²⁵ Exact functional consequences for SV2A upon LEV binding are not well understood, however studies suggest that LEV modulates the release of neurotransmitters. LEV exhibits additional mechanisms, and a striking characteristic of LEV is its ability to rescue connexin 43 (Cx43) gap junction (GJ) coupling in astrocytes which is impaired in epilepsy.⁴⁸ Since LEV binds to SV2A with modest affinity, brivaracetam (BRV, Briviact[®]), a 10- to 15-fold more potent derivative of LEV, was developed for improved antiepileptic properties. Brivaracetam has recently been approved by EMA and FDA as an add-

5 Project summary and outlook

on AED to treat partial onset seizures. Our group has recently reported the development of LEV and BRV in radiolabeled form.⁵⁷⁻⁵⁸

In the present study, a radioligand binding assay with [³H]BRV was established that is suitable for testing compound libraries for interaction with human SV2A expressed in Chinese hamster ovary (CHO) cells. The testing of 500 approved drugs in competition binding studies using [³H]BRV as a radioligand resulted in a hit rate of 3%. Hits were defined as compounds inhibiting the radioligand by $\geq 90\%$ at 20 μM test concentration. Subsequent testing at 2 μM resulted in the identification of the antihistaminic prodrug loratadine (K_i 1.16 μM), the antimalarial drug quinine (K_i 2.03 μM), and the anti-obesity drug rimonabant (K_i 2.73 μM) as the most potent SV2A ligands of the investigated library. Based on flexible alignment of brivaracetam, loratadine, and quinine, a pharmacophore model was generated which indicated an excellent steric and electronic fit of three drugs and in line with previously known structure-activity relationships (SARs). There are no reports on antiepileptic effects of loratadine, and it is also not likely due to its poor penetration through the blood-brain barrier (BBB) and its prodrug properties. On the other hand, several studies showed quinine to act as an antiepileptic agent. We conclude that the interaction of quinine with SV2A may explain its anticonvulsive effects observed in animal and clinical studies. This hypothesis warrants further investigations, for instance in SV2A-deficient animal models, or in the presence of negative allosteric modulators of SV2A.

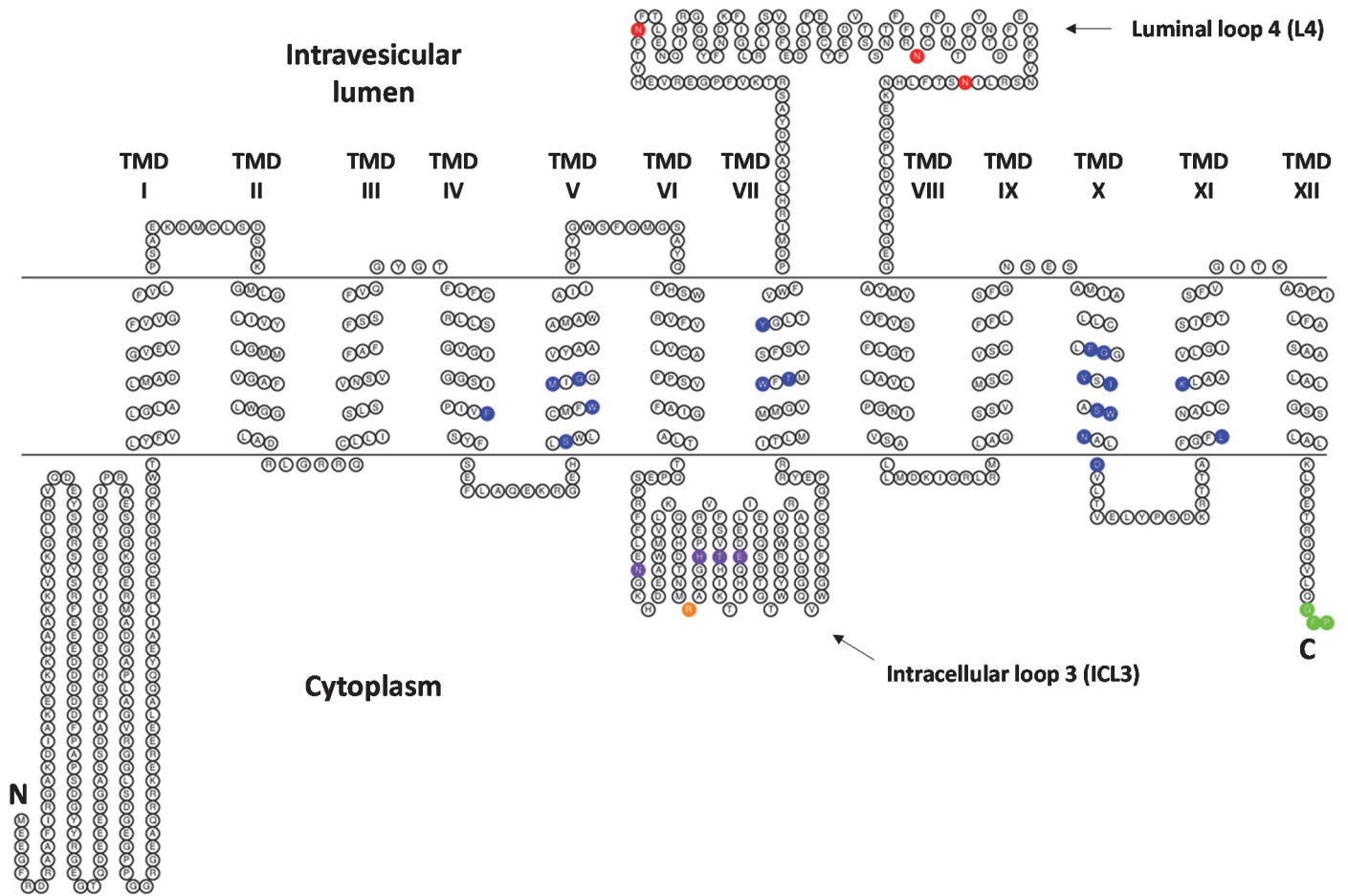


Figure I: Topology model of the human SV2A. The snake plot diagram was prepared by using the TOPO2 program along with the transmembrane domain predictions using the HMMTOP software.⁸⁰⁻⁸¹ Transmembrane domains are indicated with Roman numbers and N & C represent N- and C-termini. The amino acids depicted in blue color have been previously demonstrated to alter racetam binding by mutagenesis and docking studies.¹⁷⁷⁻¹⁷⁹ Amino acids shown in purple within ICL3 have been previously mutated to test the affinity of mutants for racetams, however binding was not altered.³⁸ The mutation of arginine within ICL3 depicted in orange color at position 383 is suggested to be a causal factor in intractable epilepsy.¹⁷⁶ The green GFP tag at the C-terminus indicates a green fluorescent protein (GFP) and the amino acids in red color denotes the N-glycosylation sites.

5 Project summary and outlook

Rimonabant is a potent antagonist of the cannabinoid CB₁ receptor and activation of this receptor was reported to result in anticonvulsive effects, while its blockade exerts proconvulsive effects.¹⁴³ However, paradoxically a single-time administration of rimonabant after a short interval of brain trauma prevented animals from developing seizures and we hypothesize that this might be due to its interaction with SV2A.¹⁴⁴ This finding prompted the idea of testing 80 cannabinoids including the most important components of the cannabis plant, the psychoactive Δ^9 -Tetrahydrocannabinol (THC) and the non-psychoactive cannabidiol (CBD). This screening campaign resulted in the identification of JWH-031 (K_i 0.618 μ M), AM-2232 (K_i 0.401 μ M), and CBD (K_i 0.719 μ M) (see Figure II & Figure III) as potent ligands for SV2A, however THC displayed no affinity for SV2A. Quite recently the CBD-containing preparation Epidiolex[®] obtained an orphan drug designation from EMA and FDA for the treatment of childhood-onset epilepsy syndromes, Lennox-Gastaut syndrome (LGS) and Dravet syndrome.¹⁴¹ Plausible CBD targets involved in translating its anticonvulsive effects are not well understood. The current results suggest that the anticonvulsive effects of CBD might be – at least partly – attributed to its interaction with SV2A, however further research in animal models is warranted. Moreover, since JWH-031 and AM-2232 are potent agonists at the CB₁R, the resulting SARs may provide a basis for the development of dual-target antiepileptic compounds.

The LEV/BRV binding site on SV2A remains elusive. As a contribution to the identification of the binding site, a possible involvement of the intracellular cytoplasmic loop 3 (ICL3) of

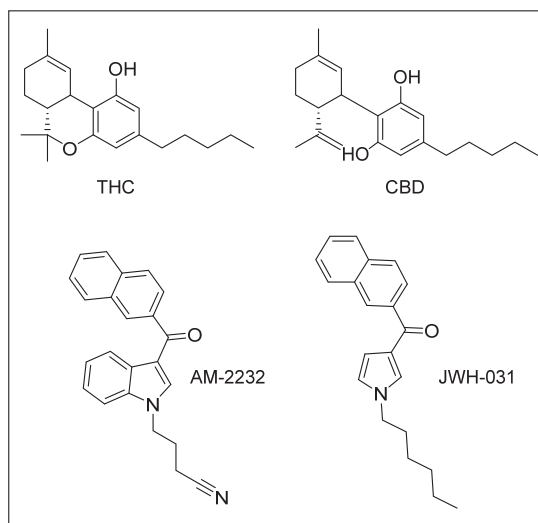


Figure II: Chemical structures of cannabinoids.

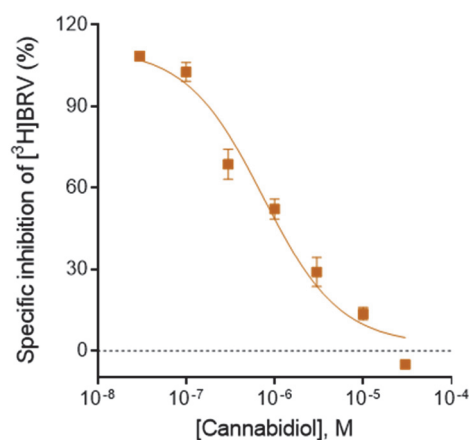


Figure III: Concentration-dependent specific inhibition of [³H]BRV binding to recombinant human SV2A by CBD, K_i value: $0.719 \pm 0.166 \mu$ M.

5 Project summary and outlook

SV2A to LEV/BRV binding was investigated. The ICL3 of SV2A contains an ATP binding site, and many SV2A-specific non-conserved amino acids. A point mutation (R383Q), which was reported to be responsible for intractable epilepsy in a patient, is also located in the ICL3 of SV2A.¹⁷⁶ Competition binding experiments with [³H]BRV on the SV2A-R383Q mutant by unlabeled LEV (IC_{50} wt 1.81 μ M vs. IC_{50} mutant 2.14 μ M) and BRV (IC_{50} wt 0.099 μ M vs. IC_{50} mutant 0.116 μ M) showed no significant differences in the IC_{50} values compared to wild-

type SV2A. However, JWH-031 (IC_{50} wt 0.643 μ M vs. IC_{50} mutant 5.99 μ M, 9-fold shift) and CBD (IC_{50} wt 0.748 μ M vs. IC_{50} mutant 20.7 μ M, 28-fold shift) showed significant shifts in IC_{50} values. Chimeric proteins were constructed with the whole ICL3 of SV2A exchanged for that of SV2B (SV2A-SV2B-ICL3) and the ICL3 of SV2B exchanged for that of SV2A (SV2B-SV2A-ICL3). Interestingly, specific [³H]BRV binding was completely abolished in both chimeric proteins (see Figure IV), which is in line with the previous findings with exon 5 and/or exon 6 deletion mutants of SV2A.³⁸ These results indicate a possible involvement of the ICL3 of SV2A for LEV/BRV binding. To further narrow down the site within the ICL3 that is involved in LEV/BRV binding, chimeric proteins with small regions exchanged within the ICL3 should be constructed and tested in the future. Botulinum neurotoxin A (BoNT/A) and galactose are known to interact with SV2A. In the present study, investigations to find out the effects of (BoNT/A) and galactose on [³H]BRV binding to SV2A demonstrated that neither of them affected [³H]BRV binding.

Cx43 is the most widely expressed GJ protein in humans, and it is the predominant Cx found in astrocytes. Over the last decade Cx43 GJs have gained increased attention as promising potential therapeutic targets for treating brain disorders including epilepsy. Since LEV was previously demonstrated to modulate Cx43 GJs in astrocytes, the affinity of [³H]BRV for Cx43 was investigated using radioligand binding. The results indicated that there appears to be no

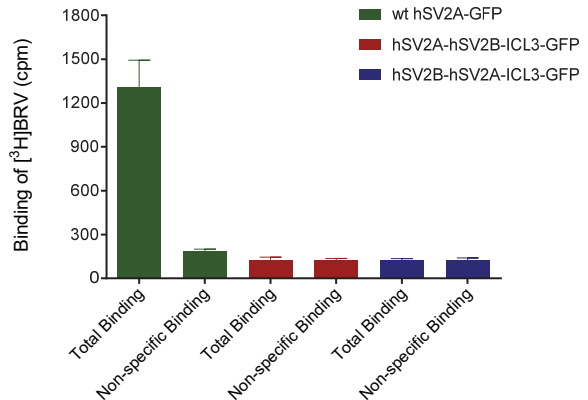


Figure IV: Evaluation of [³H]BRV binding to recombinant wt hSV2A (green), hSV2A-hSV2B-ICL3 chimera (red), and hSV2B-hSV2A-ICL3 chimera (blue). Total binding was determined in the absence of LEV and non-specific binding was determined in the presence of LEV (1 mM).

5 Project summary and outlook

direct high-affinity binding site for BRV neither on human nor on mouse Cx43. To date, only few, moderately potent and selective ligands of Cx43 are known, probably due to lack of suitable screening assays and test systems. In the current study, a new high-throughput screening assay for Cx43 GJ modulators was developed. The assay works based on the principle that activation of the G_s protein-coupled human adenosine receptor ($A_{2A}AR$) in a

donor cell line with a specific agonist (CGS21680) generates cAMP, which crosses via Cx43 GJs into biosensor cells harboring cAMP sensitive luciferase. Upon cAMP-mediated activation the luciferase catalyzes the oxidation of luciferin producing luminescence (see Figure V). The Z' -factor of the current assay was determined to be 0.5, which confirms its suitability as an HTS assay. The newly developed assay has the potential to be deployed for screening large compound libraries for Cx43 GJ modulators, investigating Cx43 mutants and heterotypic GJ coupling, and the same method can be applied to other Cx subtypes.

Membrane proteins constitute targets for around 60% of all approved drugs.²³⁶ Monitoring the expression of recombinant membrane proteins is mostly crucial to rely on the outcomes of pharmacological assays. Several types of tags are used for labeling recombinant membrane proteins to facilitate monitoring of their expression. Green fluorescence protein (GFP) is extensively used for tagging recombinant proteins. Detection and quantification of recombinant proteins fused to GFP are most frequently performed by fluorescence microscopy, flow cytometry, or by measuring fluorescence in suspension or in solution after solubilization. However, these methods have limitations such as low sensitivity and lack of precision due to high background autofluorescence. In the present study, a fast and robust method was

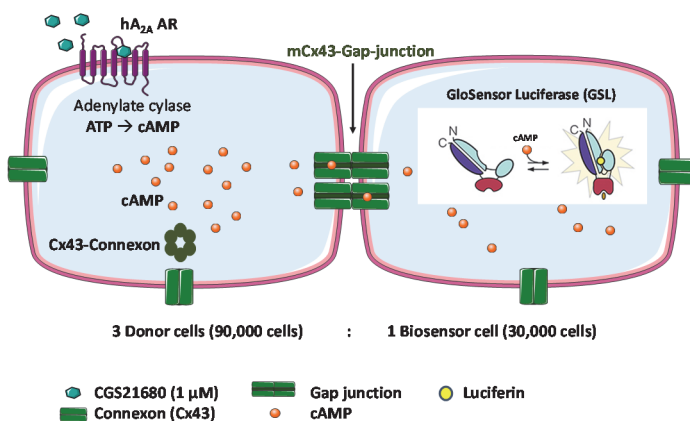


Figure V: Design of the Cx43 GJ assay. HeLa cells expressing $hA_{2A}AR$ and $mCx43$ are denoted as donor cells and HeLa cells expressing GSL and $mCx43$ are indicated as biosensor cells.

5 Project summary and outlook

established to quantify GFP-tagged membrane proteins in cell homogenates by using capillary gel electrophoresis coupled to a laser-induced fluorescence detector (CGE-LIF) (see Figure VI). CGE-

LIF was found to be highly sensitive displaying a limit of detection (LOD) of 0.168 $\mu\text{g/ml}$ (5 nM) for GFP. The CGE-LIF method showed higher sensitivity (at least 5-

fold) as compared to fluorimetric measurement in a microplate. We quantified three different types of GFP-tagged membrane proteins expressed in CHO cells, namely SV2A, A_{2A}AR, and Cx43. Quantification of SV2A and A_{2A}AR using classical radioligand binding assays confirmed the results obtained with CGE-LIF. Importantly, the new method involves separation of the target proteins and their degradation products prior to quantification. We anticipate broad applicability of the method for any fluorophore-tagged proteins and for multiplex protein detection.

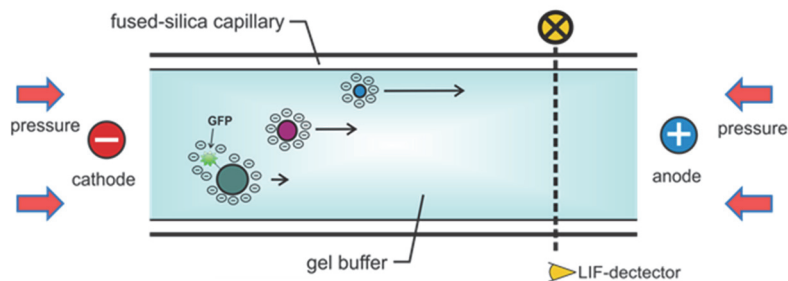


Figure VI: Schematic representation for the detection of GFP-tagged proteins using CGE-LIF. Cellular homogenate containing recombinant GFP-tagged protein (green circle) and non-fluorescent cellular proteins (violet and blue circles) is diluted in a Tris buffer containing 1% SDS. The sample is then electrokinetically injected into a fused-silica capillary filled with a gel buffer containing semi-liquid gel. The complex mixture of cellular proteins in the homogenate is resolved in the applied electric field based on their molecular weights by applying a high voltage. The proteins are negatively charged due to their inclusion in SDS micelles and then migrate from cathode to anode. Only the GFP-tagged proteins are detected by a LIF detector.

6 Experimental section

6.1 Materials

6.1.1 Chemicals

2-Arachidonylglycerol	Sigma, 80676
2-Mercaptoethanol	Applichem, A4338
Adenosine	Sigma, A9251
Agarose	Roth, 2267.2
AM-251	Biotrend, BN0063
AM-281	Sigma, A0980
AM-630	Tocris, 1120
Ampicillin sodium salt	Applichem, A0839
Anandamide	Tocris, 1339
Anhydrotetracycline hydrochloride	Riedel-de-Haen, 37919
Brivaracetam	Briviact® ampoules (10 mg/ml) Prof. Dr. Ivar von Kügelgen, University of Bonn
Bromophenol blue sodium salt	Applichem, 3640
BSA/Albumin fraction V	Applichem, A1391
Calcium chloride dehydrate	Fluka, 21097
Calcium-5	Molecular devices, R8186
Carbenoxolone disodium salt	Alfa Aesar, J63714
CGS21680	Tocris, 1063
Cinchonidine	Merck-Schuchardt AG, 485-71-2
Cinchonine	Merck-Schuchardt AG, 118-10-5
Coomassie BrilliantBlue G-250	Sigma, 27815-25G-F
D-(+)-Galactose	Alfa Aesar, A12813
D-(+)-Glucose	Sigma, G-7012
D-(+)-Sucrose	Applichem, A4734,5
Desloratadine	Tocris, 5958

6 Experimental section

DMSO	Applichem, A3608
DMSO for cell culture	Applichem, A3672
EDTA	Roth, 8040.3
Ethanol	ZVE University of Bonn, 123974
FCS	Sigma, F-0804
Fluo-4	ThermoFischer Scientific, F14201
Forskolin	Applichem, 66575-29-9
G418	Calbiochem, 345810
Glacial acetic acid	Merck, 1.00063.1011
Glycerol	AppliChem, A1123
HEPES	Sigma, H-3375
Hydrochloric acid 37%	Applichem, A 0659
IBMX	Fluka, 58620
Isopropanol	ZVE University of Bonn, 123903
JWH-031, AM-2232, AM-679, JWH-234, JWH-175, AM-1235, JWH-368, JWH-016, JWH-309	Provided by Dr. Cornelius Hess, Institute of Forensic Medicine, Bonn
Luria Bertani (LB) agar	Invitrogen, 22700-041
LB powder medium	Applichem, A0954,901
Levetiracetam	Chemos GmbH, Art No. 134992
Lipofectamine2000	Invitrogen, 11668019
Liquid scintillation cocktail	LumaSafe™, Perkin Elmer, 3087
Magnesium chloride	Sigma, M8266
MSX-2	Synthesis in AK Prof. Dr. C. E. Müller
NECA	Sigma, E-2387
PEI solution (50% in H ₂ O)	Sigma, P-3143-1L
Pen-strep solution	Gibco, 15140
Polybrene (Hexadimethrine bromide)	Aldrich, 10,768-9
SDS solution 20%	Applichem, A0675
Sodium butyrate	Fluka, 19364
Sodium chloride	Sigma, P-9541

6 Experimental section

Sodium hydroxide	Fluka, 71689
TRIS	Roth, AE15.3
Tween20	Sigma, P9416
WIN 55,212-2	Tocris, 1038
Zeocin™	Invitrogen, R25001

All other test compounds used in this study and are not listed were obtained from Pharma-Zentrum Bonn compound library (<https://www.pharmchem1.uni-bonn.de/pharmchem1-en/mueller-laboratory/compound-library>).

6.1.2 Instruments and consumables

Amicon Ultra-15 10k Centrifugal Filter	Amicon-Millipore
Analytical balance	Sartorius CP225D SBC 42, SCALTEC
Autoclave	VX-95, Systec
Cell culture flasks	Cell Star – Greiner Bio-One
Centrifuges	Mikro 200, Hettich Allegra 21 R, Beckman Coulter Avanti J-201, Beckman
Confocal microscope	A1Eclipse Ti, Nikon
Drying cabinet	T6120, Heraeus
Electrophoresis chamber	Schütt Labortechnik
Electrophoresis power supply	Power Pac 300, ELITE 300 Plus, Schütt Labortechnik
Gel documentation system	Universal hood II Geldoc, BioRad
Glass homogenizer, Potter	Sartorius
Glass-fiber filters (GF/C) and (GF/B)	Whatman®
Hamilton syringe	Syringes 705, Roth
Harvester	Brandel M24 Gaithersburg, MD, USA and Brandel M48 Gaithersburg, MD, USA
Hemocytometer (cell counting chamber)	Marienfeld Germany

6 Experimental section

Incubator for cells	Heraeus HERAcell 240 and INC 246, Mettler
Incubator/shaker for bacteria	Innova 4200, New Brunswick Scientific
Liquid scintillation analyzer	Tri-Carb 2810 TR, Perkin-Elmer
Microplates	Greiner Bio-one
Microscope	Wilovert, Hund Wetzlar Axiovert 25, Zeiss
Microwave	Microwave 800, Severin
Multimode microplate reader	Mithras LB 940, Berthold Technologies
pH-meter	691 pH Meter, Metrohm Seven Easy, Mettler Toledo
Photometer	DU-530, Beckman
Pipette tips	Sarstedt
Pipettes	Eppendorf
Reaction tubes	Eppendorf
Rocking shaker	ELMI Digital Rocking Shaker DRS-12
Safety cabinet	NUNC [®] Safe flow 1.2 NUNC [®] MICROFLOW
Steril filter	Filtropur 0.22 µm, 831826001, Sarstedt
Thermal block	Thermomixer comfort, Eppendorf
Thermocycler	T Personal, Biometra
Tip Sonicator	Sonoplus HD2070, Bandelin
Tissue homogenizer	Ultra-turrax T25 basic, IKA
UV-Base	UV-Star Biometra
Vortex mixer	UNIMAG Zx ³ , UniEquip Vortex Genius 3, IKA MS2 Minishaker, IKA
Water bath	WNB 14, Memmert
Western blot equipment	BioRad and Invitrogen

6 Experimental section

6.1.3 Software

Graphpad Prism, version 6, San Diego, California, USA

ClustalW2, European Bioinformatics Institute

DNAtrans 2.0, Dr. A. Schiedel / J. Bosmann

Microsoft Office 2013

Chromas Lite, sequence analysis, Conor McCarthy

Clone Manager, version 9

ChemDraw Prime 16, Cambridge Software

TOPO2, <http://www.sacs.ucsf.edu/cgi-bin/tmhmm.py>

Needle, EMBL-EBI, http://www.ebi.ac.uk/Tools/psa/emboss_needle/

Multiple Sequence Alignment Tools, <http://www.ebi.ac.uk/Tools/msa/>

Oligoanalyzer 3.1, <https://eu.idtdna.com/calc/analyzer>

HMMTOP, Prediction of transmembrane helices, <http://www.enzim.hu/hmmtop/>

NisEelement viewer for Nikon microscope images

NEBuilder assembly tool, <http://nebuilder.neb.com/>

Servier medical art, <http://www.servier.com/Powerpoint-image-bank>

<http://multalin.toulouse.inra.fr/multalin/>

6 Experimental section

6.1.4 Materials for molecular biology

6X Gel Loading Dye, blue	New England BioLabs, B7021S
Bradford Assay Dye Reagent Concentrate	Bio-Rad, 5000006
EnduRen™ Live Cell Substrate	Promega, E6481
Enhanced GFP Protein (EU056363.1)	ABM, 33P, Canada
GelRed™	Biotrend, 41002
GloSensor™ cAMP Reagent	Promega, E1290
Lamda DNA/EcoRI + HindIII	Thermo Scientific, SM0281
Lipofectamine™ 2000 Transfection Reagent	Invitrogen, 11668019
Pierce™ ECL Western Blotting Substrate	Thermo Scientific, 32106
ProLong Gold antifade reagent	Invitrogen, P36930
Protease inhibitor cocktail	Sigma, P8340
Protein Marker	Thermo Scientific, 26619
RIPA	Thermo Scientific, 89900
ΦX174 DNA-HaeIII Digest	Thermo Scientific, SM0251

Enzymes

Pyrobest™ DNA Polymerase	TaKaRa
Q5® High-Fidelity DNA Polymerase	New England BioLabs
Restriction enzymes	New England BioLabs
T4 DNA ligase	New England BioLabs

Antibodies

Donkey anti-rabbit-HRP	Jackson Immuno Research, Hamburg, Germany
Goat anti-mouse-HRP	Germany
Mouse monoclonal anti-eGFP	Covance, Freiburg, Germany
Rabbit polyclonal anti-Cx43	Provided by Prof. Dr. Christian Steinhäuser

Kits

DNA clean & concentrator™-5 Kit	Zymo Research, D4003
---------------------------------	----------------------

6 Experimental section

Gibson Assembly® Master Mix	New England BioLabs, E2611S
HiPure Plasmid Filter Midiprep kit	Invitrogen, K210014
HisPur™ Ni-NTA, 3 ml resin bed	Thermo Scientific, 88226
Plasmid Miniprep Kit Classic	Zymo Research, D4015
Zymoclean Gel DNA Recovery Kit	Zymo Research, D4001
ZymoPURE™ Plasmid Maxiprep Kit	Zymo Research, D4028

6.1.5 Plasmids

pcDNA™4/ <i>myc</i> -His A vector	Invitrogen, V863-20
pGloSensor™-20F cAMP Plasmid	Promega, E1171
pLVX-IRES-mCherry	Clontech, 631237
pASK-IBA43plus	IBA GmbH, Germany
pMK-RQ-BoNTA-HCR (codon optimized)	LifeTechnologies, 1562951
pUC19	Thermo Scientific, SD0061
pMJ-mCx43-IRES-GFP	AK Prof. Dr. Klaus Willecke,
pGEM-T-hCx43	LIMES Institute, Bonn
pCMV-hSV2A-GFP (NM_014849.3)	Dr. Simone Hildenbrand
pCMV-hSV2B-GFP (NM_014848.4)	
pLXSN-hA _{2A} AR (NM_001278500.1)	Dr. Elisabetta De Filippo
pcDNA3.1+ <i>Renilla</i> luciferase8 (RLuc8)	Dr. Benjamin Seibt

6.1.6 Media and supplements for cell culture

DMEM	Dulbecco's Modified Eagle Medium, Life Technologies, 41966029
DMEM/F12	Life Technologies, 31330038
FCS	Sigma-Aldrich, F0804
G418	Calbiochem, 345810
Hygromycin B	Merck, 400052
PS	Penicillin-Streptomycin solution, Gibco 15140
Trypsin	Lonza, 17-160

6 Experimental section

6.1.7 Primers

The underlined and bold bases in primer sequences represent restriction sites. The underlined and bold single base in the primer sequences used for mutagenesis indicates mutated base. The overlapping regions in primers used for Gibson assembly are represented with lowercase bases and uppercase bases indicate the annealing sequence.

Primers for cloning

	Sequence (5'-3')
f-hSV2A-NotI	GAGCTAG <u>GCGGCCGC</u> ACCATGGAAGAGGGCTTCCGAGAC
r-GFP-HindIII	CATCAT <u>AAGCTT</u> TTACTTGTACAGCTCGTCCATGC
f-hSV2B -NotI	GAGCTAG <u>GCGGCCGC</u> ACCATGGATGACTACAAGTATCAG
f-hSV2A- EcoRI	GAGCTAG <u>GAATTC</u> ACCATGGAAGAGGGCTTCCGAGAC
r-hSV2A- XhoI	CATCAT <u>CTCGAG</u> TTACTTGTACAGCTCGTCCATGC
f-Cx43-XhoI (h, m)	GAGCTA <u>CTCGAG</u> ACCATGGGTGACTGGAGCGCC
r-hCx43-XbaI	CATCAT <u>TCTAGA</u> TTAGATCTCCAGGTCATCATCAGGCCG
r-mCx43-XbaI	CATCAT <u>TCTAGA</u> TTAAATCTCCAGGTCATCAGGCCGAGG
f-mCX43-HindIII	AGACCCAAGCTGGCTAGTT <u>AAGCTT</u> ACCATGGGTGACTGGAGC
r-mCX43-XhoI	AAGGGCCCTCTAGA <u>CTCGAG</u> TTAAATCTCCAGGTCATCAGGC
f-hCX43- HindIII	AGACCCAAGCTGGCTAGTT <u>AAGCTT</u> ACCATGGGTGACTGGAGC
r-hCX43-XhoI	AAGGGCCCTCTAGA <u>CTCGAG</u> TTAGATCTCCAGGTCATCAGGC

Primers for mutagenesis

	Sequence (5'-3')
f-hSV2A-R383Q	CAGGTCCATGATACCAACATGC <u>A</u> AGCCAAAGGACATCCTGAGCG
r-hSV2A-R383Q	CGCTCAGGATGTCCTTGGCT <u>I</u> GCATGTTGGTATCATGGACCTG

Primers for Gibson assembly

	Sequence (5'-3')
f-(hSV2A-hSV2B-ICL3-GFP) 1	agaccaagctggctagttaagcttACCATGGAAGAGGGCTTCCG
r-(hSV2A-hSV2B-ICL3-GFP) 1	ctggcatgaaGGTCAGAGCCCCAATGGCAAAC
f-(hSV2A-hSV2B-ICL3-GFP) 2	ggctctgaccTTCATGCCAGAGAGCCCAAG
r-(hSV2A-hSV2B-ICL3-GFP) 2	tcagagtgatCATTCTGTAGGGCCCCATCAC
f-(hSV2A-hSV2B-ICL3-GFP) 3	ctacagaatgACTACTCTGATGATGATGGGTGTG
r-(hSV2A-hSV2B-ICL3-GFP) 3	gttcgaagggccctctagactcgagTTACTTGTACAGCTCGTCCATGC
f-(hSV2B-hSV2A-ICL3-GFP) 1	agaccaagctggctagttaagcttACCATGGATGACTACAAGTATCAGGAC

6 Experimental section

r-(hSV2B-hSV2A-ICL3-GFP) 1	caggctgcgtCTTCAGGGCCACCATGGACAC
f-(hSV2B-hSV2A-ICL3-GFP) 2	ggccctgaagACGCAGCCTGAGAGCCCCCG
r-(hSV2B-hSV2A-ICL3-GFP) 2	tcagtgattGCGCCGATATTCGGGACCAAACAGG
f-(hSV2B-hSV2A-ICL3-GFP) 3	atatggcgcAATACACTGATTCTGGCCGTGG
r-(hSV2B-hSV2A-ICL3-GFP) 3	gttttgtcgaagggccctctagaTTACTTGTACAGCTCGTCCATGC
f-(mCx43-GFP) 1	agaccaagctggctagttaagcttACCATGGGTGACTGGAGC
r-(mCx43-GFP) 1	cgccccctcgacAATCTCCAGGTCATCAGGC
f-(mCx43-GFP) 2	cctggagattGTCGACGGGGGCGGCGGA
r-(mCx43-GFP) 2	gttcgaagggccctctagactcgagTTACTTGTACAGCTCGTCCATGCCGAGAGTG
f-(hA _{2A} -GFP) 1	agaccaagctggctagttaagcttACCATGCCCATCATGGGC
r-(hA _{2A} -GFP) 1	cgccccctcgacGGACACTCCTGCTCCATC
f-(hA _{2A} -GFP) 2	aggagtgtccGTCGACGGGGGCGGCGGA
r-(hA _{2A} -GFP) 2	gttcgaagggccctctagactcgagTTACTTGTACAGCTCGTCCATGCCGAGAGTG
f-mCx43 1	agaccaagctggctagttaagcttACCATGGGTGACTGGAGC
r-mCx43 1	aagggccctctagactcgagTTAAATCTCCAGGTCATCAGGC
f-hCx43 1	agaccaagctggctagttaagcttACCATGGGTGACTGGAGC
r-hCx43 1	aagggccctctagactcgagTTAGATCTCCAGGTCATCAGGC

Primers for sequencing

	Sequence (5'-3')
f-hSV2A-1051	CTGACCACGCAGCCTGAG
r-hSV2A-1341	AGTGATGCGCCGATATTCG
r-hSV2A-1462	GGAACACTTTGGTGCGGGATG
f-hSV2B-697	GGAGAACACCTCAGTTGGC
f-hSV2B-1345	CACCAACATGGGAAACTTGTG

f, forward; r, reverse; h, Human; m, Mouse.

6.1.8 Bacteria and growth media

Chemocompetent <i>E. coli</i> Top 10 <i>Invitrogen, C4040-10</i>	Untransformed cells were grown in basal Luria Bertani (LB) medium. Transformed cells depending on the antibiotic resistance were grown in LB medium
Chemocompetent <i>E. coli</i> DH5 α <i>New England Biolabs, C2987I</i>	supplemented with either 100 μ g/ml ampicillin or 50 μ g/ml kanamycin.

6 Experimental section

6.1.9 Cell lines and culture media

CHO-K1 (Ovary cells) ATCC, CRL-61 Non-transfected cells were cultivated in basal DMEM-F12 medium supplemented with 10% FCS, 100 U/ml penicillin G, and 100 µg/ml streptomycin (“full medium”). For transfected cells selection reagent either 200 – 800 µg/ml G418 or 100 – 200 µg/ml zeocin was additionally added to the medium (“selection medium”).

GP⁺envAM12 (Embryo-fibroblasts) ATCC, CRL-9641 HXM medium was prepared by supplementing basal DMEM medium with 10% FCS, 100 U/ml penicillin G, 100 µg/ml streptomycin, 1% ultraglutamine, 200 µg/ml hygromycin B, 15 µg/ml hypoxanthine, 250 µg/ml xanthine, and 25 µg/ml mycophenolic acid.

HeLa (Cervical carcinoma) Prof. Dr. K. Willecke Non-transfected cells were cultivated in basal DMEM medium supplemented with 10% FCS, 100 U/ml penicillin G, and 100 µg/ml streptomycin (“full medium”). For transfected cells selection reagent either 200 – 800 µg/ml G418 or 100 – 200 µg/ml zeocin was additionally added to the medium (“selection medium”).

ATCC, American Type Culture Collection

6.1.10 Buffers, media and gels

PBS buffer

NaCl (137 mM), KCl (2.5 mM), Na₂HPO₄ (7.5 mM), and KH₂PO₄ (1.5 mM) were dissolved in deionized water and pH was adjusted to 7.4 with HCl (37%). The buffer was autoclaved and stored at room temperature.

Tris-HCl buffer (50 mM), pH 7.4 (buffer for radioligand binding assays)

Tris (50 mM) was dissolved in deionized water and pH was adjusted to 7.4 with HCl (37%). The buffer was stored at 4°C.

MgCl₂ solution (10 mM), pH 7.4

MgCl₂ (10 mM) was dissolved in Tris-HCl buffer (50 mM), pH 7.4. The buffer was stored at 4°C.

6 Experimental section

Polyethyleneimine (PEI) solution (0.1%)

PEI solution (50% in H₂O) was diluted (1:500) in deionized water. The solution was stored at 4°C.

Tris (20 mM) / Sucrose (250 mM) solution, pH 7.4 (homogenization solution)

Tris (20 mM) was prepared by dissolving D(+)-Sucrose (250 mM) in Tris (50 mM, pH 7.4) under stirring and concentration was corrected with deionized water. The solution was stored for maximum two weeks at 4°C.

Tris-acetate-EDTA buffer (TAE), pH 8 (buffer for agarose gel electrophoresis)

Tris (40 mM) was dissolved in in deionized water and pH was adjusted to 8.0 using acetic acid followed by addition of Na₂EDTA (2 mM). The buffer was stored at room temperature.

HBSS buffer with 0.1% BSA (buffer for Cx43 gap junction assay)

HEPES (20 mM), NaCl (13 mM), Glucose (5.5 mM), KCl (5.4 mM), NaHCO₃ (4.2 mM), CaCl₂ (1.25 mM), MgCl₂ (1 mM), MgSO₄ (0.8 mM), KH₂PO₄ (0.44 mM) and Na₂HPO₄ (0.34 mM) were dissolved in autoclaved water and pH was adjusted to 7.4. The buffer was stored at 4°C. BSA (0.1%, w/v) was dissolved in buffer prior to use.

Laemmli sample buffer 5X

SDS (10%, v/v), glycerol (50%, v/v), β-mercaptoethanol (25%, v/v), bromphenol blue (0.25% w/v), Tris-HCl (250 mM) were dissolved in deionized water and pH was adjusted to 6.8. The buffer was stored at 4°C and used under the fume hood.

TBST buffer for Western blot

Tris (20 mM), NaCl (150 mM), Tween 20 (0.1%) were dissolved in deionized water and pH was adjusted to 7.6. The buffer was stored at RT.

Proteins transfer buffer for Western blot

Tris (25 mM), glycine (190 mM), and methanol (20%, v/v) were dissolved in deionized water and pH was adjusted to 8.3. The buffer was stored at RT

6 Experimental section

Gel staining solutions with colloidal Coomassie BrilliantBlue G-250

Solution A: Methanol (50%, v/v), phosphoric acid (2%, v/v) were diluted in deionized water.

Solution B: Solution A was supplemented with ammonium sulfate (1.3 M).

Solution C: Solution B was supplemented with Coomassie G-250 (0.066%, w/v).

LB medium

LB medium powder (25 g) was added to 1 L deionized water and the suspension was autoclaved. The medium was stored at 4°C.

LB agar plates

LB agar (32 g) was added to 1 L deionized water and the suspension was autoclaved. Antibiotic (ampicillin/kanamycin) was added after the solution has cooled down to about 50°C. The agar was then poured into the petridishes for solidification. The plates were stored at 4°C.

6.1.11 Radioligands

Precursors of the radioligands were synthesized in AK Prof. Dr. C. E. Müller and labeling was performed by Quotient Bioresearch, UK.

<i>Radioligand</i>	<i>Specific activity</i>	<i>Supplier code</i>	<i>Supplier</i>
[³ H]BRV	94 Ci/mmol	TRQ40419	Quotient Bioresearch, UK
[³ H]LEV	98 Ci/mmol	TRQ40411	Quotient Bioresearch, UK
[³ H]MSX-2	84 Ci/mmol	TRQ40688	Quotient Bioresearch, UK

6 Experimental section

6.2 Molecular Biology

6.2.1 Transformation

Transformation refers to the taking up of exogenous DNA by bacteria. Bacteria were made chemocompetent by incubating the cells with calcium chloride (CaCl₂). CaCl₂ improves the binding of the DNA to the cell wall and further the uptake is improved by heat shock (raising the temperature to 42°C for 40 s). Plasmid-DNA which has to be transformed mostly contains resistance genes against antibiotics. Therefore, the selection of the transformed bacteria is done by adding the particular antibiotic to the growth medium.²⁶⁵

6.2.1.1 Preparation of competent bacteria

An overnight grown preculture (4 ml) of *E. coli* TOP10 was added to 40 ml LB medium and grown to an OD₅₅₀ of 0.5 (37°C, 220 rpm). The culture was centrifuged (1700 g, 4°C, 20 min) and the pellet was resuspended in 20 ml of sterile ice cold 0.1 M CaCl₂ solution followed by incubation for 30 min on ice. The suspension was centrifuged (1700 g, 4°C, 20 min) and the pellet was resuspended in 2 ml of ice cold 0.1 M CaCl₂ solution and incubated for another 30 min on ice. Glycerol (0.5 ml) was added to the bacterial suspension and 100 µl aliquots were stored at -80°C.

6.2.1.2 Transformation of competent bacteria

Transformation with the desired plasmid was performed using *E. coli* competent bacteria. A frozen aliquot (100 µl) of bacterial suspension was thawed on ice for 30 min. Plasmid (10 – 50 ng) was mixed with the bacterial suspension and further incubated on ice for 30 min. The bacterial suspension was then heat shocked (42°C, 40 s) in a thermoblock. The mixture was again incubated on ice for 2 min. LB medium (200 µl) was added to the cells and the culture was incubated on a thermoblock (37°C, 300 rpm, 1 h). Finally the whole mixture was spread on an LB agar plate containing the antibiotic for which the plasmid confers resistance gene, e.g. ampicillin and kanamycin. The plates were inverted and incubated (37°C, 18 h) and single clones were picked for further analysis.

6 Experimental section

6.2.2 Isolation and purification of plasmids

Most of the current methods used for isolation of amplified plasmids from bacteria are based on the procedure introduced by Birnboim and Doly.²⁶⁶ The bacterial pellet is treated with a mixture of sodium dodecylsulfate (SDS), sodium hydroxide (NaOH) and ethylenediaminetetraacetic acid (EDTA). The increased pH by NaOH helps to denature the bacterial DNA and SDS denatures the proteins. EDTA captures the divalent cations from the bacterial nucleases, thereby preventing the degradation of plasmid-DNA. The pH of the reaction is neutralized by the addition of a weak acid, e.g. acetic acid. The neutralization causes an incomplete renaturation of bacterial genomic DNA and it can be separated by centrifugation or filtration. The supernatant obtained by this procedure contains the plasmid-DNA. The plasmid-DNA is then precipitated with ethanol and can be separated by centrifugation or filtration. This method yields purified plasmid-DNA.

6.2.2.1 Plasmid Mini-preparation

Single clones were picked from the overnight grown LB plates and incubated in 4 ml of antibiotic containing LB medium followed by incubation in shaker (37°C, 220 rpm, 18 h). The Zymo Research miniprep-*Classic* kit was used for plasmid isolation and plasmid was eluted in sterile water. The procedure was performed according to the manufacturer's protocol.

6.2.2.2 Plasmid Maxi-preparation

Maxi-preparation was used for larger yield of plasmids. Bacterial preculture was prepared by inoculating LB medium (4 ml) with bacterial glycerol stock (50 µl) followed by incubation in a shaker (37°C, 220 rpm, 6 h). The preculture was then transferred to LB medium (100 ml) containing antibiotics in an Erlenmeyer flask followed by incubation in the shaker (37°C, 220 rpm, 18 h). The maxiprep kit from Zymo Research was used for the plasmid isolation according to manufacturer's protocol and plasmid was eluted in sterile water.

6.2.3 Preparation of glycerol stocks

The glycerol stocks were prepared by adding 200 µl of sterile glycerol to 800 µl of bacterial suspension in fresh LB medium without antibiotics. The stocks were stored at -20°C for 24 h followed by long term storage at -80°C.

6 Experimental section

6.2.4 Gel electrophoresis

Electrophoresis is a technique capable of separating macromolecules (DNA, RNA, and proteins) based on their sizes under electric current. DNA carries negative charge due to the phosphate group backbone, therefore it moves towards the positive electrode during electrophoresis. The size of the DNA molecule is the decisive factor for its separation, since the other two important factors for standard electrophoresis, i.e. the shape and charge-to-mass ratio of molecules are identical for DNA samples. A gel is prepared by boiling agarose in water which forms a meshwork of small pores. These pores are suitable to separate nucleic acids ranging from 1 – 30 kbp for 0.5% agarose gel and 1 – 300 bp with even single nucleotide differentiation for 40% agarose gels. For the visualization of the DNA fragments, a DNA intercalating dye, e.g. GelRed™ is used, which gives fluorescent signals when exposed to UV light.²⁶⁵

Agarose was added to TAE buffer to get a final concentration of 1% and the solution was heated in a microwave oven until the agarose was dissolved and the solution was clear. After the solution reached a temperature of about 45°C, the GelRed™ DNA stain was added to the (1:10000) liquid gel. The liquid gel solution was added to gel casting chamber and combs were inserted. After the hardening of the gel, the whole chamber with the gel was placed in the electrophoresis chamber filled with TAE buffer. Samples were mixed with 6X gel-loading dye and loaded in the wells. Lambda DNA/HindIII and phiX174 DNA HaeIII were used as DNA ladders for size comparison. A voltage of 100 V was applied for 30 min and DNA bands were visualized under UV light in a gel documentation system.

6.2.5 Restriction digest with endonucleases

Restriction endonucleases were discovered in the early 1950s,²⁶⁵ when it was shown that some bacterial strains are immune to bacteriophage infection. Bacteria produce enzymes which add methyl groups to their DNA, so that it can be differentiated from the invading foreign DNA. Among all three types I, II and III of endonucleases, type II is the most important for foreign DNA digestion. The recognition sequence for endonucleases are palindromes (sequence read the same in either direction), when cut by restriction enzymes, they produce either blunt or sticky ends. The destruction of bacterial DNA is lethal for bacteria, therefore, it is protected from type II endonucleases due to the methylation of their DNA, which blocks the degrading

6 Experimental section

enzyme action. The type II endonucleases has a wide range of applications in molecular biology particularly in recombinant DNA technology.

Different restriction enzymes were used for cloning and subcloning of DNA fragments. All components of the reaction mixture were pipetted as shown in Table 10. The restriction digest mixture was incubated at 37°C for 1 h with high fidelity enzymes and with fast digest enzymes at 37°C for 20 min followed by the deactivation of enzymes (80°C, 10 min) on a thermoblock. The restriction products were then purified using DNA clean and concentrator kit according to manufacturer's protocol. In case the digested products were separated on agarose gel, the corresponding bands containing DNA were carefully cut-out and DNA was recovered using Gel DNA recovery kit.

Table 10: General pipetting scheme of restriction digest for vectors and inserts

Components	Concentration
10X Reaction Buffer	1:10 dilution
10X BSA (if required)	1:10 dilution
Sterile H ₂ O	X μ l
Enzyme(s)	1 U/ μ g of DNA
Template DNA (PCR product or vector)	0.5 – 1 μ g
Final volume	20 – 30 μ l

6.2.5.1 Dephosphorylation of digested vector

Dephosphorylation of the digested vector was performed to prevent the re-ligation of the cut vector. The components of the dephosphorylation used and concentrations are listed in Table 11. The reaction mixture was incubated at 37°C for 25 min on a thermoblock followed by heat inactivation at 65°C for 5 min.

Table 11: Pipetting scheme of dephosphorylation reaction mixture

Components	Concentration
NEB-Buffer 2	1:10 dilution
10x Phosphatase buffer	1:10 dilution
Sterile H ₂ O	X μ l
Antarctic phosphatase	1 μ l
Digested vector	~ 100 ng
Final volume	25 μ l

6 Experimental section

6.2.6 Ligation

The joining of two DNA fragments is known as ligation and the enzyme catalyzing this reaction is called the DNA ligase. Ligation takes place between the phosphate group (5' terminus) and hydroxyl group (3' terminus) by the formation of a covalent phosphodiester bond by DNA ligase. Ligation requires ATP and the reaction is carried out in three steps, i) adenylation (addition of AMP) to the active center of the enzyme, ii) transfer of AMP to the 5' phosphate end, and iii) formation of a phosphodiester bond by the release of AMP. In contrast to blunt end ligation, sticky end ligation is much more efficient and requires only a low concentration of DNA molecules.^{181,265}

Ligation of the digested vector and the insert was performed using the T4 DNA ligase enzyme. The reaction mixture as listed in Table 12 was incubated at room temperature for at least 1 h or alternatively incubated overnight at 16°C.

Table 12: Components of ligation reaction

Material	Concentration
DNA Insert	~ 150 ng
Plasmid	~ 50 ng
10X Buffer	1:10 dilution
T4 ligase	5 U
ATP	100 mM
Sterile H ₂ O	X µl
Total Volume	20 – 25 µl

6.2.7 Polymerase chain reaction (PCR)

The polymerase chain reaction (PCR) was invented by Kary Mullis in 1985 for which he received a Nobel Prize in 1993.²⁶⁷ PCR technique extended the range of DNA analysis such as DNA cloning, DNA-based phylogeny, functional analysis of genes, diagnosis of hereditary diseases, and detection of pathogens. PCR allows amplification of the target DNA-sequence using minute amounts of DNA. It is carried out in a reaction tube by mixing the template DNA with a set of oligonucleotides (primers), DNA polymerase, deoxynucleotides, and their corresponding buffers. The mixture is incubated at a series of preprogrammed temperatures in a thermal cycler. The DNA in the mixture is denatured by heating to 98°C resulting in the disruption of double and triple hydrogen bonds holding the complementary strands of DNA

6 Experimental section

together. Thereafter the mixture is cooled down to 50 – 60°C, allowing the annealing of two primers to the specific sequence site in the template DNA. The annealing temperature is usually kept 2 – 3°C lower than the melting temperature (T_m) of the primers to ensure efficient annealing. The approximate melting temperature of a primer can be calculated by the following Equation 1.^{265, 268}

$$T_m = 4 \times (n^*(C) + n(G)) + 2 \times (n(A) + n(T))$$

Equation 1: Calculation of melting temperature (T_m) of a primer.

n: Number of nucleotides

A, C, G, and T: adenine, cytosine, guanine, and thymine nucleotides

The primers are chemically synthesized and are typically 18 – 30 bp long with ~50% GC nucleobase content. The temperature of the PCR mixture is raised to 72°C, which is the optimum working temperature of DNA polymerase (DNA pol). DNA pol attaches to the 3' end of the primer which is annealed to the target DNA sequence and incorporates ~ 1000 nucleotides/min synthesizing a new strand of DNA. Mg^{2+} is a cofactor for the DNA pol and also plays a role in the primer annealing, therefore, its concentration shall be taken into account during PCR. The denaturation-annealing-synthesis cycles are repeated 25 – 32 times which results in the exponential increase of double stranded template DNA.²⁶⁹

The PCR reactions were performed using a high-fidelity DNA polymerase enzyme (Pyrobest or Q5). The addition of 2 – 5% of DMSO in some amplification reactions particularly with GC rich DNA resulted in a better yield. As a negative control water in place of DNA was used. A general PCR reaction scheme is shown in Table 13 and a general program cycle in Table 14.

Table 13: General pipetting scheme for a PCR reaction

Components	Concentration
Forward-Primer	0.3 μ M
Reverse-Primer	0.3 μ M
dNTPs	1 mM
10X buffer	1:10 dilution
Polymerase	1 U / reaction
Sterile H ₂ O	X μ l
Template DNA	~ 20 ng
Final volume	25.0 μ l

6 Experimental section

Table 14: Standard PCR program

	Process	Temperature	Time	Cycles
Step 1	Initial denaturation	98°C	4 min	1x
Step 2	Denaturation	98°C	30 s	} 32x
Step 3	Primer hybridization	$T_m - 4^\circ\text{C}$	30 s	
Step 4	Elongation	72°C	1 min / 1Kb	
Step 5	Terminal elongation	72°C	10 min	
Step 6	Storage	4°C		

6.2.8 Site-directed mutagenesis

Site-directed mutagenesis is a simple and versatile technique to create a desired mutation at any point in a gene using the PCR technique. The mutations are introduced in the gene by using a pair of complementary primers containing desired mutations and a plasmid containing the gene of interest. Generally a small plasmid such as pUC19 with ~ 2.7 kbp is used for site-directed mutagenesis. The whole plasmid will be amplified with this method like a normal PCR reaction with minor changes of primer concentration and low temperature for primer hybridization as shown in Table 15 and Table 16. After amplification, the DNA was purified using DNA clean and concentrator kit according to manufacturer's protocol.

Table 15: General Pipetting scheme for a PCR-mediated site-directed mutagenesis reaction

Components	Concentration
f-primer	1 μM
r-primer	1 μM
dNTPs	2 mM
10X buffer	1:10 dilution
Ster. H ₂ O	X μl
Pyrobest enzyme	1 U / reaction
Template DNA	~20 ng
Final volume	25.0 μl

Table 16: PCR program for site-directed mutagenesis

	Process	Temperature	Time	Cycles
Step 1	Initial denaturation	94°C	4 min	1x
Step 2	Denaturation	94°C	30 s	} 20x
Step 3	Primer hybridization	55°C	30 s	
Step 4	Elongation	72°C	1 min / 1Kb	
Step 5	Terminal elongation	72°C	10 min	
Step 6	Storage	4°C		

6 Experimental section

After the PCR-mutagenesis the reaction mixture contains both the mutated plasmid and mother plasmid due to the semi-conservative nature of DNA replication. However, the mother plasmids without mutations can be selectively degraded by the action of restriction enzyme DpnI.²⁷⁰ DpnI digests the methylated DNA and since the mother plasmid is Dam methylated, they are sensitive to DpnI digestion.

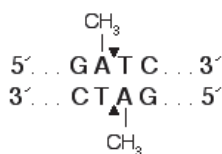


Figure 46: Recognition site of DpnI enzyme on methylated DNA.

Pipetting scheme for the DpnI digestion mixture is demonstrated in Table 17. The reaction mixture was incubated for 90 min at 37°C in a thermoblock. Thereafter DpnI was inactivated at 80°C for 20 min. Subsequently mixture was used to transform chemocompetent *E. coli* cells for plasmid amplification.

Table 17: Pipetting scheme for DpnI digestion of methylated DNA

Components	Volumes (µl)
Purified PCR product	10
10X NEB-4 buffer	2
DpnI (20U)	1
Sterile H ₂ O	7
Final volume	20

6.2.9 Primer design

The primers used in this study were longer than 18 bases. The primers were designed by keeping the GC-content of at least 48% and melting temperature below 70°C. The primers for site-directed mutagenesis contained at least 15 nucleotides complementary to the anti-sense strand flanking both 3' and 5' ends of the introduced mutation. The flanking with extra nucleotides on both ends provides stable annealing of the primer, despite the mismatch in the middle of the primer sequence. The primers used for the Gibson assembly method were designed by using the NEBuilder assembly online tool. Furthermore all the designed primers were analyzed using the online tool Oligoanalyzer 3.1 for formation of hairpins.

6.2.10 Sequencing

Isolated and purified plasmids from putative positive clones were sequenced to verify the success of cloning and to confirm the mutation free sequences. The analysis was performed by GATC Biotech AG, Germany. Sample for sequencing was prepared by diluting 1 µg DNA in 30 µl of sterile water.

6.2.11 Gibson assembly: one-step assembly of multiple DNA fragments

Gibson assembly method is a novel method for assembling multiple DNA fragments of variable lengths and end compatibilities. This method is highly suitable for assembling large and complex DNA constructs without relying on the availability of restriction sites. In this approach, multiple overlapping double stranded DNA fragments obtained by PCR amplification are combined with Gibson master mix and incubated at 50°C for 1 h. This single-tube isothermal reaction then results in seamlessly joined DNA construct or plasmid (see Figure 47). The Gibson assembly method make use of the following three enzymes for assembling multiple DNA fragments:

- i. Exonucleases (5'-T5) recess double stranded DNA from 5'-end creating a single-stranded 3' overhang that is complementary to 3' overhang of adjacent DNA fragment at overlap region.
- ii. DNA polymerase (Phusion[®] pol) fills the gaps in the annealed fragments. *Taq* pol can also be used in this method, however Phusion[®] pol is preferred due to its inherent proof-reading activity and high-fidelity.
- iii. DNA ligase subsequently covalently seals the nicks in the assembled DNA.
- iv. The general pipetting scheme for the Gibson assembly method is given in Table 18. After mixing up the DNA fragments (0.02 – 0.05 pmols) with Gibson master mix. The mixture is incubated in a thermocycler at 50°C for 60 minutes, followed by subsequent transformation of competent *E. coli* directly with 2 µl of reaction mixture. The assembled DNA constructs can as well be stored at -20°C for future transformations.

6 Experimental section

$$pmols = \frac{DNA \text{ in } ng * 1000}{base \text{ pairs} * 650 \text{ Daltons}}$$

Equation 2: Formula to calculate amount of DNA in moles

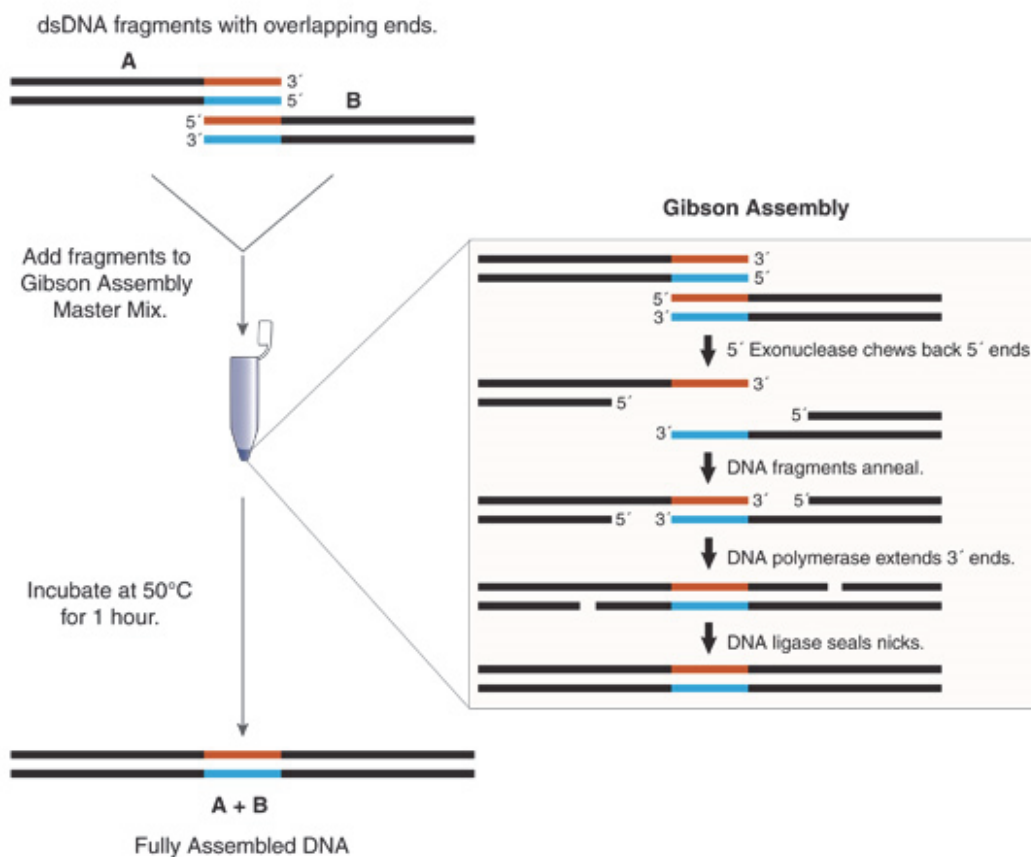


Figure 47: Schematic diagram of Gibson assembly method for generating constructs with multiple DNA fragments. DNA fragments sharing terminal sequence are PCR amplified. The double-stranded DNA sequences are mixed with Gibson assembly master mix. This mix possesses three enzymatic activities, i.e. 5'-exonuclease creates single-stranded 3' overhangs, polymerase fills the gaps in the annealed fragments and DNA ligase seals nicks in the assembled DNA.²⁷¹

Table 18: General pipetting scheme of Gibson assembly method

Components	2 – 3 Fragment Assembly	4 – 6 Fragment Assembly
Total amount of Fragments	X μ l (0.02 – 0.5 pmol)	X μ l (0.2 – 1 pmol)
Gibson Assembly Master Mix (2X)	10 μ l	10 μ l
Deionized H ₂ O	10 – X μ l	10 – X μ l
Total Volume	20 μ l	20 μ l

6 Experimental section

6.3 Expression and purification of BoNT/A-HCR

BoNT/A-HCR sequence was used as described earlier by Benoit et al. (2014).¹⁷³ Codon-optimized cDNA of BoNT/A-RBD (871 – 1296 amino-acids, Swiss-Prot P10845) for expression in *E. coli* with restriction sites at 3' SacII and at 5' KpnI was subcloned into the bacterial expression vector pASK-IBA43plus with an *N*-terminus 6xHis-tag. *E. coli* top 10 cells were transformed either with expression plasmid containing BoNT/A-HCR or only vector as control. Cultures were grown in 400 ml LB medium supplemented with 100 µg/ml ampicillin at 37°C for 4 – 8 h in a shaking incubator to an OD₅₅₀ = 0.5. The cultures were then induced with 100 µg anhydrotetracycline and grown at lower temperature of 30°C for 16 h in a shaking incubator. The cells were harvested by centrifugation at 6000 g for 20 min and 1 g wet pellet was resuspended in 1 ml of ice cold lysis buffer (50 mM NaH₂PO₄, 300 mM NaCl, 10 mM Imidazole, pH 8) supplemented with protease inhibitor cocktail 10 µl/ml in lysis buffer. Cell lysis was performed by ultrasonication (3x, 10 s, 5 cycles, 50% power) on ice and lysate was cleared by centrifugation at 20000 g for 30 min at 4°C. The 6xHis-tagged BoNT/A-HCR was purified from the lysate via immobilized metal affinity chromatography (IMAC) by using 3 ml spin columns containing nickel-charged nitrilotriacetic acid (Ni-NTA) according to manufacture's protocol for purification under native conditions (HisPur™ Ni-NTA, 3 ml resin bed, 88226, Thermo Scientific™, Germany). The residual imidazole from the elute was removed, and BoNT/A-HCR was concentrated in assay buffer (50 mM Tris-HCl, pH 7.4) by using ultrafiltration with molecular weight cutoff of 10 kDa according to manufacturer's protocol (Amicon-Millipore, Germany). For long term storage 30% glycerol was added to purified proteins and stored at -20°C for 24 h and subsequently at -80°C.

6 Experimental section

6.4 Cell culture

6.4.1 Cultivation of cells

Mammalian cells were cultivated in different cell culture flasks (25 cm², 75 cm², 175 cm², and dishes) with required culture medium (see Section 6.1.9). All steps were performed under sterile conditions (laminar air flow hood). The cultures were incubated at 37°C in a humidified atmosphere with 5% CO₂ in an incubator. Cells were regularly passaged after they had reached a confluence of 80 – 90%. The old medium was decanted and the cells were washed twice with sterile PBS to remove residual medium. The cells were detached using a trypsin 0.01% solution containing 0.6 mM EDTA with incubation at 37°C for 2 – 3 min. Cells adhere to the culture flask surface via integrin proteins present at the plasma membrane. Trypsin, which belongs to a family of serine proteases, cleaves these integrin proteins and cells get detached. Additionally, EDTA reduces the divalent cations, needed for the integrin stability.²⁶⁵

6.4.2 Cryopreservation of cells

Cell line stocks were prepared by trypsinization of a confluent 175 cm² flask. Cells were resuspended in culture medium (10 ml) without antibiotics and centrifuged (1200 g, 5 min, RT). The pellet was then resuspended in 3 ml of the freezing medium containing 10% DMSO and 90% FCS. Freezing medium (2X) for HeLa cells was prepared by diluting DMSO (20%, v/v) and FCS (30%, v/v) in DMEM basal medium. Suspended HeLa cells were mixed (1:1) with freezing medium. Aliquots (1 ml each) were pipetted in cryovials and stored first in a freezing box for gradual cooling from RT to -80°C at a rate of 1°C/min and after 24 h stored at -80°C or in liquid nitrogen for long term storage.

6.4.3 Counting and seeding of cells

Cells were detached and resuspended in an appropriate amount of culture medium (5 – 10 ml) and centrifuged (5 min, 200 g, RT). The pellet was again resuspended in 5 – 10 ml of culture medium and 10 µl of cell suspension was added under the coverslip of a haemocytometer (Neubauer-chamber improved, depth: 0.100 mm). The cells were counted in two big squares and the average was multiplied by 10⁴ which gave the number of cells/ml. The cell suspension was corrected to a defined number of cells per ml according to the following formula:

6 Experimental section

$$V_{cell\ suspension} (ml) = \frac{C_{required} \left(\frac{cells}{ml}\right)}{C_{counted} \left(\frac{cells}{ml}\right)} * V_{final} (ml)$$

Equation 3: Formula for calculating the number of cells in a given suspension

V: volume (ml)

C: number of cells per milliliter (cells/ml)

6.4.4 Lipofection

Lipofection is a method to transfect cultured cells with a foreign DNA. This technique employs small liposomes, which contain synthetic cationic lipids. Upon interaction with DNA, they form lipid-DNA complexes. These complexes get fused with the plasma membrane of cells, thereby transport the foreign DNA into the cytoplasm with high efficiency. Lipofection can be used for both transient and stable DNA expressions and is found to be more effective as compared to other methods like calcium phosphate or the DEAE-dextran transfection methods.²⁷²

For transfection, cells (2×10^6) were seeded in a 25 cm² culture flask containing full medium followed by incubation (37°C, 16 h). The old culture medium was exchanged against 6.25 ml of new full culture medium without antibiotics and the culture was incubated (37°C, 3 h). Basal medium (600 µl) without any supplements was mixed with 25 µl of Lipofectamine 2000 and incubated for 5 min at RT. plasmid-DNA (10 µg) was diluted in basal medium without any supplements to make a final volume of 625 µl. Both solutions were mixed giving a mixture of 1225 µl, which was incubated for 20 min at RT. The transfection mixture was then dropwise added to the cells followed by incubation (37°C, 5% CO₂, 24 – 48 h). The culture medium was then replaced against selection medium containing the antibiotic corresponding to selection markers.

6 Experimental section

6.4.4.1 Retroviral transfection

Various methods of gene delivery into the cells are available such as DNA injection, lipofection, and gene gun technology. However gene delivery using genetically engineered retroviruses is one of the most effective methods.²⁷³ Retroviruses are special viruses, which after infecting the cells can reverse transcribe their own RNA into DNA by the virally encoded enzyme reverse transcriptase.²⁷³ This DNA copy is then integrated into the host genome by a virally encoded enzyme called integrase. Thereafter the host transcriptional and translational machinery is used for the expression of viral genes.

The retrovirus genome contains the essential genes for viral production, i.e. *gag*, *pol*, *env*, and the packaging signal (Ψ) along with other genes flanked on both ends by long terminal repeats (LTRs). The *gag* gene encodes for group-specific antigen on capsids, the *pol* gene for the viral polymerase and the *env* gene for the viral envelope. LTRs are large redundant DNA sequences where the viral promoters and transcriptional enhancers are located. These regions are essential for reverse transcription and replication. The packaging signal sequence (Ψ) interacts with the viral proteins to ensure proper packaging of the viral RNA into the virion.²⁷³ The use of competent retrovirus is not feasible, since the infected cell will die. Therefore, genetically engineered viruses are used in which all viral protein coding regions are removed other than genes responsible for viral RNA encapsulation, reverse transcription and integration.²⁷⁴ The packaging cell line is created using helper virus DNA in which *gag* and *pol* genes are encoded on one plasmid while the *env* gene is encoded on a separate plasmid. This strategy prevents the possibility of recombination events and their related dangers.²⁷⁵ The retroviral transfection mechanism is illustrated in Figure 48.

The cell line GP⁺envAM12 is an example of packaging cell line derived from mouse fibroblasts and used for the retroviral vector system. These packaging cells harbor two plasmids, one contains the *env* gene and a selection marker for hygromycin B while the second plasmid contains the *gag* and *pol* genes of the murine leukemia virus (MuLV) and an additional *gpt* gene encoding a xanthine-guanine phosphoribosyltransferase.²⁷⁵⁻²⁷⁷ The presence of hygromycin B, hypoxanthine, xanthine and mycophenolic acid in the culture medium (HXM medium) causes a selection pressure on the cells preventing them from losing the three viral genes. Mycophenolic acid inhibits the *de novo* purine synthesis, therefore cells expressing

6 Experimental section

xanthine-guanine phosphoribosyltransferase for purine synthesis and confer hygromycin B resistance will survive. Since the viral packaging signal (Ψ) is missing in the packaging cells to avoid the formation of replication-competent viruses, a separate plasmid is used. This plasmid contains the gene of interest in the multiple cloning site and a packaging signal (Ψ). Both of these genes are flanked by LTRs. The retroviral plasmids have an origin of replication and antibiotic resistance for propagation in bacteria. Examples of such plasmids are pLXSN and pLVX-IRES-mCherry, which were used in this work. While retroviruses can infect mitotically active cell types, lentiviruses, a subtype of retroviruses, can infect almost all types of mammalian cells including non-dividing cell, stem cells, and primary cells.²⁷⁸ The lentiviral plasmid (pLVX-IRES-mCherry) was utilized in this study, which allowed the isolation of monoclonal cells with high recombinant protein expression using fluorescence assisted cell sorting (FACS). However, a drawback of this plasmid was the absence of antibiotic selection marker which may result in low yield of recombinant protein over increasing passages.

In order to increase the infectivity of viruses, a vector encoding the glycoprotein G of the vesicular stomatitis virus (VSV-G) was co-transfected with retroviral plasmid. The VSV-G-molecules gets integrated in the cellular membrane and eventually in the retrovirus envelope. The retrovirus with glycoproteins will not only infect by binding to specific receptors but also by binding to phospholipids non-specifically.²⁷⁹ The last step is the harvesting of viruses containing the gene of interest from the medium. These viruses are then added to the target cells. The successfully transfected cells can then be selected based on either a resistance gene such as neomycin or a fluorescence protein like mCherry.

6 Experimental section

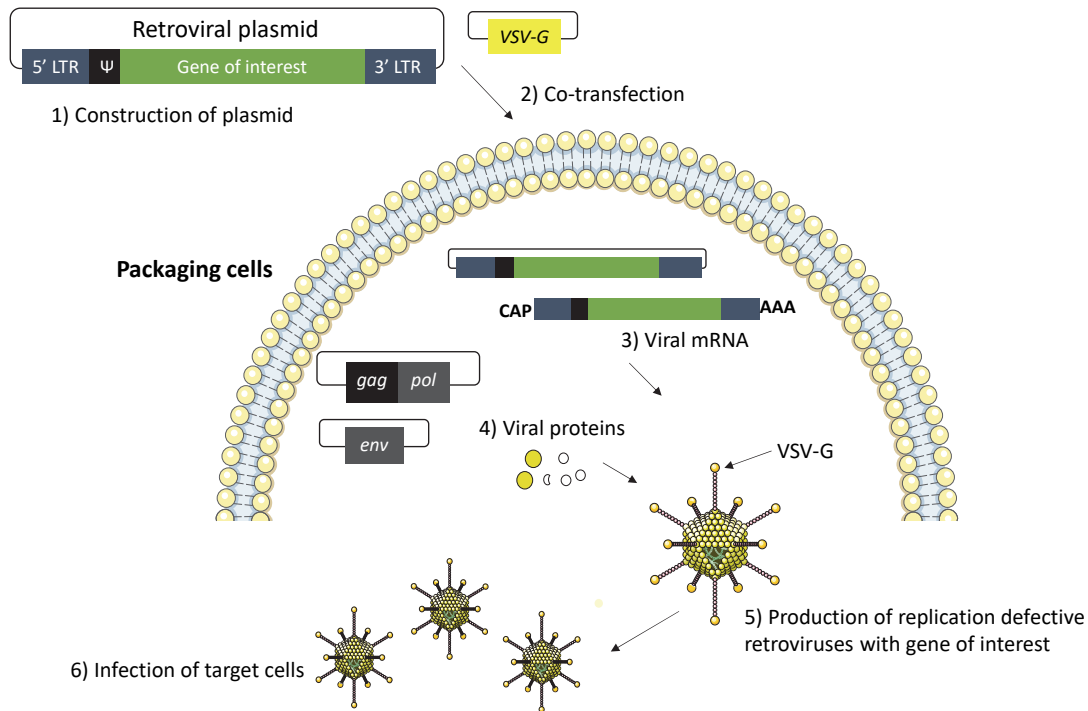


Figure 48: Production of retroviruses in helper cells. (1) A recombinant retroviral plasmid is constructed which contains the gene of interest (green), the virus packaging signal Ψ (black), and the essential sequences LTRs (blue). (2) A helper cell is co-transfected with a retroviral plasmid and a *VSV-G* encoding plasmid. (3) The viral mRNA is transcribed from the retroviral plasmid by the transcriptional machinery of the helper cell. (4) Helper cells harbor two separate plasmids responsible for expression of structural proteins of viruses. (5) The packaging sequence (Ψ) on the recombinant viral RNA is recognized by the packaging proteins resulting in the formation of virus cores which are enveloped by cell membrane containing VSV-G envelope proteins. (6) Subsequently infectious virions bud from the cell and are collected in the medium. These virions can be further utilized for transducing the target cells. LTR: long terminal repeat, Ψ : packaging signal, VSV-G: glycoprotein G of the vesicular stomatitis virus. Diagram concept taken from Hu and Pathak (2000).²⁷³

Packaging cells GP⁺envAM12 (1.5×10^6 cells) were seeded in a 25 cm² flask with 5 ml of DMEM medium supplemented with FCS (10%), penicillin (100 U/ml), and streptomycin (100 µg/ml) followed by incubation (37°C, 5% CO₂, 24 h) prior to transfection. Next day the cells were transfected using Lipofectamine 2000 with 10 µg of DNA comprising the retroviral plasmid (6.25 µg) and VSV-G plasmid (3.75 µg). After 15 h of transfection, the old culture medium was exchanged with 3 ml of fresh medium DMEM medium containing FCS (10%), penicillin (100 U/ml), streptomycin (100 µg/ml), and sodium butyrate (5 mM) followed by incubation (32°C, 5% CO₂, 48 h). The supernatant (3 ml) containing the virus particles was removed and sterile filtered using a 2 µm filter to harvest the viruses. The filtrate containing the viruses was mixed with 6 µl of polybrene solution (4 mg / ml in H₂O, sterile filtered). Subsequently, the medium of the target cell line (CHO-K1 or HeLa) a 25 cm² flask was

6 Experimental section

replaced with mixture and the cells were incubated at 37°C for 2.5 h. After the incubation, mixture containing the viruses was discarded and 5 ml of fresh culture medium supplemented with antibiotic like G418 dependent on the cell line (see Section 6.1.9) was added to the cells followed by incubation (37°C, 5% CO₂, 48 – 72 h). After three days of incubation, the medium was regularly changed until the non-transfected cell death process ended.

6.5 Protein sample preparations

6.5.1 Rat cortical membrane preparations

Membrane preparations of rat cortex were used for performing some of the radioligand binding assays. Frozen rat brains were thawed in ice-cold sucrose solution (0.32 M). The brains were then placed top side on an ice-cold glass plate and cortex was carefully dissected along the two hemispheres with a scalpel. The cortical tissue was stored in ice-cold sucrose solution (0.32 M). The cortical tissue in sucrose solution was disrupted with a Potter glass homogenizer for about 3 min followed by centrifugation (1000 g, 4°C, 10 min). The supernatant was carefully collected and centrifuged (37000 g, 4°C, 1 h), whereas the pellet (P1) was discarded. The supernatant was decanted and pellet (P2) was resuspended and homogenized (Ultraturrax, setting 3, 10 s) in ice-cold deionized water. The homogenate was centrifuged (37000 g, 4°C, 1 h) and again the resulting pellet was resuspended and homogenized (Ultraturrax, setting 3, 10 s) in ice-cold Tris-HCl buffer and pelleted by centrifugation (37000 g, 4°C for 1 h). Subsequently, the supernatant was decanted and the pellet was resuspended and homogenized (Ultraturrax, setting 3, 10 s) in a small volume of ice-cold Tris-HCl buffer. The homogenized cortical membrane preparations were aliquoted in 1.5 ml tubes for shock-freezing in liquid nitrogen and stored at -80°C for future use.

6.5.2 Preparation of cellular homogenates

Mammalian expression plasmid pcDNA4-hSV2A-GFP was constructed by cloning cDNA of wt human SV2A (NM_014849.3) fused to green fluorescence protein (GFP) at the C-terminus into the pcDNATM4/*myc*-His-A vector with restriction enzyme HindIII and XhoI. CHO-K1 cells were transfected with pcDNA4-hSV2A-GFP conferring zeocin resistance using Lipofectamine2000. A stable cell line expressing hSV2A-GFP was established by using 100

6 Experimental section

$\mu\text{g/ml}$ zeocin in selection medium. Single clones with strong fluorescence signal were selected by fluorescence-assisted cell sorting (FACS, Aria™ III cell sorter, BD Biosciences). Single clones were further cultivated in selection medium and early cell passages (P4 – P8) were used for the preparation of cellular homogenate for binding assays. For homogenate preparation, cells in culture dishes (152 cm^2) were grown to 80 – 90% confluence and washed with 10 ml of PBS followed by scraping them off with a rubber scraper in 3 – 5 ml of ice-cold buffer (PBS / 2 mM EDTA). The collected cells were then pelleted by centrifugation (1000 g, 10 min, 4°C). The pellet was resuspended in ice-cold homogenization solution (20 mM Tris-HCl, 250 mM sucrose, pH 7.4) and homogenized two times (Ultraturrax, setting 5, 15 s) with 5 min incubation on ice between two repetitions. The homogenate was then supplemented with a protease inhibitor cocktail, 10 $\mu\text{l/ml}$ of homogenate, and aliquots with a concentration of 5 – 8 mg/ml were shock-frozen in liquid nitrogen and stored at -80°C until further use.

The cDNA of the human A_{2A} adenosine receptor (hA_{2A}AR, NM_001278500.1) and enhanced GFP from corresponding mother plasmids were amplified using overlapping primers for the pcDNA™4/myc-His A vector. The overlapping primers were designed with the NEBuilder Assembly tool (NewEngland Biolabs). Amplified cDNA of the hA_{2A}AR and GFP were assembled with the pcDNA™4/myc-His A vector in such a way that the GFP was fused at the C-terminus of the hA_{2A}AR using the Gibson assembly cloning kit (NewEngland Biolabs) as explained in Section 6.2.11. For the construction of an expression plasmid for mouse connexin 43 (mCx43, NM_010288.3) fused to enhanced GFP at the C-terminus, the cDNA of mCx43 was amplified using overlapping primers designed with the NEBuilder Assembly tool. The plasmid pcDNA4-mCx43-GFP was constructed as described for pcDNA4-hA_{2A}AR-GFP, using the Gibson assembly cloning kit. The CHO-K1 cells were transiently transfected with each of the plasmid using Lipofectamine2000 as explained in Section 6.4.4. Cellular homogenates with both cell lines were prepared as described above for the hSV2A-GFP expressing cells.

6.5.3 Cell membrane and cell debris preparations

The cell membranes and cell debris were used in some radioligand binding assays. Cells were grown to a confluence of 80% in a culture dish and medium was aspirated followed by a washing step with 5 ml PBS. At this step dishes containing the cells were either stored at -80°C

6 Experimental section

until further use or the procedure was continued. Cells were scrapped off with a rubber scraper in 3 ml of ice-cold buffer (PBS / 2 mM EDTA) and collected in a beaker on ice. Cells were homogenized using Ultraturrax (level 6, 15 s) and the step was repeated. Cell homogenate is then centrifuged (4°C, 1000 g, 10 min) to separate pellet (P1) from supernatant (S1). The pellet (P1) contained the cellular components like cell debris and cell nuclei and the supernatant (S1) contained the membranes. The supernatant (S1) was centrifuged (4°C, 38000 g, 10 min) to obtain a pellet (P2). Meanwhile, the pellet (P1) was resuspended in small volume of Tris-HCl and aliquoted in 1.5 ml tubes, which after shock-freezing in liquid nitrogen were stored at -80°C. The pellet (P2) was resuspended in 50 mM Tris-HCl (0.1 ml / dish) and small aliquots of 1 ml were prepared. The aliquots of cell membrane suspensions were also shock-frozen in liquid nitrogen and stored at -80°C until further use. Bradford method was used for the determination of protein concentration as explained in Section 6.6.2.

6.6 Recombinant protein analysis

6.6.1 Fluorescence microscopy

CHO-K1 transfectants of SV2A-GFP or its variants were seeded on coverslips, 2 days prior to fixation in standard culture medium without zeocin. Cells were washed two times with PBS and third time with DAPI (1:10000, v/v) diluted in PBS. Coverslips were incubated with ice-cold 1:1 methanol/aetone (v/v) mixture and incubated in freezer (-20°C, 20 min). After the incubation, cells were washed 3x with PBS. Subsequently, the coverslips were mounted onto the glass slides with mounting medium (ProLong Gold antifade reagent, Invitrogen). The enhanced GFP tagged proteins were excited by a wavelength of 488 nm and emission was detected at 515 nm using a confocal microscope.

6.6.2 Bradford assay

The Bradford protein assay (1976) is widely used to determine the total protein concentration in a given a sample.²⁶³ This method measures the presence of the basic amino acid residues arginine, lysine, and histidine, which form a complex with Coomassie dye under acidic conditions producing a dark blue color. Five to eight dilutions of BSA protein as standard with a range of 10 to 500 µg/ml were prepared. In a 96-well transparent plate 10 µl of protein sample

6 Experimental section

was diluted in 190 μl of Bradford reagent and incubated for 5 min at RT in dark. Subsequently, the absorbance of the samples were measured at 595 nm. A calibration curve was obtained by plotting the concentrations on the X-axis and their corresponding absorbance values on the Y-axis (see Figure 49). Absorbance of the unknown protein was incorporated in the line equation and solving it for X gave the protein concentration (see Figure 49).

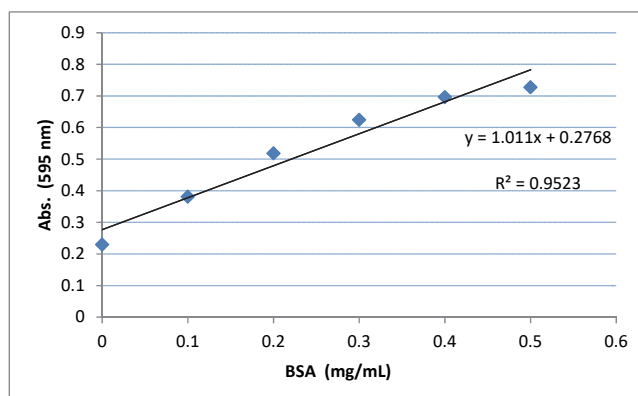


Figure 49: Example of a calibration curve with BSA as standard for Bradford protein assay. Abs, absorbance; BSA, bovine serum albumin.

6.6.3 Fluorimetric measurement

Samples containing pure GFP or GFP-fused proteins were diluted in buffer (50 mM Tris-HCl, pH 7.4) and added to the wells in a 96-well solid-bottom black plate (Nunc, ThermoScientific). For fluorescent measurements the volume was corrected and either 50 or 100 μl of sample/well was used. Background fluorescence was measured using either buffer for purified GFP or cellular homogenate of non-transfected CHO cells for GFP-fused proteins in cellular homogenates. Fluorimetric measurements of enhanced GFP were conducted with a microplate fluorimeter (Mithras LB940) at room temperature using an either of the two filter set combinations (excitation: 485/14 nm and emission: 535/25 nm) or (excitation: 450/30 nm and emission: 510/12 nm).

6 Experimental section

6.6.4 Capillary gel electrophoresis system

The capillary gel electrophoresis with laser-induced fluorescence detector (CGE-LIF) studies have been performed by Dr. Sangyong Lee (AK Müller, University of Bonn).

All experiments were performed on a P/ACE MDQ Capillary Electrophoresis system with a laser-induced fluorescence detector (Beckman Instruments, Fullerton, CA, USA). Data processing was performed by 32 Karat software supplied with the CE instrument. The analysis was performed on 50 μm ID bare-fused silica capillaries with a total length of 60 cm (50 cm effective length) obtained from Polymicro Technologies (Kehl, Germany). The excitation and emission wavelengths of the laser-induced fluorescence detector were 488 and 520 nm, respectively. The capillary and sample tray were kept at 25°C during the measurement. In order to form a semiliquid gel in the capillary, preconditioning was performed with 0.1 N NaOH, 0.1 N HCl, and water at 50 psi (3.4 bar) for 5, 2 and 2 min, respectively, followed by SDS-MW gel buffer (AB Sciex, Darmstadt, Germany) at 40 psi (2.8 bar) for 10 min, and eventually a separation voltage of – 15 kV was applied for 30 min. This preconditioning step was carried out twice and repeated again after 6 sample runs. Electrokinetic injection was at – 5 kV for 20 s and separation took place with an applied voltage of – 15 kV. To keep the semi-liquid gel inside the capillary, a pressure of 30 psi (2.0 bar) was applied to both sides of the capillary during the separation.

6.6.4.1 Protein quantification with CGE-LIF

Initially a calibration curve was determined with the standard green fluorescence protein using various concentrations. The protein samples were diluted in the reaction buffer (100 mM Tris, pH 9.0 supplemented with 1% SDS). The dilution factors for each protein sample are shown in the results section. The unknown protein concentration was calculated as shown in the following example using hSV2A-GFP protein:

6 Experimental section

Calculation example using hSV2A-GFP

Peak area of hSV2A: **69044**

Equation of calibration curve: $Y = 423700000 * X - 0.00002178$

$$69044 = 423700000 * X - 0.00002178$$

Solving equation for X: $X = 162.95492 \text{ ng/ml}$

The crude cellular homogenate containing hSV2A-GFP was diluted (1:100) in reaction buffer, therefore concentration corrected:

$$162.95492 \text{ ng/ml} * 100$$

$$= 16295.4921 \text{ ng/ml}$$

Since molecular weight of hSV2A-GFP is 117 kDa:

$$= 117 \times 1000 \text{ Da} = 117000 \text{ Da} = 117000 \text{ g/mol}$$

$$= (16295.4921 \text{ ng/ml}) / (117000 \text{ g/mol})$$

$$= 0.1393 \text{ (ng/ml} * \text{ mol/g)}$$

$$= 0.1393 \text{ nmol/ml}$$

$$= 139.3 \text{ pmol/ml}$$

Total protein concentration in cell homogenate measured with Bradford assay: ~5.00 mg/ml

Hence, the concentration of hSV2A-GFP in the cellular homogenate can be calculated as follows:

$$139 \text{ pmol/ml} / 5.00 \text{ mg/ml protein}$$

$$= 139 \text{ pmol} / 5.00 \text{ mg protein}$$

$$= \mathbf{27.9 \text{ pmol/mg protein}}$$

6 Experimental section

6.6.5 SDS PAGE

Crude cellular homogenates were solubilized using 10% RIPA buffer and solution was cleared by centrifugation (10,000 g, 20 min, 4°C). The protein samples (20 µg – 100 µg of protein) were mixed with the required volume of 5X Laemmli sample buffer. Samples were reduced and denatured by heating for 5 min, BoNT/A-HCR sample at 50°C, SV2A sample at 40°C, GFP sample at 95°C, and Cx43 at 65°C. The samples were then loaded into the wells of a 10% SDS-PAGE gel along with the standard protein ladder and separated by electrophoresis using running buffer (25 mM Tris base, 192 mM glycine, 0.1% SDS, pH 8.3) for 40 min at 200 V. After the proteins were separated on the gel, the gel was used for Western blot. The gel used to analyze the purity of BoNT/A-HCR was further stained for protein bands with colloidal Coomassie BrilliantBlue G-250 solutions (see Section 6.1.10 for A, B, C solutions). The gel was incubated under shaking in solution A for 1 h at RT and washed 3x with deionized water. The gel was then incubated in solution B under shaking for 1 h at RT. The solution B was discarded and the gel was incubated overnight under shaking in solution C. Subsequently, the gel was washed several times with water until the bands became clear and the gel was scanned.

6.6.6 Western Blot analysis

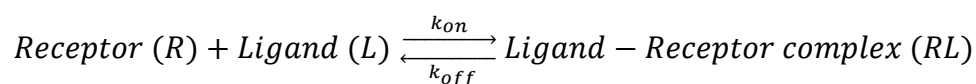
Proteins from the SDS PAGE gel were transferred onto a nitrocellulose membrane (Protran – Whatman, Sigma, Germany) using transfer buffer (see Section 6.1.10). The protein transfer was monitored by staining the membrane with Ponceau S solution (0.1%) for 2 min. The membrane was blocked for 1 h at room temperature in blocking solution, 5% skimmed milk powder in TBST buffer (see Section 6.1.10). After discarding the blocking solution, the membrane was incubated overnight at 4°C with the appropriate dilution of the primary antibody in dilution solution (2.5% milk in TBST). The primary antibodies were discarded and the membrane was washed three times with TBST for 5 min each. Finally, the membrane was incubated for 1 h at room temperature with horseradish peroxidase (HRP) conjugated secondary antibodies appropriately diluted in dilution solution. After the incubation, the membrane was again washed three times with TBST for 5 min each. Subsequently, the HRP substrate was added to the membrane (Pierce™ ECL Western Blotting Substrate) and an X-ray film was developed in the dark room according the manufacturer's protocol.

6 Experimental section

6.7 Radioligand binding assays

Radioligand binding assays are highly useful tools to characterize the interaction between a radioligand and its protein target such as receptor, transporters, and enzymes.²⁸⁰ These assays can be used to determine the affinity of various ligands for a specific protein target as well as to determine the density and distribution of this target in a given tissue or protein sample. Radioligand binding experiments can be majorly subdivided into three types, i) saturation binding experiments, ii) competition binding experiments, and iii) kinetic binding experiments. Saturation binding experiments are performed to determine the affinity of a radioligand (K_d) for a protein target and the target density (B_{max}) in specific tissues or samples. Competition binding experiments are useful to determine the affinity (K_i) of unlabeled ligands, which compete with the radioligand for specific protein target. Kinetic binding experiments provide the information of association kinetic constant (K_{on}) and dissociation kinetic constant (K_{off}) of the radioligand.

Radioligand binding experiments work based on the law of mass action:



Equation 4: Equilibrium of receptor-ligand binding based on law of mass action

K_{on} : association rate constant (1/M * min)

K_{off} : dissociation rate constant (1/min)

$$K_d = \frac{k_{off}}{k_{on}}$$

Equation 5: Calculation of equilibrium dissociation constant K_d

K_d : kinetic equilibrium dissociation constant (M)

Radioligand assays are performed by incubating the radioligand with a preparation containing protein of interest for a certain amount of time to reach steady-state conditions. After the incubation period the protein-bound radioligand is separated from free radioligand generally by using filtration technique. It is important to note that the radioligands should possess high affinity ($K_d < 5$ nM) for target protein, high specific activity ($[^3\text{H}]$ ligands > 30 Ci/mmol), and low non-specific binding (10 – 30%). Unfortunately there is no general procedure for all

6 Experimental section

radioligand assays and therefore assay conditions like temperature, ionic strength of buffer, and presence of divalent ions are mostly required to be optimized.²⁸⁰⁻²⁸¹

6.7.1 Competition radioligand binding assay

Competition experiments are extremely useful to determine the affinity of an unlabeled compound indirectly by measuring its ability to compete binding of a fixed concentration of the radioligand. By plotting logarithmic concentrations of the competitor on the X-axis against the specific binding of the radioligand on the Y-axis, a sigmoidal inhibition curve is obtained with inflection point corresponding to the IC_{50} value of the unlabeled drug. The IC_{50} value corresponds to the concentration of the unlabeled compound at which specific binding of the radioligand is inhibited by 50%. The equilibrium inhibition constant K_i of the unlabeled compound, which gives affinity of compound for a receptor, is obtained from IC_{50} value and K_d of the radioligand using Cheng-Prusoff equation (see Equation 6). The higher the K_i of the unlabeled compound, the lower will be its affinity to the receptor.

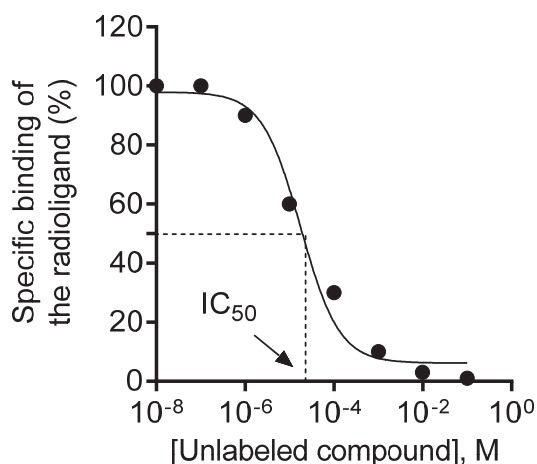


Figure 50: Typical curve of a competition binding experiment. Different concentrations of unlabeled compound are incubated with the same amount of protein and fixed concentration of the radioligand. The concentration of the unlabeled compound at which specific binding of the radioligand is inhibited by 50% corresponds to the IC_{50} value.

6 Experimental section

$$K_i = \frac{IC_{50}}{1 + \frac{L}{K_d}}$$

Equation 6: Cheng-Prusoff equation

K_i : equilibrium inhibition constant (M)

IC_{50} : half maximal inhibitory concentration (M)

L : concentration of radioligand (M)

K_d : equilibrium dissociation constant of radioligand (M)

Competitive [^3H]BRV binding assays were performed essentially as described.^{49, 104} However, protein preparations were adapted according to the requirements of the investigation. Cellular homogenate (200 μg of protein / assay vial) was incubated with [^3H]BRV (3 nM) and the test compound for 240 min at 4°C in 500 μl of cold (4°C) assay buffer (50 mM Tris-HCl, pH 7.4), supplemented with 2 mM MgCl_2 (see Table 19). The assay racks were placed on a rocking shaker and the whole setup was placed in the refrigerator during incubation. The test compounds were dissolved either in the assay buffer or in DMSO. The final DMSO concentration in the assay did not exceed 0.5% since this concentration had no effect on the results. Non-specific binding was determined in the presence of a high concentration of unlabeled LEV (1 mM), whereas total binding was determined in the absence of LEV. Specific binding was determined by subtracting non-specific binding from total binding. For compounds dissolved in DMSO, non-specific and total binding was determined in the presence of the corresponding DMSO concentration. [^3H]BRV bound to SV2A was separated from unbound [^3H]BRV by rapid vacuum filtration using double-layered GF/C glass fiber filters pre-soaked for 30 min at 4°C in aqueous polyethylenimine (PEI) solution (0.1%). The filters were rapidly washed three times with ice-cold assay buffer (1 ml each) using a manual harvester and subsequently dried in a drying oven (50°C, 90 min). Filters were transferred to scintillation vials and radioactivity on the filters was determined by incubating them in 2.5 ml of scintillation cocktail for at least 9 h before measuring with a liquid scintillation counter (Tri-Carb 2810 TR). The Cheng-Prusoff equation²⁸² was used to calculate K_i values inserting the previously determined K_d value of 75 nM for [^3H]BRV and the employed radioligand concentration of 3 nM.³⁸ For data analysis Prism 6 (GraphPad Inc., La Jolla, CA) was used.

6 Experimental section

Table 19: Pipetting scheme for competition experiments using [³H]BRV

	Total binding (μ l)	Non-specific binding (μ l)	Competitive binding (μ l)
MgCl ₂ solution (10 mM)	100	100	100
Tris-HCl buffer (50 mM, pH 7.4)	200	190	190
levetiracetam solution (50 mM)	-	10	-
dilution of competitor	-	-	10
[³ H]BRV in Tris-HCl buffer	100	100	100
protein in Tris-HCl buffer	100	100	100
total volume	500	500	500

6.7.2 Homologous competition binding assay

A competition binding assay is called “homologous binding assay” when the same compound in the labeled and the unlabeled form is used and both show the same affinity for the protein target.²⁸³ This assay can be used as an alternative to the saturation assay to calculate the B_{max} and the K_d values, where much less amount of the expensive radioligand is needed.²⁵⁹ The calculations are performed using the equations shown below:

For homologous competition assay:

$$K_d = IC_{50} - L$$

Equation 7: Calculation of K_d in homologous binding assay which is equal to K_i

K_d : equilibrium dissociation constant (M)

K_i : equilibrium inhibition constant (M)

IC_{50} : half maximal inhibitory concentration (M)

L: concentration of radioligand (M)

The maximum number of binding sites (B_{max}) in homologous competition assay (De Blasi et al. 1989)²⁵⁹ are calculated as follows:

$$B_{max} = \frac{(Top - Bottom) * IC_{50}}{L}$$

Equation 8: Calculation of B_{max} in homologous competition assay

B_{max} : maximum number of binding sites (cpm)

6 Experimental section

Top: total binding of radioligand (cpm)

Bottom: non-specific binding of radioligand (cpm)

IC₅₀: half maximal inhibitory concentration (M)

L: concentration of radioligand (M)

The B_{max} (cpm) is converted to B_{max} (fmol/mg) according to Deupree et al. (2002)²⁸³ follows:

$$B_{max} (fmol/mg) = \frac{B_{max} (cpm) * 100}{eff. (\%) * 2.2 * spec. activity \left(\frac{Ci}{mmol} \right) * Protein (mg)}$$

Equation 9: Conversion of B_{max} (cpm) to B_{max} (fmol/mg)

B_{max}: maximum number of binding sites

eff.: counter efficiency (cpm/dpm = cpm in %)

2.2: conversion factor for cpm to dpm (1 Ci \cong 2.2 x 10¹² dpm)

spec. activity: specific activity of radioligand (Ci/mmol)

Protein: total amount of protein per vial

Concentration-dependent homologous competition of [³H]BRV binding using unlabeled BRV was performed as described for levetiracetam (LEV) (see Section 6.7.1). Non-specific binding was determined in the presence of high concentration of LEV (1 mM). Bound [³H]BRV was separated from unbound radioligand by rapid filtration with a manual harvester using a double layer of GF/C filter which had been pre-soaked in 0.1% polyethylenimine (PEI) for 30 min. The filters were washed three times (1 ml each) with ice-cold assay buffer and were dried at 50°C for 90 min in a drying oven. The dried filters with [³H]BRV were transferred into scintillation vials and 2.5 ml of scintillation cocktail (Luma Safe, Perkin Elmer) was added. The vials were incubated for 9 h and radioactivity was counted with a liquid scintillation counter with 52% counting efficiency (Tri-Carb 2810 TR).

Homologous competition assays with hA_{2A}AR-GFP were essentially performed as described.²⁶⁰ Cellular homogenate of CHO-hA_{2A}AR-GFP (400 µg of protein) were incubated with [³H]MSX-2 (1 nM) and increasing concentrations of unlabeled MSX-2 in a final volume of 400 µl of assay buffer (50 mM Tris-HCl, pH 7.4) at room temperature for 30 min (see Table 20). Non-specific binding was determined in the presence of CGS15943 (10 µM), whereas total binding was determined in the absence of CGS15943. Specific binding was calculated by

6 Experimental section

subtracting the non-specific binding from the total binding. Bound [^3H]MSX-2 was separated from unbound radioligand by rapid filtration with a manual harvester using a GF/B filter that was pre-soaked in 0.3% PEI for 30 min. Filters were rapidly washed three times (2 ml each) with ice-cold assay buffer. The filters with [^3H]MSX-2 were transferred into scintillation vials and 2.5 ml of scintillation cocktail (Luma Safe, Perkin Elmer) was added. After an incubation of 9 h, radioactivity was counted with a liquid scintillation counter with 52% counting efficiency (Tri-Carb 2810 TR). For data analysis Prism 6 (GraphPad Inc., La Jolla, CA) was used.

Table 20: Pipetting scheme for homologous competition experiments with [^3H]MSX-2

	Total binding (μl)	Non-specific binding (μl)	Competitive binding (μl)
Tris-HCl buffer (50 mM, pH 7.4)	196	196	196
100% DMSO	4	-	-
CGS15943 solution (4 mM)	-	4	-
dilution of competitor	-	-	4
[^3H]MSX-2 in Tris-HCl buffer	100	100	100
protein in Tris-HCl buffer	100	100	100
total volume	400	400	400

6.8 Cx43 gap junction assay

6.8.1 Plasmids and cell lines for Cx43 gap junction assay

The cDNAs of wt mouse Cx43 (NCBI sequence: NM_010288.3) and wt human Cx43 (NCBI sequence: NM_000165.4) were amplified from the plasmids pmj-mCX43-IRES-GFP and pGEM-T-hCx43 (generous gift from Prof. Klaus Willecke) using overlapping primers containing restriction sites, HindIII at 5' and XhoI at 3' end, respectively (for primers see Section 6.1.7). After the restriction digest, mCx43 and hCx43 were cloned into the mammalian expression vector pcDNATM4/myc-His A to obtain the plasmids pcDNA4-mCx43 and pcDNA4-hCx43 suitable for transient transfections. The HeLa cell line stably expressing the hA_{2A}AR was transiently co-transfected with pcDNA4-mCx43 using Lipofectamine2000 to establish the donor cells for generating cAMP. Native HeLa cells were transiently co-transfected with the plasmid pGloSensor-20F cAMP (Promega) and pcDNA4-mCx43 using

6 Experimental section

Lipofectamine 2000 (Invitrogen) to establish the biosensor cell line containing the cAMP sensitive GloSensor luciferase. For the experiments to evaluate the intercellular communication in native HeLa cells, donor and biosensor cells were without additional transfection of the pcDNA4-mCx43 plasmid were obtained.

6.8.2 Plate preparation for the Cx43 gap junction assay

On the day of the experiment donor and biosensor cells were harvested by trypsinization, resuspended in full DMEM medium, cell aggregates were dislodged by slow pipetting, and cells were counted. Initially 30,000 biosensor cells per well were dispensed in a 96-well solid bottom white plate followed by 90,000 donor cells to maintain a 3:1 ratio of donor and biosensor cells. Both, donor and biosensor cells, were mixed by pipetting and the co-culture was incubated for 4 h at 37°C in an incubator. After the incubation, the full DMEM medium was replaced by HBSS buffer supplemented with 0.1% BSA, 200 µM IBMX and 2% GloSensor cAMP reagent (“assay buffer”) followed by incubation for 45 min in the dark at room temperature. For the evaluation of Cx43 GJ inhibitors, the compounds were added directly when DMEM full medium was replaced with the assay buffer. The plate was then placed in a plate reader without any filter for the basal luminescence readout. Subsequently, either CGS21680 (1 µM), or DMSO (1%), or forskolin (10 µM), respectively, was added, and luminescence from each well was measured in a kinetic mode for 1 s with an interval of 2 min over a total duration of 20 min (see Figure 51).

6 Experimental section

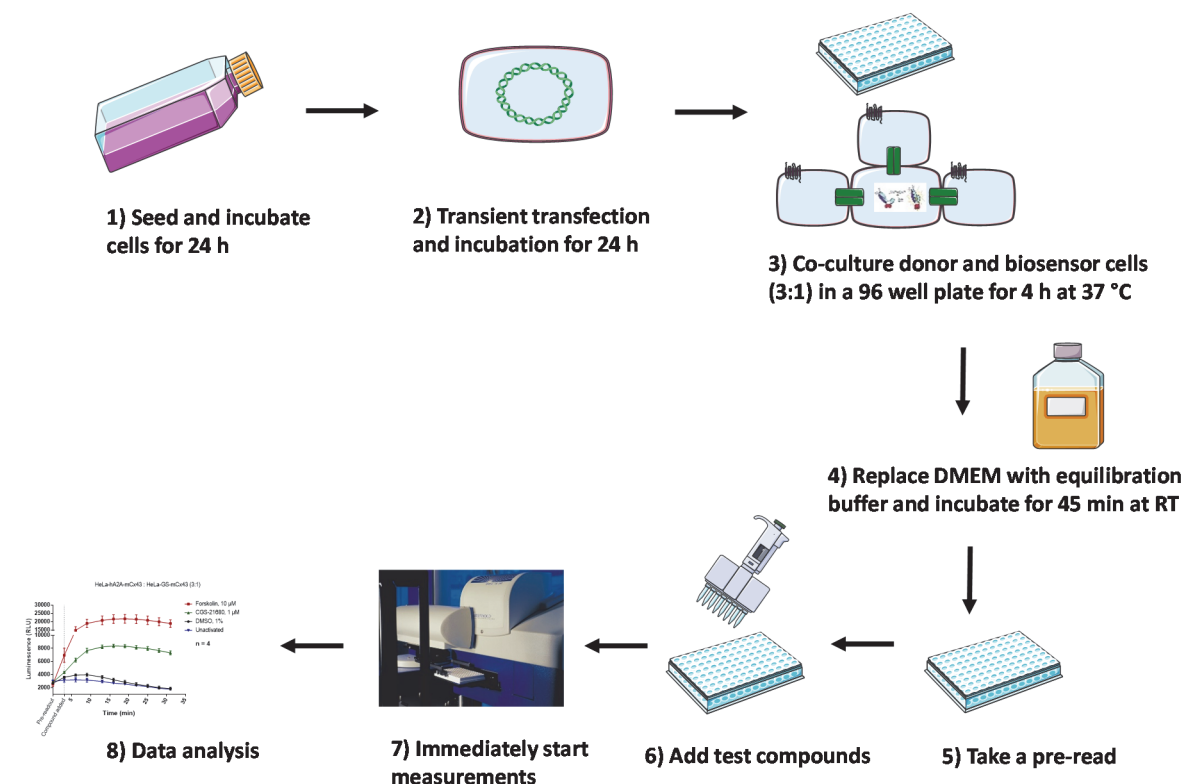


Figure 51: Workflow for performing Cx43 gap junction assay

6.9 Pharmacophore modeling

The pharmacophore modeling studies have been performed by Dr. Vigneshwaran Namasivayam (AK Prof. Dr. C. E. Müller, University of Bonn)

The three selected drugs brivaracetam, loratadine, and quinine, which showed high affinity for SV2A, were flexibly aligned using the flexible alignment module implemented in Molecular Operating Environment (MOE 2014.09).²⁸⁴ This method utilizes the stochastic search procedure and simultaneously searches for the conformational space of the defined molecules and the space of alignment of those molecules.²⁸⁵ The method flexibly aligns the selected small molecules by maximizing steric and feature overlap using the MMFF94x forcefield.²⁸⁶ Each resulting alignment is given a score that quantifies the quality of the alignment in terms of both internal strain and overlap of molecular features. The similarity terms including hydrogen bond donor, acceptor, hydrophobicity and volume, were used in the flexible alignment with the default settings for the other parameters. The presented flexible alignment of the three drugs

6 Experimental section

was selected on the basis of overall score, strain energy and visual inspection of the alignment. This alignment was then used as a template for the pharmacophore model generation. The pharmacophore model was generated using the pharmacophore elucidator feature in MOE 2014.09. The pharmacophore features were calculated automatically with the consensus pharmacophore function. This function clusters the features into potential pharmacophore features which are more conserved than a tolerance and threshold value. For the presented pharmacophore model, the tolerance distance of 1.5 Å and the threshold of 50% conservation was used.

7 Abbreviations

2-AG	2-arachidonylglycerol
A _{2A} AR	adenosine A _{2A} receptor
AA-5HT	<i>N</i> -arachidonylserotonin
AED	antiepileptic drug
AM	acetoxymethyl ester
AM-404	<i>N</i> -arachidonylaminophenol
AMPA	α -amino-3-hydroxy-5-methyl-4 isoxazole propionic acid
ANOVA	analysis of variance
AP	action potential
ATP	adenosine-5'-triphosphate
b	base(s)
BBB	blood-brain barrier
B _{max}	maximum number of binding sites
BoNT	Botulinum neurotoxin
bp	base pair(s)
BRV	brivaracetam
BSA	bovine serum albumin
cAMP	3',5'-cyclic adenosine monophosphate
CBD	cannabidiol
CBX	carbenoxolone
cDNA	complementary DNA
CGE	capillary gel electrophoresis
cGMP	3',5'-cyclic guanosine monophosphate
CGS21680	2-(4-[2-carboxyethyl]-phenethylamino)adenosine-5'- <i>N</i> -ethyluronamide
CHO	Chinese hamster ovary
Ci	Curie
CK1	casein kinase 1
CMV	cytomegalovirus

7 Abbreviations

CNS	central nervous system
cpm	counts per minute
CRE	cAMP response element
CSF	cerebrospinal fluid
Cx	connexin
Da	Dalton
DAPI	4',6-diamidino-2-phenylindole
DMEM	Dulbecco's Modified Eagle's Medium
DMSO	dimethyl sulfoxide
DNA	deoxyribonucleic acid
dpm	disintegrations per minute
dsDNA	double-stranded DNA
<i>E. coli</i>	<i>Escherichia coli</i>
e.g.	<i>exempli gratia</i> (for example)
EDTA	ethylenediaminetetraacetic acid
EEG	electroencephalogram
EMA	European Medicines Agency
et al.	<i>et alii</i> (and others)
f	forward
FACS	fluorescence-assisted cell sorting
FC	flow cytometry
FDA	Food and Drug Administration
FRAP	fluorescence recovery after photobleaching
g	gram
GABA	γ -aminobutyric acid
GABA-T	GABA transaminase
GAD	glutamic acid decarboxylase
GFP	green fluorescent protein
GJ	gap junction
GJIC	gap junctional intercellular communication
GPCR	G protein-coupled receptor

7 Abbreviations

GSL	GloSensor luciferase
GSS	GloSensor substrate
h	hour(s)
h	human
HC	hemichannel
HCR	heavy chain C-terminal receptor
HEPES	<i>N</i> -(2-hydroxyethyl)piperazine- <i>N'</i> -(2-ethanesulfonic acid)
HRP	horseradish peroxidase
HTS	high-throughput screening
HVA	high voltage- activated
HXM	hypoxanthine xanthine mycophenolic acid
Hz	hertz
i.p.	intraperitoneal
IBE	International Bureau for Epilepsy
IBMX	3-isobutyl-1-methylxanthine
IC ₅₀	half maximal inhibitory concentration
ICL	intracellular cytoplasmic loop
ICL3	intracellular cytoplasmic loop three
ILAE	International League Against Epilepsy
KA	kainic acid
K _D	equilibrium dissociation constant
K _i	equilibrium inhibition constant
k _{off}	dissociation kinetic constant
k _{on}	association kinetic constant
l	liter
L	ligand
L4	Luminal loop four
LacY	lactose permease
LAMP	local activation of molecular fluorescence probe
LC	light chain
LEV	levetiracetam

7 Abbreviations

LIF	laser-induced fluorescence detector
LOD	limit of detection
LOQ	limit of quantification
LTR	long terminal repeat
LVA	low voltage-activated
LY	Lucifer yellow
m	meter
M	Molar
MES	maximal electroshock
MFS	major facilitator superfamily
min	minute(s)
MRI	magnetic resonance imaging
mRNA	messenger RNA
MSX-2	3-(3-hydroxypropyl)-7-methyl-8-(<i>m</i> -methoxystyryl)-1-propargylxanthine
MTLE	mesial temporal lobe epilepsy
MTLE-HS	MTLE and hippocampal sclerosis
MuLV	murine leukemia virus
NECA	<i>N</i> -ethylcarboxamidoadenosine
NMDA	<i>N</i> -methyl- <i>D</i> -aspartate
NMR	nuclear magnetic resonance
OD	optical density
ODDD	Oculodentodigital Dysplasia
PAM	positive allosteric modulator
PBS	phosphate-buffered saline
PCR	polymerase chain reaction
PDE	phosphodiesterase
PEI	polyethylenimine
PET	positron emission tomography
PKA	cAMP-dependent protein kinase
PKC	protein kinase C
PKG	cGMP-dependent protein kinase

7 Abbreviations

PSG	polysialoganglioside
PTZ	pentylenetetrazole
r	reverse
R	receptor
RFU	relative fluorescence units
RIPA	radioimmunoprecipitation assay
RNA	ribonucleic acid
rpm	rounds per minute
RSD	relative standard deviation
RT	room temperature
s	second(s)
s.c.	subcutaneous(ly)
SARs	structure-activity relationships
SDS	sodium dodecylsulfate
SDS PAGE	sodium dodecylsulfate polyacrylamide gel electrophoresis
SEL	seletracetam
SEM	standard error of the mean
SNAP	synaptosome-associated protein
SSA	succinic semialdehyde
SSA-D	SSA-dehydrogenase
SV2	synaptic vesicle protein 2
SV2A	synaptic vesicle protein 2A
Syt	synaptotagmin
TAE	Tris Acetate EDTA buffer
<i>Taq</i>	<i>Thermus aquaticus</i>
TBI	traumatic brain injury
TBST	Tris-buffered saline with 0.1% Tween 20
TGFβ1	transforming growth factor β1
THC	Δ ⁹ -Tetrahydrocannabinol
T _m	melting temperature
TMD	transmembrane domain

7 Abbreviations

TRE	treatment-resistant epilepsy
Tris	tris(hydroxymethyl)aminomethane
TRPV1	transient receptor potential vanilloid receptor type 1
Trx	thioredoxin reductase system
VAMP	vesicle-associated membrane protein
vs.	versus
VSV-G	vesicular stomatitis virus
WHO	World Health Organization
wt	wild-type
YFP	yellow fluorescent protein
ZO-1	zona occludens-1

8 References

1. Reynolds, E. H.; Rodin, E. The clinical concept of epilepsy. *Epilepsia* **2009**, *50 Suppl.* 3, 2-7.
2. England, M. J.; Liverman, C. T.; Schultz, A. M.; Strawbridge, L. M. Epilepsy across the spectrum: promoting health and understanding. A summary of the Institute of Medicine report. *Epilepsy Behav.* **2012**, *25*, 266-276.
3. Dannhardt, G.; Kiefer, W. Antiepileptika - Wirkprinzipien und Strukturelle Parameter. *Pharm. Unserer Zeit* **2007**, *36*, 270-281.
4. Fisher, R. S.; van Emde Boas, W.; Blume, W.; Elger, C.; Genton, P.; Lee, P.; Engel, J., Jr. Epileptic seizures and epilepsy: definitions proposed by the International League Against Epilepsy (ILAE) and the International Bureau for Epilepsy (IBE). *Epilepsia* **2005**, *46*, 470-472.
5. Fisher, R. S.; Acevedo, C.; Arzimanoglou, A.; Bogacz, A.; Cross, J. H.; Elger, C. E.; Engel, J., Jr.; Forsgren, L.; French, J. A.; Glynn, M.; Hesdorffer, D. C.; Lee, B. I.; Mathern, G. W.; Moshe, S. L.; Perucca, E.; Scheffer, I. E.; Tomson, T.; Watanabe, M.; Wiebe, S. ILAE official report: a practical clinical definition of epilepsy. *Epilepsia* **2014**, *55*, 475-482.
6. Scheffer, I. E.; Berkovic, S.; Capovilla, G.; Connolly, M. B.; French, J.; Guilhoto, L.; Hirsch, E.; Jain, S.; Mathern, G. W.; Moshé, S. L.; Nordli, D. R.; Perucca, E.; Tomson, T.; Wiebe, S.; Zhang, Y.-H.; Zuberi, S. M. ILAE classification of the epilepsies: Position paper of the ILAE Commission for Classification and Terminology. *Epilepsia* **2017**, *58*, 512-521.
7. Böhme, I.; Lüddens, H. Zielstrukturen für Antiepileptika *Pharm. Unserer Zeit* **2007**, *36*, 262-268.
8. Shorvon, S. D. The etiologic classification of epilepsy. *Epilepsia* **2011**, *52*, 1052-1057.
9. Wu, Y. W.; Sullivan, J.; McDaniel, S. S.; Meisler, M. H.; Walsh, E. M.; Li, S. X.; Kuzniewicz, M. W. Incidence of Dravet Syndrome in a US Population. *Pediatrics* **2015**, *136*, e1310-e1315.
10. Al-Banji, M. H.; Zahr, D. K.; Jan, M. M. Lennox-Gastaut syndrome: Management update. *Neurosciences* **2015**, *20*, 207-212.
11. Perucca, E. An Introduction to Antiepileptic Drugs. *Epilepsia* **2005**, *46*, 31-37.

8 References

12. Rogawski, M. A.; Loscher, W. The neurobiology of antiepileptic drugs. *Nat. Rev. Neurosci.* **2004**, *5*, 553-564.
13. Catterall, W. A. From ionic currents to molecular mechanisms: the structure and function of voltage-gated sodium channels. *Neuron* **2000**, *26*, 13-25.
14. Meldrum, B. S.; Rogawski, M. A. Molecular targets for antiepileptic drug development. *Neurotherapeutics.* **2007**, *4*, 18-61.
15. Surges, R.; Volynski, K. E.; Walker, M. C. Is Levetiracetam different from other antiepileptic drugs? Levetiracetam and its cellular mechanism of action in epilepsy revisited. *Ther. Adv. Neurol. Disord.* **2008**, *1*, 13-24.
16. Rundfeldt, C. The new anticonvulsant retigabine (D-23129) acts as an opener of K⁺ channels in neuronal cells. *Eur. J. Pharmacol.* **1997**, *336*, 243-249.
17. Main, M. J.; Cryan, J. E.; Dupere, J. R.; Cox, B.; Clare, J. J.; Burbidge, S. A. Modulation of KCNQ2/3 potassium channels by the novel anticonvulsant retigabine. *Mol. Pharmacol.* **2000**, *58*, 253-262.
18. Ängelsten, M.; Ben-Menachem, E.; Rönnebeck, L.; Hansson, E. Novel Mechanisms of Action of Three Antiepileptic Drugs, Vigabatrin, Tiagabine, and Topiramate. *Neurochem. Res.* **2003**, *28*, 333-340.
19. Qian, A.; Johnson, J. W. Channel gating of NMDA receptors. *Physiol. Behav.* **2002**, *77*, 577-582.
20. Subramaniam, S.; Rho, J. M.; Penix, L.; Donevan, S. D.; Fielding, R. P.; Rogawski, M. A. Felbamate block of the N-methyl-D-aspartate receptor. *J. Pharmacol. Exp. Ther.* **1995**, *273*, 878-886.
21. Schmidt, D.; Schachter, S. C. Drug treatment of epilepsy in adults. *Br. Med. J.* **2014**, *348*.
22. Rogawski, M. A.; Cavazos, J. E. Mechanisms of action of antiepileptic drugs. In *Wyllie's treatment of epilepsy: principles and practices*, Sixth ed.; Wyllie, E.; Gidal, B.; Goodkin, H.; Loddenkemper, T.; Sirven, J., Eds. Wolters Kluwer: Philadelphia, 2014; pp 522-529.
23. Gryder, D. S.; Rogawski, M. A. Selective antagonism of GluR5 kainate-receptor-mediated synaptic currents by topiramate in rat basolateral amygdala neurons. *J. Neurosci.* **2003**, *23*, 7069-7074.

8 References

24. Bromfield, E.; Cavazos, J.; Sirven, J., Neuropharmacology of Antiepileptic Drugs. In *An Introduction to Epilepsy* [Online] Bromfield, E.; Cavazos, J.; Sirven, J., Eds. American Epilepsy Society, West Hartford (CT): <https://www.ncbi.nlm.nih.gov/books/NBK2513/>, **2006** (accessed 13.03.2017).
25. Löscher, W.; Gillard, M.; Sands, Z. A.; Kaminski, R. M.; Klitgaard, H. Synaptic vesicle glycoprotein 2A ligands in the treatment of epilepsy and beyond. *CNS Drugs* **2016**, *30*, 1055-1077.
26. Remy, S.; Beck, H. Molecular and cellular mechanism of pharmacoresistance in epilepsy *Brain* **2006**, *129*, 18-35.
27. Armijo, J.; Adin, J.; Sanchez, M. Mechanism of action of antiepileptic drugs and new antiepileptic drugs. *Rev. Neurol.* **2006**, *43 Suppl. 1*, 17-41.
28. Goldberg, E. M.; Coulter, D. A. Mechanisms of epileptogenesis: a convergence on neural circuit dysfunction. *Nat. Rev. Neurosci.* **2013**, *14*, 337-349.
29. Stafstrom, C. E. Mechanisms of action of antiepileptic drugs: the search for synergy. *Curr. Opin. Neurol.* **2010**, *23*, 157-163.
30. Lason, W.; Dudra-Jastrzebska, M.; Rejdak, K.; Czuczwar, S. J. Basic mechanisms of antiepileptic drugs and their pharmacokinetic/pharmacodynamic interactions: an update. *Pharmacol. Rep.* **2011**, *63*, 271-292.
31. Rogawski, M. A.; Loscher, W.; Rho, J. M. Mechanisms of action of antiseizure drugs and the ketogenic diet. *Cold Spring Harb. Perspect. Med.* **2016**, *6*, pii: a022780.
32. Wahab, A. Difficulties in treatment and management of epilepsy and challenges in new drug development. *Pharmaceuticals* **2010**, *3*, 2090-2110.
33. Kalachnik, J. E.; Hanzel, T. E.; Sevenich, R.; Harder, S. R. Brief report: clonazepam behavioral side effects with an individual with mental retardation. *J. Autism Dev. Disord.* **2003**, *33*, 349-354.
34. Keranen, T.; Sivenius, J. Side effects of carbamazepine, valproate and clonazepam during long-term treatment of epilepsy. *Acta Neurol. Scand. Suppl.* **1983**, *97*, 69-80.
35. Kazzi, Z. N.; Jones, C. C.; Morgan, B. W. Seizures in a pediatric patient with a tiagabine overdose. *J. Med. Toxicol.* **2006**, *2*, 160-162.
36. Pellock, J. M.; Brodie, M. J. Felbamate: 1997 Update. *Epilepsia* **1997**, *38*, 1261-1264.

8 References

37. Harris, J. A.; Murphy, J. A. Retigabine (ezogabine) as add-on therapy for partial-onset seizures: an update for clinicians. *Ther. Adv. Chronic Dis.* **2011**, *2*, 371-376.
38. Hildenbrand, S. Levetiracetam and Brivaracetam: synthesis of radioligands as pharmacological tools for studying their interactions with target proteins. PhD, University of Bonn, 2012.
39. Baker, G. A.; Jacoby, A.; Buck, D.; Stalgis, C.; Monnet, D. Quality of life of people with epilepsy: a European study. *Epilepsia* **1997**, *38*, 353-362.
40. Klitgaard, H.; Matagne, A.; Nicolas, J. M.; Gillard, M.; Lamberty, Y.; De Ryck, M.; Kaminski, R. M.; Leclercq, K.; Niespodziany, I.; Wolff, C.; Wood, M.; Hannestad, J.; Kervyn, S.; Kenda, B. Brivaracetam: Rationale for discovery and preclinical profile of a selective SV2A ligand for epilepsy treatment. *Epilepsia* **2016**, *57*, 538-548.
41. Ulloa, C. M.; Towfigh, A.; Safdieh, J. Review of levetiracetam, with a focus on the extended release formulation, as adjuvant therapy in controlling partial-onset seizures. *Neuropsychiatr. Dis. Treat.* **2009**, *5*, 467-476.
42. Abou-Khalil, B. Levetiracetam in the treatment of epilepsy. *Neuropsychiatr. Dis. Treat.* **2008**, *4*, 507-523.
43. Lynch, B. A.; Lambeng, N.; Nocka, K.; Kensel-Hammes, P.; Bajjalieh, S. M.; Matagne, A.; Fuks, B. The synaptic vesicle protein SV2A is the binding site for the antiepileptic drug levetiracetam. *Proc. Natl. Acad. Sci. U. S. A.* **2004**, *101*, 9861-9866.
44. Klitgaard, H.; Matagne, A.; Gobert, J.; Wülfert, E. Evidence for a unique profile of levetiracetam in rodent models of seizures and epilepsy. *Eur. J. Pharmacol.* **1998**, *353*, 191-206.
45. Gower, A. J.; Noyer, M.; Verloes, R.; Gobert, J.; Wülfert, E. ucb L059, a novel anti-convulsant drug: pharmacological profile in animals. *Eur. J. Pharmacol.* **1992**, *222*, 193-203.
46. Löscher, W.; Hönack, D. Profile of ucb L059, a novel anticonvulsant drug, in models of partial and generalized epilepsy in mice and rats. *Eur. J. Pharmacol.* **1993**, *232*, 147-158.
47. Kaminski, R. M.; Rogawski, M. A.; Klitgaard, H. The potential of antiseizure drugs and agents that act on novel molecular targets as antiepileptogenic treatments. *Neurotherapeutics.* **2014**, *11*, 385-400.

8 References

48. Bedner, P.; Dupper, A.; Hüttmann, K.; Müller, J.; Herde, M. K.; Dublin, P.; Deshpande, T.; Schramm, J.; Häussler, U.; Haas, C. A.; Henneberger, C.; Theis, M.; Steinhäuser, C. Astrocyte uncoupling as a cause of human temporal lobe epilepsy. *Brain* **2015**, *138*, 1208-1222.
49. Noyer, M.; Gillard, M.; Matagne, A.; Henichart, J. P.; Wülfert, E. The novel antiepileptic drug levetiracetam (ucb L059) appears to act via a specific binding site in CNS membranes. *Eur. J. Pharmacol.* **1995**, *286*, 137-146.
50. Kaminski, R. M.; Matagne, A.; Leclercq, K.; Gillard, M.; Michel, P.; Kenda, B.; Talaga, P.; Klitgaard, H. SV2A protein is a broad-spectrum anticonvulsant target: functional correlation between protein binding and seizure protection in models of both partial and generalized epilepsy. *Neuropharmacology* **2008**, *54*, 715-720.
51. Bialer, M.; White, H. S. Key factors in the discovery and development of new antiepileptic drugs. *Nat. Rev. Drug Discov.* **2010**, *9*, 68-82.
52. FDA approves Briviact to treat partial onset seizures (2016). <http://www.fda.gov/NewsEvents/Newsroom/PressAnnouncements/ucm486827.htm> (accessed 10.02.2017).
53. Markham, A. Brivaracetam: First Global Approval. *Drugs* **2016**, *76*, 517-522.
54. Gillard, M.; Fuks, B.; Leclercq, K.; Matagne, A. Binding characteristics of brivaracetam, a selective, high affinity SV2A ligand in rat, mouse and human brain: relationship to anti-convulsant properties. *Eur. J. Pharmacol.* **2011**, *664*, 36-44.
55. Yates, S. L.; Fakhoury, T.; Liang, W.; Eckhardt, K.; Borghts, S.; D'Souza, J. An open-label, prospective, exploratory study of patients with epilepsy switching from levetiracetam to brivaracetam. *Epilepsy Behav.* **2015**, *52*, 165-168.
56. Wood, M.; Gillard, M. Evidence for a Differential interaction of brivaracetam and levetiracetam with the SV2A protein (P5.246). *Neurology* **2016**, *86*.
57. Hildenbrand, S.; Baqi, Y.; Müller, C. E. Synthesis of tritium-labeled levetiracetam ((2S)-2-(2-oxopyrrolidin-1-yl)butanamide) with high specific activity. *J. Labelled Comp. Radiopharm.* **2011**, *55*, 48-51.
58. Hildenbrand, S.; Schoch, S.; von Lehe, M.; Surges, R.; Müller, C. E. Tritium-labeled brivaracetam with high specific activity: preparation, characterization and application in human brain samples. *ChemMedChem* **2012**, *7*, 1369-1374.

8 References

59. Bajjalieh, S. M.; Frantz, G. D.; Weimann, J. M.; McConnell, S. K.; Scheller, R. H. Differential expression of synaptic vesicle protein 2 (SV2) isoforms. *J. Neurosci.* **1994**, *14*, 5223-5235.
60. Janz, R.; Goda, Y.; Geppert, M.; Missler, M.; Südhof, T. C. SV2A and SV2B function as redundant Ca²⁺ regulators in neurotransmitter release. *Neuron* **1999**, *24*, 1003-1016.
61. Bajjalieh, S. M.; Peterson, K.; Shinghal, R.; Scheller, R. H. SV2, a brain synaptic vesicle protein homologous to bacterial transporters. *Science* **1992**, *257*, 1271-1273.
62. Janz, R.; Südhof, T. C. SV2C is a synaptic vesicle protein with an unusually restricted localization: anatomy of a synaptic vesicle protein family. *Neuroscience* **1999**, *94*, 1279-1290.
63. Bajjalieh, S. M.; Peterson, K.; Linial, M.; Scheller, R. H. Brain contains two forms of synaptic vesicle protein 2. *Proc. Natl. Acad. Sci. U. S. A.* **1993**, *90*, 2150-2154.
64. Mendoza-Torreblanca, J. G.; Vanoye-Carlo, A.; Phillips-Farfan, B. V.; Carmona-Aparicio, L.; Gomez-Lira, G. Synaptic vesicle protein 2A: basic facts and role in synaptic function. *Eur. J. Neurosci.* **2013**, *38*, 3529-3539.
65. Madeo, M.; Kovacs, A. D.; Pearce, D. A. The human synaptic vesicle protein, SV2A, functions as a galactose transporter in *Saccharomyces cerevisiae*. *J. Biol. Chem.* **2014**, *289*, 33066-33071.
66. Kwon, S. E.; Chapman, E. R. Glycosylation is dispensable for sorting of synaptotagmin 1 but is critical for targeting of SV2 and synaptophysin to recycling synaptic vesicles. *J. Biol. Chem.* **2012**, *287*, 35658-35668.
67. Lynch, B.; Matagne, A.; Brännström, A.; von-Euler, A.; Jansson, M.; Hauzenberger, E.; Söderhäll, J. Visualization of SV2A conformations in situ by the use of protein tomography. *Biochem. Biophys. Res. Commun.* **2008**, *375*, 491-495.
68. Wan, Q.; Zhou, Z.; Thakur, P.; Vila, A.; Sherry, D.; Janz, R.; Heidelberger, R. SV2 acts via presynaptic calcium to regulate neurotransmitter release. *Neuron* **2011**, *66*, 884-895.
69. Reigada, D.; Diez-Perez, I.; Gorostiza, P.; Verdaguer, A.; Gomez de Aranda, I.; Pineda, O.; Vilarrasa, J.; Marsal, J.; Blasi, J.; Aleu, J.; Solsona, C. Control of neurotransmitter release by an internal gel matrix in synaptic vesicles. *Proc. Natl. Acad. Sci. U. S. A.* **2003**, *100*, 3485-3490.

8 References

70. Budzinski, K. L.; Allen, R. W.; Fujimoto, B. S.; Kensel-Hammes, P.; Belnap, D. M.; Bajjalieh, S. M.; Chiu, D. T. Large structural change in isolated synaptic vesicles upon loading with neurotransmitter. *Biophys. J.* **2009**, *97*, 2577-2584.
71. Yao, J.; Bajjalieh, S. Synaptic vesicle protein 2 binds adenine nucleotides. *J. Biol. Chem.* **2008**, *283*, 20628-20634.
72. Schivell, A. E.; Batchelor, R. H.; Bajjalieh, S. M. Isoform-specific, calcium-regulated interaction of the synaptic vesicle proteins SV2 and synaptotagmin. *J. Biol. Chem.* **1996**, *271*, 27770-27775.
73. Crowder, K. M.; Gunther, J. M.; Jones, T. A.; Hale, B. D.; Zhang, H. Z.; Peterson, M. R.; Scheller, R. H.; Chavkin, C.; Bajjalieh, S. M. Abnormal neurotransmission in mice lacking synaptic vesicle protein 2A (SV2A). *Proc. Natl. Acad. Sci. U. S. A.* **1999**, *96*, 15268-15273.
74. Kaminski, R. M.; Gillard, M.; Leclercq, K.; Hanon, E.; Lorent, G.; Dassel, D.; Matagne, A.; Klitgaard, H. Proepileptic phenotype of SV2A-deficient mice is associated with reduced anticonvulsant efficacy of levetiracetam. *Epilepsia* **2009**, *50*, 1729-1740.
75. Yang, X. F.; Rothman, S. M. Levetiracetam has a time- and stimulation-dependent effect on synaptic transmission. *Seizure* **2009**, *18*, 615-619.
76. Yang, X. F.; Weisenfeld, A.; Rothman, S. M. Prolonged exposure to levetiracetam reveals a presynaptic effect on neurotransmission. *Epilepsia* **2007**, *48*, 1861-1869.
77. Yang, X.; Bogner, J., Jr.; He, T.; Mohammed, M.; Niespodziany, I.; Wolff, C.; Esguerra, M.; Rothman, S. M.; Dubinsky, J. M. Brivaracetam augments short-term depression and slows vesicle recycling. *Epilepsia* **2015**, *56*, 1899-1909.
78. Löscher, W.; Reissmüller, E.; Ebert, U. Anticonvulsant efficacy of gabapentin and levetiracetam in phenytoin-resistant kindled rats. *Epilepsy Res.* **2000**, *40*, 63-77.
79. Leclercq, K.; Kaminski, R. M. Status epilepticus induction has prolonged effects on the efficacy of antiepileptic drugs in the 6-Hz seizure model. *Epilepsy Behav.* **2015**, *49*, 55-60.
80. Johns, S. J. TOPO2: Transmembrane protein display software. <http://www.sacs.ucsf.edu/TOPO2/> (accessed 15.04.2017).
81. Tusnády, G. E.; Simon, I. The HMMTOP transmembrane topology prediction server. *Bioinformatics* **2001**, *17*, 849-850.

8 References

82. Abbaci, M.; Barberi-Heyob, M.; Blondel, W.; Guillemin, F.; Didelon, J. Advantages and limitations of commonly used methods to assay the molecular permeability of gap junctional intercellular communication. *Biotechniques* **2008**, *45*, 33-52, 56-62.
83. Söhl, G.; Maxeiner, S.; Willecke, K. Expression and functions of neuronal gap junctions. *Nat. Rev. Neurosci.* **2005**, *6*, 191-200.
84. Vinken, M.; Vanhaecke, T.; Papeleu, P.; Snykers, S.; Henkens, T.; Rogiers, V. Connexins and their channels in cell growth and cell death. *Cell. Signal.* **2006**, *18*, 592-600.
85. Jeanson, T.; Pondaven, A.; Ezan, P.; Mouthon, F.; Charveriat, M.; Giaume, C. Antidepressants impact connexin 43 channel functions in astrocytes. *Front. Cell. Neurosci.* **2015**, *9*.
86. Solan, J. L.; Lampe, P. D. Connexin43 phosphorylation: structural changes and biological effects. *Biochem. J.* **2009**, *419*, 261-272.
87. Chen, Q.; Boire, A.; Jin, X.; Valiente, M.; Er, E. E.; Lopez-Soto, A.; S. Jacob, L.; Patwa, R.; Shah, H.; Xu, K.; Cross, J. R.; Massagué, J. Carcinoma–astrocyte gap junctions promote brain metastasis by cGAMP transfer. *Nature* **2016**, *533*, 493-498.
88. Baldwin, M. R.; Barbieri, J. T. Association of botulinum neurotoxin serotypes A and B with synaptic vesicle protein complexes. *Biochemistry* **2007**, *46*, 3200-3210.
89. Chen, S. Clinical uses of botulinum neurotoxins: current indications, limitations and future developments. *Toxins (Basel)* **2012**, *4*, 913-939.
90. Lam, K.-H.; Yao, G.; Jin, R. Diverse binding modes, same goal: the receptor recognition mechanism of botulinum neurotoxin. *Prog. Biophys. Mol. Biol.* **2015**, *117*, 225-231.
91. Strotmeier, J.; Mahrhold, S.; Krez, N.; Janzen, C.; Lou, J.; Marks, J. D.; Binz, T.; Rummel, A. Identification of the synaptic vesicle glycoprotein 2 receptor binding site in botulinum neurotoxin A. *FEBS Lett.* **2014**, *588*, 1087-1093.
92. Blum, F. C.; Chen, C.; Kroken, A. R.; Barbieri, J. T. Tetanus toxin and botulinum toxin a utilize unique mechanisms to enter neurons of the central nervous system. *Infect. Immun.* **2012**, *80*, 1662-1669.
93. Gu, S.; Jin, R. Assembly and function of the botulinum neurotoxin progenitor complex. *Curr. Top. Microbiol. Immunol.* **2013**, *364*, 21-44.

8 References

94. Walker, T. J.; Dayan, S. H. Comparison and overview of currently available neurotoxins. *J. Clin. Aesthet. Dermatol.* **2014**, *7*, 31-39.
95. EMA: List of nationally authorised medicinal products. Active substance(s): botulinum toxin a - haemagglutinin complex (2016) (accessed 14.03.2017).
96. Dong, M.; Yeh, F.; Tepp, W. H.; Dean, C.; Johnson, E. A.; Janz, R.; Chapman, E. R. SV2 is the protein receptor for botulinum neurotoxin A. *Science* **2006**, *312*, 592-596.
97. Rossetto, O.; Pirazzini, M.; Montecucco, C. Botulinum neurotoxins: genetic, structural and mechanistic insights. *Nat. Rev. Micro.* **2014**, *12*, 535-549.
98. Haghikia, A.; Ladage, K.; Hinkerohe, D.; Vollmar, P.; Heupel, K.; Dermietzel, R.; Faustmann, P. M. Implications of antiinflammatory properties of the anticonvulsant drug levetiracetam in astrocytes. *J. Neurosci. Res.* **2008**, *86*, 1781-1788.
99. Stienen, M. N.; Haghikia, A.; Dambach, H.; Thöne, J.; Wiemann, M.; Gold, R.; Chan, A.; Dermietzel, R.; Faustmann, P. M.; Hinkerohe, D.; Prochnow, N. Anti-inflammatory effects of the anticonvulsant drug levetiracetam on electrophysiological properties of astroglia are mediated via TGFbeta1 regulation. *Br. J. Pharmacol.* **2011**, *162*, 491-507.
100. Gillard, M.; Fuks, B.; Michel, P.; Vertongen, P.; Massingham, R.; Chatelain, P. Binding characteristics of [³H]ucb 30889 to levetiracetam binding sites in rat brain. *Eur. J. Pharmacol.* **2003**, *478*, 1-9.
101. Matagne, A.; Margineanu, D. G.; Potschka, H.; Löscher, W.; Michel, P.; Kenda, B.; Klitgaard, H. Profile of the new pyrrolidone derivative seletracetam (ucb 44212) in animal models of epilepsy. *Eur. J. Pharmacol.* **2009**, *614*, 30-37.
102. Daniels, V.; Wood, M.; Leclercq, K.; Kaminski, R. M.; Gillard, M. Modulation of the conformational state of the SV2A protein by an allosteric mechanism as evidenced by ligand binding assays. *Br. J. Pharmacol.* **2013**, *169*, 1091-1101.
103. Mercier, J.; Archen, L.; Bollu, V.; Carre, S.; Evrard, Y.; Jnoff, E.; Kenda, B.; Lallemand, B.; Michel, P.; Montel, F.; Moureau, F.; Price, N.; Quesnel, Y.; Sauvage, X.; Valade, A.; Provins, L. Discovery of heterocyclic nonacetamide synaptic vesicle protein 2A (SV2A) ligands with single-digit nanomolar potency: opening avenues towards the first SV2A positron emission tomography (PET) ligands. *ChemMedChem* **2014**, *9*, 693-698.
104. Gillard, M.; Chatelain, P.; Fuks, B. Binding characteristics of levetiracetam to synaptic vesicle protein 2A (SV2A) in human brain and in CHO cells expressing the human recombinant protein. *Eur. J. Pharmacol.* **2006**, *536*, 102-108.

8 References

105. Finnema, S. J.; Nabulsi, N. B.; Eid, T.; Detyniecki, K.; Lin, S.-f.; Chen, M.-K.; Dhaher, R.; Matuskey, D.; Baum, E.; Holden, D.; Spencer, D. D.; Mercier, J.; Hannestad, J.; Huang, Y.; Carson, R. E. Imaging synaptic density in the living human brain. *Sci. Transl. Med.* **2016**, *8*, 348ra396.
106. Warnock, G. I.; Aerts, J.; Bahri, M. A.; Bretin, F.; Lemaire, C.; Giacomelli, F.; Mievis, F.; Mestdagh, N.; Buchanan, T.; Valade, A.; Mercier, J.; Wood, M.; Gillard, M.; Seret, A.; Luxen, A.; Salmon, E.; Plenevaux, A. Evaluation of 18F-UCB-H as a novel PET tracer for synaptic vesicle protein 2A in the brain. *J. Nucl. Med.* **2014**, *55*, 1336-1341.
107. Nabulsi, N. B.; Mercier, J.; Holden, D.; Carre, S.; Najafzadeh, S.; Vandergeten, M. C.; Lin, S. F.; Deo, A.; Price, N.; Wood, M.; Lara-Jaime, T.; Montel, F.; Laruelle, M.; Carson, R. E.; Hannestad, J.; Huang, Y. Synthesis and Preclinical Evaluation of 11C-UCB-J as a PET Tracer for Imaging the Synaptic Vesicle Glycoprotein 2A in the Brain. *J. Nucl. Med.* **2016**, *57*, 777-784.
108. Estrada, S.; Lubberink, M.; Thibblin, A.; Sprycha, M.; Buchanan, T.; Mestdagh, N.; Kenda, B.; Mercier, J.; Provins, L.; Gillard, M.; Tytgat, D.; Antoni, G. [(11)C]UCB-A, a novel PET tracer for synaptic vesicle protein 2A. *Nucl. Med. Biol.* **2016**, *43*, 325-332.
109. Oprea, T. I.; Mestres, J. Drug repurposing: far beyond new targets for old drugs. *AAPS J.* **2012**, *14*, 759-763.
110. Tanabe, K. K.; Cusack, J. C. In *Surgery: basic science and clinical evidence*. Springer: Berlin, 2001.
111. Xia, W.; Bringmann, P.; McClary, J.; Jones, P. P.; Manzana, W.; Zhu, Y.; Wang, S.; Liu, Y.; Harvey, S.; Madlansacay, M. R. High levels of protein expression using different mammalian CMV promoters in several cell lines. *Protein Expression Purif.* **2006**, *45*, 115-124.
112. Zhang, J. H.; Chung, T. D.; Oldenburg, K. R. A simple statistical parameter for use in evaluation and validation of high throughput screening assays. *J. Biomol. Screen.* **1999**, *4*, 67-73.
113. Carpenter, J. W.; Laethem, C.; Hubbard, F. R.; Eckols, T. K.; Baez, M.; McClure, D.; Nelson, D. L.; Johnston, P. A. Configuring radioligand receptor binding assays for HTS using scintillation proximity assay technology. *Methods Mol. Biol.* **2002**, *190*, 31-49.
114. WHO, 19th WHO Model List of Essential Medicines. 2015.

8 References

115. Miadonna, A.; Milazzo, N.; Lorini, M.; Marchesi, E.; Tedeschi, A. Inhibitory effect of the H1 antagonist loratadine on histamine release from human basophils. *Int. Arch. Allergy Immunol.* **1994**, *105*, 12-17.
116. Barenholtz, H. A.; McLeod, D. C. Loratadine: a nonsedating antihistamine with once-daily dosing. *DICP* **1989**, *23*, 445-450.
117. Kay, G. G.; Harris, A. G. Loratadine: a non-sedating antihistamine. Review of its effects on cognition, psychomotor performance, mood and sedation. *Clin. Exp. Allergy* **1999**, *29 Suppl. 3*, 147-150.
118. Obach, R. S. Pharmacologically Active Drug Metabolites: Impact on Drug Discovery and Pharmacotherapy. *Pharmacol. Rev.* **2013**, *65*, 578-640.
119. Lin, C. C.; Radwanski, E.; Affrime, M.; Cayen, M. Pharmacokinetics of loratadine in pediatric subjects. *Am. J. Ther.* **1995**, *2*, 504-508.
120. Achan, J.; Talisuna, A. O.; Erhart, A.; Yeka, A.; Tibenderana, J. K.; Baliraine, F. N.; Rosenthal, P. J.; D'Alessandro, U. Quinine, an old anti-malarial drug in a modern world: role in the treatment of malaria. *Malar. J.* **2011**, *10*, 144-156.
121. Foley, M.; Tilley, L. Quinoline antimalarials: Mechanisms of action and resistance. *Int. J. Parasitol.* **1997**, *27*, 231-240.
122. Clifford, M.; Leah, M.; Charles, N. Antiepileptic properties of quinine: A systematic review. *Ann. Neurosci.* **2012**, *19*, 14-20.
123. Nassiri-Asl, M.; Zamansoltani, F.; Torabinejad, B. Antiepileptic effects of quinine in the pentylenetetrazole model of seizure. *Seizure* **2009**, *18*, 129-132.
124. Bostanci, M. O.; Bagirici, F. Anticonvulsive effects of quinine on penicillin-induced epileptiform activity: an in vivo study. *Seizure* **2007**, *16*, 166-172.
125. Gajda, Z.; Szupera, Z.; Blazso, G.; Szente, M. Quinine, a blocker of neuronal Cx36 channels, suppresses seizure activity in rat neocortex in vivo. *Epilepsia* **2005**, *46*, 1581-1591.
126. Srinivas, M.; Hopperstad, M. G.; Spray, D. C. Quinine blocks specific gap junction channel subtypes. *Proc. Natl. Acad. Sci. U. S. A.* **2001**, *98*, 10942-10947.
127. Etemadi, F.; Sayyah, M.; Pourbadie, H. G.; Babapour, V. Facilitation of hippocampal kindling and exacerbation of kindled seizures by intra-cal injection of quinine: a possible role of Cx36 gap junctions. *Iran. Biomed. J.* **2016**, *20*, 266-272.

8 References

128. Pukrittayakamee, S.; Wanwimolruk, S.; Stepniewska, K.; Jantra, A.; Huyakorn, S.; Looareesuwan, S.; White, N. J. Quinine pharmacokinetic-pharmacodynamic relationships in uncomplicated falciparum malaria. *Antimicrob. Agents Chemother.* **2003**, *47*, 3458-3463.
129. Silamut, K.; White, N. J.; Looareesuwan, S.; Warrell, D. A. Binding of quinine to plasma proteins in falciparum malaria. *Am. J. Trop. Med. Hyg.* **1985**, *34*, 681-686.
130. Reddy, D. S.; Golub, V. M. The pharmacological basis of cannabis therapy for epilepsy. *J. Pharmacol. Exp. Ther.* **2016**, *357*, 45-55.
131. Devinsky, O.; Cilio, M. R.; Cross, H.; Fernandez-Ruiz, J.; French, J.; Hill, C.; Katz, R.; Di Marzo, V.; Jutras-Aswad, D.; Notcutt, W. G.; Martinez-Orgado, J.; Robson, P. J.; Rohrback, B. G.; Thiele, E.; Whalley, B.; Friedman, D. Cannabidiol: pharmacology and potential therapeutic role in epilepsy and other neuropsychiatric disorders. *Epilepsia* **2014**, *55*, 791-802.
132. Di Marzo, V. A brief history of cannabinoid and endocannabinoid pharmacology as inspired by the work of British scientists. *Trends. Pharmacol. Sci.* **2006**, *27*, 134-140.
133. De Petrocellis, L.; Di Marzo, V. Non-CB1, non-CB2 receptors for endocannabinoids, plant cannabinoids, and synthetic cannabimimetics: focus on G-protein-coupled receptors and transient receptor potential channels. *J. Neuroimmune Pharmacol.* **2010**, *5*, 103-121.
134. Rosenberg, E. C.; Tsien, R. W.; Whalley, B. J.; Devinsky, O. Cannabinoids and Epilepsy. *Neurotherapeutics : the journal of the American Society for Experimental NeuroTherapeutics* **2015**, *12*, 747-768.
135. Oliére, S.; Jolette-Riopel, A.; Potvin, S.; Jutras-Aswad, D. Modulation of the endocannabinoid system: vulnerability factor and new treatment target for stimulant addiction. *Front. Mol. Psychiatry* **2013**, *4*.
136. Iannotti, F. A.; Silvestri, C.; Mazzarella, E.; Martella, A.; Calvigioni, D.; Piscitelli, F.; Ambrosino, P.; Petrosino, S.; Czifra, G.; Bíró, T.; Harkany, T.; Tagliatalata, M.; Di Marzo, V. The endocannabinoid 2-AG controls skeletal muscle cell differentiation via CB1 receptor-dependent inhibition of Kv7 channels. *Proc. Natl. Acad. Sci. U. S. A.* **2014**, *111*, E2472-E2481.
137. Andradas, C.; Blasco-Benito, S.; Castillo-Lluva, S.; Dillenburg-Pilla, P.; Diez-Alarcia, R.; Juanes-García, A.; García-Taboada, E.; Hernando-Llorente, R.; Soriano, J.; Hamann, S.; Wenners, A.; Alkatout, I.; Klapper, W.; Rocken, C.; Bauer, M.; Arnold, N.; Quintanilla, M.; Megías, D.; Vicente-Manzanares, M.; Urigüen, L.; Gutkind, J. S.; Guzmán, M.; Pérez-Gómez, E.; Sánchez, C. Activation of the orphan receptor GPR55

8 References

- by lysophosphatidylinositol promotes metastasis in triple-negative breast cancer. *Oncotarget* **2016**, *7*, 47565-47575.
138. Finlay, D. B.; Joseph, W. R.; Grimsey, N. L.; Glass, M. GPR18 undergoes a high degree of constitutive trafficking but is unresponsive to N-Arachidonoyl Glycine. *PeerJ* **2016**, *4*, e1835.
139. Blair, R. E.; Deshpande, L. S.; DeLorenzo, R. J. Cannabinoids: is there a potential treatment role in epilepsy? *Expert Opin. Pharmacother.* **2015**, *16*, 1911-1914.
140. Devinsky, O.; Marsh, E.; Friedman, D.; Thiele, E.; Laux, L.; Sullivan, J.; Miller, I.; Flamini, R.; Wilfong, A.; Filloux, F.; Wong, M.; Tilton, N.; Bruno, P.; Bluvstein, J.; Hedlund, J.; Kamens, R.; Maclean, J.; Nangia, S.; Singhal, N. S.; Wilson, C. A.; Patel, A.; Cilio, M. R. Cannabidiol in patients with treatment-resistant epilepsy: an open-label interventional trial. *Lancet. Neurol.* **2016**, *15*, 270-278.
141. Pharmaceuticals, G., GW Pharmaceuticals Announces Epidiolex® Receives Orphan Drug Designation from the European Medicines Agency for the Treatment of Lennox-Gastaut Syndrome. Schultz, S., Ed. GLOBE NEWSWIRE: <https://globenewswire.com/news-release/2017/03/29/946290/0/en/GW-Pharmaceuticals-Announces-Epidiolex-Receives-Orphan-Drug-Designation-from-the-European-Medicines-Agency-for-the-Treatment-of-Lennox-Gastaut-Syndrome.html>, 2017.
142. Wallace, M. J.; Blair, R. E.; Falenski, K. W.; Martin, B. R.; DeLorenzo, R. J. The endogenous cannabinoid system regulates seizure frequency and duration in a model of temporal lobe epilepsy. *J. Pharmacol. Exp. Ther.* **2003**, *307*, 129-137.
143. Blair, R. E.; Deshpande, L. S.; Sombati, S.; Falenski, K. W.; Martin, B. R.; DeLorenzo, R. J. Activation of the cannabinoid type-1 receptor mediates the anticonvulsant properties of cannabinoids in the hippocampal neuronal culture models of acquired epilepsy and status epilepticus. *J. Pharmacol. Exp. Ther.* **2006**, *317*, 1072-1078.
144. Echevoyen, J.; Armstrong, C.; Morgan, R. J.; Soltesz, I. Single Application of a CB1 receptor antagonist rapidly following head injury prevents long-term hyperexcitability in a rat model. *Epilepsy Res.* **2009**, *85*, 123-127.
145. Rinaldi-Carmona, M.; Barth, F.; Heaulme, M.; Alonso, R.; Shire, D.; Congy, C.; Soubrie, P.; Breliere, J. C.; Le Fur, G. Biochemical and pharmacological characterisation of SR141716A, the first potent and selective brain cannabinoid receptor antagonist. *Life Sci.* **1995**, *56*, 1941-1947.

8 References

146. Lan, R.; Liu, Q.; Fan, P.; Lin, S.; Fernando, S. R.; McCallion, D.; Pertwee, R.; Makriyannis, A. Structure-activity relationships of pyrazole derivatives as cannabinoid receptor antagonists. *J. Med. Chem.* **1999**, *42*, 769-776.
147. Lan, R.; Gatley, J.; Lu, Q.; Fan, P.; Fernando, S. R.; Volkow, N. D.; Pertwee, R.; Makriyannis, A. Design and synthesis of the CB1 selective cannabinoid antagonist AM281: a potential human SPECT ligand. *AAPS PharmSci.* **1999**, *1*, E4.
148. Makriyannis, A.; Deng, H., Cannabimimetic indole derivatives. Google Patents: 2007.
149. Felder, C. C.; Joyce, K. E.; Briley, E. M.; Mansouri, J.; Mackie, K.; Blond, O.; Lai, Y.; Ma, A. L.; Mitchell, R. L. Comparison of the pharmacology and signal transduction of the human cannabinoid CB1 and CB2 receptors. *Mol. Pharmacol.* **1995**, *48*, 443-450.
150. Florek-Luszczki, M.; Wlaz, A.; Zagaja, M.; Andres-Mach, M.; Kondrat-Wrobel, M. W.; Luszczki, J. J. Effects of WIN 55,212-2 (a synthetic cannabinoid CB1 and CB2 receptor agonist) on the anticonvulsant activity of various novel antiepileptic drugs against 6 Hz-induced psychomotor seizures in mice. *Pharmacol. Biochem. Behav.* **2015**, *130*, 53-58.
151. Wiley, J. L.; Compton, D. R.; Dai, D.; Lainton, J. A.; Phillips, M.; Huffman, J. W.; Martin, B. R. Structure-activity relationships of indole- and pyrrole-derived cannabinoids. *J. Pharmacol. Exp. Ther.* **1998**, *285*, 995-1004.
152. Iwamura, H.; Suzuki, H.; Ueda, Y.; Kaya, T.; Inaba, T. In vitro and in vivo pharmacological characterization of JTE-907, a novel selective ligand for cannabinoid CB2 receptor. *J. Pharmacol. Exp. Ther.* **2001**, *296*, 420-425.
153. Showalter, V. M.; Compton, D. R.; Martin, B. R.; Abood, M. E. Evaluation of binding in a transfected cell line expressing a peripheral cannabinoid receptor (CB2): identification of cannabinoid receptor subtype selective ligands. *J. Pharmacol. Exp. Ther.* **1996**, *278*, 989-999.
154. Ibeas Bih, C.; Chen, T.; Nunn, A. V.; Bazelot, M.; Dallas, M.; Whalley, B. J. Molecular Targets of Cannabidiol in Neurological Disorders. *Neurotherapeutics : the journal of the American Society for Experimental NeuroTherapeutics* **2015**, *12*, 699-730.
155. Jones, N. A.; Hill, A. J.; Smith, I.; Bevan, S. A.; Williams, C. M.; Whalley, B. J.; Stephens, G. J. Cannabidiol Displays Antiepileptiform and Antiseizure Properties In Vitro and In Vivo. *J. Pharmacol. Exp. Ther.* **2010**, *332*, 569-577.

8 References

156. Wallace, M. J.; Wiley, J. L.; Martin, B. R.; DeLorenzo, R. J. Assessment of the role of CB1 receptors in cannabinoid anticonvulsant effects. *Eur. J. Pharmacol.* **2001**, *428*, 51-57.
157. Smith, M. D.; Wilcox, K. S.; White, S., Analysis of Cannabidiol Interactions with Antiseizure Drugs. American Epilepsy Society Abst. #1.215: https://www.aesnet.org/meetings_events/annual_meeting_abstracts/view/2326854, 2015.
158. Guy, G.; Flint, M. A single centre, placebo-controlled, four period, crossover, tolerability study assessing, pharmacodynamic effects, pharmacokinetic characteristics and cognitive profiles of a single dose of three formulations of cannabis based medicine extracts (CBMEs)(GWPD9901), plus a two period tolerability study comparing pharmacodynamic effects and pharmacokinetic characteristics of a single dose of a cannabis based medicine extract given via two administration routes (GWPD9901 EXT). *J. Cannabis Ther.* **2004**, *3*, 35-77.
159. Gronewold, A.; Skopp, G. A preliminary investigation on the distribution of cannabinoids in man. *Forensic Sci. Int.* **2011**, *210*, e7-e11.
160. Daniel Friedman; Maria Roberta Cilio; Nicole Tilton; Joseph Sullivan; Julie Hedlund; Evan Rosenberg; Judith Bluvstein; Orrin Devinsky, The effect of epidiolex (cannabidiol) on serum levels of concomitant anti-epileptic drugs in children and young adults with treatment-resistant epilepsy in an expanded access program. American Epilepsy Society https://www.aesnet.org/meetings_events/annual_meeting_abstracts/view/1868391 2014.
161. Ujváry, I.; Hanuš, L. Human metabolites of cannabidiol: a review on their formation, biological activity, and relevance in therapy. *Cannabis Cannabinoid Res.* **2016**, *1:1*, 90–101.
162. Högestätt, E. D.; Jönsson, B. A.; Ermund, A.; Andersson, D. A.; Björk, H.; Alexander, J. P.; Cravatt, B. F.; Basbaum, A. I.; Zygmunt, P. M. Conversion of acetaminophen to the bioactive N-acylphenolamine AM404 via fatty acid amide hydrolase-dependent arachidonic acid conjugation in the nervous system. *J. Biol. Chem.* **2005**, *280*, 31405-31412.
163. Pertwee, R. G.; Howlett, A. C.; Abood, M. E.; Alexander, S. P.; Di Marzo, V.; Elphick, M. R.; Greasley, P. J.; Hansen, H. S.; Kunos, G.; Mackie, K.; Mechoulam, R.; Ross, R. A. International Union of Basic and Clinical Pharmacology. LXXIX. Cannabinoid receptors and their ligands: beyond CB(1) and CB(2). *Pharmacol. Rev.* **2010**, *62*, 588-631.

8 References

164. Hess, C.; Schoeder, C. T.; Pillaiyar, T.; Madea, B.; Müller, C. E. Pharmacological evaluation of synthetic cannabinoids identified as constituents of spice. *Forensic Toxicol.* **2016**, *34*, 329-343.
165. Huffman, J. W.; Zengin, G.; Wu, M. J.; Lu, J.; Hynd, G.; Bushell, K.; Thompson, A. L.; Bushell, S.; Tartal, C.; Hurst, D. P.; Reggio, P. H.; Selley, D. E.; Cassidy, M. P.; Wiley, J. L.; Martin, B. R. Structure-activity relationships for 1-alkyl-3-(1-naphthoyl)indoles at the cannabinoid CB(1) and CB(2) receptors: steric and electronic effects of naphthoyl substituents. New highly selective CB(2) receptor agonists. *Bioorg. Med. Chem.* **2005**, *13*, 89-112.
166. Huffman, J. W.; Mabon, R.; Wu, M. J.; Lu, J.; Hart, R.; Hurst, D. P.; Reggio, P. H.; Wiley, J. L.; Martin, B. R. 3-Indolyl-1-naphthylmethanes: new cannabimimetic indoles provide evidence for aromatic stacking interactions with the CB(1) cannabinoid receptor. *Bioorg. Med. Chem.* **2003**, *11*, 539-549.
167. Huffman, J. W.; Padgett, L. W.; Isherwood, M. L.; Wiley, J. L.; Martin, B. R. 1-Alkyl-2-aryl-4-(1-naphthoyl)pyrroles: new high affinity ligands for the cannabinoid CB1 and CB2 receptors. *Bioorg. Med. Chem. Lett.* **2006**, *16*, 5432-5435.
168. Aung, M. M.; Griffin, G.; Huffman, J. W.; Wu, M.; Keel, C.; Yang, B.; Showalter, V. M.; Abood, M. E.; Martin, B. R. Influence of the N-1 alkyl chain length of cannabimimetic indoles upon CB(1) and CB(2) receptor binding. *Drug Alcohol Depend.* **2000**, *60*, 133-140.
169. Behrenswerth, A.; Volz, N.; Toräng, J.; Hinz, S.; Bräse, S.; Müller, C. E. Synthesis and pharmacological evaluation of coumarin derivatives as cannabinoid receptor antagonists and inverse agonists. *Bioorg. Med. Chem.* **2009**, *17*, 2842-2851.
170. Bossolan, G.; Trindade, C. E.; Barreiros, R. C. Blood galactose and glucose levels in mothers, cord blood, and 48-hour-old breast-fed full-term infants. *Neonatology* **2007**, *91*, 121-126.
171. Torre, E. R.; Steward, O. Protein synthesis within dendrites: glycosylation of newly synthesized proteins in dendrites of hippocampal neurons in culture. *J. Neurosci.* **1996**, *16*, 5967-5978.
172. Murrey, H. E.; Gama, C. I.; Kalovidouris, S. A.; Luo, W. I.; Driggers, E. M.; Porton, B.; Hsieh-Wilson, L. C. Protein fucosylation regulates synapsin Ia/Ib expression and neuronal morphology in primary hippocampal neurons. *Proc. Natl. Acad. Sci. U. S. A.* **2006**, *103*, 21-26.
173. Benoit, R. M.; Frey, D.; Hilbert, M.; Kevenaer, J. T.; Wieser, M. M.; Stirnimann, C. U.; McMillan, D.; Ceska, T.; Lebon, F.; Jaussi, R.; Steinmetz, M. O.; Schertler, G. F.;

8 References

- Hoogenraad, C. C.; Capitani, G.; Kammerer, R. A. Structural basis for recognition of synaptic vesicle protein 2C by botulinum neurotoxin A. *Nature* **2014**, *505*, 108-111.
174. Dong, M.; Liu, H.; Tepp, W. H.; Johnson, E. A.; Janz, R.; Chapman, E. R. Glycosylated SV2A and SV2B mediate the entry of botulinum neurotoxin E into neurons. *Mol. Biol. Cell* **2008**, *19*, 5226-5237.
175. Elger, C. E.; Heils, A., Variante des humanen SV2A-proteins und deren Einfluss auf die Therapieantwort bei Epilepsie. Google Patents: 2007.
176. Serajee, F. J.; Huq, A. M. homozygous mutation in synaptic vesicle glycoprotein 2A gene results in intractable epilepsy, involuntary movements, microcephaly, and developmental and growth retardation. *Pediatr. Neurol.* **2015**, *52*, 642-646 e641.
177. Lee, J.; Daniels, V.; Sands, Z. A.; Lebon, F.; Shi, J.; Biggin, P. C. Exploring the interaction of SV2A with racetams using homology modelling, molecular dynamics and site-directed mutagenesis. *PLoS One* **2015**, *10*, e0116589.
178. Shi, J.; Anderson, D.; Lynch, B. A.; Castaigne, J. G.; Foerch, P.; Lebon, F. Combining modelling and mutagenesis studies of synaptic vesicle protein 2A to identify a series of residues involved in racetam binding. *Biochem. Soc. Trans.* **2011**, *39*, 1341-1347.
179. Correa-Basurto, J.; Cuevas-Hernández, R. I.; Phillips-Farfán, B. V.; Martínez-Archundia, M.; Romo-Mancillas, A.; Ramírez-Salinas, G. L.; Pérez-González, Ó. A.; Trujillo-Ferrara, J.; Mendoza-Torreblanca, J. G. Identification of the antiepileptic racetam binding site in the synaptic vesicle protein 2A by molecular dynamics and docking simulations. *Front. Cell. Neurosci.* **2015**, *9*, 125.
180. Hutchison, C. A., 3rd; Phillips, S.; Edgell, M. H.; Gillam, S.; Jahnke, P.; Smith, M. Mutagenesis at a specific position in a DNA sequence. *J. Biol. Chem.* **1978**, *253*, 6551-6560.
181. Lehman, I. R. DNA ligase: structure, mechanism, and function. *Science* **1974**, *186*, 790-797.
182. An, Y.; Wu, W.; Lv, A. A PCR-after-ligation method for cloning of multiple DNA inserts. *Anal. Biochem.* **2010**, *402*, 203-205.
183. Gibson, D. G.; Smith, H. O.; Hutchison, C. A.; Venter, J. C.; Merryman, C. Chemical synthesis of the mouse mitochondrial genome. *Nat Meth* **2010**, *7*, 901-903.

8 References

184. Gibson, D. G.; Young, L.; Chuang, R.-Y.; Venter, J. C.; Hutchison, C. A.; Smith, H. O. Enzymatic assembly of DNA molecules up to several hundred kilobases. *Nat. Methods* **2009**, *6*, 343-345.
185. Kar, R.; Batra, N.; Riquelme, M. A.; Jiang, J. X. Biological role of connexin intercellular channels and hemichannels. *Arch. Biochem. Biophys.* **2012**, *524*, 2-15.
186. Salameh, A. Life cycle of connexins: regulation of connexin synthesis and degradation. *Adv. Cardiol.* **2006**, *42*, 57-70.
187. Laird, D. W. Life cycle of connexins in health and disease. *Biochem. J.* **2006**, *394*, 527-543.
188. Dbouk, H. A.; Mroue, R. M.; El-Sabban, M. E.; Talhouk, R. S. Connexins: a myriad of functions extending beyond assembly of gap junction channels. *Cell Commun. Signal.* **2009**, *7*, 4.
189. Thevenin, A. F.; Kowal, T. J.; Fong, J. T.; Kells, R. M.; Fisher, C. G.; Falk, M. M. Proteins and mechanisms regulating gap-junction assembly, internalization, and degradation. *Physiology (Bethesda)* **2013**, *28*, 93-116.
190. Thomas, M. A.; Zosso, N.; Scerri, I.; Demaurex, N.; Chanson, M.; Staub, O. A tyrosine-based sorting signal is involved in connexin43 stability and gap junction turnover. *J. Cell Sci.* **2003**, *116*, 2213-2222.
191. Laing, J. G.; Beyer, E. C. The gap junction protein connexin43 is degraded via the ubiquitin proteasome pathway. *J. Biol. Chem.* **1995**, *270*, 26399-26403.
192. Naus, C. C.; Laird, D. W. Implications and challenges of connexin connections to cancer. *Nat. Rev. Cancer* **2010**, *10*, 435-441.
193. Solan, J. L.; Lampe, P. D. Specific Cx43 phosphorylation events regulate gap junction turnover in vivo. *FEBS Lett.* **2014**, *588*, 1423-1429.
194. Imanaga, I.; Hai, L.; Ogawa, K.; Matsumura, K.; Mayama, T. Phosphorylation of connexin in functional regulation of the cardiac gap junction. *Exp. Clin. Cardiol.* **2004**, *9*, 161-164.
195. Haq, N.; Grose, D.; Ward, E.; Chiu, O.; Tigue, N.; Dowell, S. J.; Powell, A. J.; Chen, M. X. A high-throughput assay for connexin 43 (Cx43, GJA1) gap junctions using codon-optimized aequorin. *Assay Drug Dev. Technol.* **2013**, *11*, 93-100.

8 References

196. De Vuyst, E.; Boengler, K.; Antoons, G.; Sipido, K. R.; Schulz, R.; Leybaert, L. Pharmacological modulation of connexin-formed channels in cardiac pathophysiology. *Br. J. Pharmacol.* **2011**, *163*, 469-483.
197. Silberstein, S. D. Tonabersat, a novel gap-junction modulator for the prevention of migraine. *Cephalalgia.* **2009**, *29 Suppl. 2*, 28-35.
198. Morioka, N.; Suekama, K.; Zhang, F. F.; Kajitani, N.; Hisaoka-Nakashima, K.; Takebayashi, M.; Nakata, Y. Amitriptyline up-regulates connexin43-gap junction in rat cultured cortical astrocytes via activation of the p38 and c-Fos/AP-1 signalling pathway. *Br. J. Pharmacol.* **2014**, *171*, 2854-2867.
199. Fatemi, S. H.; Folsom, T. D.; Reutiman, T. J.; Lee, S. Expression of astrocytic markers aquaporin 4 and connexin 43 is altered in brains of subjects with autism. *Synapse.* **2008**, *62*, 501-507.
200. Mostafavi, H.; Khaksarian, M.; Joghataei, M. T.; Hassanzadeh, G.; Soleimani, M.; Eftekhari, S.; Soleimani, M.; Mousavizadeh, K.; Hadjighassem, M. R. Fluoxetine upregulates connexin 43 expression in astrocyte. *Basic Clin. Neurosci.* **2014**, *5*, 74-79.
201. Sun, J. D.; Liu, Y.; Yuan, Y. H.; Li, J.; Chen, N. H. Gap junction dysfunction in the prefrontal cortex induces depressive-like behaviors in rats. *Neuropsychopharmacology.* **2012**, *37*, 1305-1320.
202. Quesseveur, G.; Portal, B.; Basile, J. A.; Ezan, P.; Mathou, A.; Halley, H.; Leloup, C.; Fioramonti, X.; Deglon, N.; Giaume, C.; Rampon, C.; Guiard, B. P. Attenuated levels of hippocampal Connexin 43 and its phosphorylation correlate with antidepressant- and anxiolytic-like activities in mice. *Front. Cell. Neurosci.* **2015**, *9*, 490.
203. Liu, X.; Gangoso, E.; Yi, C.; Jeanson, T.; Kandelman, S.; Mantz, J.; Giaume, C. General anesthetics have differential inhibitory effects on gap junction channels and hemichannels in astrocytes and neurons. *Glia* **2016**, *64*, 524-536.
204. Duchene, A.; Perier, M.; Zhao, Y.; Liu, X.; Thomasson, J.; Chauveau, F.; Pierard, C.; Lagarde, D.; Picoli, C.; Jeanson, T.; Mouthon, F.; Dauvilliers, Y.; Giaume, C.; Lin, J. S.; Charveriat, M. Impact of astroglial connexins on modafinil pharmacological properties. *Sleep* **2016**, *39*, 1283-1292.
205. Guan, X.; Wilson, S.; Schlender, K. K.; Ruch, R. J. Gap-junction disassembly and connexin 43 dephosphorylation induced by 18 β -glycyrrhetic acid. *Mol. Carcinog.* **1996**, *16*, 157-164.

8 References

206. Lee, J. Y.; Choi, E. J.; Lee, J. A new high-throughput screening-compatible gap junctional intercellular communication assay. *BMC Biotechnol.* **2015**, *15*, 90.
207. Stewart, W. W. Functional connections between cells as revealed by dye-coupling with a highly fluorescent naphthalimide tracer. *Cell* **1978**, *14*, 741-759.
208. el-Fouly, M. H.; Trosko, J. E.; Chang, C. C. Scrape-loading and dye transfer. A rapid and simple technique to study gap junctional intercellular communication. *Exp. Cell Res.* **1987**, *168*, 422-430.
209. Raptis, L. H.; Brownell, H. L.; Firth, K. L.; Mackenzie, L. W. A novel technique for the study of intercellular, junctional communication: electroporation of adherent cells on a partly conductive slide. *DNA Cell Biol.* **1994**, *13*, 963-975.
210. Suter, S.; Trosko, J. E.; el-Fouly, M. H.; Lockwood, L. R.; Koestner, A. Dieldrin inhibition of gap junctional intercellular communication in rat glial cells as measured by the fluorescence photobleaching and scrape loading/dye transfer assays. *Fundam. Appl. Toxicol.* **1987**, *9*, 785-794.
211. Kavanagh, T. J.; Martin, G. M.; el-Fouly, M. H.; Trosko, J. E.; Chang, C. C.; Rabinovitch, P. S. Flow cytometry and scrape-loading/dye transfer as a rapid quantitative measure of intercellular communication in vitro. *Cancer Res.* **1987**, *47*, 6046-6051.
212. Dakin, K.; Zhao, Y.; Li, W. H. LAMP, a new imaging assay of gap junctional communication unveils that Ca²⁺ influx inhibits cell coupling. *Nat. Methods* **2005**, *2*, 55-62.
213. Neyton, J.; Trautmann, A. Single-channel currents of an intercellular junction. *Nature* **1985**, *317*, 331-335.
214. Churchill, G. C.; Lurtz, M. M.; Louis, C. F. Ca²⁺ regulation of gap junctional coupling in lens epithelial cells. *Am. J. Physiol. Cell Physiol.* **2001**, *281*, C972-C981.
215. Lurtz, M. M.; Louis, C. F. Intracellular calcium regulation of connexin43. *Am. J. Physiol. Cell Physiol.* **2007**, *293*, C1806-1813.
216. Roemer, E.; Lammerich, H.-P.; Conroy, L. L.; Weisensee, D. Characterization of a gap-junctional intercellular communication (GJIC) assay using cigarette smoke. *Toxicol. Lett.* **2013**, *219*, 248-253.

8 References

217. Dukic, A. R.; McClymont, D. W.; Tasken, K. A cell-based high-throughput assay for gap junction communication suitable for assessing Connexin 43-ezrin interaction disruptors using IncuCyte ZOOM. *J. Biomol. Screen.* **2016**.
218. Bathany, C.; Beahm, D.; Felske, J. D.; Sachs, F.; Hua, S. Z. High throughput assay of diffusion through Cx43 gap junction channels with a microfluidic chip. *Anal. Chem.* **2011**, *83*, 933-939.
219. Shaner, N. C.; Campbell, R. E.; Steinbach, P. A.; Giepmans, B. N. G.; Palmer, A. E.; Tsien, R. Y. Improved monomeric red, orange and yellow fluorescent proteins derived from *Discosoma* sp. red fluorescent protein. *Nat. Biotechnol.* **2004**, *22*, 1567-1572.
220. Clontech pLVX-IRES-mCherry Vector Information (PT5061-5, Catalog No. 631237). http://www.clontech.com/xxclt_ibcGetAttachment.jsp?cItemId=46586 (accessed 20.03.2017).
221. Falk, M. M. Connexin-specific distribution within gap junctions revealed in living cells. *J. Cell Sci.* **2000**, *113* (Pt 22), 4109-4120.
222. Promega Technical Manual: EnduRen™ Live Cell Substrate, E6481. <https://www.promega.de/-/media/files/resources/protocols/technical-manuals/0/enduren-live-cell-substrate-protocol.pdf> (accessed 15.04.2017).
223. Meda, P. Assaying the molecular permeability of connexin channels. In *Connexin methods and protocols*, Bruzzone, R.; Giaume, C., Eds. Springer Science & Business Media: 2001; Vol. 154, pp 201-224.
224. Homolya, L.; Hollo, Z.; Germann, U. A.; Pastan, I.; Gottesman, M. M.; Sarkadi, B. Fluorescent cellular indicators are extruded by the multidrug resistance protein. *J. Biol. Chem.* **1993**, *268*, 21493-21496.
225. Barbier, A. J.; Baron, B. M. Development of a prototype reporter-based assay for the evaluation of gap junctional intercellular communication. *Biotechnol. Lett.* **2001**, *23*, 1559-1563.
226. Gupta, A.; Anderson, H.; Buo, A. M.; Moorer, M. C.; Ren, M.; Stains, J. P. Communication of cAMP by connexin43 gap junctions regulates osteoblast signaling and gene expression. *Cell. Signal.* **2016**, *28*, 1048-1057.
227. Trehan, A.; Rotgers, E.; Coffey, E. T.; Huhtaniemi, I.; Rivero-Müller, A. CANDLES, an assay for monitoring GPCR induced cAMP generation in cell cultures. *Cell Commun. Signal.* **2014**, *12*, 70.

8 References

228. Fan, F.; Binkowski, B. F.; Butler, B. L.; Stecha, P. F.; Lewis, M. K.; Wood, K. V. Novel Genetically Encoded Biosensors Using Firefly Luciferase. *ACS Chem. Biol.* **2008**, *3*, 346-351.
229. Pettengill, M. A.; Lam, V. W.; Ojcius, D. M. The Danger Signal Adenosine Induces Persistence of Chlamydial Infection through Stimulation of A2b Receptors. *PLoS One* **2009**, *4*, e8299.
230. Valiunas, V. Cyclic nucleotide permeability through unopposed connexin hemichannels. *Front. Pharmacol.* **2013**, *4*, 75.
231. De Filippo, E.; Namasivayam, V.; Zappe, L.; El-Tayeb, A.; Schiedel, A. C.; Müller, C. E. Role of extracellular cysteine residues in the adenosine A(2A) receptor. *Purinergic Signalling* **2016**, *12*, 313-329.
232. Taniguchi, T.; Inagaki, R.; Murata, S.; Akiba, I.; Muramatsu, I. Microphysiometric analysis of human $\alpha(1a)$ -adrenoceptor expressed in Chinese hamster ovary cells. *Br. J. Pharmacol.* **1999**, *127*, 962-968.
233. Crassous, P. A.; Flavahan, S.; Flavahan, N. A. Acute dilation to $\alpha(2)$ -adrenoceptor antagonists uncovers dual constriction and dilation mediated by arterial $\alpha(2)$ -adrenoceptors. *Br. J. Pharmacol.* **2009**, *158*, 1344-1355.
234. Bull, S. C.; Doig, A. J. Properties of Protein Drug Target Classes. *PLoS One* **2015**, *10*, e0117955.
235. Rask-Andersen, M.; Almén, M. S.; Schiöth, H. B. Trends in the exploitation of novel drug targets. *Nat. Rev. Drug Discov.* **2011**, *10*, 579-590.
236. Yildirim, M. A.; Goh, K.-I.; Cusick, M. E.; Barabasi, A.-L.; Vidal, M. Drug[mdash]target network. *Nat. Biotechnol.* **2007**, *25*, 1119-1126.
237. Crivat, G.; Taraska, J. W. Imaging proteins inside cells with fluorescent tags. *Trends Biotechnol.* **2012**, *30*, 8-16.
238. Lotze, J.; Reinhardt, U.; Seitz, O.; Beck-Sickinger, A. G. Peptide-tags for site-specific protein labelling in vitro and in vivo. *Mol. Biosyst.* **2016**, *12*, 1731-1745.
239. Chalfie, M.; Tu, Y.; Euskirchen, G.; Ward, W. W.; Prasher, D. C. Green fluorescent protein as a marker for gene expression. *Science* **1994**, *263*, 802-805.
240. Zimmer, M. Green fluorescent protein (GFP): applications, structure, and related photophysical behavior. *Chem. Rev.* **2002**, *102*, 759-781.

8 References

241. Ehrmann, M. A.; Scheyhing, C. H.; Vogel, R. F. In vitro stability and expression of green fluorescent protein under high pressure conditions. *Lett. Appl. Microbiol.* **2001**, *32*, 230-234.
242. Hink, M. A.; Griep, R. A.; Borst, J. W.; van Hoek, A.; Eppink, M. H.; Schots, A.; Visser, A. J. Structural dynamics of green fluorescent protein alone and fused with a single chain Fv protein. *J. Biol. Chem.* **2000**, *275*, 17556-17560.
243. Cormack, B. P.; Valdivia, R. H.; Falkow, S. FACS-optimized mutants of the green fluorescent protein (GFP). *Gene* **1996**, *173*, 33-38.
244. Soboleski, M. R.; Oaks, J.; Halford, W. P. Green fluorescent protein is a quantitative reporter of gene expression in individual eukaryotic cells. *FASEB J.* **2005**, *19*, 440-442.
245. Marjanovic, I.; Kanduser, M.; Miklavcic, D.; Keber, M. M.; Pavlin, M. Comparison of flow cytometry, fluorescence microscopy and spectrofluorometry for analysis of gene electrotransfer efficiency. *J. Membr. Biol.* **2014**, *247*, 1259-1267.
246. Turner, E. H.; Lauterbach, K.; Pugsley, H. R.; Palmer, V. R.; Dovichi, N. J. Detection of green fluorescent protein in a single bacterium by capillary electrophoresis with laser-induced fluorescence. *Anal. Chem.* **2007**, *79*, 778-781.
247. Nemeth, E.; Tuttle, M. S.; Powelson, J.; Vaughn, M. B.; Donovan, A.; Ward, D. M.; Ganz, T.; Kaplan, J. Hepcidin Regulates Cellular Iron Efflux by Binding to Ferroportin and Inducing Its Internalization. *Science* **2004**, *306*, 2090-2093.
248. Ali, I.; Aboul-Enein, H. Y.; Gupta, V. K. Microchip-Based Nano Chromatography and Nano Capillary Electrophoresis in Genomics and Proteomics. *Chromatographia* **2009**, *69*, 13-22.
249. Deeb, S. E.; Wätzig, H.; El-Hady, D. A. Capillary electrophoresis to investigate biopharmaceuticals and pharmaceutically-relevant binding properties. *Trends Anal. Chem.* **2013**, *48*, 112-131.
250. Laing, T. D.; Marenco, A. J.; Moore, D. M.; Moore, G. J.; Mah, D. C.; Lee, W. E. Capillary electrophoresis laser-induced fluorescence for screening combinatorial peptide libraries in assays of botulinum neurotoxin A. *J. Chromatogr. B: Anal. Technol. Biomed. Life Sci.* **2006**, *843*, 240-246.
251. Ban, E.; Song, E. J. Recent developments and applications of capillary electrophoresis with laser-induced fluorescence detection in biological samples. *J. Chromatogr. B: Anal. Technol. Biomed. Life Sci.* **2013**, *929*, 180-186.

8 References

252. Babu, C. V.; Chung, B. C.; Lho, D. S.; Yoo, Y. S. Capillary electrophoretic competitive immunoassay with laser-induced fluorescence detection for methionine-enkephalin. *J. Chromatogr. A* **2006**, *1111*, 133-138.
253. Korf, G. M.; Landers, J. P.; O'Kane, D. J. Capillary electrophoresis with laser-induced fluorescence detection for the analysis of free and immune-complexed green fluorescent protein. *Anal. Biochem.* **1997**, *251*, 210-218.
254. Jin, Y.; Chen, C.; Meng, L.; Chen, J.; Li, M.; Zhu, Z.; Lin, J. A CE-LIF method to monitor autophagy by directly detecting LC3 proteins in HeLa cells. *Analyst* **2012**, *137*, 5571-5575.
255. Satori, C. P.; Arriaga, E. A. Describing autophagy via analysis of individual organelles by capillary electrophoresis with laser induced fluorescence detection. *Anal. Chem.* **2013**, *85*, 11391-11400.
256. Swearingen, K. E.; Loomis, W. P.; Kehimkar, B.; Cookson, B. T.; Dovichi, N. J. Quantification of green fluorescent protein in cellular supernatant by capillary electrophoresis with laser-induced fluorescence detection for measurement of cell death. *Talanta* **2010**, *81*, 948-953.
257. Marala, R. B.; Mustafa, S. J. Immunological characterization of adenosine A2A receptors in human and porcine cardiovascular tissues. *J. Pharmacol. Exp. Ther.* **1998**, *286*, 1051-1057.
258. Müller, C. E.; Jacobson, K. A. Recent developments in adenosine receptor ligands and their potential as novel drugs. *Biochim. Biophys. Acta* **2011**, *1808*, 1290-1308.
259. DeBlasi, A.; O'Reilly, K.; Motulsky, H. J. Calculating receptor number from binding experiments using same compound as radioligand and competitor. *Trends Pharmacol. Sci.* **1989**, *10*, 227-229.
260. Borrmann, T.; Hinz, S.; Bertarelli, D. C. G.; Li, W.; Florin, N. C.; Scheiff, A. B.; Müller, C. E. 1-Alkyl-8-(piperazine-1-sulfonyl)phenylxanthines: Development and Characterization of Adenosine A2B Receptor Antagonists and a New Radioligand with Subnanomolar Affinity and Subtype Specificity. *J. Med. Chem.* **2009**, *52*, 3994-4006.
261. Danish, A.; Namasivayam, V.; Schiedel, A. C.; Müller, C. E. Interaction of Approved Drugs with Synaptic Vesicle Protein 2A. *Arch. Pharm.* **2017**, 1700003-n/a.
262. Palomares, L. A.; Estrada-Mondaca, S.; Ramirez, O. T. Production of recombinant proteins: challenges and solutions. *Methods Mol. Biol.* **2004**, *267*, 15-52.

8 References

263. Bradford, M. M. A rapid and sensitive method for the quantitation of microgram quantities of protein utilizing the principle of protein-dye binding. *Anal. Biochem.* **1976**, *72*, 248-254.
264. Franco, V.; French, J. A.; Perucca, E. Challenges in the clinical development of new antiepileptic drugs. *Pharmacol. Res.* **2016**, *103*, 95-104.
265. Brown, T. A. In *Gene Cloning and DNA Analysis: An Introduction*. Wiley: UK, 2006.
266. Birnboim, H. C.; Doly, J. A rapid alkaline extraction procedure for screening recombinant plasmid DNA. *Nucleic Acids Res.* **1979**, *7*, 1513-1523.
267. Mullis, K. B.; Faloona, F. A. Specific synthesis of DNA in vitro via a polymerase-catalyzed chain reaction. *Methods Enzymol.* **1987**, *155*, 335-350.
268. Wallace, R. B.; Shaffer, J.; Murphy, R. F.; Bonner, J.; Hirose, T.; Itakura, K. Hybridization of synthetic oligodeoxyribonucleotides to phi chi 174 DNA: the effect of single base pair mismatch. *Nucleic Acids Res.* **1979**, *6*, 3543-3557.
269. Bartlett, J. M.; Stirling, D. A short history of the polymerase chain reaction. *Methods Mol. Biol.* **2003**, *226*, 3-6.
270. Weiner, M. P.; Costa, G. L. Rapid PCR site-directed mutagenesis. *PCR Methods Appl.* **1994**, *4*, S131-136.
271. NEB Data sheet: Gibson Assembly® Master Mix, E2611S. <https://www.neb.com/products/e2611-gibson-assembly-master-mix> (accessed 10.03.2017).
272. Felgner, P. L.; Gadek, T. R.; Holm, M.; Roman, R.; Chan, H. W.; Wenz, M.; Northrop, J. P.; Ringold, G. M.; Danielsen, M. Lipofection: a highly efficient, lipid-mediated DNA-transfection procedure. *Proc. Natl. Acad. Sci. U. S. A.* **1987**, *84*, 7413-7417.
273. Hu, W. S.; Pathak, V. K. Design of retroviral vectors and helper cells for gene therapy. *Pharmacol. Rev.* **2000**, *52*, 493-511.
274. Miller, A. D. Retrovirus packaging cells. *Hum. Gene Ther.* **1990**, *1*, 5-14.
275. Markowitz, D.; Goff, S.; Bank, A. Construction and use of a safe and efficient amphotropic packaging cell line. *Virology* **1988**, *167*, 400-406.
276. Markowitz, D.; Goff, S.; Bank, A. A safe packaging line for gene transfer: separating viral genes on two different plasmids. *J. Virol.* **1988**, *62*, 1120-1124.

8 References

277. Mulligan, R. C.; Berg, P. Selection for animal cells that express the Escherichia coli gene coding for xanthine-guanine phosphoribosyltransferase. *Proc. Natl. Acad. Sci. U. S. A.* **1981**, *78*, 2072-2076.
278. Clontech Lenti-X™ Lentiviral Expression Systems User Manual, PT5135-1. http://www.clontech.com/US/Products/Viral_Transduction/Lentiviral_Vector_Systems/ibcGetAttachment.jsp?cItemId=17579 (accessed 10.03.2017).
279. Cronin, J.; Zhang, X. Y.; Reiser, J. Altering the tropism of lentiviral vectors through pseudotyping. *Curr. Gene Ther.* **2005**, *5*, 387-398.
280. Bylund, D. B.; Toews, M. L. Radioligand binding methods: practical guide and tips. *Am. J. Physiol. Lung Cell Mol. Physiol.* **1993**, *265*, 421-429.
281. Davenport, A. P.; Russell, F. D. Radioligand Binding Assays: Theory and Practice. In *Current Directions in Radiopharmaceutical Research and Development*, Mather, S. J., Ed. Springer Netherlands: Dordrecht, 1996; pp 169-179.
282. Yung-Chi, C.; Prusoff, W. H. Relationship between the inhibition constant (K_i) and the concentration of inhibitor which causes 50 per cent inhibition (IC_{50}) of an enzymatic reaction. *Biochem. Pharmacol.* **1973**, *22*, 3099-3108.
283. Deupree, J.; Bylund, D. Basic principles and techniques for receptor binding. *Tocris Reviews* **2002**, *18*, 1-7.
284. Molecular Operating Environment (MOE) Chemical Computing Group Inc.,: 1010 Sherbooke St. West, Suite #910, Montreal, QC, Canada, H3A 2R7, 2016.
285. Labute, P.; Williams, C.; Feher, M.; Sourial, E.; Schmidt, J. M. Flexible alignment of small molecules. *J. Med. Chem.* **2001**, *44*, 1483-1490.
286. Halgren, T. A. Merck molecular force field. 1. Basis, form, scope, parameterization, and performance of MMFF94. *J. Comput. Chem.* **1996**, *17*, 490-519.
287. Corpet, F. Multiple sequence alignment with hierarchical clustering. *Nucleic Acids Res.* **1988**, *16*, 10881-10890.
288. Clarke, T. C.; Thomas, D.; Petersen, J. S.; Evans, W. H.; Martin, P. E. The antiarrhythmic peptide rotigaptide (ZP123) increases gap junction intercellular communication in cardiac myocytes and HeLa cells expressing connexin 43. *Br. J. Pharmacol.* **2006**, *147*, 486-495.

8 References

289. Shishido, S. N.; Nguyen, T. A. Induction of apoptosis by PQ1, a gap junction enhancer that upregulates connexin 43 and activates the MAPK signaling pathway in mammary carcinoma cells. *Int. J. Mol. Cell. Med.* **2016**, *17*, 178.

9 Appendices

Table A1: Quantification of GFP-tagged proteins by CE-LIF

hSV2A-GFP	peak area	mg/ml	ng/ml	1:100 dilution (ng/ml)	nmol/l	pmol/ml	total amount (mg/ml)	pmol/mg
Test 1	69044	0.00016295	162.95492	16295.4921	0.1393	139.3	5.00	27.9
Test 2	60554	0.00014292	142.91716	14291.7158	0.1222	122.2	5.00	24.4
Test 3	69134	0.00016317	163.16734	16316.7335	0.1395	139.5	5.00	27.9
mean								26.7

hA _{2A} AR-GFP	peak area	mg/ml	ng/ml	1:20 dilution (ng/ml)	nmol/l	pmol/ml	total amount (mg/ml)	pmol/mg
Test 1	2011	0.00000475	4.74628	94.9257	1.3184119	1.32	12.0	0.110
Test 2	2412	0.00000569	5.69271	113.8541	1.5813075	1.58	12.0	0.132
Test 3	2245	0.00000530	5.29856	105.9712	1.4718223	1.47	12.0	0.123
mean								0.121

mCx43-GFP	peak area	mg/ml	ng/ml	1:2 dilution (ng/ml)	nmol/l	pmol/ml	total amount (mg/ml)	pmol/mg
Test 1	2341	0.00000553	5.52514	11.0503	0.1579	0.158	4.70	0.0336
Test 2	3282	0.00000775	7.74605	15.4921	0.2213	0.221	4.70	0.0471
Test 3	2692	0.00000635	6.35355	12.7071	0.1815	0.182	4.70	0.0386
mean								0.0398

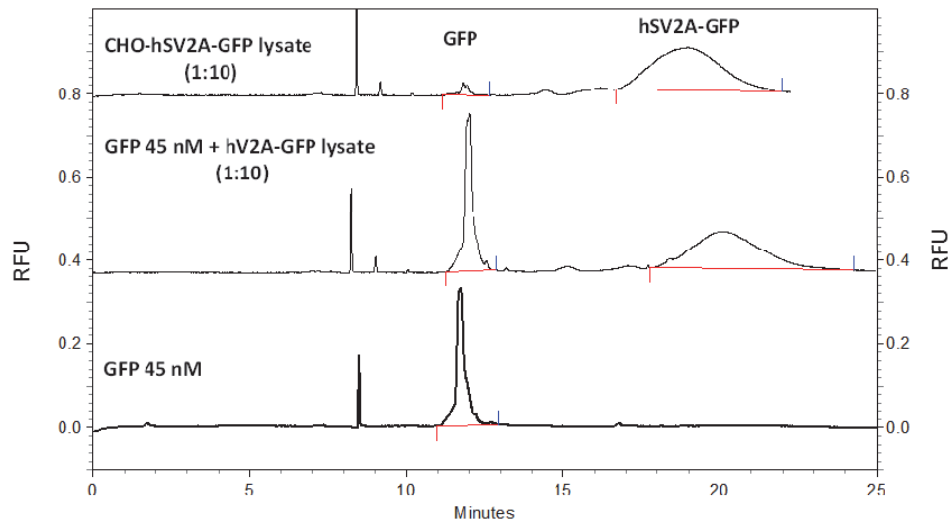


Figure A1: Separation of free GFP (standard) and hSV2A-GFP in cellular homogenate. RFU: relative fluorescence unit.

9 Appendices

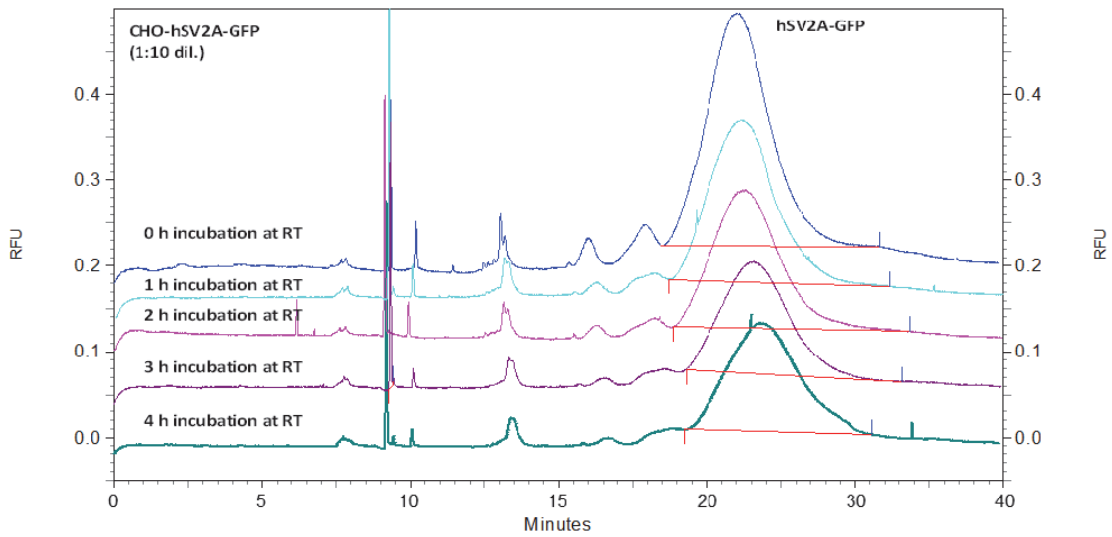


Figure A3: Effect of 1% SDS in sample buffer on peak area of hSV2A-GFP measured at different incubation time points. RT: room temperature, RFU: relative fluorescence unit.

9 Appendices

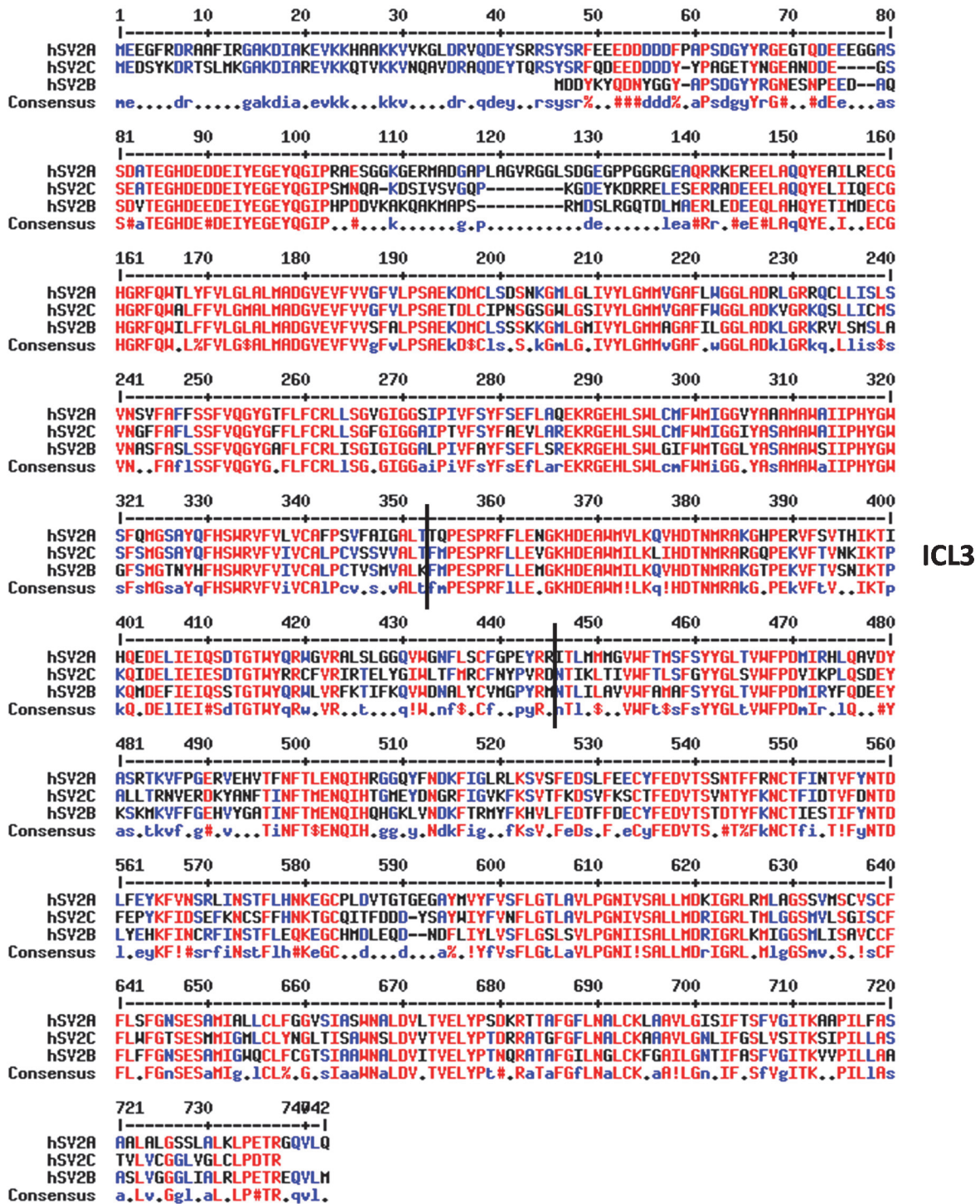


Figure A3: Multiple sequence alignment of human SV2A, SV2B, and SV2C. The alignment was performed using Multalin tool.²⁸⁷

Amino acid sequences of SV2A, SV2B and their chimeric variants

Protein sequence of human wild-type SV2A

MEEGFRDRAAFIRGAKDIAKEVKKHAAKVVVGLDRVQDEYSRRSYSRFEEDDDDDDFPAPSDGYRGEQTQDE
EEGGASSDATEGHDEDEDEIYEGEYQGI PRAESGGKGERMADGAPLAGVRGGLSDGEGPPGGRGEAQRRKEREEL
AQQYEAILRECGHGRFQWTLYFVLGLALMADGVEVFVVGFLVPSAEKDMCLSDSNKGMGLIVYLGMMVGAFLW
GGLADRLGRRQCLLISLSVNSVFAFFSSVFGYGTFLFCRLLSGVGIGGSIPIVFSYFSEFLAQEKRGEHLSWL
CMFWMIGGVYAAAMAWAIIPHYGWSFQMGSAIQFHWSRVFVLVCAFPSVFAIGALTTPESPRFFLENGKHDEA
WMVLKQVHDTNMR**AK**GHPERVFSVTHIKTIHQEDELIEIQSDTGTWYQRWGVRLSLGGQVWGNFLSCFGPEYR
RITLMMMGVWFTMSFSYYGLTVWFPDMIRHLQAVDYASRTKVFPGERVEHVTFNFTLENQIHRGGQYFNDKFIG
LRLKSVSFEDSLFEECYFEDVTSNTFFRNCTFINTVFYNTDLFEYKFNVSRLINSTFLHNKEGCPLDVTGTGE
GAYMVYFVSVFLGTLAVLPGNIVSALLMDKIGRLRMLAGSSVMSCVSCFFLSFGNSESAMIALLCFLGGVSIASW
NALDVLTVELYPSDKRTTAFGFLNALCKLAAVLGISIFTSFVGITKAAPILFASAALALGSSLALKLPETRGQV
LQ

Protein sequence of human wild-type hSV2B

MDDYKYQDNYYGGYAPSDGYRGNESNPEEDAQSDVTEGHDEEDEIYEGEYQGI PHPDDVKAKQAKMAPSRMDSL
RGQTDLMAERLEDEEQLAHQYETIMDECCHGRFQWILFFVLGLALMADGVEVFVVSFALPSAEKDMCLSSSKKG
MLGMIVYLGMMAGAFILGGLADKLGRKRVLSMSLAVNASFASLSSVFGYGAFLFCRLISGIGIGGALPIVFAY
FSEFLSREKRGEHLSWLGIFWMTGGLYASAMAWSIIPHYGWGFSMGTNYHFHWSRVFVIVCALPCTVSMVALKF
MPESPRFLLLEMGKHDEAWMILKQVHDTNMR**AK**GTPEKVFTVSNIKTPKQMDIEIQSSTGTWYQRWLVRFKTI
FKQVWDNALYCVMGPYRMNTLILAVVWFAMAFSYYGLTVWFPDMIRYFQDEEYKSKMKVFFGEHVYGATINFTM
ENQIQHGHKLVNDKFTRMVFKHVLFEDECFYFEDVTSSTDTYFKNCTIESTIFYNTDLYEHKFINCRFINST
FLEQKEGCHMDLEQDNDFLIYLVSVFLGSLSVLPGNII SALLMDRIGRLKMIIGGSMLISAVCCFFLFFGNSESAM
IGWQCLFCGTSIAAWNALDVITVELYPTNQRATAFGILNGLCKFGAILGNTIFASFVGITKVVPIILLAAASLVG
GGLIALRLPETREQVLI

Protein sequence of human hSV2A-hSV2B-ICL3

MEEGFRDRAAFIRGAKDIAKEVKKHAAKVVVGLDRVQDEYSRRSYSRFEEDDDDDDFPAPSDGYRGEQTQDE
EEGGASSDATEGHDEDEDEIYEGEYQGI PRAESGGKGERMADGAPLAGVRGGLSDGEGPPGGRGEAQRRKEREEL
AQQYEAILRECGHGRFQWTLYFVLGLALMADGVEVFVVGFLVPSAEKDMCLSDSNKGMGLIVYLGMMVGAFLW
GGLADRLGRRQCLLISLSVNSVFAFFSSVFGYGTFLFCRLLSGVGIGGSIPIVFSYFSEFLAQEKRGEHLSWL
CMFWMIGGVYAAAMAWAIIPHYGWSFQMGSAIQFHWSRVFVLVCAFPSVFAIGALTMPESPRFLLLEMGKHDEA
WMILKQVHDTNMR**AK**GTPEKVFTVSNIKTPKQMDIEIQSSTGTWYQRWLVRFKTI FKQVWDNALYCVMGPYR
MITLMMMGVWFTMSFSYYGLTVWFPDMIRHLQAVDYASRTKVFPGERVEHVTFNFTLENQIHRGGQYFNDKFIG
LRLKSVSFEDSLFEECYFEDVTSNTFFRNCTFINTVFYNTDLFEYKFNVSRLINSTFLHNKEGCPLDVTGTGE
GAYMVYFVSVFLGTLAVLPGNIVSALLMDKIGRLRMLAGSSVMSCVSCFFLSFGNSESAMIALLCFLGGVSIASW
NALDVLTVELYPSDKRTTAFGFLNALCKLAAVLGISIFTSFVGITKAAPILFASAALALGSSLALKLPETRGQV
LQ

Protein sequence of human hSV2B-hSV2A-ICL3

MDDYKYQDNYYGGYAPSDGYRGNESNPEEDAQSDVTEGHDEEDEIYEGEYQGI PHPDDVKAKQAKMAPSRMDSL
RGQTDLMAERLEDEEQLAHQYETIMDECCHGRFQWILFFVLGLALMADGVEVFVVSFALPSAEKDMCLSSSKKG
MLGMIVYLGMMAGAFILGGLADKLGRKRVLSMSLAVNASFASLSSVFGYGAFLFCRLISGIGIGGALPIVFAY
FSEFLSREKRGEHLSWLGIFWMTGGLYASAMAWSIIPHYGWGFSMGTNYHFHWSRVFVIVCALPCTVSMVALKT
QPESPRFFLENGKHDEAWMVLKQVHDTNMR**AK**GHPERVFSVTHIKTIHQEDELIEIQSDTGTWYQRWGVRLSL
GGQVWGNFLSCFGPEYRRNTLILAVVWFAMAFSYYGLTVWFPDMIRYFQDEEYKSKMKVFFGEHVYGATINFTM
ENQIQHGHKLVNDKFTRMVFKHVLFEDECFYFEDVTSSTDTYFKNCTIESTIFYNTDLYEHKFINCRFINST
FLEQKEGCHMDLEQDNDFLIYLVSVFLGSLSVLPGNII SALLMDRIGRLKMIIGGSMLISAVCCFFLFFGNSESAM
IGWQCLFCGTSIAAWNALDVITVELYPTNQRATAFGILNGLCKFGAILGNTIFASFVGITKVVPIILLAAASLVG
GGLIALRLPETREQVLI

Colors: Red color indicates the intracellular loop 3 (ICL3) in SV2A, SV2B, and chimeric variants. Yellow highlighted amino acid in SV2A wt depicts the arginine at position 383

Curriculum Vitae

Curriculum Vitae

PERSONAL DATA

AWARDS & SCHOLARSHIPS

EXPERIENCE

SCIENTIFIC PUBLICATIONS

Danish, A.; Namasivayam, V.; Schiedel, A. C.; Müller, C. E. Interaction of Approved Drugs with Synaptic Vesicle Protein 2A. *Arch. Pharm.* **2017**, DOI: 10.1002/ardp.201700003 (ahead of print).

Danish, A.; Namasivayam, V.; Müller, C. E. (*in preparation*). Cannabidiol (CBD) interacts with the levetiracetam binding site of synaptic vesicle protein SV2A.

Danish et al. (*in preparation*). Screening assay for connexin (Cx43) gap junctions.

Danish, A.*; Lee, SY.*; Müller, C. E. (*in preparation*). Quantification of green fluorescent protein (GFP)-tagged membrane proteins by capillary gel electrophoresis. *Both authors contributed equally to this study.

SCIENTIFIC CONFERENCES

Poster and short oral presentation (March, 2016)

Danish, A.; Schiedel, A.; Müller, C. E. Interaction of cannabinoids with the levetiracetam binding site of synaptic vesicle protein SV2A. Frontiers in Medicinal Chemistry in Bonn, Germany.

Poster and short oral presentation (July, 2015)

Danish, A.; Hildenbrand, S.; Schiedel, A.; Müller, C. E. Mutagenesis studies to elucidate the binding site of the antiepileptic drug Levetiracetam. V Paul Ehrlich MedChem Symposium in Krakow, Poland.

Acknowledgements

Acknowledgements

Firstly, I would like to express my sincere gratitude to my advisor Prof. Dr. Christa E. Müller for providing me the opportunity to work on such an interesting topic. This PhD study has intensively trained me to effectively conduct research in the field of pharmacology and molecular biology. I would like to thank you for your continuous support, for your valuable time, your motivation, your patience, your immense knowledge, your competence, and your constructive critic in writing this dissertation. You have taught me how good research is done and most importantly how it is documented. I could not imagine completing this thesis without your full support and guidance, which makes you a highly successful mentor. Thank you again.

I would like to express my special appreciation and thanks to my co-supervisor PD Dr. Anke Schiedel. You have been a tremendous mentor for me. Your support in research in the form of teaching lab skills, advices, scientific discussions as well as your motivation have been invaluable. I am grateful to you in particular for those moments when execution of some experiments was challenging, but together with your support, experience, and competence we found a feasible solution. Your readiness to help any time is highly appreciable.

Furthermore, I would like to thank Prof. Dr. Christian Steinhäuser for the collaboration project and for being so kind to act as a co-examiner in my PhD examination committee. I hope that our collaborative efforts will result in a useful contribution to the gap junction research community.

I would also like to specially thank Prof. Dr. Rainer Manthey for his immediate willingness to take up the role of the external co-examiner in my PhD examination committee.

I am highly indebted to Friedrich-Ebert-Stiftung for awarding me a PhD scholarship and for providing me a platform, which was, is, and will be extremely useful for the grooming of my personality and ideology. I would like to offer my special thanks to Mrs. Kathrein Hölscher for her continuous support, encouragement, flexibility, and extremely friendly nature. I am also highly thankful to Mrs. Beate Eckstein for providing assistance in various matters and for her friendliness.

Acknowledgements

I have greatly benefited from the Bonn International Graduate School of Drug Sciences (BIGS DrugS) through its pharmaceutical lecture series, scientific hands-on workshops, and PhD student colloquiums.

I want to thank Dr. Vigneshwaran Namasivayam for performing molecular modeling studies and also for being a dear friend. The discussions with you during the coffee breaks were always insightful and were never less than a career counselling appointments. I am indebt to Dr. Sang-Yong Lee for performing the capillary electrophoresis studies and also for being a nice friend. Your motivation was contagious and kept me motivated for the development of new protein analytical method. I received generous support from Clara Schöder with regard to cannabinoid library. Without you the screening of cannabinoids would have been certainly difficult.

I would like to thank Dr. Dominik Thimm. Your advice and comments were an enormous help for me in performing pharmacological assays and data analysis.

I am deeply grateful to my office mates-cum-friends Dr. Elisabetta De Filippo and Muhammad Rafehi for creating such a pleasant and joyful atmosphere. The moments I spent with you guys will always stay in nice memories.

I want to thank my fellow labmates plus friends Dr. Sonja Hinz and Isaac Attah for the stimulating discussions. I am also thankful to other AK Müller group members who are currently working or have worked in the past, in particular Markus Kuschak, Dr. Wessam Alnouri, Dr. Thanigaimalai Pillaiyar, Mahmoud Rashed, and Dr. Nader Boshta for being so helpful and friendly. All in all it was an amazing experience to work with such a highly-skilled team.

I would like to offer my thanks to Prof. Dr. Diana Imhof and all other colleagues from the 4th semester practical course of instrumental analytics. It was a great pleasure to work with you all.

Last but not least, I owe my deepest gratitude to my family: my parents, my sibblings, Hafsa, my friends in Bonn, and my friends in Pakistan. Without your emotional support, encouragement, and help, probably bringing this journey to an end would have not been possible.